CR 152399

LEAR SIEGLER, INC.
ASTRONICS DIVISION

DEVELOPMENT AND EVALUATION OF AUTOMATIC LANDING CONTROL LAWS FOR POWERED LIFT STOL AIRCRAFT

NASA CR-152399, January, 1981

3171 SOUTH BUNDY DRIVE
SANTA MONICA, CA. 90406
AREA CODE 213 391-7211

NASA CR-152399

DEVELOPMENT AND EVALUATION OF AUTOMATIC LANDING CONTROL LAWS FOR POWERED LIFT STOL AIRCRAFT

JANUARY, 1981

By

B. Feinreich and G. Gevaert

Prepared under Contract No. NAS2-10324 by

LEAR SIEGLER INC., ASTRONICS DIVISION,

Santa Monica, California 90406

for

AMES RESEARCH CENTER

NATIONAL AERONAUTICS AND SPACE ADMINISTRATION

Abstract

Automatic flare and decrab control laws were developed for a powered lift STOL aircraft, incorporated in the airborne digital computer on NASA's Augmentor Wing Jet STOL Research Airplane, evaluated on two simulations and in over 200 flight test landings using MLS for approach guidance. The extensive technology base which exists for conventional takeoff and landing aircraft has been adapted to the unique requirements of the powered lift STOL airplane. Three longitudinal autoland control laws were developed. In additon to conventional controllers, direct lift and direct drag control were used in the longitudinal axis. A fast time simulation was used for the control law synthesis, with emphasis on stochastic performance prediction and evaluation. Through iterative refinements, good correlation with flight test results was obtained. This simulation was used to extrapolate the statistical landing data base beyond the two sigma level established in flight to the improbable level required by the FAA for certification. Excellent touchdown sink-rate control was obtained, with range accuracy consistent with Cat III performance requirements.

TABLE OF CONTENTS

LIST OF FIGURES

LIST OF FIGURES (CONTINUED)

LIST OF TABLES

REFERENCES

1. N. M. Shah, G. Gevaert, L. O. Lykken, "The Effect of Aircraft Environment on Category III Autoland Performance and Safety", AIAA 4th Aircraft Design, Flight Test, and Operations Meeting, August, 1972.

2. Gevaert, G., Lykken, L. O., and Shah, N., "A Simulation Program for Category III Autoland Certification" Summer Computer Simulation Conference, June, 1972.

3. Mineck, D. W., Derr, R. E., Lykken, L. O., Hall, J. C., "Avionic Flight Control System for the Lockheed L-1011 Tristar", SAE Aerospace Control and Guidance Systems Committee Meeting No. 30, September, 1972.

4. Anon., "Automatic Landing Systems", FAA, AC 20-57A, 12 January, 1971.

5. Gevaert, G., Feinreich, B., "The Development of Advanced Automatic Flare and Decrab for Powered Lift Short Haul Aircraft Using A Microwave Landing System", NASA CR-151948, April, 1977.

6. Hindson, W. S., Hardy, G. H., Innis, R. C., "Evaluation of Several STOL Control and Flight Director Concepts from Flight Tests of a Powered-Lift Aircraft Flying Steep, Curved Approaches." NASA TP 1641 (to be published).

7. Quigley, H. C., Innis, R. C., Grossmith, S., "A Flight Investigation of the STOL characteristics of an Augmented Jet Flap STOL Research Aircraft", NASA TM X-62, 334, May, 1974.

8. Scott, B. C., Hynes, C. S., Martin, P. W., and Bryder, R. B.: "Progress Toward Development of Civil Airworthiness Criteria for Powered-Lift Aircraft" NASA TMX-73, 124, 1976.

9. Neuman, F., Watson, D. M., Bradbury, P., "Operational Description of an Experimental Digital Avionics System for STOL Airplanes" NASA TM X-62, 448, 1975.

10. De Hoff, R. L., Reed, W. B., Trankle, T. L., Hall, Jr., W. E., "Identification of Spey Engine Dynamics in the Augmentor Wing Jet STOL Research Aircraft from Flight Data" NASA CR-152054, October, 1977.

11. Anon., "Planning and Design Criteria for Metropolitan STOL Ports", FAA Advisory Circular 150/5300-8, November, 1970.

12. BCAR Paper 367, Issue 3. "Airworthiness Requirements for Automatic Landing Including Automatic Landing in Restricted Visibility Down To Category 3," June, 1970.

13. BCAR Paper 423, Issue 2. "Airworthiness Requirements for Landing in Restricted Visibility, Category 2 Operation," February, 1969.

14. Feinreich, B., Gevaert, G., Hardy, G. H., Watson, D. M., "Development of Automatic Landing Control Laws for Powered Lift Short Haul Aircraft." AIAA Paper No. 80-1759, August, 1980.

REFERENCES (continued)

A-1 W.B. Cleveland, R.F. Vomaske, and S.R.M. Sinclair, "Augmentor Wing Jet STOL Research Aircraft Simulation Model", NASA TMX 62149, April, 1972.

A-2 R.K. Heffley, R.L. Stapleford, R.C. Rumold and J.M. Lehman, "A STOL Airworthiness Investigation Using a Simulation of an Augmentor Wing Transport", NASA TMX 62396, October, 1974.

A-3 "Microwave Landing System Study - Area Navigation Impact on Autopilots", LSI ADR-765, 4 March, 1974.

LIST OF SYMBOLS

a_x^c	Nozzle commanded deceleration rate
a_y	Lateral acceleration
h_{ALN}	Altitude where runway alignment begins
$\dot{h}$	Rate of climb
$\ddot{h}$	Vertical acceleration
$\dot{h}_e$	Sink rate error
h_{FL}	Radar altitude at which flare sink rate control begins
h_G	Main landing gear height
h_{GS}	Radar altitude at which glide slope error starts fading out
h_o	Altitude where runway alignment ends
h_{RA}	Radar altitude
$\hat{h}_{RA}$	Filtered radar altitude derived sink rate
$h_{\theta FL}$	Radar altitude at which the pitch flare maneuver begins
$\dot{h}_{TD}^c$	Commanded touchdown sinkrate
k_{CH}	Choke gain
k_h	Glideslope deviation gain
k_{IF}	Flare integrator gain
k_{IG}	Glideslope error integrator gain
k_{NCH}	Engine RPM to choke gain
k_{NF}	RPM feedback gain
k_q	Pitch rate gain
k_r	Yaw rate gain
k_{VI}	Speed integrator gain
k_{VN}	Speed gain to nozzle
$k_{V\theta}$	Speed to pitch gain
k_W	Wheel command gain
k_Y	Lateral position error gain
k_{YI}	Lateral position error integral gain
$k_{\dot{Y}}$	Lateral position rate error gain
$k_{\dot{Y}a}$	Additional lateral position rate error gain at align
$k_{\dot{Y}A}$	Runway alignment lateral acceleration gain
$k_{\delta TC}$	Throttle command gain
$k_{\delta TF}$	Throttle feedback gain
$k_{\dot{\delta}T}$	Throttle rate command gain
k_θ	Pitch attitude gain
$k_{\phi I}$	Roll integral gain
$k_{\dot{\phi}}$	Roll rate feedback gain
k_ψ	Yaw feedback gain
$k_{\psi I}$	Yaw error integral gain
$k_{\psi\phi}$	Yaw to roll crossfeed gain at align
NH	High pressure engine RPM
n_Y	Lateral acceleration (in g's)
q	Pitch rate
$\bar{q}$	Dynamic Pressure
r	Yaw rate
$\dot{r}$	Yaw acceleration

LIST OF SYMBOLS (cont)

S	Laplace operator
t	Ambient temperature
u_A	Incremental airspeed deviation from trim
U_w	Wind speed
V_C	Calibrated airspeed
$\hat{V}_C$	Filtered calibrated airspeed
V_{REF}	Reference approach airspeed
V_T	True airspeed
W	Aircraft gross weight
X	Distance along the runway measured from the Glide-Path Intercept Point
$\ddot{X}$	Longitudinal acceleration
$\hat{Y}$	Filtered lateral position error
$\hat{\dot{Y}}$	Filtered lateral position error rate
$\ddot{Y}$	Lateral acceleration at the c.g.
$\ddot{Y}_R$	Lateral acceleration in runway axes
α_A	Incremental angle of attack with respect to trim
γ_{AIR}	Aerodynamic flight path angle
Δh_f	Filtered glide slope error
Δh_{GS}	Glideslope deviation
$\hat{\Delta h}_{GS}$	Filtered glideslope deviation
$\hat{\Delta \dot{h}}_{GS}$	Filtered glideslope deviation rate
Δh_{100}	Glide slope deviation at 30.5 meters (100 ft) radar altitude
ΔY_{LOC}	Lateral position error
$\Delta\psi$	Runway heading error
$\Delta\psi_i$	Heading error when the alignment maneuver begins
$\Delta\psi_o$	Heading error commanded when the alignment maneuver ends
δ_{CH}	Choke deflection
δ^C_{CH}	Choke command
δ_e	Incremental elevator deflection with respect to trim
δ^C_e	Elevator command
δ_F	Flap position
δ_N	Nozzle deflection
δ^C_N	Nozzle angle command
δ^P_N	Trim table nozzle command
δ_{NH}	Incremental engine RPM with respect to trim
δ_{NREF}	Reference nozzle position
δ_R	Rudder deflection
δ^C_R	Rudder command
δ_T	Incremental throttle deflection with respect to trim
δ^C_T	Throttle position command
$\dot{\delta}^C_T$	Throttle rate command
δ^P_T	Trim table throttle command
δ_W	Wheel deflection
δ^C_W	Wheel command
θ	Pitch attitude
θ_o	Pre-flare pitch attitude
θ_{TD}	Touchdown pitch attitude
θ^C_{TD}	Touchdown pitch attitude command
θ^P	Trim table pitch command
μ	Mean value
σ	Standard deviation

τ_{BN}	Beam noise time constant
τ_{CH}	Choke time constant
$\tau_{\ddot{h}}$	Vertical accelerometer time constant
τ_I	Lateral accelerometer time constant
τ_u	Horizontal turbulence time constant
τ_w	Vertical turbulence time contant
τ_2	Yaw to roll crossfeed time contant
ϕ	Roll ttitude
ϕ_{ALN}	Runway alignment roll command
$\dot{\phi}$	Roll rate
ψ	Heading
ψ_{RWY}	Runway heading
ω_{GS}	Glide slope complementary filter frequency
ω_{RA}	Radar altimeter complementary filter frequency
ω_Y	Localizer complementary filter frequency

ACRONYMS AND ABBREVIATIONS

BN	Beam Noise
CAA	The British Civil Aviation Authority
CAT III	Category III (Weather Minima)
CG	Center of Gravity
CTL	Controls
CTOL	Conventional Takeoff and Landing
deg	Degrees
DLC	Direct Lift Control
FAA	Federal Aviation Administration
ft	Feet
g	Gravity Acceleration
GPIP	Glide-Path Intercept Point
HW	Headwind
HWS	Shearing Headwind
kt	Knots
m	Meters
NALF	Naval Auxiliary Landing Field
NASA	National Aviation and Space Administration
psf	Pounds Per Square Foot
RMS	Root Mean Squared
RPM	Revolutions Per Minute
RPS	Radians Per Second
sec	Second
STOL	Short Takeoff and Landing
TD	Touchdown
TW	Tailwind
TWS	Shearing Tailwind

1.0 Introduction and Summary

1.1 Introduction

The Ames Research Center of NASA is conducting a series of investigations to generate and verify through ground based simulation and flight research a data base to aid in the design and certification of advanced propulsive lift short takeoff and landing (STOL) aircraft. One portion of this program is concerned with obtaining technical information on automatic landing systems for STOL aircraft including flight path control performance and touchdown state dispersion in the presence of environmental disturbances. As part of this program, Lear Siegler's Astronics Division developed automatic landing control laws for the Augmenter Wing Jet STOL Research Airplane.

The technology for the development and certification of Category III automatic landing systems for conventional takeoff and landing (CTOL) jet transports is well developed and documented, as noted in References 1 to 3 for one commercial aircraft and Reference 4 for the FAA requirements. No comparable technology exists for automatic landing systems for STOL airplanes in general and for powered lift STOL airplanes in particular.

The objective of the automatic landing work reported here is to gain understanding of the problems impacting the design of powered lift short-haul airplanes that are to be landed automatically on STOL runways in adverse weather conditions. This understanding was attained by a limited coverage of important elements that are normally included in the certification process of a CAT III automatic landing system for CTOL airplanes with major emphasis on fault-free performance. The control law development concentrated on the final approach to touchdown phase of the landing, with the majority of the effort expended on longitudinal and vertical control because this is where the peculiarities of the powered-lift STOL vehicle are most prominent.

The development and flight validation of the automatic landing system control laws was conducted in three phases. In the first phase, reported in Reference 5, Lear Siegler developed both longitudinal and lateral candidate autoland control laws for a powered lift STOL airplane using an Augmenter Wing Jet STOL airplane as an example. This development was based on previous company experience with automatic landing system designs and on control strategies which were emerging from manual operation of the Augmenter Wing airplane by NASA pilots. For discussion of these manual operations, see Reference 6.

In Phase 2, candidate automatic landing control laws were selected by NASA for implementation. NASA personnel supervised the development and qualification of the flight software on the airborne hardware simulation resident at the Ames Research Center, conducted the flight testing and analyzed the performance of these control laws. As the flight program progressed, models and control laws were refined in a joint effort of Lear Siegler and NASA, culminating in the configurations presented in this report.

Although a lateral control law was flight qualified and evaluated, the main thrust of the program remained on the longitudinal control laws. Three longitudinal control laws emerged for comparison. The primary emphasis in all three longitudinal laws was on achieving an accurate touchdown sink-rate with secondary emphasis on touchdown range dispersion.

In the third phase of the program, Lear Siegler used the results of the NASA flight testing to validate a high speed analog simulation which was then used to generate a large statistical data base to establish the automatic landing system performance at the 10^{-6} probability (improbable event) level.

1.2 Summary

This report describes the development of a family of automatic landing system control laws and shows that this type of control law is capable of meeting requirements like those applied by the FAA to CTOL automatic landing systems. The results presented in this report are derived from both simulation and flight data. A comparison of flight and simulation establishes the validity of the simulation both as a design tool and as a mechanism for extrapolating the flight data to the improbable event.

The report contains eight sections describing the development and evaluation of the automatic landing control laws. Section 2 is a brief description of the Augmenter Wing Airplane, the STOL approach conditions, the airplane's peculiar controls and its avionic system. Section 3 described the design and evaluation process employed in this program including two simulations and flight tests. Section 4 contains a detailed description of the final longitudinal and lateral control laws that emerged from this program. Section 5 describes the longitudinal landing performance results that were obtained in the simulation. It provides data for the effects of various environment, airframe and system variations. Section 6 describes the simulation landing performance results for the lateral/directional axis. Section 7 gives a comparison between simulation and flight results. The conclusions derived from this work are presented in Section 8. Appendix A is a summary of airframe, controllers, sensors and disturbance mathematical models that were used in the simulation. Appendix B contains backup data for the simulation results that are presented in Section 5.

2.0 The Research Airplane and the Approach Condition

The Augmenter Wing Airplane is briefly described in this section. The STOL approach condition that was used in this program is defined, the controls available on this airplane and its avionic system are described.

2.1 The Airplane

The Augmenter Wing Airplane shown in Figure 2-1 is a modified de Havilland C-8A Buffalo airplane with the wingspan reduced to increase wing loading. This airplane is equipped with jet augmenter flaps as shown in Figure 2-2, incorporating flow blocking devices called chokes, has drooped ailerons with boundary layer control and incorporates full span leading edge slats. The two original turboprop engines were replaced by two Rolls Royce Spey 801 split flow turbo-fan engines which were supplied by the Canadian government as part of the joint program between NASA and the Canadian Department of Trade, Industry and Commerce. The cold flow from the engines is ducted to the augmenter flaps and ailerons and the hot thrust is vectorable through the conical exhaust nozzles. A more detailed description of the aircraft and its characteristics is given in Reference 7.

Figure 2-1 The Augmenter Wing Airplane

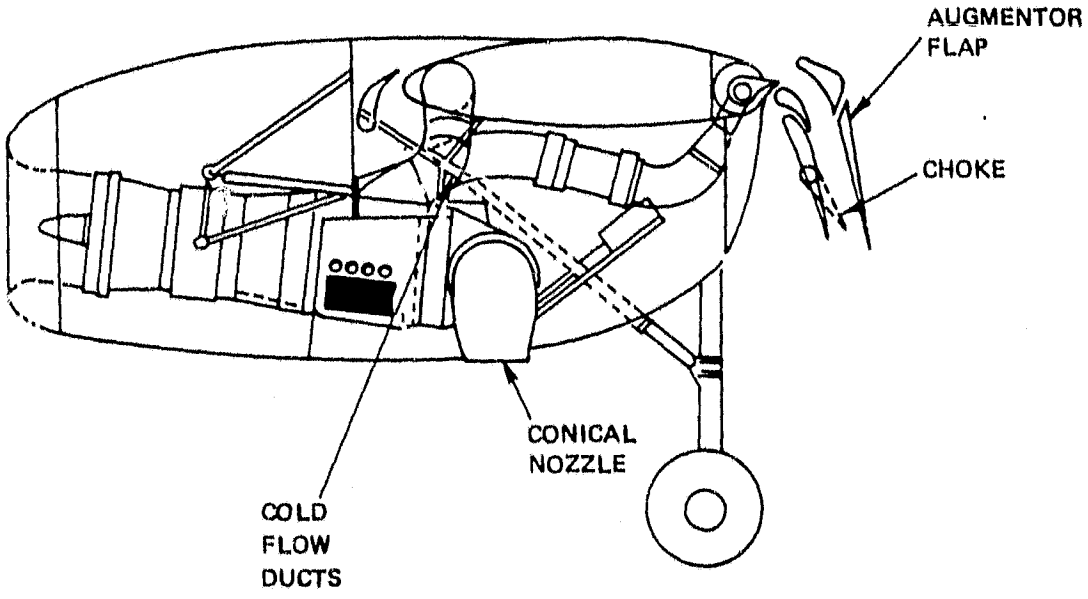

FIGURE 2-2. ENGINE NACELLE AND CROSS SECTION OF THE JET AUGMENTOR FLAP

2.2 The Approach Condition

The nominal landing approach condition of the Augmenter Wing Jet STOL Research airplane is compared in Table 2-I with that of the L-1011 which is a typical example of a CTOL transport airplane. (These numbers are representative and approximate; they are given in order to highlight the differences between the two aircraft rather than to provide exact data for each one.)

TABLE 2-I STOL VERSUS CTOL LANDING APPROACH CONDITIONS

	AUG WING	L-1011
Airspeed, kt	70	135
Glide Slope Angle, deg	7.5	2.75
Thrust Inclination, deg	90	0
Wing Loading N/m^2 (psf)	2378 (49.7)	4359 (91.1)
Lift Coefficient	3.0	1.5
Approach/Full Thrust, %	85	25
Lift, Aerodynamic, %	40	100
Cold Flow, %	40	0
Hot Thrust, %	20	0

The Augmenter Wing Jet STOL Research airplane was flown on a 7.5 degree glide slope at speeds near 70 knots for the final approach. At this low approach speed, the airplane operates on the backside of the power curve. Because of this and the near vertical thrust orientation in the approach configuration, the most effective control for path is the throttle and the most effective control for speed is the elevator. These characteristics are in sharp contrast to the conventional jet transport where during the approach the path is primarily controlled with the elevator and the speed is primarily controlled with the throttle. Reference 6 contains a more complete discussion of the operating characteristics of the Augmenter Wing airplane.

2.3 The Airplane Controls and Avionics System

The Augmenter Wing airplane incorporates four controls that can be used in the longitudinal axis for the control of glide path and automatic flare. The throttle regulates RPM which in turn regulates hot thrust through the exhaust nozzles and cold thrust through the augmenter flaps. The autothrottle was mechanized to give a lift control authority of +0.1g and -0.07g's about the nominal trim point while observing engine limitations and preserving lift margins. Direct lift control is available through the symmetric actuation of the chokes (Figure 2-2) which can block the flow through the inboard augmenter flaps. These fast acting chokes, when used, are modulated ±30 percent of full closure about a nominal 30 percent position to provide approximately ±0.1g's of lift authority. When the chokes are used, they are complemented with the throttle to improve overall path control bandwidth at the expense of some overall reduction in powered lift augmentation. The powered lift lost by biasing the chokes must be replaced by increasing the aerodynamic lift through a small increase in approach reference airspeed. The thrust conical nozzles, (Figure 2-2) which can be vectored from 6^{o} to 104^{o} from horizontal are always used to trim engine RPM and for some control configurations are also used as a direct drag device for short term speed control. As a trim device, the nozzles are adjusted to compensate for temperature and wind in order to maintain the engine RPM in a nominal operating range to provide for both upward and downward path corrections. The maximum RPM limitation is established to avoid structural damage to the nozzles when the nozzles are down. The minimum RPM is set to maintain a minimum value of lift margin as described subsequently. When used as a longitudinal speed control device, the nozzles have a longitudinal authority of +0.13 and -0.09g's for typical nozzle trim values near 75^{o}. A hydraulic powered elevator is the fourth control which is always used for long term speed corrections and is also used, in the absence of short term nozzle vectoring, to provide short term speed control.

Roll is controlled with ailerons, spoilers and outboard augmenter flap chokes which are mechanically geared to the wheel. A split segment but otherwise conventional powered rudder is used to control yaw.

A unique characteristic of a powered lift aircraft is that it can approach at speeds below the power off stall speed. In order to provide adequate safety margins, CTOL aircraft use an approach speed of 1.3 times the power off stall speed. For powered lift aircraft, this would be an excessive requirement and other means must be used to provide safety margins comparable to that used for the CTOL vehicle. Reference 8 describes a comprehensive study of this problem. On the Augmenter Wing aircraft, a lift margin of 0.4g's was used to ensure a safe approach speed. Lift margin is defined as the difference in g's between the trim lift value and the maximum lift available from pitch rotation alone with the throttle held constant. Since the lift margin is a function of speed and thrust, limits must be placed not only on the approach speed, but also on the minimum value of engine RPM.

The airplane is equipped with the STOLAND digital avionics system (Reference 9) providing versatile navigation, guidance, control and display functions.

A microwave landing system was used for approach guidance, providing azimuth, elevation and distance information.

3.0 Design and Evaluation Methods

The methods used in the design and evaluation of the automatic landing control laws that have been developed are described in this section. The roles of the two simulations and flight tests are explained as well as the sequence and interrelations of these activities. Simulation models are given in Appendix A.

3.1 Design and Evaluation Process

The design and evaluation process used in this program includes several of the major elements that constitute the certification process of a CTOL airplane CAT III automatic landing system as reported in References 1 through 3. Figure 3-1 depicts the major elements and flow paths included in the current program. A simulation is used to define and refine the control laws and verify that they produce acceptable landing performance with environmental disturbances. Initial flight test results are used to refine control laws and airframe models used in the simulation. When good correlation is established between flight and simulation results, the simulation can be used to expand the limited statistical flight data base ($\approx 10^2$) to the extreme event levels ($\approx 10^6$) required for certification.

Using the simulation, data was taken for various levels of environmental disturbances, airframe variations and system errors, covering a wider range than possible in flight. Probability distributions were generated for all touchdown state variables.

In two major areas this program was less comprehensive than a full certification program: Heavy emphasis during the control law development was placed on performance with no system failures. Less consideration was given to failure effects and redundancy requirements. The system flown was nonredundant, relying on pilot monitoring to ensure safety.

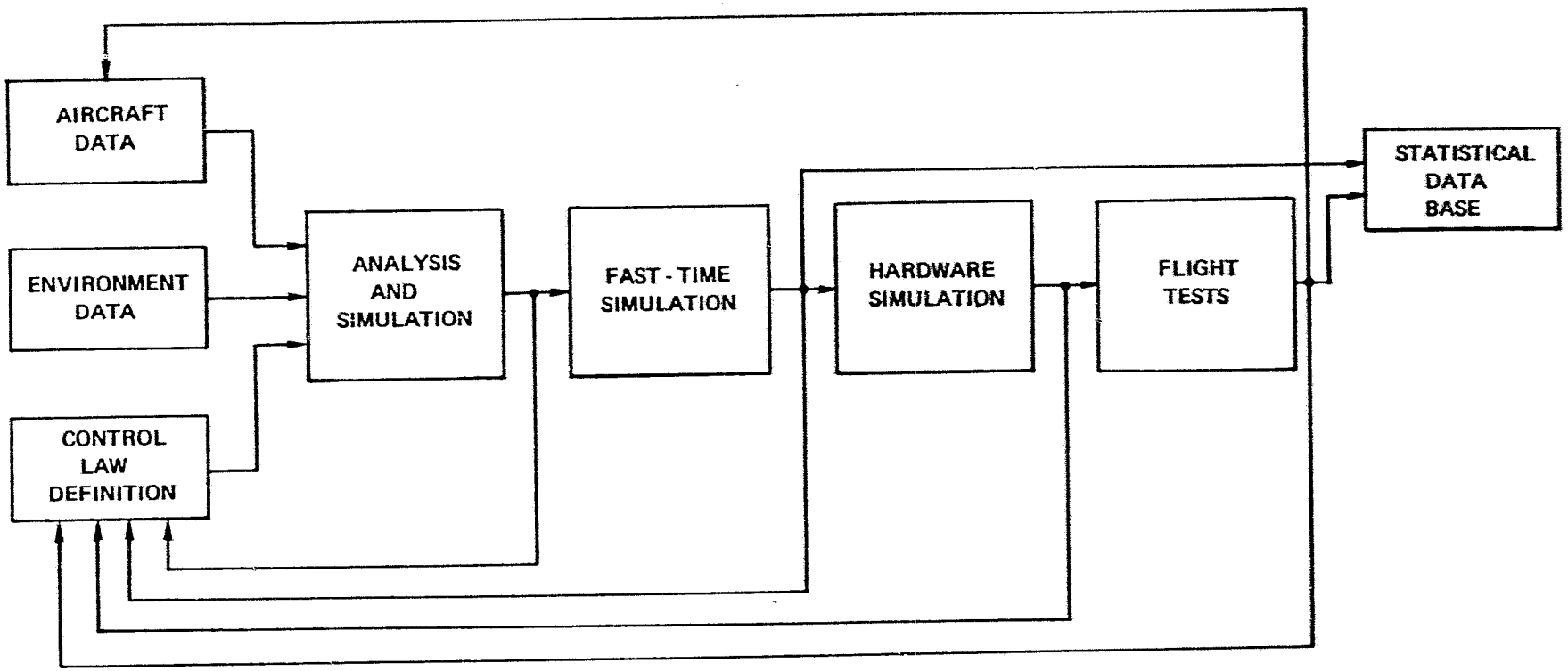

FIGURE 3-1. DESIGN AND EVALUATION PROCESS

In a full certification program, correlation between simulation and flight is verified through the collection of actual disturbance data as encountered in flight on a landing by landing basis, inserting the same disturbances in the simulation, and correlating the results for a limited number of landings. This was not done in this program due to contract funding constraints. Total population results for a given control law configuration is used for correlation instead.

3.2 Simulation

A fast-time simulation was the major tool used in synthesizing and evaluating the automatic landing control laws. Mathematical models of the airframe, controllers, sensors and the environment were assembled and used in the simulation. The normal set of uncoupled, linearized, small perturbation equations of motion were used in separate longitudinal and lateral simulations. Longitudinal dynamics were included in the lateral simulation to the extent necessary to account for the ground speeds associated with different headwinds. Important nonlinearities were modeled, including lift and drag variations associated with changing nozzle angles and with engine RPM settings. Lift, pitching moment, and drag variation due to ground effects were also included.

Controller dynamics were modeled, including rate and position limits and significant hysteresis effects. Special care was taken in accurately modelling engine dynamics because the engine is used as the major flight path angle controller and has a strong impact on performance. Engine modelling was based on the identification work described in Reference 10. Separate paths were used for computing cold and hot thrust responses, with different time constants used for thrust increase or decrease.

Sensor dynamics and error models which contribute to landing dispersions were also included, such as radar altimeter dynamics and offsets, and dynamic and static vertical gyro and accelerometer errors. MLS noise was modeled and included in the simulation. Winds, shears and turbulence consistent with the definitions in the FAA Advisory Circular 20-57A (Reference 4) were used.

For statistical data collection, the simulation was run in fast time repetitive operation mode, starting at 1000 feet above the runway with the airplane stabilized on the glide slope or localizer, and terminating at touchdown. The 30.5 meters (100 foot) approach window states were recorded, as were the touchdown states: vertical and lateral velocity, touchdown point on the runway, and pitch, roll and heading angles.

Appendix A contains a detailed description of the models used in the simulation.

3.3 Hardware Simulation and Flight Tests

The automatic landing control laws were programmed into flight control computer software, with testing and validation on the NASA Ames Research Center real time hardware simulator. This total nonlinear six degrees of freedom simulation includes flight control and display computer hardware and pilot interface. The simulation facility was used to qualify each software revision prior to flight.

Flight tests were conducted by NASA Ames Research Center at Crows Landing Naval Auxiliary Landing Field (NALF) in California. The flight test landings were made on a simulated 518.3 by 30.5 meters (1700 by 100 feet) STOL runway with boundaries painted, in accordance with Reference 11, on a longer and wider runway. The runway geometry is shown in Figure 3-2. The Glide Path Intercept Point is 79.3 meters (260 ft) beyond the threshold. All landing distance results in this report are referenced to the GPIP.

The marked touchdown zone extends from 24.4 m (80 ft) to 85.4 m (280 ft) beyond the GPIP.

A microwave landing system was installed. A data collection and reduction system with airborne and ground based elements was used to record flight test results.

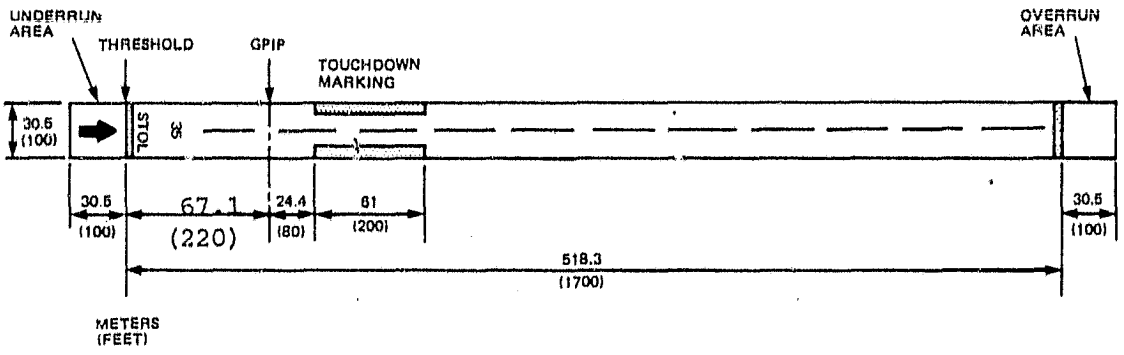

FIGURE 3-2. STOL RUNWAY GEOMETRY

4.0 Control Laws Description

The final version of the automatic landing control laws that emerged from this program after several iterations of refinements resulting from simulator and flight evaluation is defined in this section. A family of control laws with different complexity levels is presented in pitch as well as the final lateral/directional control law.

4.1 Longitudinal

The glide slope track and flare control laws that have been developed for the Augmenter Wing airplane are shown in the block diagram of Figure 4-1 and the gains are defined in Table 4-I. A backside of the power curve control technique is used, controlling flight path angle with engine RPM, augmented by the DLC chokes. The elevator is used for attitude stabilization and control and for long term airspeed trim changes. Short term airspeed deviations are controlled through the use of the conical nozzles which are also used for longitudinal trim control to account for the aerodynamic flight path angles resulting from differing wind components. The trim tables shown in Figure 4-1 pre-position the throttles, nozzles and pitch attitude, and the closed loop control laws correct for deviations from trim. The trim tables outputs are held constant below 91.5 meters (300 ft) radar altitude. Raw glide slope deviation, computed from elevation and range information, is combined with vertical acceleration in a complementary filter to produce estimates of glide slope deviation and rate which are used for tracking the glide slope. The output of the radar altimeter is blended with vertical acceleration in another complementary filter to produce a sink-rate signal that is used in the flare. These complementary filters had been previously defined in the course of prior Augmenter Wing programs and were used in this automatic landing program. These filters are defined by the block diagrams of Figure 4-2.

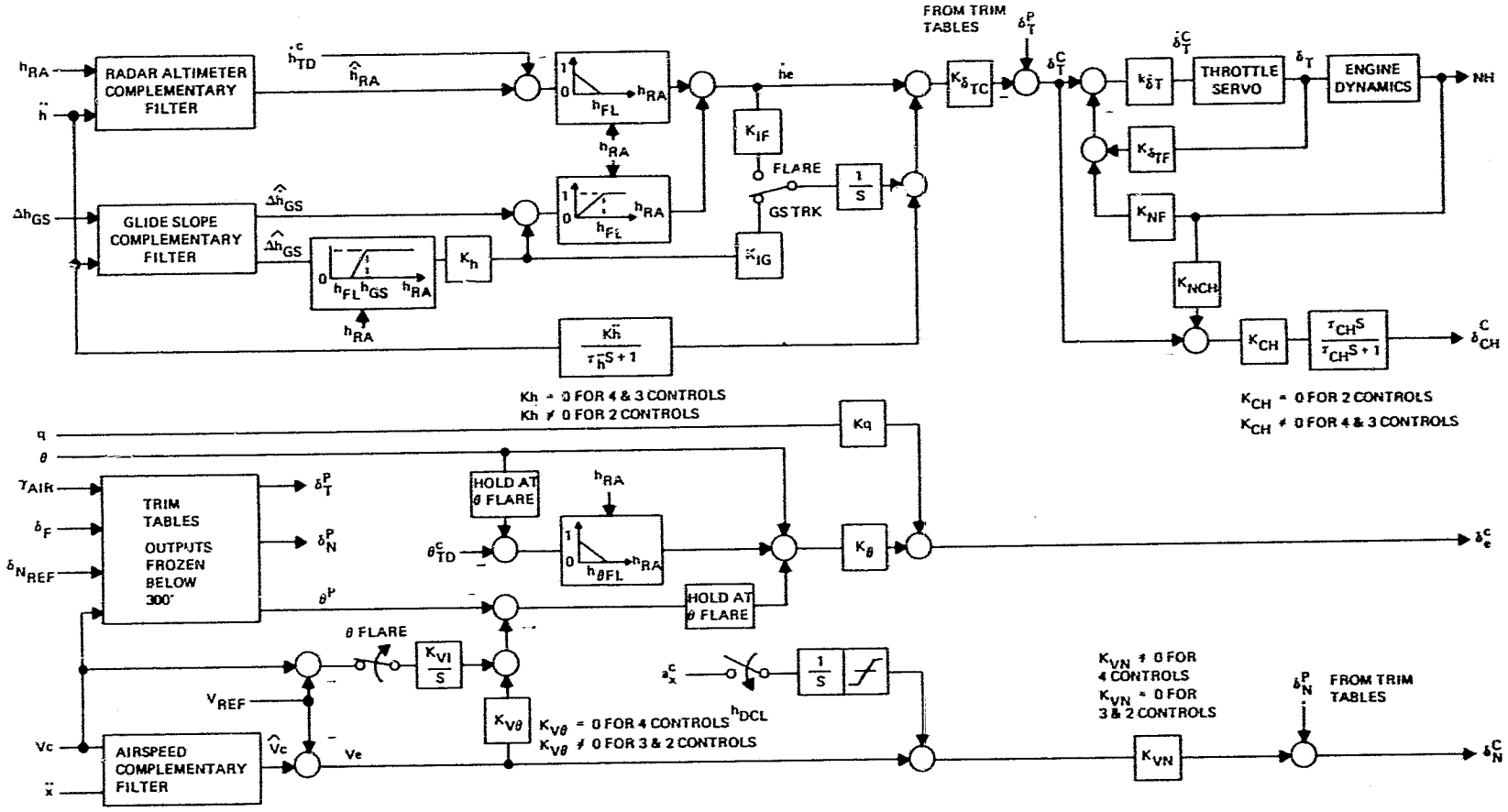

FIGURE 4-1. GLIDE SLOPE TRACK AND FLARE BLOCK DIAGRAM

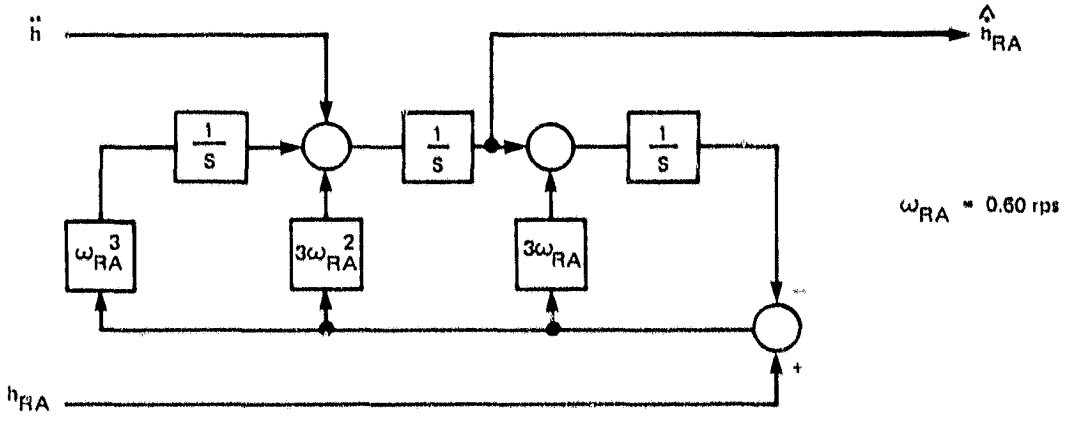

1) RADAR ALTIMETER

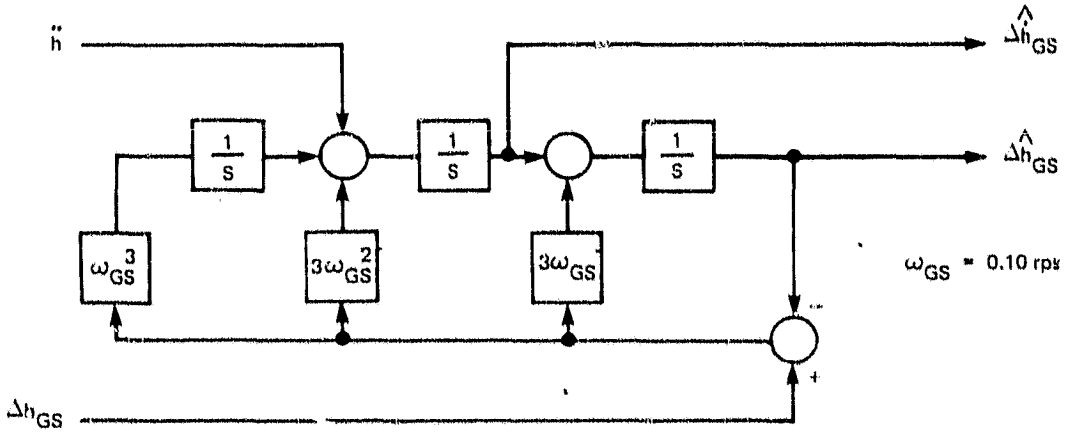

2) GLIDE SLOPE

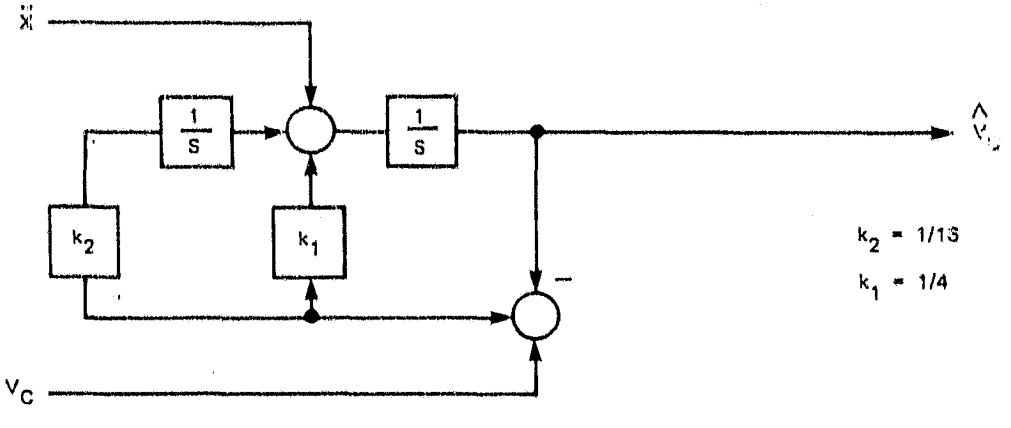

3) AIRSPEED

0301-1A0

FIGURE 4-2. LONGITUDINAL FILTERS

TABLE 4-I LONGITUDINAL GAIN LIST

Gains	Four Control	Three Control*	Two Control*
K_h $\frac{m/sec}{m}$ $(\frac{fps}{ft})$	0.50		
K_{IG} 1/sec	0.0429		
K_{IF} 1/sec	0.50		0.25
$K_{\dot{h}}$ $\frac{m/sec}{m/sec^2}$ $(\frac{fps}{fps^2})$	0		0.667
K_{STC} $\frac{deg}{m/sec}$ $(\frac{deg}{fps})$	3.44 (1.05)		2.29 (0.70)
K_{ST} $\frac{deg/sec}{deg}$	4.0		
K_{STF} $\frac{deg}{deg}$	0.45		
K_{NF} $\frac{deg}{\dot{v}}$	0.765		
K_{NCH} $\frac{deg}{\dot{v}}$	1.39		
K_{CH} $\frac{\dot{v}}{deg}$	10.5		0
K_θ $\frac{deg}{deg}$	5.0		
K_q $\frac{deg}{deg/sec}$	2.1		
$K_{v\theta}$ $\frac{deg}{kt}$	0	0.42	0.42
K_{vI} $\frac{deg/sec}{kt}$	0.051		
K_{vN} $\frac{deg}{kt}$	5.6	0	0
Time Constants			
$\tau_{\dot{h}}$ sec	0.25		
τ_{CH} sec	10.0		
Constants			
h_{GS} m (ft)	30.5 (100)		
h_{OFL} m (ft)	19.8 (65)		
h_{FL} m (ft)	15.2 (50)		
$\dot{h}^c_{TD}$ $\frac{m}{sec}$ (fps)	0.96(3.15)		
θ^c_{TD} deg	9.0		
a^c_X $\frac{kt}{sec}$	-1.66		

*Only gains that differ from the Four Control values are given.

The glide slope error is faded out prior to flare initiation. Through the flare, derived sink-rate is transitioned linearly with decreasing altitude from glide slope to radar altimeter based information, minimizing the impact of terrain irregularities. A straight line $h/\dot{h}$ profile from the existing pre-flare sink-rate to the desired touchdown value is commanded in the flare as shown in Figure 4-3. This results in an exponential flare, the time constant of which is proportional to the slope of the $h/\dot{h}$ line. The flare height is constant at 15.2 m (50 ft) and the commanded touchdown sink-rate is 0.96 m/sec (3.15 fps). The pre-flare sink-rate varies with the wind conditions, resulting in a flare time constant that is shorter with tailwind than with headwind. This variation in flare time tends to compensate for wind induced touchdown position dispersion.

Vertical path errors generate a throttle position or normal acceleration command which drives engine RPM and DLC chokes in a complementary combination. Engine RPM and throttle position are used as feedbacks for the throttle loop to quicken engine response and minimize the effects of hysteresis in the throttle cables. A lag of about one second is associated with the unaugmented engine RPM response to a throttle position change. The closed loop response of the throttle servo and engine to throttle position command can be approximated by second order dynamics. In flight, with a proper choice of gains, a natural frequency of up to 2.5 radians per second (critically damped) could be obtained; attempts to further increase the bandwidth resulted in ringing primarily due to the low rate capability of the throttle servo which was designed for CTOL applications. In the simulation, a natural frequency of 2.0 rps and a damping ratio of 0.7 was used. The chokes are driven with the error between throttle position command and engine RPM complementing the response of the engine and providing fast normal acceleration while engine response is building up. This is a structure comparable to a complementary filter and it results in nearly a step in normal acceleration in response to a step in throttle command.

The ratio of commanded normal acceleration to sink-rate error is 1.4 $\frac{m/sec^2}{m/sec}\left(\frac{fps^2}{fps}\right)$ with the nominal gains.

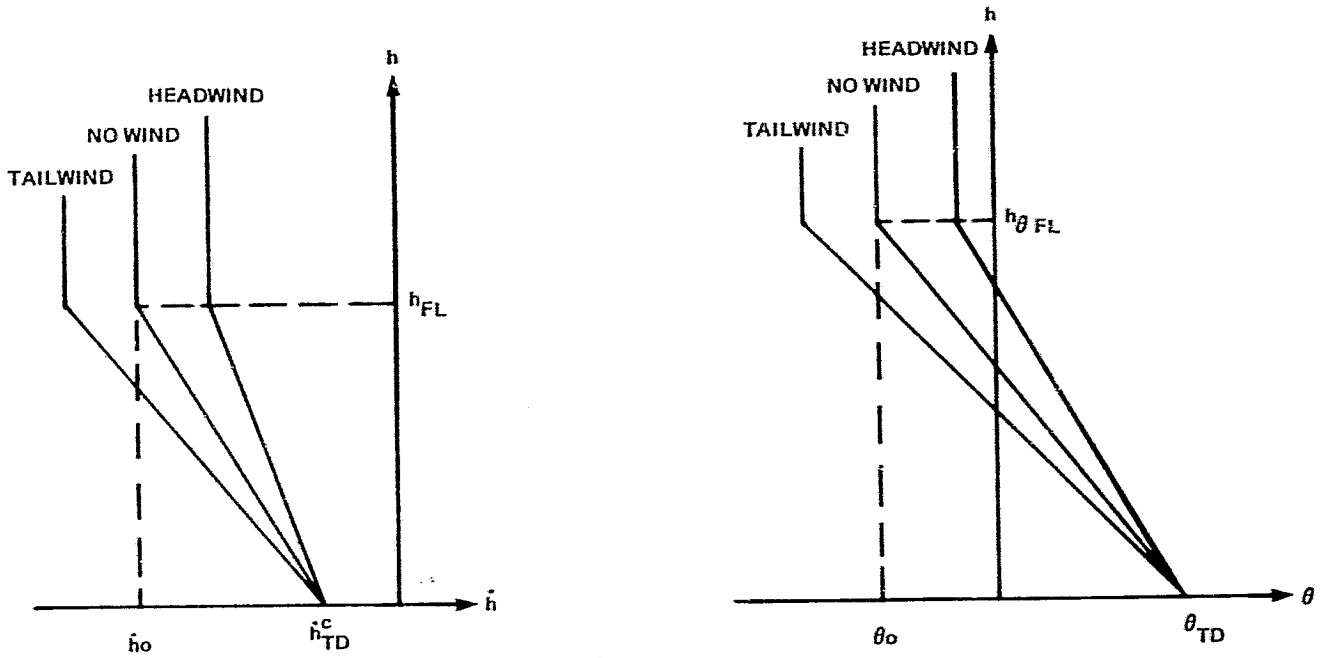

0302-1A1

FIGURE 4-3. FLARE SINK RATE AND ATTITUDE TRAJECTORIES

Pitch attitude and rate feedback to the elevator are used in stabilizing attitude. On the glide slope, the pitch attitude command provides long term speed control by summing integrated raw airspeed error with the trim table output. Through the flare, attitude is ramped with decreasing altitude from its pre-flare value to the desired touchdown value as shown in Figure 4-3. This helps arrest the sink-rate, bleed off airspeed, and puts the airplane in a proper attitude for touchdown. This form of control law is similar to the technique used by pilots for manual landings of the Augmenter Wing Airplane and manual landing of CTOL aircraft. Pitch rotation starts at a main gear height of 19.8 m (65 ft). The proper phasing between the rotation and sink-rate trajectories provide a smooth entry into the flare by reducing the initial sink-rate error. A constant 6^{0} touchdown attitude was obtained. The pre-flare attitude varies with the wind conditions, as shown in Figure 4-3. This results in a somewhat adaptive pitch flare as more rotation is obtained for the wind conditions that are associated with a higher initial sink-rate.

Raw airspeed is blended with longitudinal acceleration in a complementary filter to produce an estimate of airspeed error which drives the diverter nozzles. The details of the filter are given in Figure 4-2. A deceleration command is applied during the flare in order to touchdown at approximately 60 knots.

The control laws described above utilize all four controllers available in pitch; configurations using three and two controllers were also defined and evaluated in flight. This was done in order to establish the trade-off between landing accuracy obtainable by using all controllers and system simplicity gained by minimizing the number of active controllers. Table 4-II summarizes the allocation of controllers in the different control law configurations.

TABLE 4-II CONTROLLER ALLOCATION

Number of Controllers	4	3	2
Flight Path Angle	Throttle & choke	Throttle & choke	Throttle
Airspeed, Long Term	Pitch	Pitch	Pitch
Short Term	Nozzle	Pitch	Pitch

The nozzle is used for longitudinal trim control on all configurations. All three control law configurations are shown in Figure 4-1. For the four-control configuration, $K_{\dot{h}}$ and $K_{V\theta}$ are zero and K_{ch} and K_{vn} are non-zero. For the three-control configuration, $K_{\dot{h}}$ and K_{vn} are zero and K_{ch} and $K_{V\theta}$ are non-zero. For the two-control configuration, K_{ch} and K_{vn} are zero and $K_{\dot{h}}$ and $K_{V\theta}$ are non-zero as indicated in Table 4-I.

4.2 Lateral/Directional

Figure 4-4 is a block diagram of the localizer track and runway alignment control laws and the gains that are used with this diagram are defined in Table 4-III.

Roll control on the Augmenter Wing airplane is achieved by mechanically linking the hydraulic actuators for the Aileron, roll spoiler and outboard chokes to the control wheel. The lateral control law output commands a wheel position for roll control. Raw localizer lateral displacement computed from azimuth angle deviation and range, is blended with cross track acceleration in a complementary filter. Yaw acceleration is also added as an input to the filter during runway alignment in order to convert lateral acceleration at the center of gravity to the value at the localizer antenna, located at the airplane's nose as shown in Figure 4-5. The estimated localizer deviation and its rate are used to command bank angle. The yaw rate, lateral acceleration and bank angle signals are fed through gains, summed and gain scheduled with dynamic pressure to drive the rudder for yaw stability augmentation and turn coordination. The yaw stability augmentation had been previously defined and used in this program during localizer track without any modifications. Its details are given in Figure 4-5.

A forward slip maneuver is used for runway alignment. Beginning at an altitude of 45.7 m (150 feet), an align command is switched into the yaw axis. This reference heading command is reduced from the heading error existing at alignment initiation to zero at 15.2 m (50 feet), yielding an alignment rate which is a function of both initial heading error and aircraft sink-rate. The error from the commanded heading trajectory is integrated to maintain the steady rudder required during alignment. In the roll axis, the beam computations are maintained to guide the vehicle along the desired horizontal path, with increased cross track rate gain for better control. A bank command proportional to lagged lateral acceleration is added in align to compensate for sideslip induced cross track acceleration. A roll kicker is switched in at align to provide a predictive bank command based on initial heading error. Bank commands in

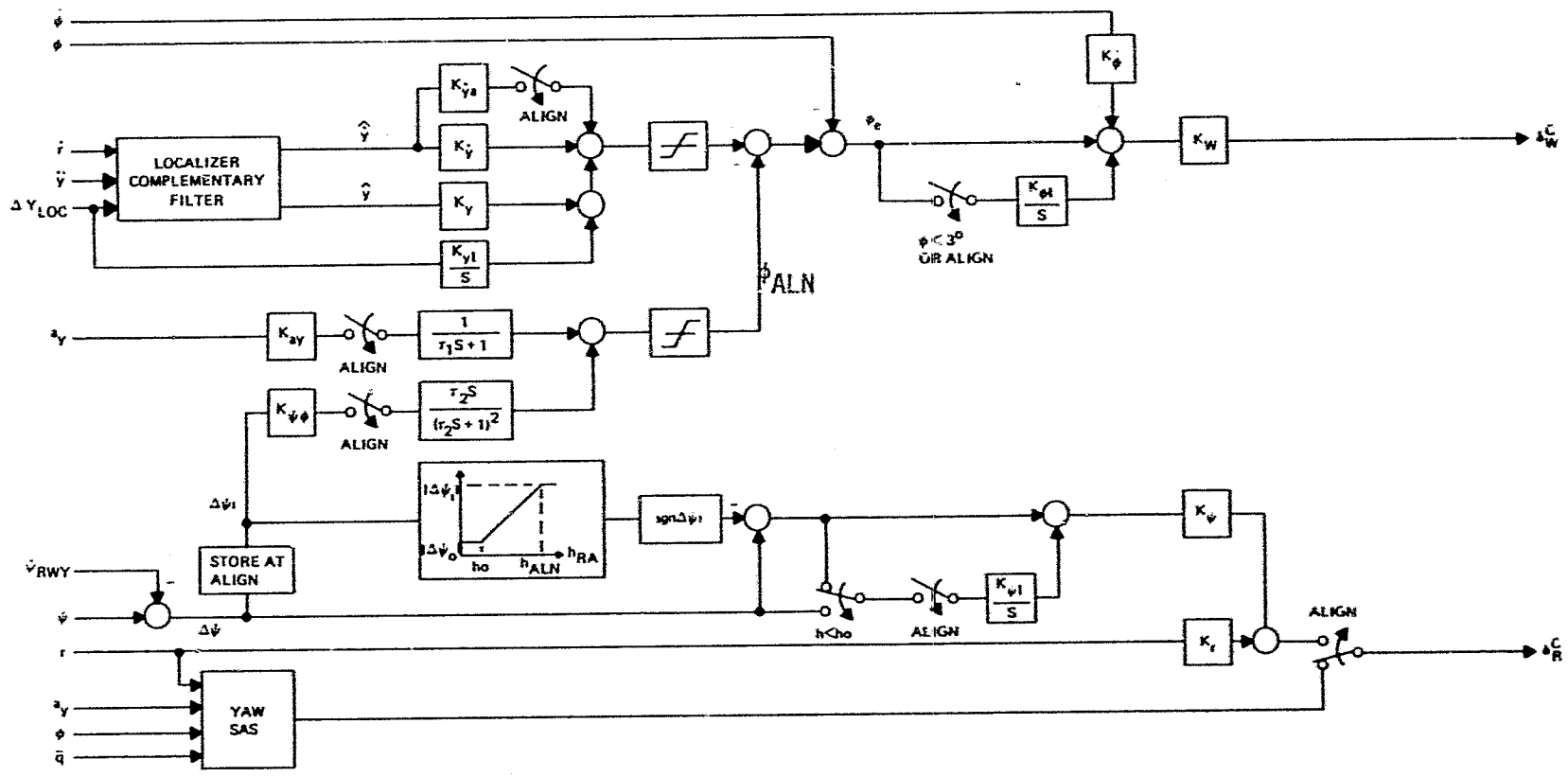

FIGURE 4-4. LOCALIZER TRACK AND RUNWAY ALIGNMENT BLOCK DIAGRAM

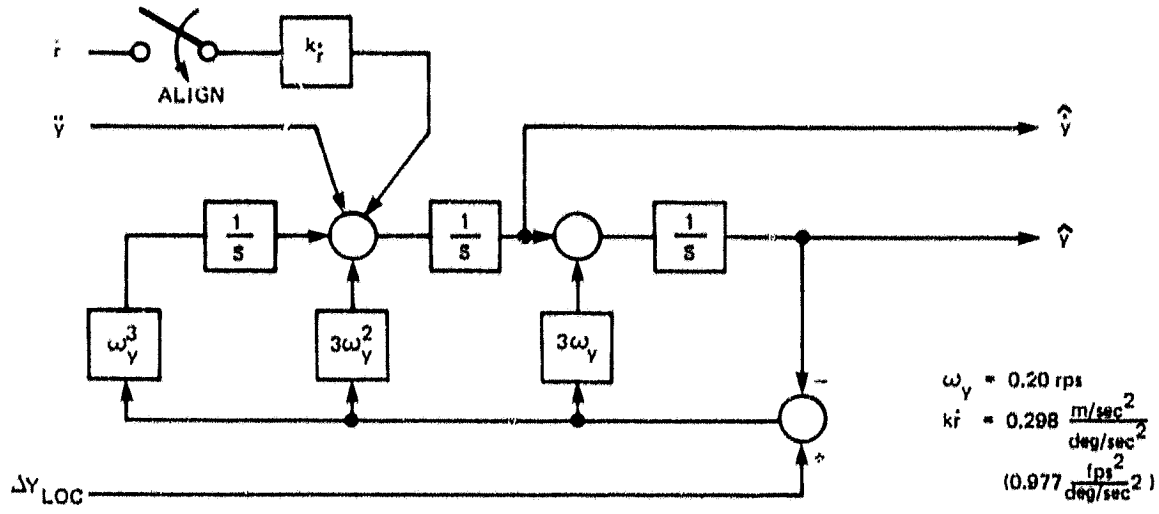

1) LOCALIZER FILTER

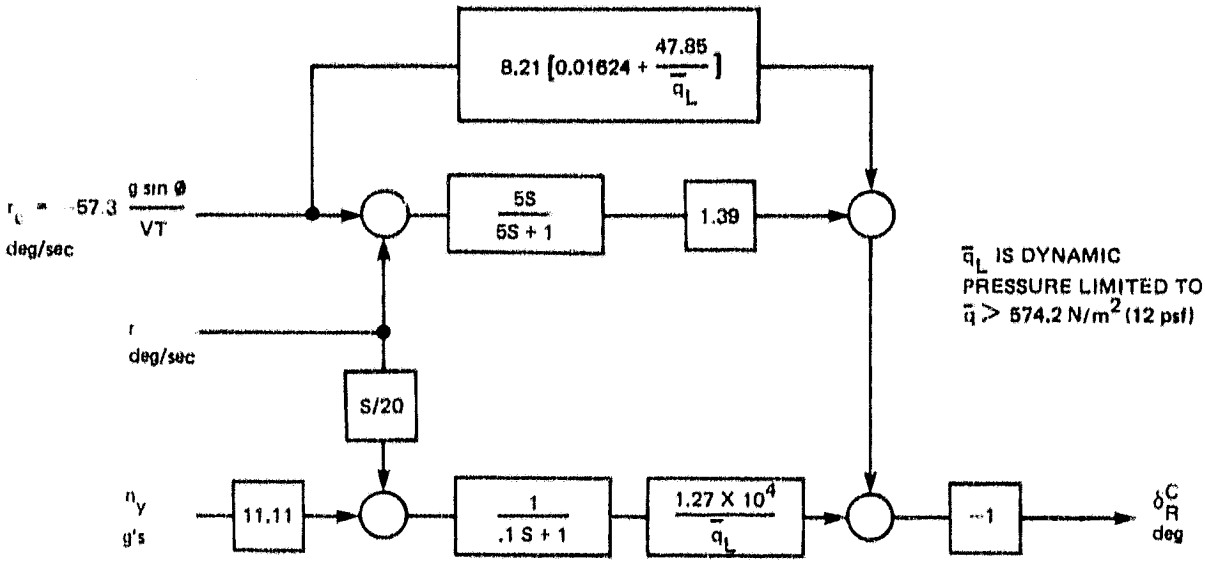

2) YAW SAS

0303-1A1

FIGURE 4-5. LOCALIZER FILTER AND YAW SAS

TABLE 4-III LATERAL/DIRECTIONAL GAIN LIST

Gains		
K_y $\frac{deg}{m}$ $(\frac{deg}{ft})$	0.197	(0.06)
K_{yI} $\frac{deg/sec}{m}$ $(\frac{deg/sec}{ft})$	0.00567	(0.00173)
$K_{\dot{y}}$ $\frac{deg}{m/sec}$ $(\frac{deg}{fps})$	2.05	(0.625)
$K_{\dot{y}a}$ $\frac{deg}{m/sec}$ $(\frac{deg}{fps})$	1.23	(0.375)
K_{ay} $\frac{deg}{m/sec^2}$ $(\frac{deg}{fps^2})$	5.84	(1.78)
$K_{\psi\phi}$ $\frac{deg}{deg}$	0.30	
$K_{\phi I}$ 1/sec	0.10	
$K_{\dot{\phi}}$ $\frac{deg}{deg/sec}$	1.0	
K_w $\frac{deg}{deg}$	7.0	
K_ψ $\frac{deg}{deg}$	3.0	
$K_{\psi I}$ 1/sec	0.20	
K_r $\frac{deg}{deg/sec}$	4.0	
Time Constants		
τ_1 sec	3.0	
τ_2 sec	2.0	
Constants		
h_{ALN} m (ft)	45.7	(150)
h_o m (ft)	15.2	(50)
ψ_o deg	0	

the localizer track path and in the align path are limited to $\pm 10^{o}$ and $\pm 5^{o}$ respectively, which is ample authority to handle steady cross winds in excess of 15 knots.

5.0 Longitudinal Simulation Results

This section describes the deterministic and statistical longitudinal landing results obtained in simulation with the best four, three and two control configurations. Landing performance is evaluated as a function of wind and turbulence level. The effect of using CAA (The British Civil Aviation Authority) rather than FAA vertical turbulence is also evaluated. Weight and temperature variations are also considered, as well as system variations such as gain, authority and sensor biases. The effect of aborting runs which are outside a glide slope track window is studied. Results for different values of sink-rate touchdown command are given.

5.1 Landing Performance Evaluation

The four, three and two control variants of the pitch control laws are described in Section 4.0. Landing results obtained from the simulation are given and discussed here.

Zero wind flare time histories are given in Figure 5-1. The pre-flare pitch attitude is -3^{o} and rotation to about 6^{o} is performed between gear height of 19.8 m (65 ft.) and touchdown for all three configurations. The airplane starts deviating up from the glide slope at about 12.2m (40 ft.) gear height, and at the same time sink-rate starts getting reduced from a pre-flare value of 5.0 m/sec (16.5 ft/sec) to the touchdown value of 0.915 ÷ 1.07 m/sec (3 ÷ 3.5 ft/sec). With no wind, the nozzles move only 4^{o} back in the four control configuration. The other two configurations do not use nozzles actively and therefore they do not move in the flare. An airspeed reduction of 9-10 knots (15-16 fps) occurs with all three configurations in the simulation. Angle of attack increases by about 3^{o} through the flare. Vertical acceleration through the flare peaks at about 0.12 g's for all configurations.

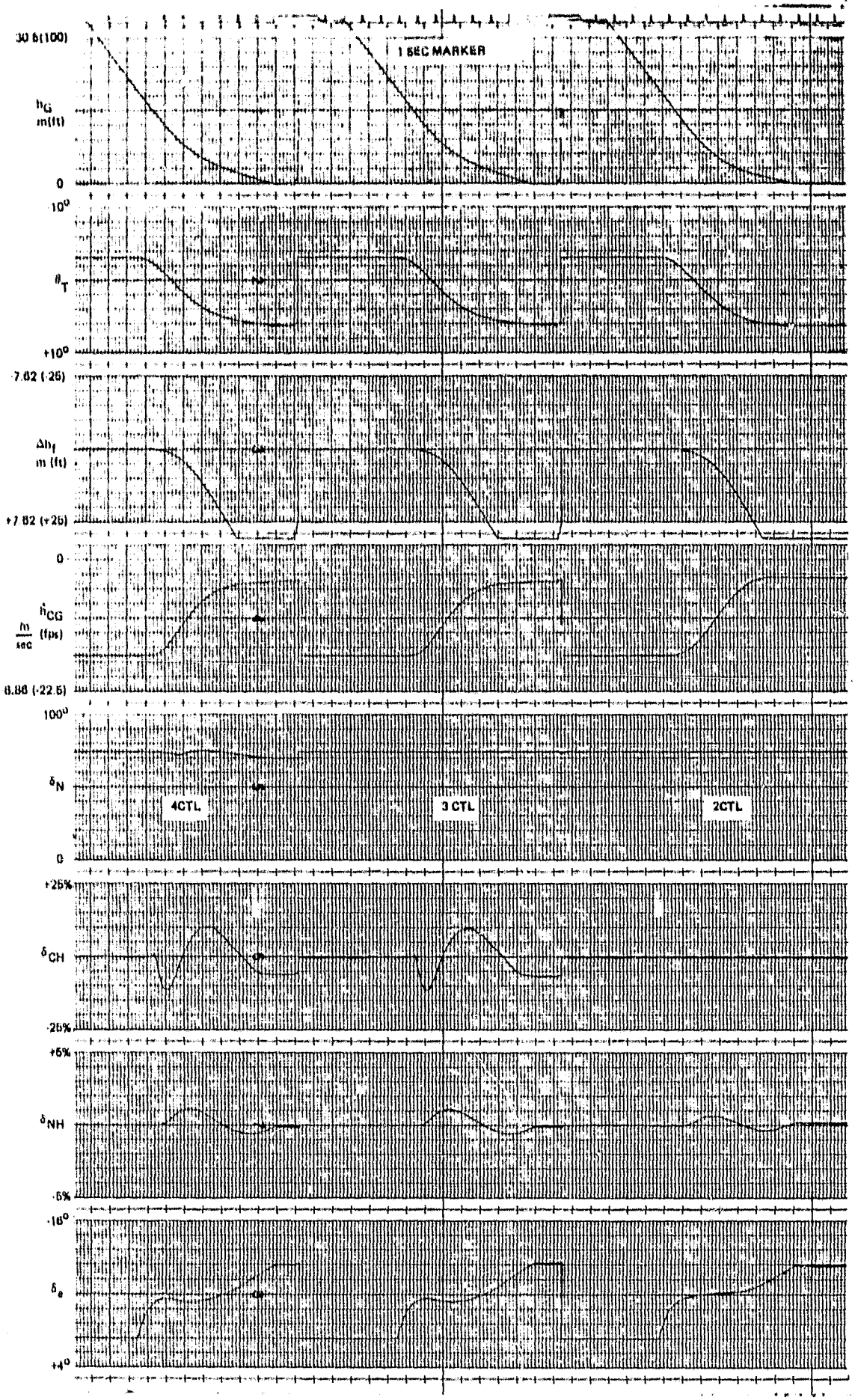

FIGURE 5-1A. FLARE TIME HISTORIES; NO WIND

Aug Wing 3/25/80

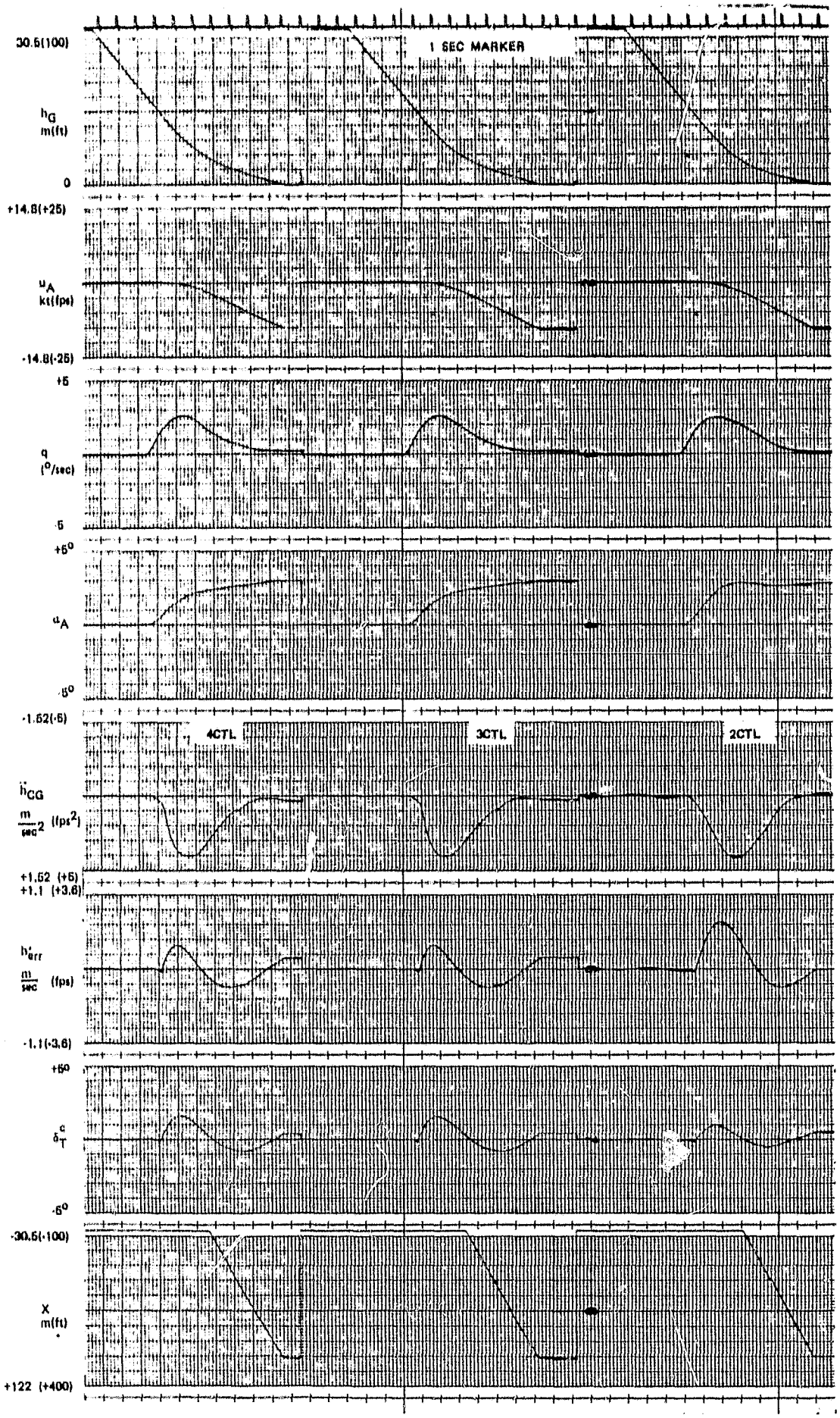

FIGURE 5-18. LANDING TIME HISTORIES; NO WIND

Aug wing 3/25/80

The $\dot{h}_{err}$ signal indicates an initial lag behind the commanded straight-line sink-rate versus altitude profile, followed by an overshoot and finally, at touchdown, the four and three control configurations are slightly behind the profile resulting in slightly higher than commanded touchdown sink-rate. The initial undershoot with the two control configuration is about twice as big as with the four and three controls due to the reduced bandwidth associated with DLC not being used. With the four and three control configurations, the chokes complement engine RPM (δ_{NH}) in controlling sink-rate. Initially, the chokes open to increase lift while RPM is increasing in order to "turn the corner" and start reducing sink-rate; then, the chokes close while RPM is going down to control the overshoot with respect to the commanded $\dot{h}$ profile. With the two-control configuration, pitch rotation and RPM only are used in controlling sink-rate.

Landing time histories of the four-control configuration with five deterministic wind profiles are shown in Figure 5-2. The wind profiles are: 25 knot shearing headwind, 25 knot steady headwind, zero headwind, 10 knot steady tailwind and 10 knot shearing tailwind as defined in Appendix A. Landing time histories of the three and two-control configurations with the same wind profiles are shown in Appendix B, Figures B-5 and B-6 respectively. All three configurations with all five wind conditions touchdown with pitch attitude close to 6^{o} and speed reduction through the flare of approximately 10 knots. The nozzles are used to control the deceleration profile with the four controls, but are stationary through the flare with the other configurations. The chokes are, of course not moving in the two-control configuration.

Table 5-I is a touchdown sink-rate and range summary for the four, three and two controller control configurations with deterministic wind disturbances. Sink-rate and range control are good with all three configurations. The sink-rate dispersion with the two-controls is somewhat bigger than with the other configurations. The shortest landings occur with the steady headwind while the longest are with the shearing tailwind. Range dispersion is 68.6 meters (225 ft) with four controls and 74.4 meters (243 feet) with the three and two controls for these deterministic disturbances.

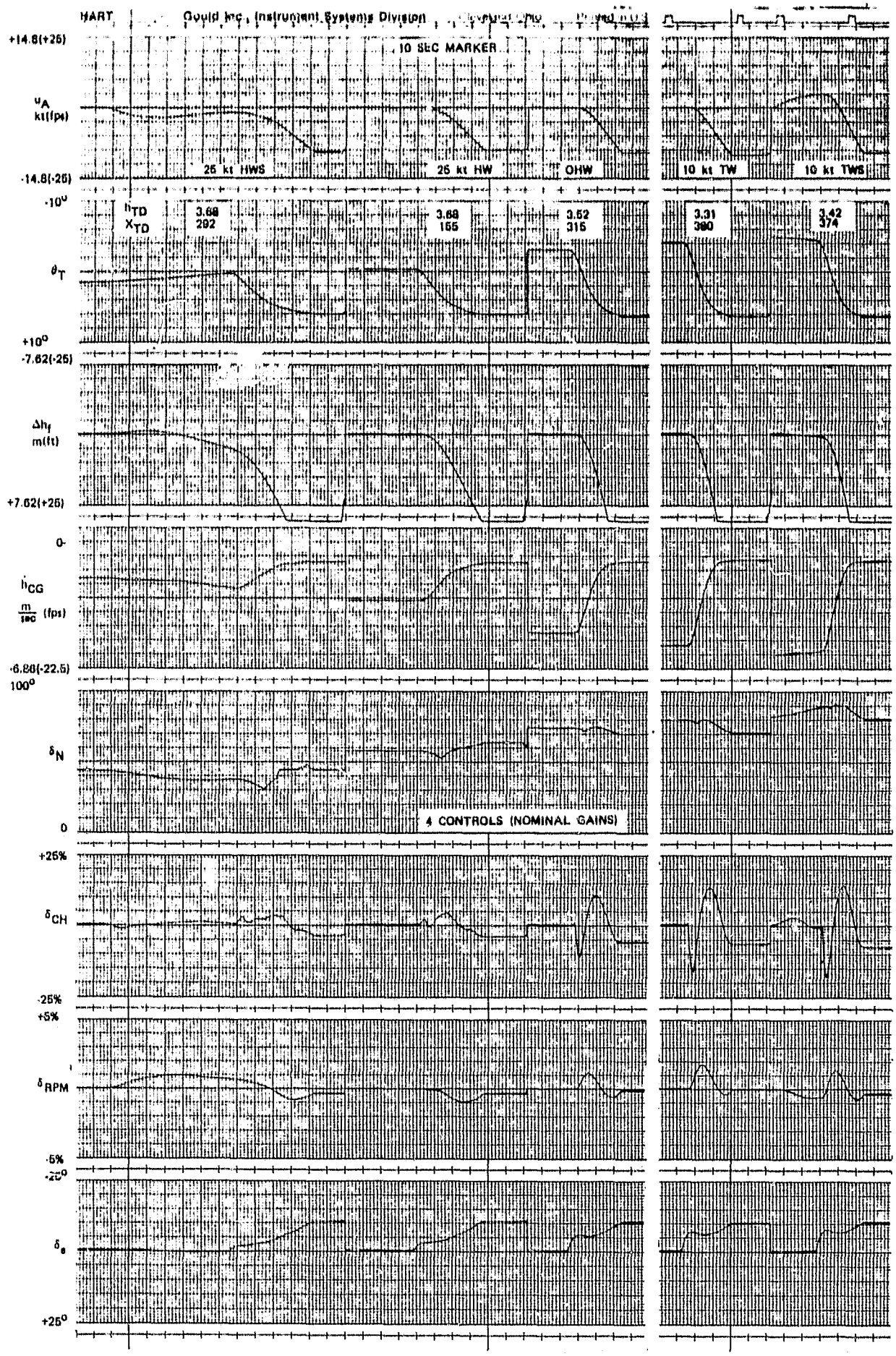

FIGURE 5-2. LANDING TIME HISTORIES: 4 CONTROLS

Aug Wing 21 March 80

TABLE 5-I DETERMINISTIC TOUCHDOWN SUMMARY

		25 knot shearing HW	25 knot steady HW	zero HW	10 knot steady TW	10 knot shearing TW
$-\dot{h}_{TD}$ m/sec (ft/sec)	4CTL	1.12 (3.68)	1.12 (3.68)	1.07 (3.52)	1.01 (3.31)	1.04 (3.42)
	3CTL	1.06 (3.48)	1.09 (3.58)	1.08 (3.55)	1.04 (3.40)	1.05 (3.45)
	2CTL	1.06 (3.49)	1.12 (3.66)	0.896 (2.94)	0.707 (2.32)	0.735 (2.41)
X_{TD} m (ft) beyond GPIP	4CTL	89.0 (292)	47.2 (155)	96.0 (315)	116 (380)	114 (374)
	3CTL	85.3 (280)	46.6 (153)	94.5 (310)	112 (369)	121 (396)
	2CTL	89.3 (293)	50.9 (167)	88.7 (291)	98.1 (322)	125 (410)

NOTE: Wind profiles are defined in Appendix A.

Table 5-II is a summary of statistical landing performance results for random disturbances as obtained from the simulation. The first column in this table defines the performance goals that were used for the automatic landing system of this powered lift STOL airplane. Requirements for CTOL transports are defined by the FAA in AC 20-57A (Reference 4). Two-sigma dispersion boundaries are defined, as well as boundaries for "improbable" events without assigning precise hazard probabilities. The British Civil Aviation Authority specifies hazard probabilities (10^{-7}), but is loose on the definition of the shape of the touchdown dispersion zone. (References 12, 13). No official requirements are available for the powered lift STOL airplane and therefore design goals had to be defined for this study. The mean targeted sink-rate was selected on the basis of flight test experience to produce a comfortable landing. The two sigma land hard is a design objective which would produce acceptable sink-rate control and a 10^{-6} hazard probability is attached to the exceedance of the Augmentor Wing Airplane's gear strength. On range, the goal for the mean was computed assuming the airplane to be on the glide slope at flare initiation and executing the commanded $h/\dot{h}$ flare trajectory with no deviations. Two sigma dispersions of ±61 m (±200 ft) were scaled down from CTOL requirements. The 10^{-6} land short requirement provides for landing within the STOL runway's safety underrun area (Figure 3-2). The 10^{-6} land long requirement depends on the airplane's stopping distance and the runway length. Such considerations were outside the scope of this study and therefore the number shown in Table 5-II is simply a linear extrapolation of the two-sigma dispersion to the 10^{-6} probability level. The 6^{o}goal for the mean pitch attitude was selected to produce adequate rotation to help arrest the airplane's sink-rate, bleed off airspeed and provide adequate nose wheel clearance. The 10^{-6} pitch attitude boundaries are based on airplane geometry.

The actual performance results that are given in Table II were computed assuming a 70% probability of encountering a 25 knot shearing headwind and 30% probability for a 10 knot shearing tailwind. The 70/30 split is based on the results of a survey of 79 major U. S. airports looking at runway orientation with respect to the prevailing winds. This ratio is applicable for airports that have bi-directional landing aids on the major runway. The assumption that each landing is made with either a limiting headwind or a limiting tailwind is conservative since the

probability of encountering 25 knot headwinds or 10 knot tailwinds is significantly lower according to Reference 4. All simulation runs were made with moderate turbulence: σ_u = 3.7 knots and σ_w = 1.5 knots. These turbulence values were not varied with altitude. The atmospheric disturbance models that were used are defined in detail in Appendix A.

The results given in Table 5-II indicate excellent sink-rate control with the four and three control configurations producing touchdown sink-rate values that are much lower than the required 3.6 m/sec (12 fps) at the 10^{-6} probability level. Sink-rate control with the two control configuration is not as good due to the reduced flight path control bandwidth. Touchdown position control is good with the four and three controls. The ± 61 m (±200 ft) 2σ requirement is met by the four control configuration and the three controls exceed it only slightly. The touchdown dispersion at the 10^{-6} level is less than 305 m (1000 ft) for the four and three control configurations. This is compatible with landing on a 518.3 m (1700 ft) long STOL runway (with a 30.5 m - 100 ft - overrun area) as recommended in Reference 11, and as shown in Figure 3-2, leaving a worst case stopping distance of 244 m (800 ft). Range dispersion with the two controls is over 40% wider than with the other configurations.

TABLE 5-II LONGITUDINAL PERFORMANCE SUMMARY

Variable		Goal	Number of Controls		
			Four	Three	Two
$-\dot{h}_{TD}$	μ	0.96 (3.15)	1.16 (3.8)	1.13 (3.7)	1.13 (3.7)
m/sec	2σ hard	1.83 (6.0)	1.68 (5.5)	1.59 (5.2)	1.89 (6.2)
(fps)	10^{-6} hard	3.66 (12.0)	2.32 (7.6)	2.26 (7.4)	3.63 (11.9)
X_{TD}	10^{-6} short	> -97.6 (-320)	-58.0 (-190)	-49.0 (-160)	-98.0 (-320)
m	2σ short	> 26.2 (86)	33.5 (110)	30.5 (100)	9.4 (31)
(ft)	μ	87.2 (286)	94.5 (310)	91.5 (300)	88.4 (290)
beyond the	2σ long	< 148 (486)	155.5 (510)	158.6 (520)	198.4 (651)
GPIP	10^{-6} long	< 237 (776)	238.0 (780)	238.0 (780)	317.0 (1040)
	10^{-6} low	> -1.0	3.0	3.3	3.0
θ_{TD}	2σ low	--	4.7	5.1	5.0
deg	μq	6.0	5.9	5.9	6.0
	2σ high	--	6.8	6.6	6.8
	10^{-6} high	< 15.0	8.0	7.4	7.8
	2σ low	-3.7 (-12)	-2.90 (-9.5)	-3.05 (-10.0)	-5.8 (-19.0)
Δh_{window}	μ	0	0.46 (1.5)	0.30 (1.0)	0
	2σ high	3.7 (12)	3.81 (12.5)	3.66 (12.0)	3.5 (11.5)

NOTES:

1. These results were obtained from the simulation with limiting shearing winds (70% HW, 30% TW), moderate turbulence and MLS beam noise.
2. Δh_{WINDOW} is glide slope tracking error at the 30.5 m (100 ft) approach window.

The touchdown ranges shown constitute a large percentage of the STOL runway and therefore, the better performance of the four and three controls is to be preferred. In this program, sink-rate control was emphasized. Better range control may be obtained by commanding higher sink-rate, or actively controlling range. Pitch attitude is well controlled for all three configurations. A 6^{o} mean with approximately $\pm 1^{o}$ 2σ dispersion is obtained. All configurations are well within the $+15^{o}$, -1^{o} boundaries determined from the airplane's geometry. Glide slope deviations at the 30.5 meter (100 ft) approach window with the four and three control configurations are within the ±3.7 meters (±12 ft) required. Deviations below the glide slope with the two controls exceed the requirement.

To summarize, good landing performance is obtained with the four and three controls and marginally acceptable performance is obtained with the two controls.

The probability distribution plots from which the Table 5-II results were obtained, are given in Appendix B, Figures B-21 through B-32.

A summary of disturbance induced activity while in glide slope track is given in Table 5-III. Control about the vertical axis is about equivalent for all three control strategies. The two control configuration has somewhat better position control, but somewhat increased vertical acceleration activity in comparison with the other two control law configurations. Airspeed control is approximately equal with the three configurations. Pitch attitude activity is lowest with the four controls and highest with the two controls as pitch is used for slow airspeed corrections only with the four controls versus fast and slow speed corrections in the three and two control configurations. Throttle, RPM and elevator activities are approximately equivalent with all configurations. Nozzle activity is higher with four controls because they are actively used for speed control in this configuration whereas the nozzles are driven by the trim tables only with the three and

TABLE 5-III GLIDE SLOPE RMS ACTIVITY WITH TURBULENCE AND BEAM NOISE

	4 Controls	3 Controls	2 Controls
Δh_f m (ft)	1.67 (5.5)	1.55 (5.1)	1.37 (4.5)
$\dot{h}_{CG}$ m/sec (fps)	0.305 (1.0)	0.305 (1.0)	0.335 (1.1)
$\ddot{h}_{CG}$ m/sec^2 (fps^2)	0.305 (1.0)	0.305 (1.0)	0.396 (1.3)
u_A knot (fps)	2.54 (4.3)	2.43 (4.1)	2.25 (3.8)
θ deg	0.3	0.8	2.0
q deg/sec	0.2	0.4	0.3
α deg	0.9	1.2	1.2
δ_T deg	1.3	1.5	1.5
$\dot{\delta}_T$ deg/sec	1.4	1.4	2.0
δ_{NH} %	0.8	0.9	0.75
δ_e deg	0.9	0.9	0.81
$\dot{\delta}_e$ deg/sec	0.8	0.9	1.0
δ_N deg	5.6	1.3	0.7
$\dot{\delta}_N$ deg/sec	2.4	0.6	0.3
δ_{CH} %	6.7	6.0	-
$\dot{\delta}_{CH}$ %/sec	12.5	11.9	-

NOTE: Data given for glide slope track at 152 m (500 ft) gear height with the following disturbances:

σ_u = 3.7 knot $\quad \sigma_w$ = 1.5 knot $\quad \sigma_{BN} = 0.06^o$

τ_u = 4.93 sec $\quad \tau_w$ = 0.247 sec $\quad \tau_{BN}$ = 0.5 sec

Disturbances are generated by passing white noise through first order filters. The τ's are the time constants of these filters.

two control configurations. Choke activity is approximately equal with the four and three controls and the chokes are not used in the two control configuration.

The four, three and two control strategies were developed in order to evaluate the tradeoff between performance and complexity as explained in Section 4.1. The performance results presented here indicate that the three control configuration is preferred as it produces performance that is equivalent to that obtained with the four control system with a lower level of complexity. It is conceivable that the nozzles could have been used more effectively in the flare to actively control range. The increased pitch activity with three controls may be objectionable from passenger comfort point of view.

5.2 The Effects of Wind and Turbulence Levels on Landing Performance

The previous section presented the longitudinal landing performance as obtained from the simulation with limiting shearing winds and moderate turbulence. In this section, simulation data for the effects of varying wind levels on landing performance is given. Deterministic winds and shears are considered. The effect of turbulence level alone and turbulence combined with shearing winds is evaluated. Wind and turbulence models compatible with FAA AC 20-57A were used as defined in Appendix A. The effect of vertical turbulence per the British CAA model was also examined and the results are given in this section.

5.2.1 Deterministic Winds and Shears

Landing time histories of the four control configuration with the standard FAA winds and shears were given in Figure 5-2 and the equivalent time histories for the three and two control configurations are given in Appendix B, Figures B-5 and B-6. The touchdown sink-rate and range results were summarized in Table 5-I. Good sink-rate and position control are obtained in all cases.

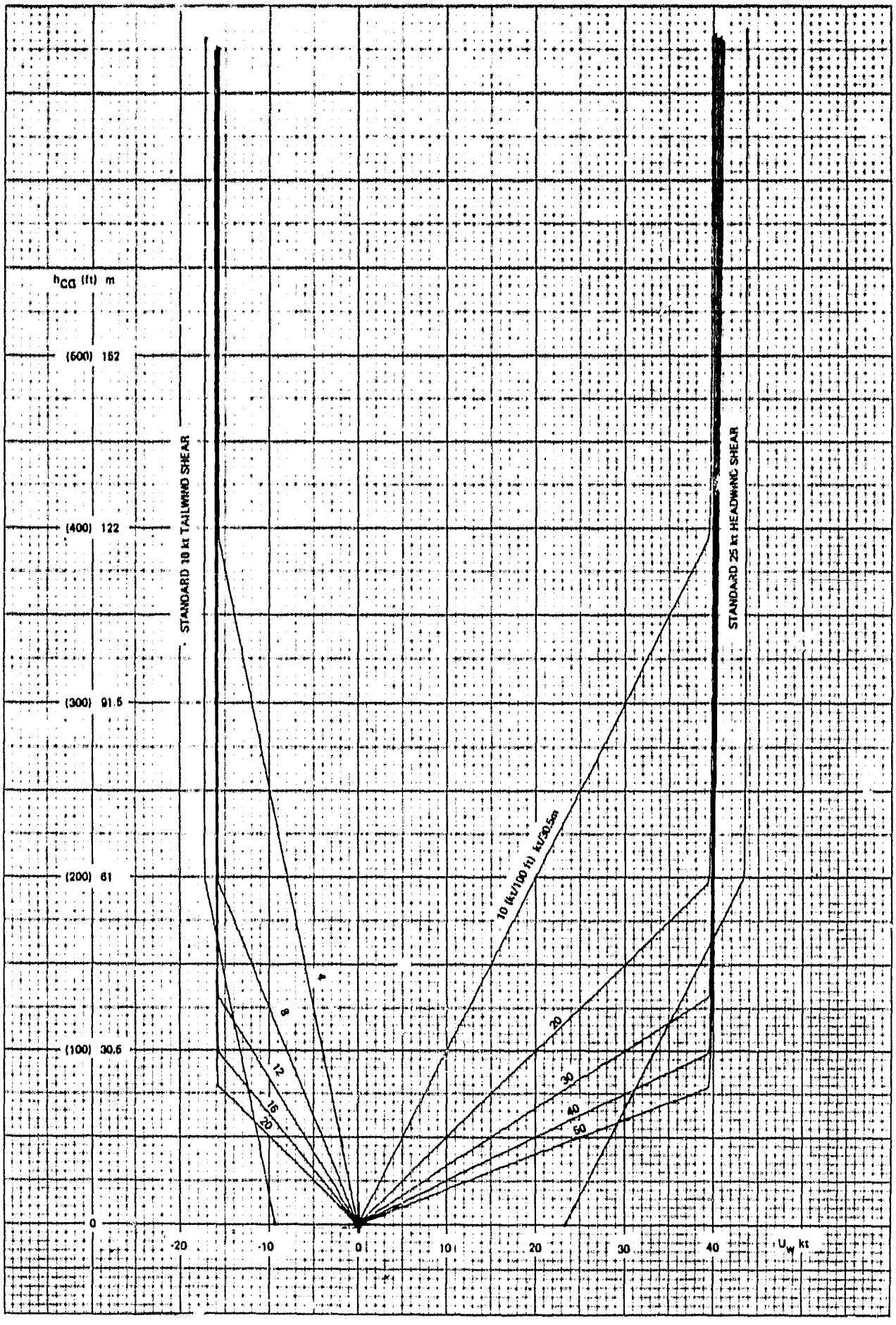

FIGURE 5-3. WIND SHEAR PROFILES

The performance of the system was also evaluated with linear shears of higher magnitudes than the standard FAA models. The shear profiles that were used are shown in Figure 5-3. The standard 25 knot shearing headwind is 25 knots at the 7.62 meter (25 ft) reference height and it shears from 43 knots at 61 meters (200 ft) to 23 knots at zero height such that the shear magnitude is 10 knots per 30.5 meters (100 ft). Above 61 meters (200 ft) the standard profile is a constant wind level. The non standard wind profiles used shear from 40 knots to zero at zero height. The altitude at which the wind starts shearing in these profiles varies to produce the desired shear level as shown in Figure 5-3. Headwind shear levels of 10, 20, 30, 40 and 50 knots per 30.5 meters (100 ft) were evaluated. The tailwind standard and non standard profiles are constructed in the same way as the headwind shears with all wind and shear levels reduced to 40% of the headwind values.

Landing time histories of the three control configuration with these shears are given in Appendix B, Figures B-7 through B-10. Landing performance results are summarized here in Figure 5-4. Touchdown sink-rate is very well controlled with variation bounded between 0.85 and 1.28 m/sec (2.8 and 4.2 fps) for all shear cases. The shape of the sink-rate curve suggests, however, that shears in excess of 50 knots per 30.5 meters (100 ft) would result in hard landings. A touchdown range dispersion of 152 meters (500 ft) was obtained for the full range of shears evaluated. This is a substantial dispersion, but it is not unreasonable considering the shear magnitudes. Δh_{100} and Δh_{50} are deviations from the glide slope at 30.5 meters (100 ft) and 15.2 meters (50 ft) gear height. These deviations depend on the magnitude of the shear and also on the height at which it starts. A maximum deviation of 2.44 meters (8 ft) occurred at 30.5 meters (100 ft) height and 2.74 meters (9 ft) at 15.2 meters (50 ft) height.

It should be noted that an airspeed reduction of up to 24 knots was associated with the high values of headwind shears. This stretches the validity of the simulation close to its limits as it does not include all lift nonlinearities.

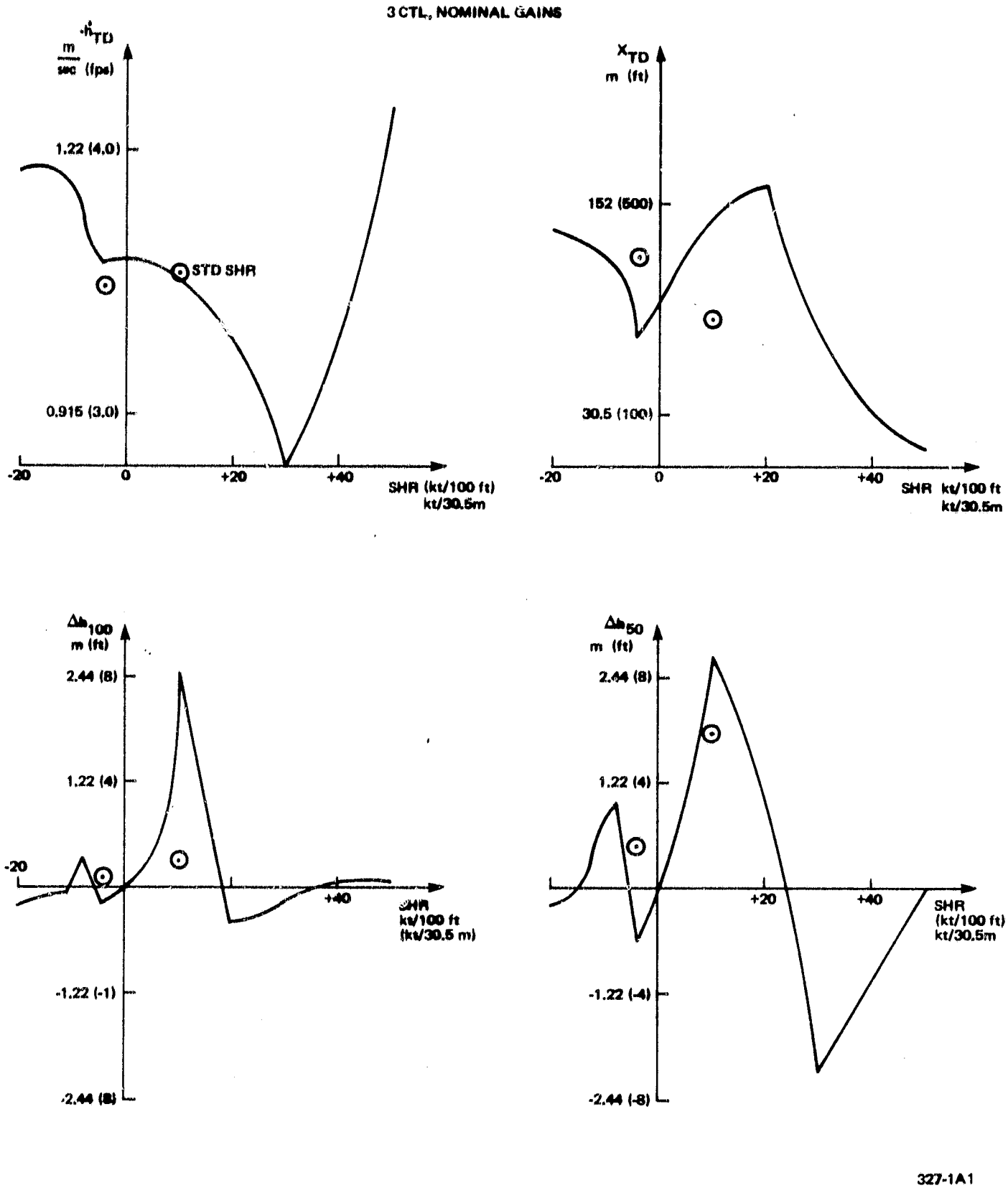

FIGURE 5-4. THE EFFECT OF WIND SHEARS ON DETERMINISTIC LANDING ACCURACY

5.2.2 The Effect of Beam Noise, Wind and Turbulence on Statistical Results

Statistical landing data were obtained in the simulation with varying levels of wind and turbulence. The results for the three control configuration are summarized here.

Mean and two-sigma landing dispersions with no steady headwind, but as a function of turbulence level are given in Figure 5-5. The RMS value for vertical turbulence is 1.5 knots for all non zero values of σ_u and it is zero for σ_u=0. All data were taken with MLS beam noise such that the zero turbulence point shows the effect of beam noise only. Turbulence was simulated according to the FAA model as defined in Appendix A.

Mean touchdown results are essentially independent of turbulence. No sink-rate dispersion is obtained with beam noise only and the two sigma dispersions grow linearly with turbulence level up to 0.30 m/sec (1.25 fps) for the full turbulence that was evaluated. Range dispersions with beam noise only are minimal at about ±3 meters (±10 ft), they grow to 91.5 meter (300 ft) ±2σ with full turbulence. Attitude dispersion with full turbulence is +0.6^{o}, -0.9^{o} at the two sigma level with respect to the 6^{o} mean touchdown value. Glide slope deviations at 30.5 meters (100 ft) height are ±2 ft 2σ due to beam noise only and ±7 ft for beam noise and full turbulence.

Figure 5-6 summarizes mean and two-sigma landing results as a function of the combination of headwinds and turbulence. Turbulence is proportional to headwind in this case, with σ_u of 3.7 knots associated with 25 knots headwind and σ_u of 1.5 knots associated with the 10 knot tailwind. Headwinds and tailwinds include shears that are proprtional to the wind levels as described in Appendix A. All data were obtained with MLS beam noise.

All the mean values are quite insensitive to headwind variations with the exception of range. The mean touchdown range varies from 70 meters (230 ft) with headwind to 122 meters (400 ft) with tailwind. The highest two sigma touchdown sink-rate is 1.45 m/sec (4.75 fps). It is obtained with the

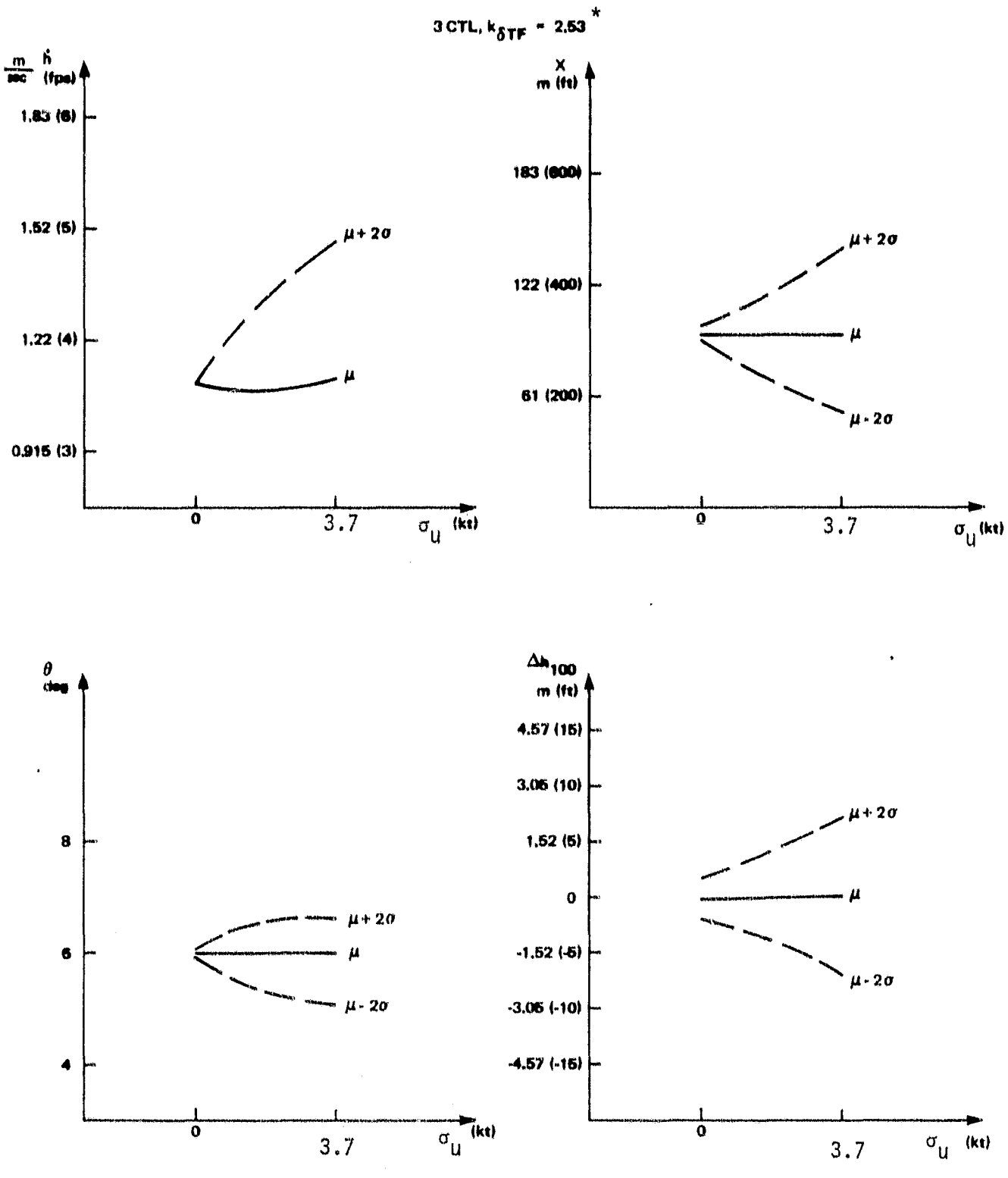

ZERO HEADWIND;
*SEE discussion in Section 5.4.3

FIGURE 5-5. THE EFFECT OF TURBULENCE ON LANDING DISPERIONS

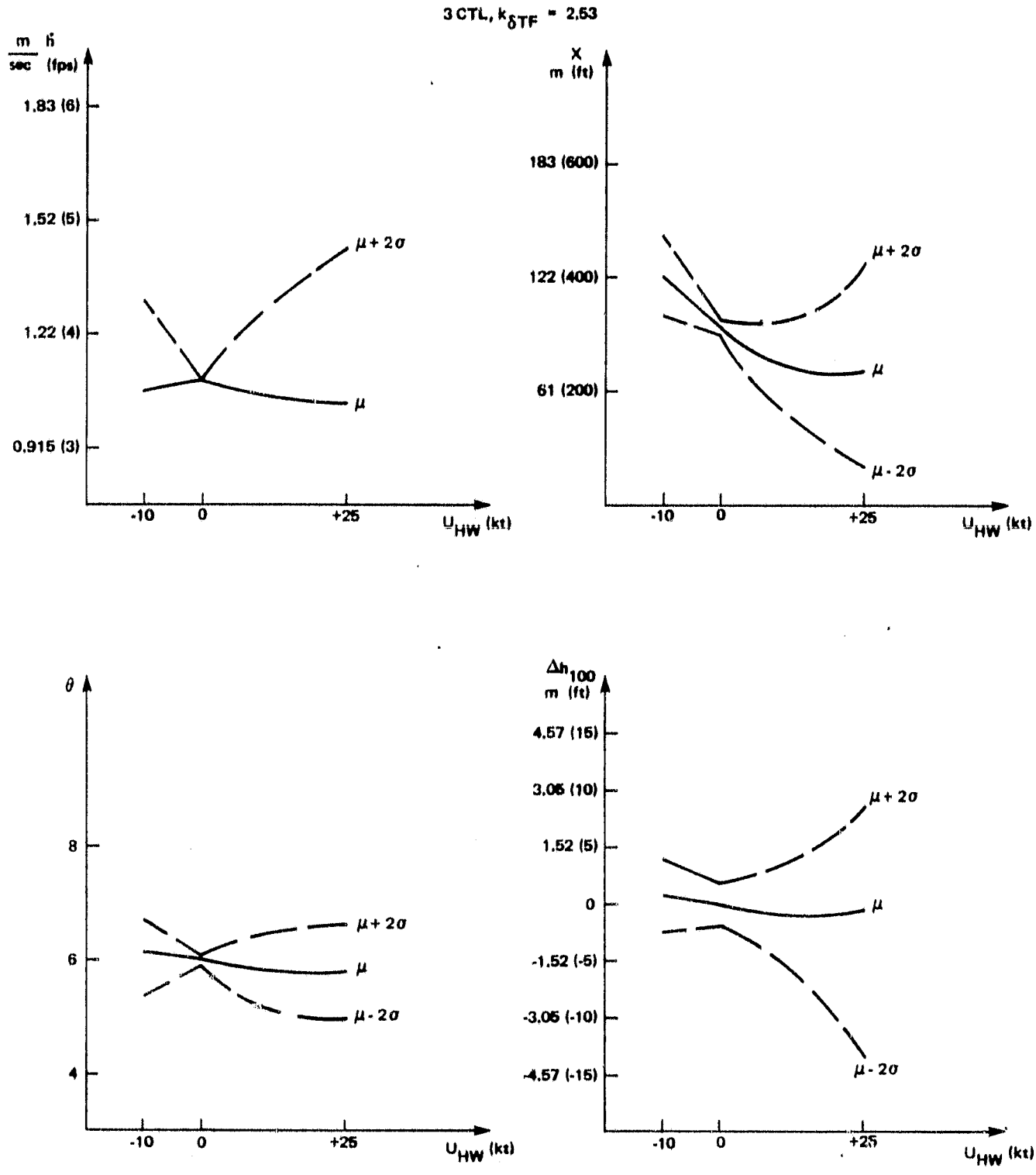

TURBULENCE PROPORTIONAL TO HEADWIND; σ_u = 3.7 kt for U_W = 25 kt

330-1A1

FIGURE 5-6. THE EFFECT OF HEADWIND AND TURBULENCE ON LANDING DISPERSIONS

25 knot headwind due to the turbulence associated with this wind level. The extreme two sigma points on range are 21 meters (70 ft) short and 143 meters (470 ft) long. The extreme two sigma values on touchdown pitch attitude vary from 5^{o} to 6.7^{o}. Glideslope deviation at 30.5 meters (100 ft) height varies from -4.11 meters (-13.5 ft) to +2.59 meters (+8.5 ft) for the combination of headwind turbulence and beam noise.

The results shown here were obtained with a throttle feedback gain, $k_{\delta TF}$, of 2.5 rather than the 0.45 value for the recommended configuration. The higher value of $k_{\delta TF}$ shifts activity from the engine to the chokes but it does not affect landing performance in the two sigma region (as long as the chokes do not reach their stops), as explained in Section 5.4.3. Thus, the results presented here are valid for the configuration with the recommended value of $k_{\delta TF}$.

Results similar to these given here for the three control configuration were obtained for the four control configuration and are given in Appendix B Figures B-1 and B-2. The probability distribution curves on which all these results are based are also given in Appendix B.

5.2.3 CAA Vertical Turbulence

The turbulence model that has been used in all previous performance evaluations is compatible with the definitions of FAA AC 20-57A and is described in Appendix A here. The vertical component of the FAA turbulence model assumes a constant scale length of 9.15 m (30 ft) and a constant RMS level of 1.5 knots. The British Civil Aviation Authority vertical turbulence model uses a scale length that is proportional to altitude, and it varies from 152 m (500 ft) at an altitude of 305 m (1000 ft) to 4.6 m (15 ft) below 9.15 m (30 ft) altitude. The rms level is proportional to total wind speed and σ_w associated with 25 knots of wind is 2.25 knots. This model is also described in Appendix A. It may be a more realistic model and it affects the control system more than the FAA model, mainly at the higher altitude because of its increased power at

lower frequencies. The effect of the CAA vertical turbulence model on performance and activity of the four control configuration was evaluated and the results are given here.

Table 5-IV compares statistical landing performance of the four control configuration with all the limiting atmospheric disturbances of the FAA model in the left column and with the CAA vertical turbulence instead of the FAA vertical turbulence in the right hand column. The performance is essentially the same with both vertical turbulence models. There is a small reduction in range dispersion with the CAA model, possibly because of the fact that its frequency near the ground is higher than the frequency of the FAA model and the airplane's trajectory does not respond to high frequency disturbances. The attitude dispersion is slightly larger with the CAA vertical turbulence probably because of its higher rms level. The probability distribution curves on which these results are based are given in Appendix B.

Table 5-V is a summary of RMS activity on the glide slope for the same four control configuration with vertical turbulence only. The CAA vertical turbulence induces higher glide slope deviation and rate, but either model is a minor contributor in this area (compare with Table 5-III). The CAA model causes more vertical acceleration-a variable on which it is the major contributor. It also induces more activity in all control surfaces.

TABLE 5-IV LANDING PERFORMANCE WITH FAA AND CAA VERTICAL TURBULENCE

			FAA		CAA	
$\dot{h}_{TD}$	μ		1.16	(3.8)	1.16	(3.8)
m/sec (fps)	2σ	hard	1.68	(5.5)	1.65	(5.4)
	10^{-6}	hard	2.32	(7.6)	2.35	(7.7)
	10^{-6}	short	-58.0	(-190)	-39.6	(-130)
X_{TD}	2σ	short	33.5	(110)	39.6	(130)
m (ft)	μ		94.5	(310)	94.5	(310)
	2σ	long	155	(510)	155	(510)
	10^{-6}	long	238	(780)	232	(760)
	10^{-6}	low	3.0		2.5	
	2σ	low	4.7		4.6	
θ_{TD}	μ		5.9		5.8	
deg	2σ	high	6.8		6.8	
	10^{-6}	high	8.0		8.1	
Δh_{100}	2σ	low	-2.90	(-9.5)	-2.90	(-9.5)
m (ft)	μ		0.46	(1.5)	0.46	(1.5)
	2σ	high	3.81	(12.5)	3.35	(11.0)
Δh_{50}	2σ	low	-2.74	(-9.0)	-2.29	(-7.5)
m (ft)	μ		1.37	(4.5)	1.37	(4.5)
	2σ	high	5.79	(19.0)	5.64	(18.5)

NOTES:

1. These results were obtained from the simulation with limiting shearing winds, moderate turbulence and MLS beam noise for the four control configuration.

2. Δh_{100} and Δh_{50} are glide slope tracking errors at 30.5 m (100 ft) and 15.2 m (50 ft) gear height respectively.

TABLE 5-V GLIDE SLOPE RMS ACTIVITY WITH VERTICAL TURBULENCE ONLY

	FAA	CAA		
h m (ft)	-	305 (1000)	152 (500)	30.5 (100)
τ_w sec	0.247	4.11	2.05	0.411
Δh_f m (ft)	0.091 (0.3)	0.19 (0.64)	0.25 (0.82)	0.14 (0.47)
$\dot{h}_{CG}$ m/sec (fps)	0.091 (0.3)	0.15 (0.49)	0.17 (0.55)	0.18 (0.59)
$\ddot{h}_{CG}$ m/sec^2 (fps^2)	0.24 (0.8)	0.17 (0.55)	0.23 (0.74)	0.36 (1.18)
u_A knots	0.10	0.15	0.19	0.15
θ deg	0.10	0.23	0.24	0.19
q deg/sec	0.12	0.15	0.17	0.25
α_A deg	0.70	0.92	1.00	1.18
δ_T deg	0.50	0.80	0.88	0.90
$\dot{\delta}_T$ deg/sec	1.0	0.87	1.06	1.63
δ_{NH} %	0.21	0.48	0,52	0.46
δ_e deg	0.30	0.78	0.81	0.78
$\dot{\delta}_e$ deg/sec	0.80	0.62	0.77	1.22
δ_N deg	0.50	1.12	1.26	0.96
$\dot{\delta}_N$ deg/sec	0.70	0.47	0.64	0.94
δ_{CH} %	3.40	3.92	4.63	6.50
$\dot{\delta}_{CH}$ %/sec	8.0	6.43	8.12	9.50

NOTE: Data given for the four controls in glide slope track with vertical turbulence only.

σ_w = 1.5 knots for the FAA model and 2.25 knots for the CAA model
τ_w is the time constant associated with vertical turbulence.

TABLE 5-IV LANDING PERFORMANCE WITH FAA AND CAA VERTICAL TURBULENCE

			FAA		CAA	
$\dot{h}_{TD}$	μ		1.16	(3.8)	1.16	(3.8)
m/sec (fps)	2σ	hard	1.68	(5.5)	1.65	(5.4)
	10^{-6}	hard	2.32	(7.6)	2.35	(7.7)
	10^{-6}	short	-58.0	(-190)	-39.6	(-130)
X_{TD}	2σ	short	33.5	(110)	39.6	(130)
m (ft)	μ		94.5	(310)	94.5	(310)
	2σ	long	155	(510)	155	(510)
	10^{-6}	long	238	(780)	232	(760)
	10^{-6}	low	3.0		2.5	
	2σ	low	4.7		4.6	
θ_{TD}	μ		5.9		5.8	
deg	2σ	high	6.8		6.8	
	10^{-6}	high	8.0		8.1	
Δh_{100}	2σ	low	-2.90	(-9.5)	-2.90	(-9.5)
m (ft)	μ		0.46	(1.5)	0.46	(1.5)
	2σ	high	3.81	(12.5)	3.35	(11.0)
Δh_{50}	2σ	low	-2.74	(-9.0)	-2.29	(-7.5)
m (ft)	μ		1.37	(4.5)	1.37	(4.5)
	2σ	high	5.79	(19.0)	5.64	(18.5)

NOTES:

1. These results were obtained from the simulation with limiting shearing winds, moderate turbulence and MLS beam noise for the four control configuration.

2. Δh_{100} and Δh_{50} are glide slope tracking errors at 30.5 m (100 ft) and 15.2 m (50 ft) gear height respectively.

TABLE 5-V GLIDE SLOPE RMS ACTIVITY WITH VERTICAL TURBULENCE ONLY

	FAA	CAA		
h m (ft)	-	305 (1000)	152 (500)	30.5 (100)
τ_w sec	0.247	4.11	2.05	0.411
Δh_f m (ft)	0.091 (0.3)	0.19 (0.64)	0.25 (0.82)	0.14 (0.47)
$\dot{h}_{CG}$ m/sec (fps)	0.091 (0.3)	0.15 (0.49)	0.17 (0.55)	0.18 (0.59)
$\ddot{h}_{CG}$ m/sec^2 (fps^2)	0.24 (0.8)	0.17 (0.55)	0.23 (0.74)	0.36 (1.18)
u_A knots	0.10	0.15	0.19	0.15
θ deg	0.10	0.23	0.24	0.19
q deg/sec	0.12	0.15	0.17	0.25
α_A deg	0.70	0.92	1.00	1.18
δ_T deg	0.50	0.80	0.88	0.90
$\dot{\delta}_T$ deg/sec	1.0	0.87	1.06	1.63
δ_{NH} %	0.21	0.48	0.52	0.46
δ_e deg	0.30	0.78	0.81	0.78
$\dot{\delta}_e$ deg/sec	0.80	0.62	0.77	1.22
δ_N deg	0.50	1.12	1.26	0.96
$\dot{\delta}_N$ deg/sec	0.70	0.47	0.64	0.94
δ_{CH} %	3.40	3.92	4.63	6.50
$\dot{\delta}_{CH}$ %/sec	8.0	6.43	8.12	9.50

NOTE: Data given for the four controls in glide slope track with vertical turbulence only.

σ_w = 1.5 knots for the FAA model and 2.25 knots for the CAA model
τ_w is the time constant associated with vertical turbulence.

In summary, the CAA vertical turbulence model induces more control activity than the FAA model and results in a smaller range dispersion along with a slight degradation of attitude dispersion.

5.3 Weight and Temperature Variations

The effects of airplane weight and ambient temperature variations as defined in Table 5-VI were evaluated in the simulation and the results are given here.

TABLE 5-VI WEIGHT AND TEMPERATURE VARIATIONS

	LIGHT	NOMINAL	HEAVY	HOT
W (10^3 lb)	(40)	(43)	(45)	(43)
(10^3 kg)	18.1	19.5	20.4	19.5
t ^oc	15	15	15	38
U_o kt	66	70	72	75
δ_{NO} deg	78	75	73	62

Approach airspeed and nozzle trim are modified to compensate for weight and temperature variations, as shown in the table. The stability derivatives for these four flight conditions are given in Appendix A.

Table 5-VII summarizes touchdown results with deterministic shearing headwinds and tailwinds. Sink-rate control is very good and very insensitive to weight, temperature and wind variations. Range dispersion is somewhat increased with respect to the nominal flight condition. The shortest landing occurs with the light flight

TABLE 5-VII TOUCHDOWN SUMMARY FOR DETERMINISTIC DISTURBANCES

Variable	Wind knots	Light	Nominal	Heavy	Hot
$-\dot{h}$ m/sec (fps)	+25	1.00 (3.29)	0.979 (3.21)	0.994 (3.26)	0.976 (3.20)
	0	1.08 (3.53)	1.06 (3.49)	1.06 (3.49)	1.03 (3.37)
	-10	1.06 (3.49)	1.04 (3.42)	1.04 (3.41)	1.01 (3.32)
$\dot{x}$ m (ft)	+25	66.2 (217)	74.4 (244)	75.6 (248)	76.2 (250)
	0	80.5 (264)	91.8 (301)	91.1 (299)	97.3 (319)
	-10	106 (347)	120 (395)	121 (396)	128 (421)
$\dot{\theta}$ deg	+25	6.1	5.9	6.2	7.0
	0	6.1	5.9	6.3	7.1
	-10	6.2	6.0	6.4	7.2

NOTES:

1. These results are for the three control configuration.
2. The winds used here are the standard shearing headwinds and tailwinds as defined in Appendix A. Headwinds are positive and tailwinds are negative.

condition in headwind and it is 8.2 meters (27 ft) shorter than the nominal flight condition with the same wind. The longest landing occurs with the hot flight condition in tailwind and it is 8 meters (26 ft) longer than with the nominal flight condition. The overall dispersion for the four flight conditions with these deterministic winds is 62.2 meters (204) versus 46 meters (151 ft) for the nominal flight condition. Touchdown pitch attitude is very tightly controlled. The hot flight condition deviates slightly from this pattern, landing about one degree higher. Landing time histories for these flight conditions and winds are given in Appendix B.

Statistical landing results for the three control configuration with moderate turbulence (σ_u= 3.7 knots, σ_w= 1.5 knots) as well as limiting shearing headwinds and tailwinds are given in Figure 5-7 for weight variation and 5-8 for temperature variation. Touchdown sink-rate is insensitive to weight and temperature variations. The maximum sink-rate spread between the mean and two sigma values is 0.52 m/sec (1.7 fps) for the nominal flight condition and it is less than that at the other weights and temperatures. Maximum range dispersion between two sigma short (with headwind) and two sigma long (with tailwind) is 148 meters (485 ft) for the nominal flight condition and 168 meters (550 ft) over the range of weight and temperature evaluated. Thus, weight and temperature variations increase range dispersions only by 13% beyond the dispersion caused by limiting winds and moderate turbulence at the nominal flight condition . The extreme -2σ to +2σ touchdown pitch attitude dispersion increases from 1.7^{0} for the nominal flight condition to 2.4^{0} over the weight and temperature range. This is a significant increase, but it does not cause any problem because attitude control is still very tight. Glide slope deviation is +2.59 meters (+8.5 ft) and -4.11 meters (-13.5 ft) on a $\pm 2\sigma$ basis at 30.5 meters (100 ft) gear height for the nominal flight condition. Over the flight condition range, these glide slope deviations are +2.74 meters (+9 ft) and -5.03 meters (-16.5 ft).

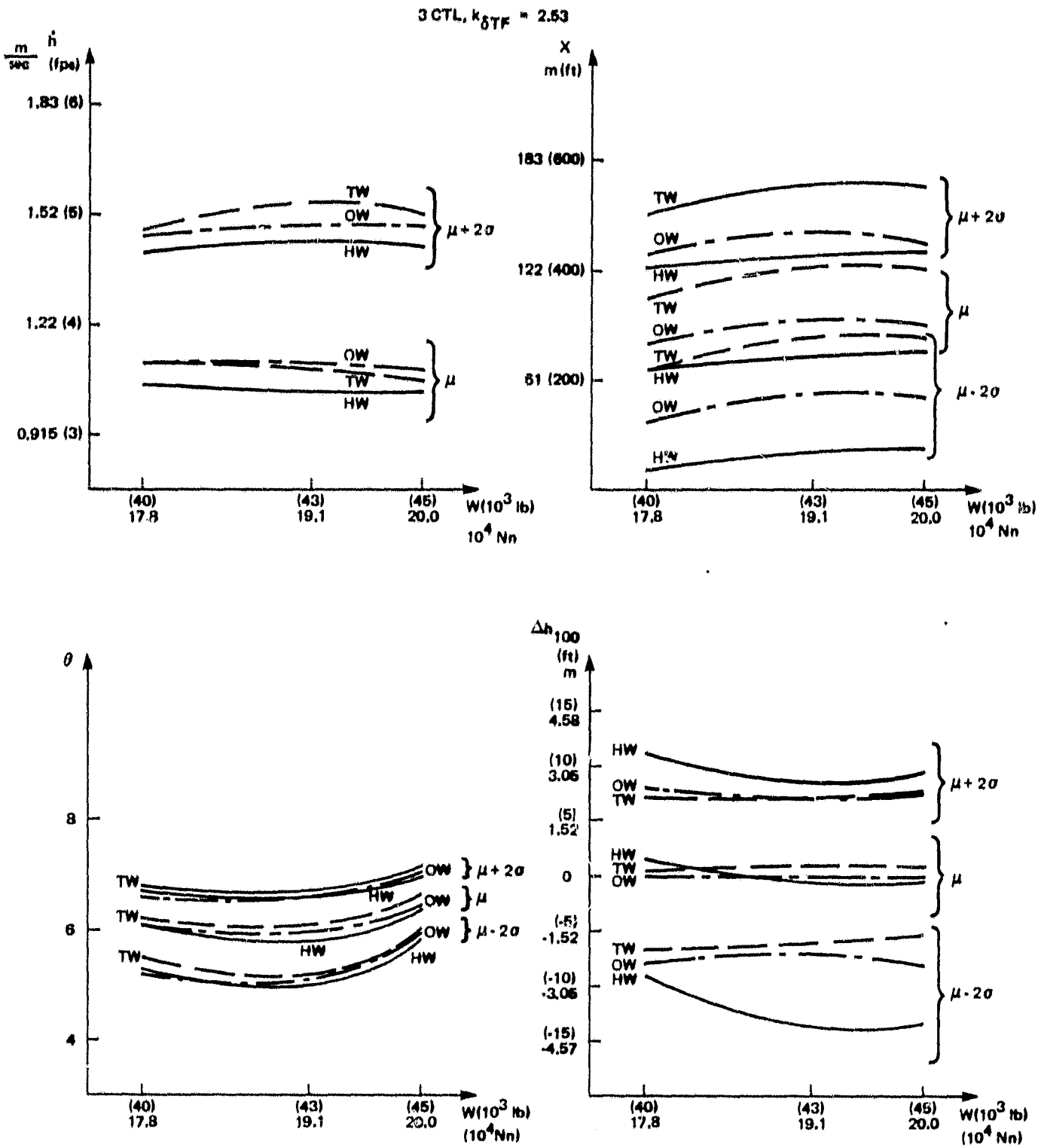

FIGURE 5-7. THE EFFECT OF WEIGHT ON LANDING DISPERSIONS

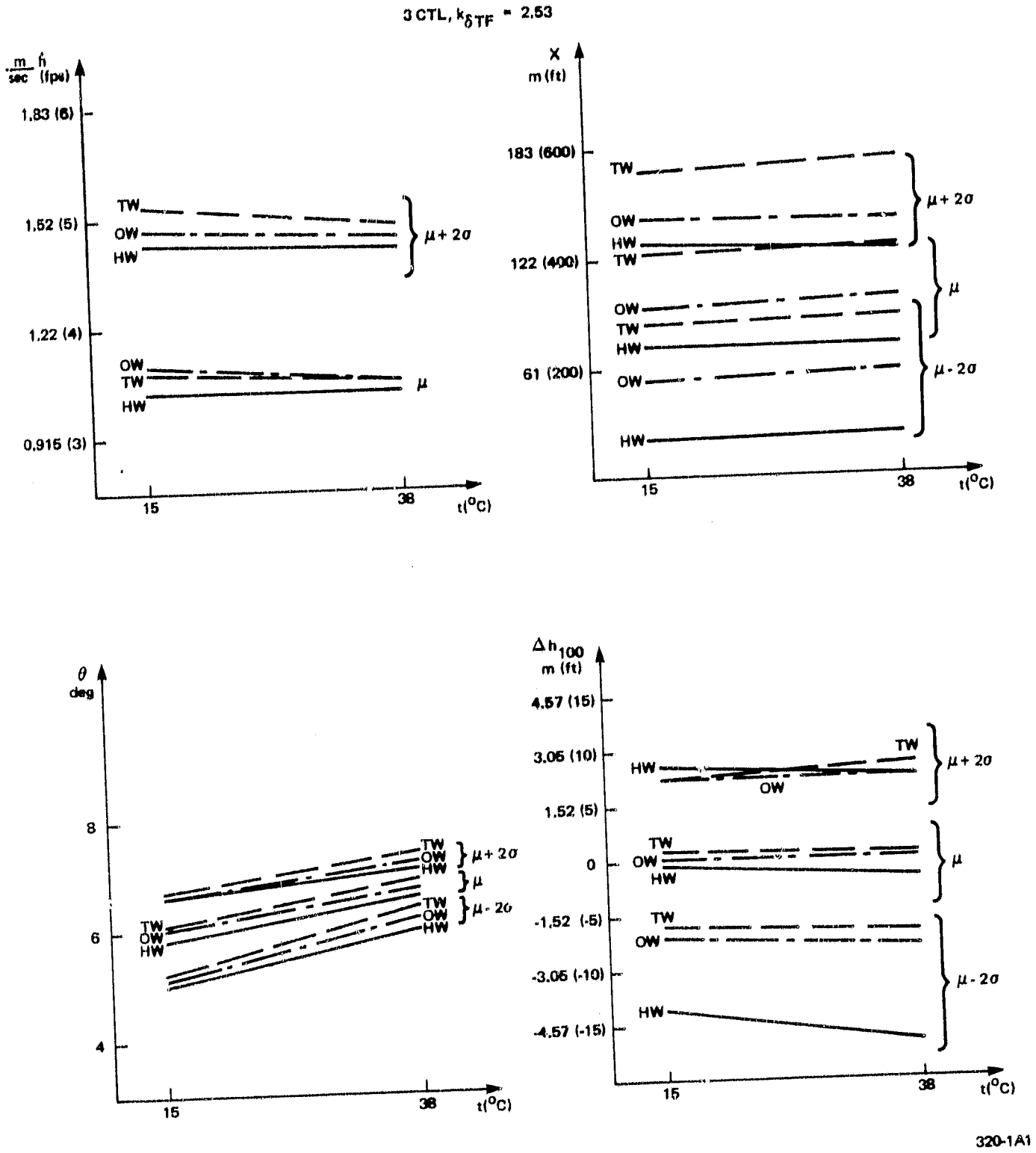

FIGURE 5-8. THE EFFECT OF TEMPERATURE ON LANDING DISPERSIONS

The conclusion from these results is that the effect of weight and temperature variations on landing dispersions is small in comparison to the dispersions caused by wind and turbulence.

The results given here are for the three control configuration. Similar results were obtained with the four control configuration and they are given in Appendix B. Data in this section was taken with the throttle feedback gain of 2.5 versus the recommended value of 0.45. As explained in Section 5.4.3, this shifts activity from RPM to the chokes, but does not affect landing performance results in the two sigma region. The probability distributions on which Figures 5-7 and 8 are based are given in Appendix B.

5.4 System Variations

This section discusses the effects of system variations on landing performance. Sensor errors such as radar altimeter and gyro biases are evaluated. The effect of gain and authority variations is studied. The effect of increased touchdown sink-rate command on range dispersion is evaluated and the effect of rejecting runs that are outside an approach window on glide slope deviation is also shown.

5.4.1 Throttle Command Gain

The throttle (and choke) command gain, $k_{\delta TC}$, sets the overall gain of the system and therefore has a direct impact on glide slope track and landing performance as well as on RPM and choke activity. Figure 5-9 summarizes the effect of reducing $k_{\delta TC}$ from its recommended value of 3.44 $\frac{deg}{m/sec}$ (1.05 $\frac{deg}{fps}$) to 2.3 $\frac{deg}{m/sec}$ (0.70 $\frac{deg}{fps}$) statistical landing performance. The data in the figure is for the three control configuration with limiting headwind and tailwind, moderate turbulence and beam noise. The 33% reduction in $k_{\delta TC}$ results in a 30% increase in touchdown sink-rate dispersion, 13% increase in range dispersion and 17% increase in glide slope deviations. These results indicate that from a performance standpoint, it is desirable to use as high a value for $k_{\delta TC}$ as stability margins and activity levels allow.

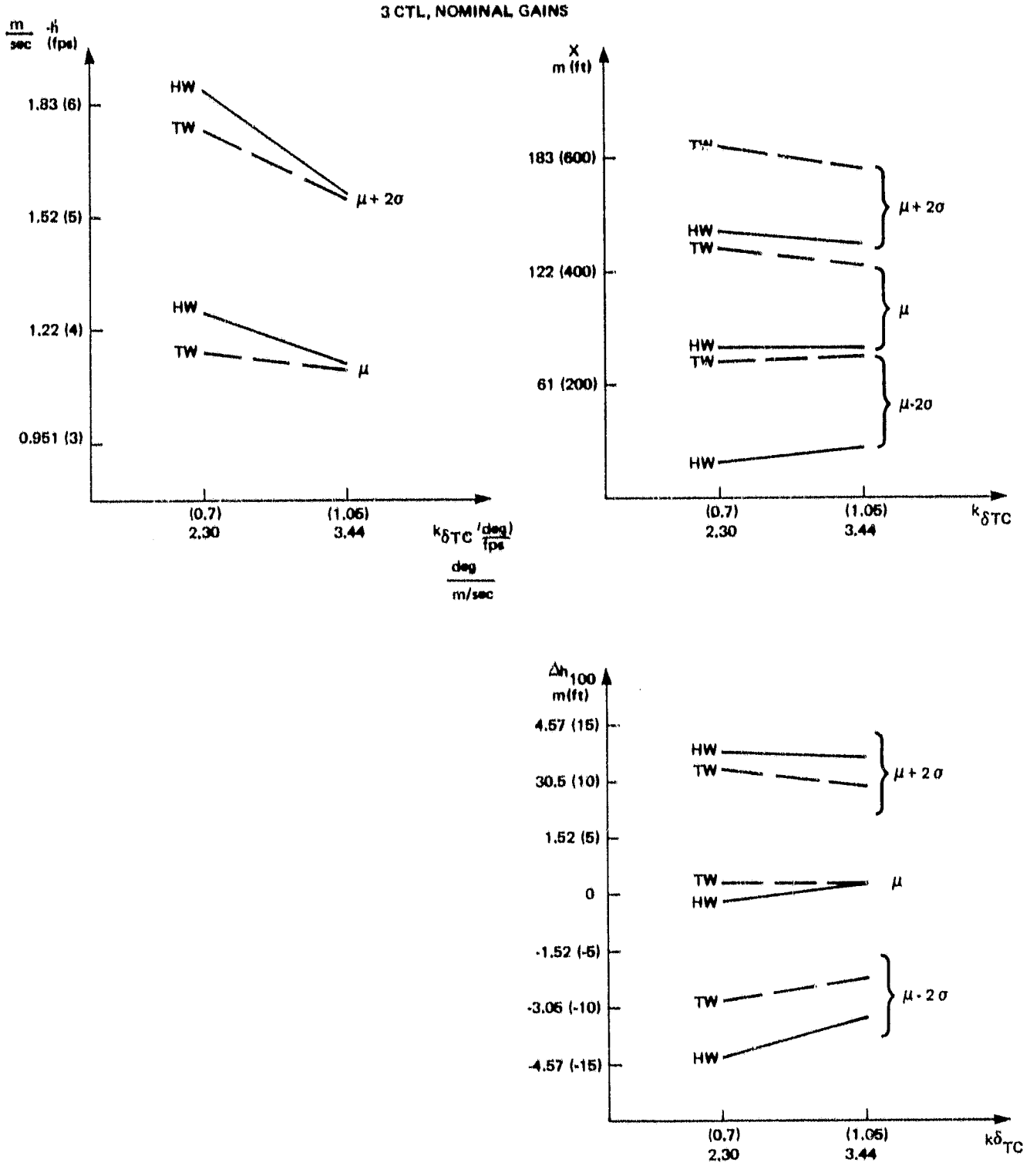

LIMITING HW, TW AND TURBULENCE & BEAM NOISE

324-1A1

FIGURE 5-9. THE EFFECT OF $K_{\delta TC}$ ON LANDING DISPERSIONS

The nominal $k_{\delta TC}$ values were 3.44 $\frac{deg}{m/sec}$ (1.05 $\frac{deg}{fps}$) for the four and three control configurations and 2.3 $\frac{deg}{m/sec}$ (0.70 $\frac{deg}{fps}$) for the two control configuration. The value used with four and three controls corresponds approximately to 1.4 m/sec^2 commanded acceleration per m/sec sink-rate error. Lower gain had to be used with the two controls because DLC is not used and therefore the lift control bandwidth is reduced. Vertical acceleration feedback had to be used with this configuration for improved stability.

Landing time histories of the three control configuration with $k_{\delta TC}$ of 2.3 $\frac{deg}{m/sec}$ (0.70 $\frac{deg}{fps}$) and probability distribution curves with reduced $k_{\delta TC}$ are given in Appendix B.

5.4.2 RPM and Choke Authority

The autothrottle in the Augmenter Wing airplane was designed to give an RPM control authority of +3%, -2% about the nominal trim point while observing maximum engine thrust and temperature limitations and preserving minimum lift margins. This corresponds to a lift control authority of approximately +0.12g and -0.08g. The chokes are modulated ±30% percent of full closure about a nominal 30% position and they provide approximately ±0.10g of direct lift control authority. Statistical data were obtained for the three control configuration with variations of these RPM and choke authority limits. The data were taken with limiting shearing headwinds and tailwinds, moderate turbulence and MLS beam noise. The probability distribution curves are given in Appendix B and the results are summarized in Table 5-VIII. The results indicate that RPM authority can be reduced to ±1% without any significant degradation in performance, as long as the full ±30% choke authority is available. The control structure in which the chokes are driven by the difference between throttle command and engine RPM causes the chokes to be driven harder when RPM limiting occurs and thus compensate for the reduction in authority. Similarly, the choke authority can be reduced to ±20% without any serious degradation in performance, provided that the full RPM authority is available. The area in which performance problems start showing up with reduced DLC authority is sink-rate

TABLE 5-VIII RPM AND CHOKE AUTHORITY SUMMARY

RPM	±3%	±2%	±1%
CHOKES			
±30%	nominal performance	no degradation	slight degradation, mainly glide slope track with headwind
±20%	some sink-rate control degradation with tailwind and slight glide slope track degradation with headwind	*	*
±10%	loss of sink-rate control with tailwind; slightly degraded sink-rate with headwind; degraded range control with tailwind; degraded glide slope track with headwind	*	*

* - not evaluated

NOTE:

1. Summary of statistical results for the three control configuration with limiting shearing headwinds and tailwinds, moderate turbulence and beam noise.

control with tailwind which is the most demanding in terms of bandwidth. When choke authority is further reduced to ±10%, sink rate control with tailwind is lost as the system loses its ability to cope with the limiting wind and moderate turbulence. With headwind, however, even with ±10% choke authority, the impact on performance is still not drastic.

The conclusion of this is that the available RPM authority of +0.1g and -0.07g and the DLC authority of ±0.1g are ample to handle the limiting disturbances that were modeled. With the RPM/chokes complementation scheme that was used, some authority reduction in either controller can be tolerated with a small impact on performance.

5.4.3 RPM and Choke Activity Variation

After some flight data was collected, an error in the implementation of the engine/choke system was discovered. This error has resulted in the throttle feedback gain, $k_{\delta TF}$, being 2.53 deg/deg rather than 0.45 deg/deg. Analysis of the engine/choke response to throttle command has shown that the wrong feedback gain results in an effective reduction in RPM gain and an increase in choke gain such that the resulting normal acceleration was unchanged as long as the chokes were not driven to their limits. This suggested that the flight data taken with this erroneous gain was still valid. This was checked in the simulation to verify the validity of the flight data and the results are given here.

Table 5-IX compares landing performance obtained with the three control configuration with the nominal $k_{\delta TF}$ versus the performance of the same configuration with the increased $k_{\delta TF}$. Performance was evaluated with limiting shearing winds, moderate turbulence and beam noise. The results show that within the two sigma region the two gains produce very similar results. Beyond that region, there is a sharp degradation in sink-rate control with the high throttle feedback gain as indicated by the increased touchdown sink-rate value at the 10^{-6} probability level. This is a result of the chokes being driven to their limits and the attendant reduction in sink-rate control bandwidth. The degradation of range control beyond the

TABLE 5-IX LANDING PERFORMANCE COMPARISON
RPM/CHOKE ACTIVITY VARIATION

RPM/Choke Activity			Nominal/Nominal	Reduced/Increased
$K_{\delta TF}$ deg/deg			0.45	2.53
$-\dot{h}_{TD}$	μ		1.13 (3.7)	1.07 (3.5)
m/sec(fps)	2σ	hard	1.59 (5.2)	1.49 (4.9)
	10^{-6}	hard	2.26 (7.4)	3.51 (11.5)
X_{TD}	10^{-6}	short	-49.0 (-160)	-67.1 (-220)
m (ft)	2σ	short	30.5 (100)	24.4 (80)
beyond the	μ		91.5 (300)	88.4 (290)
GPIP	2σ	long	158 (520)	158 (520)
	10^{-6}	long	238 (780)	268 (880)
	10^{-6}	low	3.3	4.0
θ_{TD}	2σ	low	5.1	5.1
deg	μ		5.9	5.9
	2σ	high	6.6	6.6
	10^{-6}	high	7.4	7.5
Δh_{WINDOW}	2σ	low	-3.05 (-10.0)	-3.66 (-12.0)
m (ft)	μ		0.305 (1.0)	0
	2σ	high	3.66 (12.0)	2.74 (9.0)

NOTES:

1. These results were obtained for the three control configuration from the simulation with limiting shearing winds (70% HW, 30% TW), moderate turbulence and beam noise.

2. Δh_{WINDOW} is glide slope tracking error at the 30.5 m (100 ft) approach window.

TABLE 5-X GLIDE SLOPE RMS ACTIVITY COMPARISON

RPM/Choke Activity	nominal/nominal		reduced/increased	
$K_{\delta TF}$ deg/deg	0.45		2.53	
Δh_f m (ft)	1.55	(5.1)	1.25	(4.1)
$\dot{h}_{CG}$ m/sec (fps)	0.305	(1.0)	0.244	(0.8)
$\ddot{h}_{CG}$ m/sec^2 (fps^2)	0.305	(1.0)	0.274	(0.9)
u_A knots (fps)	2.43	(4.1)	1.19	(3.9)
θ deg	0.8		0.9	
q deg/sec	0.4		0.4	
α_A deg	1.2		1.2	
δ_T deg	1.5		0.4	
$\dot{\delta}_T$ deg/sec	1.4		0.4	
δ_{NH} %	0.9		0.3	
δ_e deg	0.9		0.8	
$\dot{\delta}_e$ deg/sec	0.9		0.8	
δ_N deg	1.3		1.2	
$\dot{\delta}_N$ deg/sec	0.6		0.1	
δ_{CH} %	6.0		11.2	
$\dot{\delta}_{CH}$ %/sec	11.9		9.8	

NOTE:

Simulation data for the three control configuration in glide slope track at 152 m (500 ft) with the following disturbances:

σ_u = 3.7 knot $\quad \sigma_w$ = 1.5 knot $\quad \sigma_{BN} = 0.06^o$

τ_u = 4.93 sec $\quad \tau_w$ = 0.247 sec $\quad \tau_{BN}$ = 0.50 sec

two sigma region is not as pronounced as the degradation in sink-rate control.

Table 5-X is an activity comparison of the three control configuration with the two throttle feedback gain values. Data was taken with moderate turbulence and beam noise. It is evident that activities for the two gain values are essentially equivalent with the major exception being the expected reduction in RPM activity and the increase in choke activity for the higher $k_{\delta TF}$. Glide slope deviation and rate are somewhat better controlled with the higher $k_{\delta TF}$ probably due to the reduced longitudinal coupling of the chokes compared to RPM.

These results verify the assumption that the flight data taken with the high value of $k_{\delta TF}$ is indeed valid.

Landing time histories and probability distributions with the high $k_{\delta TF}$ are given in Appendix B.

5.4.4 Touchdown Sink-Rate Command Variation

In this program, the primary requirement placed on the STOL automatic landing control law development was that precise and soft sink-rate control be achieved. This is consistent with the current practice for CTOL Category III automatic landing systems. This requirement was met, but as a result the worst case landing dispersions constitute a large percentage of the 457m (1500 ft) to 549m (1800 ft) STOL runway length called for in the planning document for STOL ports (Reference 11). The reduction of range dispersion by commanding higher touchdown sink-rates was evaluated in the simulation and the results are given in Table 5-XI and Figure 5-10. Table 5-XI indicates that the mean touchdown sink-rate can be safely increased to 1.83 m/sec (6 fps) as the 10^{-6} land hard value of 3.05 m/sec (10 fps) is still short of the maximum allowed on the basis of gear strength which is 3.66 m/sec (12 fps). The $\pm 2\sigma$ range dispersion decreases from 116

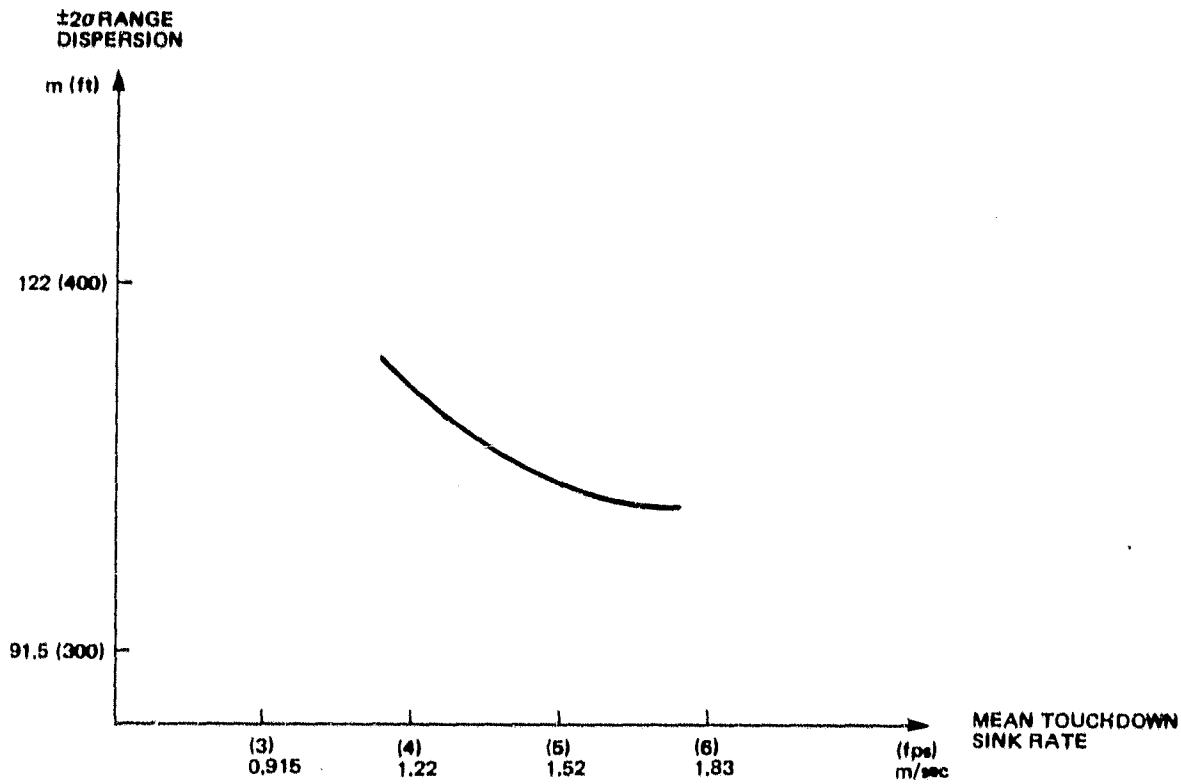

FIGURE 5-10. RANGE DISPERSION VARIATION WITH SINK RATE

TABLE 5-XI THE EFFECT OF TOUCHDOWN SINK RATE COMMAND VARIATION

	$\dot{h}^C_{TD}$ m/sec (fps)		0.96 (3.15)		1.37 (4.50)		1.83 (6.0)	
$-\dot{h}_{TD}$	μ		1.16	(3.8)	1.46	(4.8)	1.77	(5.8)
m/sec (fps)	2σ	hard	1.62	(5.3)	1.98	(6.5)	2.35	(7.7)
	10^{-6}	hard	2.23	(7.3)	2.65	(8.7)	3.05	(10)
	10^{-6}	short	-45.7	(-150)	-51.8	(-170)	-79.3	(-260)
X_{TD}	2σ	short	36.6	(120)	15.2	(50)	-6.1	(-20)
m (ft)	μ		94.5	(310)	67.0	(220)	48.8	(160)
beyond the GPIP	2σ	long	152	(500)	122	(400)	97.6	(320)
	10^{-6}	long	235	(770)	189	(620)	162	(530)

NOTE:

These are simulation results for the four control configuration with limiting shearing winds (70% HW, 30% TW), moderate turbulence and MLS beam noise. Runs exceeding (± 12 ft) at 30.5 m (100 ft) gear height were rejected.

meters (380 ft) with the 1.16 m/sec (3.8 fps) mean touchdown sink-rate to 104 m (340 ft) with the 1.77 m/sec (5.8 fps) sink-rate. This is only a 10% reduction in range dispersion. The reduction in range dispersion is somewhat bigger at the 10^{-6} probability level where it is about 14%. Also, the higher commanded sink-rate shifts the whole range footprint closer to the approach end of the runway resulting in a reduction in the land long range at the 10^{-6} probability level from 235m (770 ft) to 162 m (530 ft) while the 10^{-6} land short range becomes -79.3 m (-260 ft) which is acceptable as it is right at the threshold of the STOL runway used in this program as described in Section 3.3. Thus, some improvement in range control can be obtained from increased touchdown sink-rate. Further improvements can probably be obtained by using the direct longitudinal force control to actively control range. This can be done only if a range signal that is sufficiently accurate can be obtained.

Landing time histories with increased touchdown sink-rate commands and the associated probability distributions are given in Appendix B.

5.4.5 Rejection of Runs Outside the Approach Window

All the statistical landing data that was given up to here (with the exception of the data in Section 5.4.4), included all runs made regardless of glide slope deviation prior to flare initiation. It is common practice, however, in Category III CTOL operations to monitor the approach on the basis of glide slope deviation and execute a go around if the deviation at a predetermined decision height exceeds a given limit. The effect of rejecting approaches on this basis was evaluated and the results are given here. The decision height was at 30.5 meters (100 ft) gear height and the limit on glide slope deviation was set at ±3.66 m (±12 ft). Statistical touchdown sink-rate and range results are compared in Table 5-XII. The results indicate that the improvement in range dispersion resulting from the rejection of runs outside the approach window is very small.

TABLE 5-XII THE EFFECT OF REJECTING RUNS OUTSIDE THE APPROACH WINDOW

			All Runs		In Window	
$-\dot{h}_{TD}$	μ		1.16	(3.8)	1.16	(3.8)
m/sec (fps)	2σ	hard	1.68	(5.5)	1.62	(5.3)
	10^{-6}	hard	2.32	(7.6)	2.23	(7.3)
	10^{-6}	short	-57.9	(-190)	-45.7	(-150)
X_{TD}	2σ	short	33.5	(110)	36.6	(120)
m (ft)	μ		94.5	(310)	94.5	(310)
beyond the GPIP	2σ	long	155	(510)	152	(500)
	10^{-6}	long	238	(780)	235	(770)

NOTES:

1. These are simulation results for the four control configuration with limiting shearing winds (70% HW, 30% TW), moderate turbulence and MLS beam noise.
2. All runs are included in the left column. Runs exceeding ± 3.66 m (± 12 ft) at 30.5 m (100 ft) gear height were rejected in the right column.

The reason for this is that most of the range dispersion occurs at low height and there is no direct correlation between being high on the approach at the 30.5 m (100 ft) decision height and long on touchdown, or vice versa. If a lower decision height was used, the results might have been different.
The probability distribution plots in which runs outside the approach window were rejected, are given in Appendix B.

5.4.6 Radar Altimeter Bias

Radar altimeter biases affect the flare maneuver since the commanded sink-rate is a function of radar altitude. A positive bias would result in a positive height indication at touchdown and a harder and shorter landing. The opposite happens with a negative bias. Deterministic and statistical landing data was obtained in the simulation for the three control configuration with radar altimeter biases. Biases of up to ±1.10 m (±3.6 ft) were simulated. The probability level for a 1.10 m (3.6 ft) bias is 4.5 sigma (based on data for a typical radio altimeter used in CTOL automatic landing operations.)

Figure 5-11 summarizes the deterministic touchdown results as a function of radar altimeter bias level. Sink-rate is quite insensitive to the bias and the worst case increase in sink-rate is 0.16 m/sec (0.53 fps) for a 1.10 m (3.6 ft bias). Range variations of ±30.5 m (±100 ft) with tailwind and ±12.2 m (±40 ft) with headwind occur with biases of ±3.6 ft. The probability distribution curves with radar altimeter biases are given in Appendix B. They indicate a mean shift only due to the bias with no effect on the slopes of the curves. Thus, radar altimeter bias can be treated as a deterministic disturbance in computing its effect on total population probability distributions.

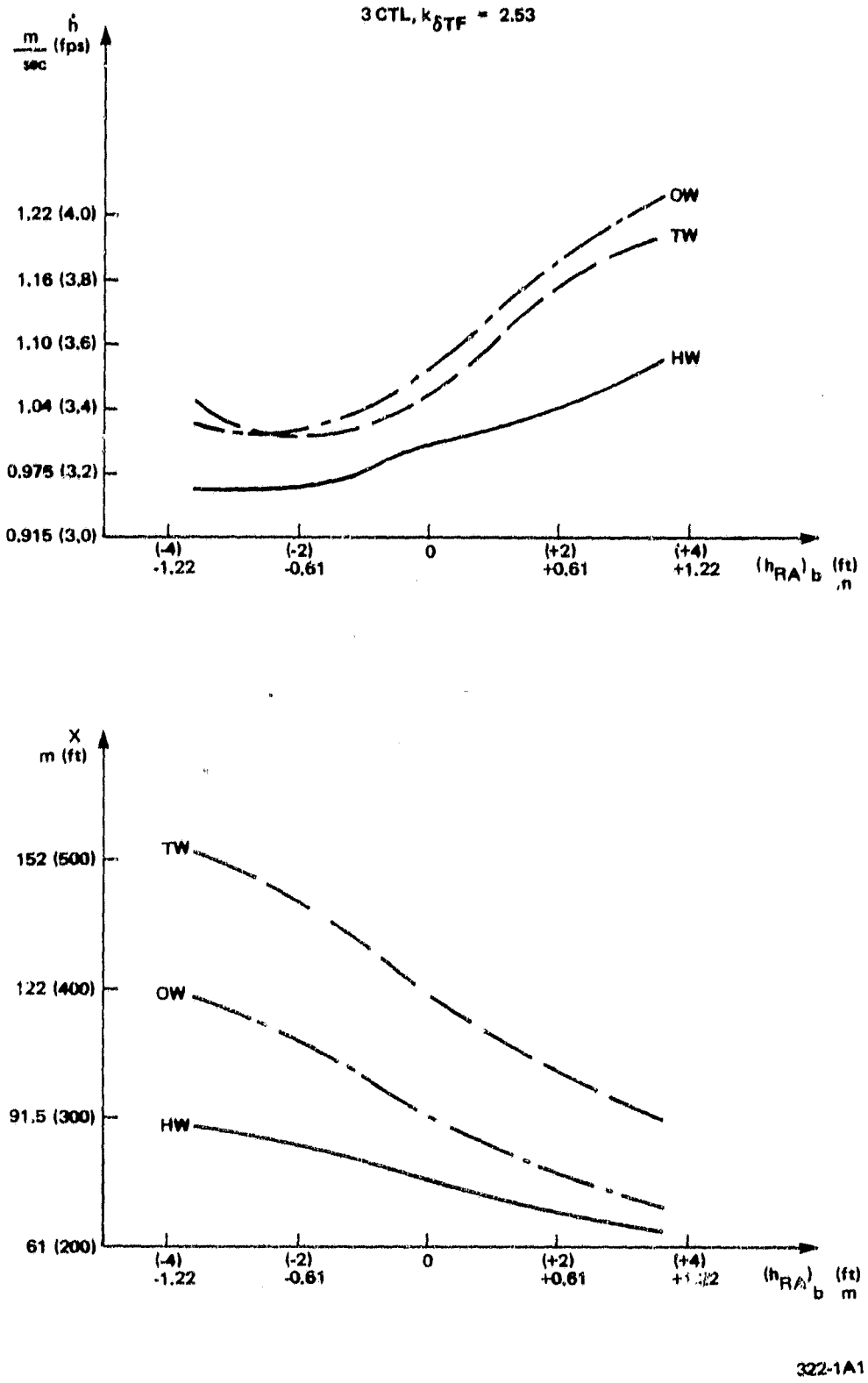

FIGURE 5-11. THE EFFECT OF RADAR ALTIMETER BIAS ON DETERMINISTIC TOUCHDOWN RESULTS

5.4.7 Pitch Attitude Gyro Bias

Pitch attitude gyro biases also affect the flare because they alter the amount of rotation that is commanded through the flare. Gyro biases of up to $\pm 2^{o}$ were simulated. This value is also at the 4.5 sigma probability level. Deterministic and statistical data was taken with gyro bias. The deterministic results are summarized in Figure 5-12. Gyro biases increase touchdown sink-rate by no more than 0.061 m/sec (0.2 fps) and their impact on range is negligible. Touchdown pitch attitude is, of course, directly affected by gyro biases and changes by $+1^{o}$ to -1.4^{o} due to bias changes of $\pm 2^{9}$. The probability distribution curves with gyro biases are given in Appendix B and, as in the case of the radar altimeter bias, a mean shift only is associated with the gyro bias, with no effect on slopes.

In summary, the effect of gyro bias is significant on touchdown attitude only.

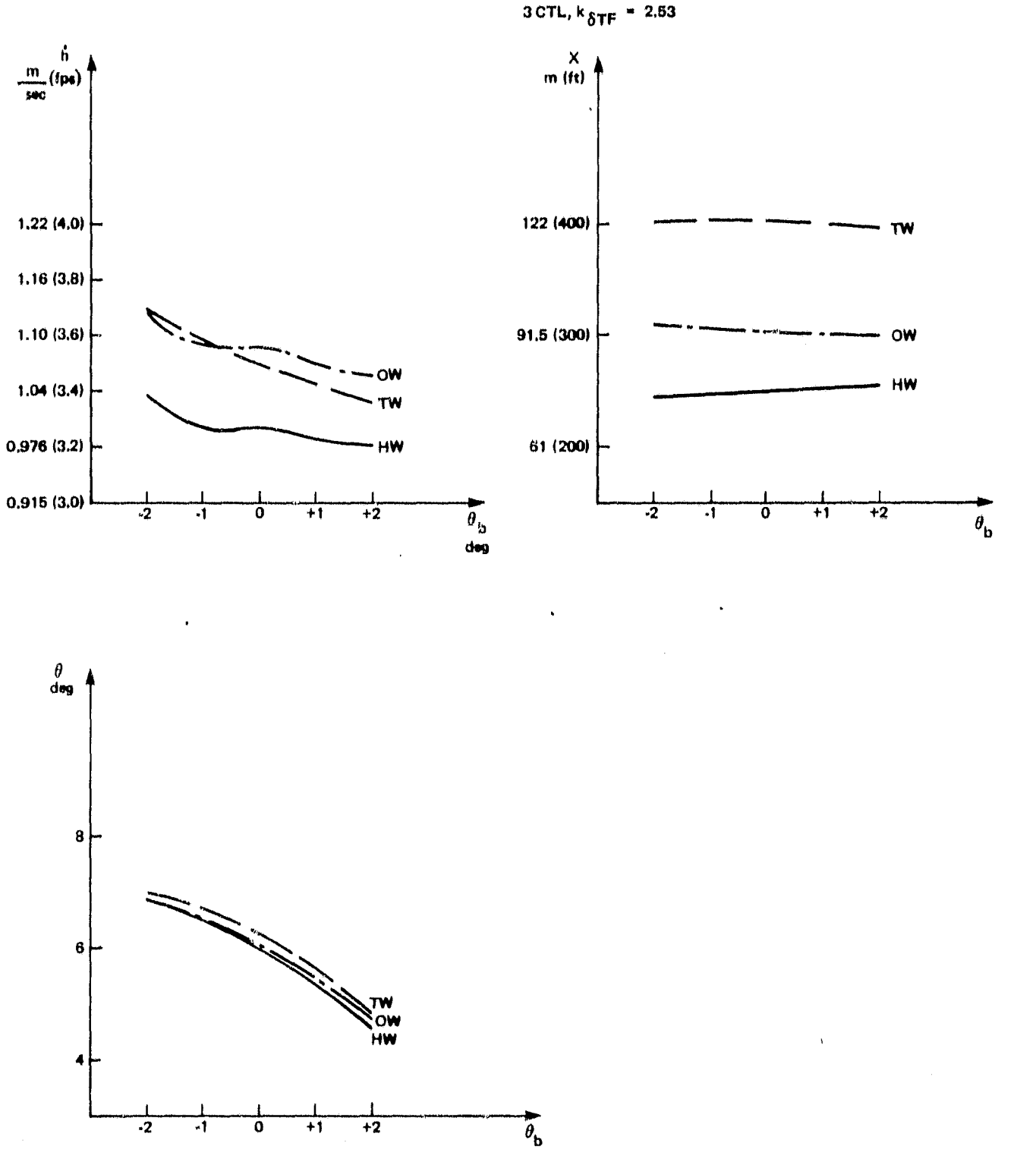

318-1A1

FIGURE 5-12. THE EFFECT OF GYRO BIAS ON DETERMINISTIC TOUCHDOWN RESULTS

6.0 Lateral/Directional Simulation Results

In this program emphasis was placed on longitudinal control laws because this is the area in which the STOL airplane peculiarities are more prominent. Lateral/directional control laws for localizer track and runway alignment were developed and evaluated in the simulations and in flight. Good correlation was not obtained, however, in this area between flight and simulation results as explained in Section 7.2. In pitch, good correlation was obtained as a result of an iterative process of refinement of airframe models and control laws and therefore the simulation results can be used to extrapolate flight test data. In the lateral/directional axis, the refinement process stopped somewhat short of this point and therefore the usefulness of the simulation results in extrapolating flight results is more restricted. The lateral simulation results are nevertheless presented here and compared with flight results in Section 7.3.

6.1 Lateral/Directional Landing Performance

The final configuration of the localizer track and runway alignment control law is described in Section 4.2. Alignment time histories with a 15 knot steady crosswind and with a 15 knot shearing crosswind, as defined in Appendix A,are shown in Figure 6-1. The initial crab angle is 13^{o} for the steady wind and 18^{o} for the shear (because the wind level at altitude is higher). The airplane banks into the wind while the crab angle is reduced. Maintaining runway heading requires about 10^{o} of rudder in both cases (the available authority is $\pm 15^{o}$). The bank attitude is about 4^{o} at touchdown. The localizer track path into roll command is retained during alignment, but an additional bank angle align, ϕ_{ALN}, path (see Figure 4-4) is needed to prevent the development of runway centerline trackling errors while reducing the high initial crab angles. The time histories show a tight localizer track with position errors of less than 0.91 m (3 ft) and rates of less than 0.91 m/sec (3 fps) throughout the maneuver. The resulting roll time history, however, is not very smooth.

Table 6-I is a summary of statistical landing performance obtained in the

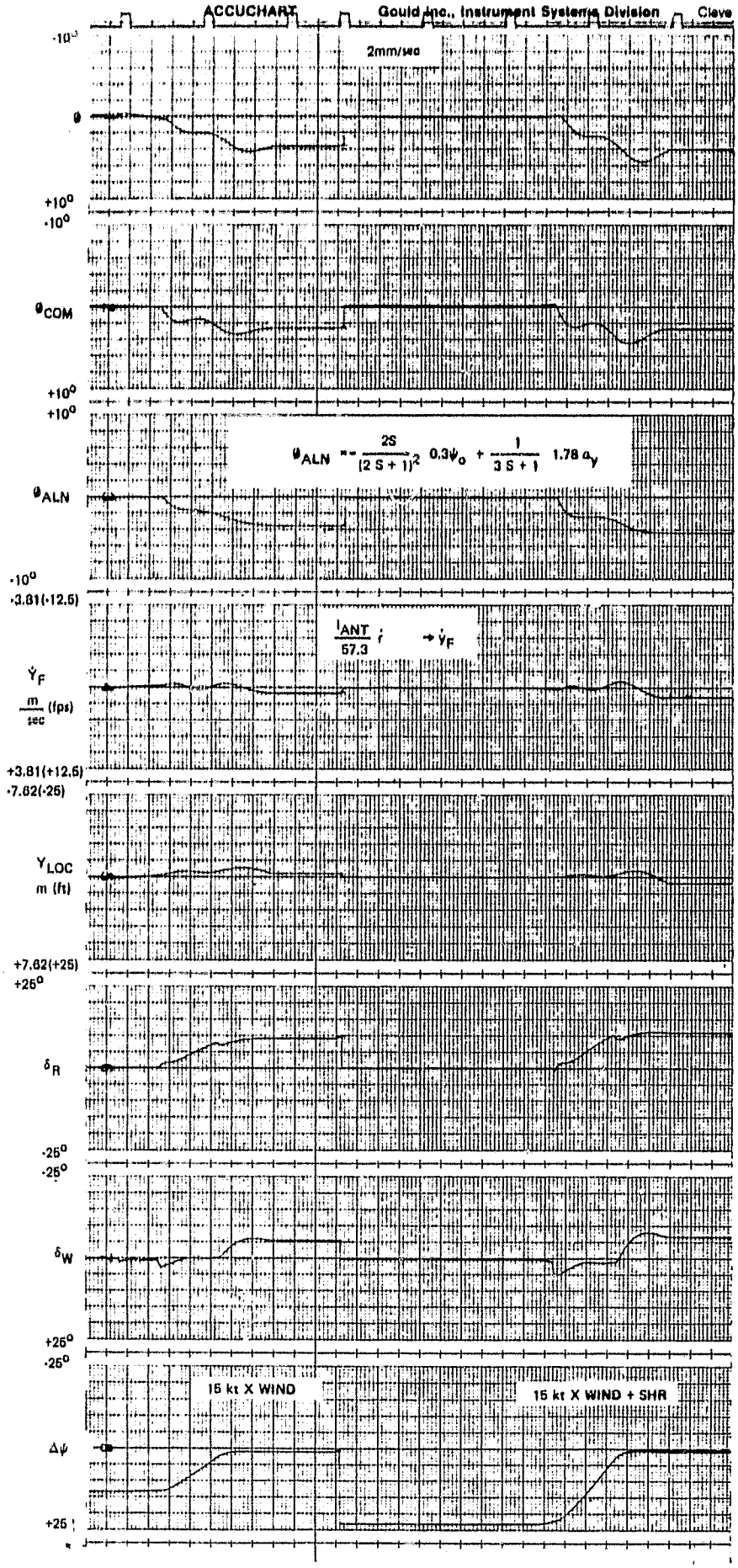

FIGURE 6-1. ALIGNMENT TIME HISTORIES;

AUG WING 35 JULY '79

simulation with limiting shearing winds, moderate turbulence and MLS beam noise. The wind and beam noise models that have been used are defined in Appendix A. The design goals are given in the left column of Table 6-I. The two sigma values for allowed touchdown position dispersion and localizer deviation at the approach window are based on the NASA Statement Of Work. The 10^{-6} lateral dispersion goal is based on the FAA AC20-57A (Reference 4) requirement for not landing any closer than five feet to the runway edge. The allowed heading deviation is based on the application of the allowed lateral deviation assuming a cross track velocity proportional to the touchdown heading error and a constant 0.2g's lateral acceleration used to arrest the lateral deviation. The allowed cross track velocity is based on gear limitations and the touchdown bank angle is based on the geometry of the Augmenter Wing Airplane. The actual performance as obtained from the simulation is given in the right hand column. All the design goals are met according to this table. However, lateral dispersions in flight were considerably bigger than predicted by the simulation, as shown in Section 7.2 and therefore more work is needed in order to refine airframe models and control laws in order to obtain good agreement between flight and simulation results. Touchdown heading error and bank attitude have significantly non zero mean values. This is due to the fact that a right crosswind was always used in the simulation.

Table 6-II is a summary of lateral activity while tracking the localizer at a gear height of 152 m (500 ft) with moderate turbulence and MLS beam noise.

TABLE 6-I LATERAL LANDING PERFORMANCE SUMMARY

Variable		Goal		Simulation	
Y_{TD}	μ	0		0	
	2σ	4.57	(15)	2.59	(8.5)
m (ft)	10^{-6}	9.15	(30)	6.40	(21)
$\dot{Y}_{TD}$	μ	0		0	
	2σ	1.22	(4)	0.305	(1.0)
m/sec (fps)	10^{-6}	3.05	(10)	0.85	(2.8)
$\Delta\psi_{TD}$	μ	0		0.9	
	2σ	4		3.0	
deg	10^{-6}	10		6.0	
ϕ_{TD}	μ	-		2.2	
	2σ	-		4.8	
deg	10^{-6}	20		9.0	
ΔY_{WINDOW}	μ	0		0.15	(0.5)
m (ft)	2σ	7.62	(25)	2.74	(9.0)

NOTES:

1. These results were obtained in the simulation with limiting shearing winds, moderate turbulence and MLS beam noise.
2. ΔY_{WINDOW} is the localizer tracking error at the 30.5 m (100 ft) approach window.

TABLE 6-II LOCALIZER TRACK RMS ACTIVITY WITH TURBULENCE AND BEAM NOISE

$\hat{y}$	m	(ft)	1.37	(4.5)
$\hat{\dot{y}}$	m/sec	(fps)	0.457	(1.5)
ϕ	deg		1.0	
ψ	deg		2.8	
δ_W	deg		4.0	
δ_R	deg		0.7	

NOTE: Data given for localizer track at 152 m (500 ft) gear height with the following disturbances:

$\sigma_\beta = 3.1^o$ $\quad \sigma_r = 1\ ^o/\text{sec}$ $\quad \sigma_y = 3.5$ ft

$L_v/U_o = 0.507$ sec $\quad 3b/\pi U_o = 0.636$ sec $\quad \tau_y = 0.5$ sec

Localizer deviations are reasonably small compared to the 25 ft allowed on a two sigma basis at the 30.5 m (100 ft) approach window. A moderate amount of cross track rate is induced by MLS beam noise. The simulation predicted roll activity is low. Heading excursions, σ_ψ, are closely related to the level of gust induced side slip, σ_β. Wheel and rudder activities are small fractions of the available authorities of $\pm 75^0$ for the wheel and $\pm 15^0$ for the rudder.

6.2 Alternate Alignment Control Law

Filtered localizer deviation and estimated rate are used to generate a roll command to track the localizer. This computation is retained during alignment, but an additional roll command is inserted in order to minimize cross track errors while the airplane gets aligned with the runway heading and a substantial sideslip angle is building up as a result. Initially this additional bank attitude command was generated as shown by the top block diagram of Figure 6-2. The difference between washed out cross track acceleration and bank attitude is filtered and limited to generate the alignment bank command. This is done in order to maintain zero cross track acceleration during the alignment maneuver. Flight test results have indicated that deviations on the order of 3-5 meters (10-15 ft) from the runway centerline have developed during alignments with crosswinds on the order of 15 knots. A simulation study of the problem has indicated that the problem could be related to the fact that the control law attempted to command zero cross track acceleration at the center of gravity while the localizer receiver antenna and cockpit on the Augmenter Wing Airplane are 8.54 meters (28 ft) ahead of the center of gravity. In localizer track, the localizer receiver antenna tracks the localizer beam and in the presence of a steady 15 knot crosswind the crab angle is higher than 12^0 and the center of gravity is 1.83 m (6 ft) off the runway centerline. Trying to rotate the airplane in yaw around the center of gravity in these conditions would cause the nose to swing away from the centerline and would introduce a disturbance in the localizer track loop. Coordinated bank and rudder commands can be used to rotate the airplane about its nose rather than the center of gravity, thereby maintaining the localizer receiver antenna and the cockpit on the runway

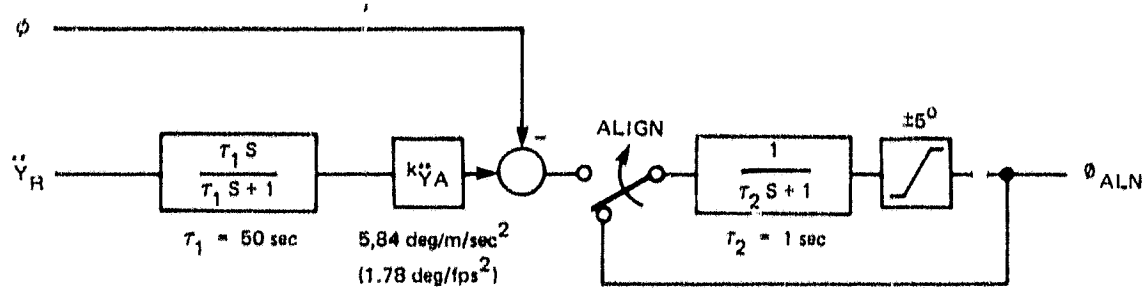

VERSION 1

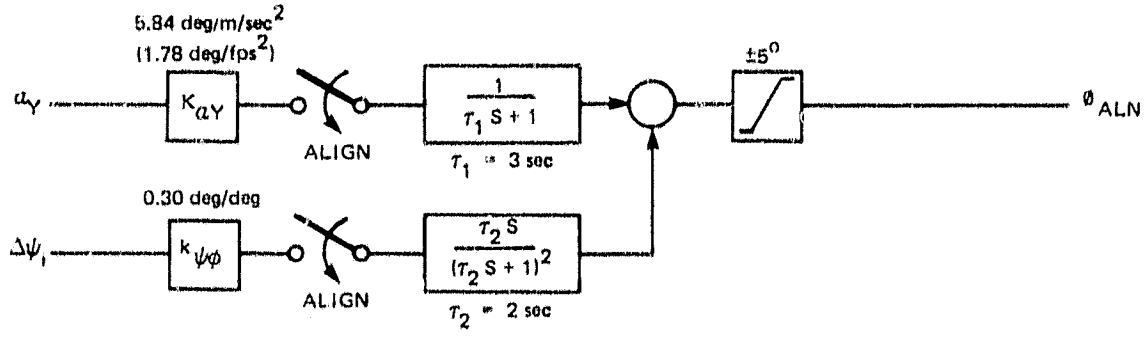

VERSION 2

0305-1A1

FIGURE 6-2. ALIGNMENT ROLL COMMAND BLOCK DIAGRAMS

centerline. The bottom block diagram of Figure 6-2 generates a roll command that approximates this desired maneuver. In this configuration lagged lateral acceleration is combined with a kicker that uses pre-alignment heading error to produce a predictive roll command. Both paths are switched in at alignment initiation. Another modification to the control law involved summing yaw acceleration with cross track acceleration at the input to the localizer complementary filter such that localizer deviation rate at the nose rather than at the center of gravity is computed. With this alignment roll command, significant improvement in localizer tracking during alignment was recorded in the simulation. Flight results, however, have not produced conclusive results with respect to one of these two configurations actually performing better than the other.

6.3 MLS Beam Filtering

High roll activity occurred in flight. Flight data was analyzed and simulation studies were conducted in order to identify potential sources of this activity. One area addressed was MLS beam noise. A three state complementary filter is used to obtain estimated localizer deviation and rate from raw deviation and cross track acceleration. The filter transfer function has three co-located poles nominally at a frequency of ω_F = 0.20 radians per second during the final approach.

Table 6-III compares activity while in the localizer track mode at 152 m (500 ft) gear height with moderate turbulence and beam noise and with ω_F of 0.20 and 0.10.

TABLE 6-III LOCALIZER TRACK RMS ACTIVITY COMPARISON

ω_F (rps)	0.20	0.10
$\hat{y}$ m (ft)	1.37 (4.5)	0.76 (2.5)
$\dot{\hat{y}}$ m/sec (fps)	0.457 (1.5)	0.061 (0.2)
ϕ deg	1.0	0.4
ψ deg	2.8	2.0
δ_W deg	4.0	3.0
δ_R deg	0.7	0.6

NOTE: Same condition and disturbances as Table 6-I.

The lower filter frequency results in a big reduction in cross track velocity activity as well as a significant reduction in roll activity and better localizer track performance. These results suggest that it is advantageous to lower the filter frequency. Using lower filter frequencies, however, increases the sensitivity of the system to accelerometer errors and the tradeoff is not obvious. The tradeoff between sensitivity to accelerometer errors and beam noise is, of course, sensitive to the models used in the simulation to define these disturbances. Flight data could have been useful in the evaluation of this tradeoff, but no flight data with ω_F=0.10 is available.

7.0 Comparison of Simulation and Flight Results

The comparison between simulation and flight results in the longitudinal and lateral axes is discussed in this section. Good correlation was obtained in pitch and therefore the simulation data can be used to extrapolate the flight data base. Additional work is needed in the lateral axis in order to obtain such correlation.

7.1 Longitudinal

Figures 7-1 through 7-6 show touchdown sink-rate and range probability distributions obtained with the simulation for the four, three and two control configurations with flight-test data points superimposed. The flight data presented in these figures is taken from Reference 14. The simulation results were taken with limiting winds and shears, limiting turbulence and MLS noise. The curves shown are based on a 70 percent probability of encountering limiting headwinds and 30 percent probability for limiting tailwinds (limiting headwinds have a magnitude of 25 knots and limiting tailwinds are 10 knots). Flight results are based on 31 landings with the four control configuration, 29 landings with three controls and 26 two control landings.

A fairly wide range of ambient conditions were encountered during the flight tests since the flights were conducted over several months of the year and different hours of the day. The distribution of winds measured at a mast near the touchdown zone is shown in Figure 7-7 for the four control configuration tests. Even though the majority of landings were made in light winds, headwinds of up to 15 knots, tailwinds up to 11 knots and crosswinds up to 20 knots were encountered. In this program, correlation of flight test and simulator results on a landing by landing basis was not attempted. Overall probability distributions obtained in flight are compared with the simulator generated probability distributions. These probability distributions are best compared in terms of their slopes. When making this comparison, steeper slopes are expected in the flight data because flying occurred in less than limiting wind conditions. Weight and temperature variations and sensor errors (such as

radar altimeter bias) in flight tend to decrease the probability distribution curve slope and reduce the difference between flight and simulation.

A comparison of simulation versus flight touchdown sink-rate results is given in Figure 7-1 for the four controls, in Figure 7-2 for the three controls and in Figure 7-3 for the two controls. Since the vertical channels of the four and three control systems are identical, the performance of the two systems is very similar as indicated by the probability distribution curves. For the two control configuration, the probability distribution curve slope is flatter than with the four and three control systems because of the reduction in bandwidth associated with this no choke configuration. The slopes of the flight test points are somewhat steeper than the slopes of the simulator curves, as expected on the basis of the lighter winds that were encountered in flight.*

The data point at 1.83 m/sec (6 fps) in Figure 7-3 tends to follow the bend in the distribution curve predicted by the simulation.

Figures 7-4, 5, 6 show the touchdown range distribution results for the same three configurations. Range is referenced to the glide path intercept point (GPIP). For the four controls most of the flight points are in good agreement with the simulation results. This is even true for the top four points which are associated with headwinds in excess of 15 knots, crosswinds between 15 and 20 knots and approaches that were not well stabilized. The crosswind conditions were beyond the design envelope of the system.

*After collecting the three control flight data, an error in the implementation of the engine - choke system was discovered, resulting in an increased throttle feedback gain. Since the gain increased the effective choke gain and reduced the effective engine gain, the overall normal acceleration was unchanged as long as the chokes were not driven to their limits. This was the case for the flight data shown in Figure 7-2. A subsequent simulator check also confirmed that for the disturbances experienced in flight, the existing flight data was valid. This simulation study is discussed in Section 5.4.3.

C-2

The simulation data in Figure 7-5 for the three control system is essentially the same as the simulation data for the four control system. Again, the flight data correlate well with the simulation data and the flight data shows the expected steeper slope associated with lighter winds. The simulation data for the two control system shown in Figure 7-6 predicts nearly the same mean range but a 50% increase in the short landing to long landing range spread as compared to the four and three control systems. The slope of the flight data probability curve is in reasonably good agreement with the simulation results, but the mean value of the flight data is 36.6 m (120 feet) short. Differences in the mean touchdown range values between flight and simulation are probably the results of a residual modeling discrepancy and coupled with the fact that range is not explicitly controlled.

The comparison of flight versus simulation touchdown performance is summarized in Table 7-I. Good agreement exists between the flight and simulation results with the exception of the difference in the mean value for range.

7.2 Lateral/Directional

Figure 7-8 shows the lateral touchdown distance distribution obtained with the simulation and in 67 landings in flight. The simulation data was taken with maximum design (15 knots) crosswinds and turbulence. The spread in the lateral touchdown distribution of the flight data is more than double than obtained from the simulation. The extreme deviations to the right of the runway's centerline (beyond 4.57 m, or 15 feet), shown by flight data, are associated with the system operating near or beyond its limits, with quartering headwinds of more than 20 knots and a left crosswind component up to 20 knots, resulting in rudder limiting in some cases. This, however, does not explain the overall wider lateral touchdown distribution of the flight data which is a result of a problem that has not been pinpointed. Other manifestations of this problem are roll excursions from side to side during alignment and not a very tight localizer track, with excursions over 6.1 m (20 feet) occurring quite often even in the light wind conditions. This compares with 2.7 m (9 feet) on a two sigma basis predicted by simulation. Unfortunately, since the emphasis in this program was on the longitudinal axis, the lateral problems were not pursued far enough to positively identify their source and solve them.

TABLE 7-I TOUCHDOWN PERFORMANCE COMPARISON

	FOUR CONTROLS		THREE CONTROLS		TWO CONTROLS	
	Flight	Simulation	Flight	Simulation	Flight	Simulation
Sink-rate $\frac{m}{sec}$ (fps)						
mean	1.16(3.8)	1.16(3.8)	0.94(3.1)	1.13(3.7)	1.00(3.3)	1.13(3.7)
two sigma, hard	1.52(5.0)	1.68(5.5)	1.31(4.3)	1.59(5.2)	1.71(5.6)	1.89(6.2)
Range m (ft)						
mean	73.2(240)	94.5(310)	97.6(320)	91.5(300)	51.8(170)	88.4(290)
two sigma, short	3.05 (10)	30.5(100)	45.7(150)	30.5(100)	-21.3(-70)	9.15(30)
two sigma, long	116(380)	152(500)	134(440)	159(520)	122(400)	198(650)

Comments: 1) Simulation results are with limiting winds and shears, limiting turbulence and MLS beam noise.

2) Range is measured from the Glidepath Intercept Point.

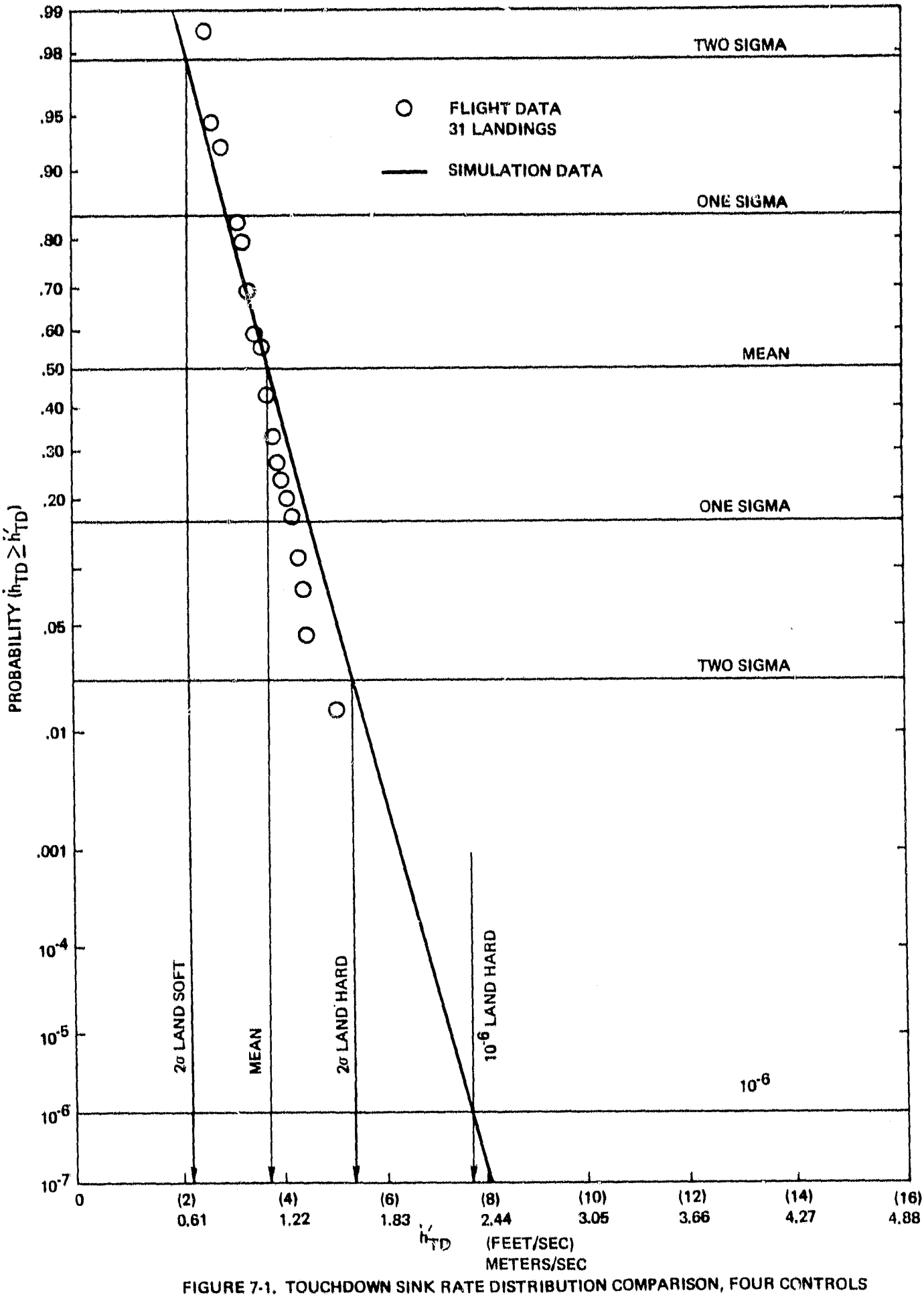

FIGURE 7-1. TOUCHDOWN SINK RATE DISTRIBUTION COMPARISON, FOUR CONTROLS

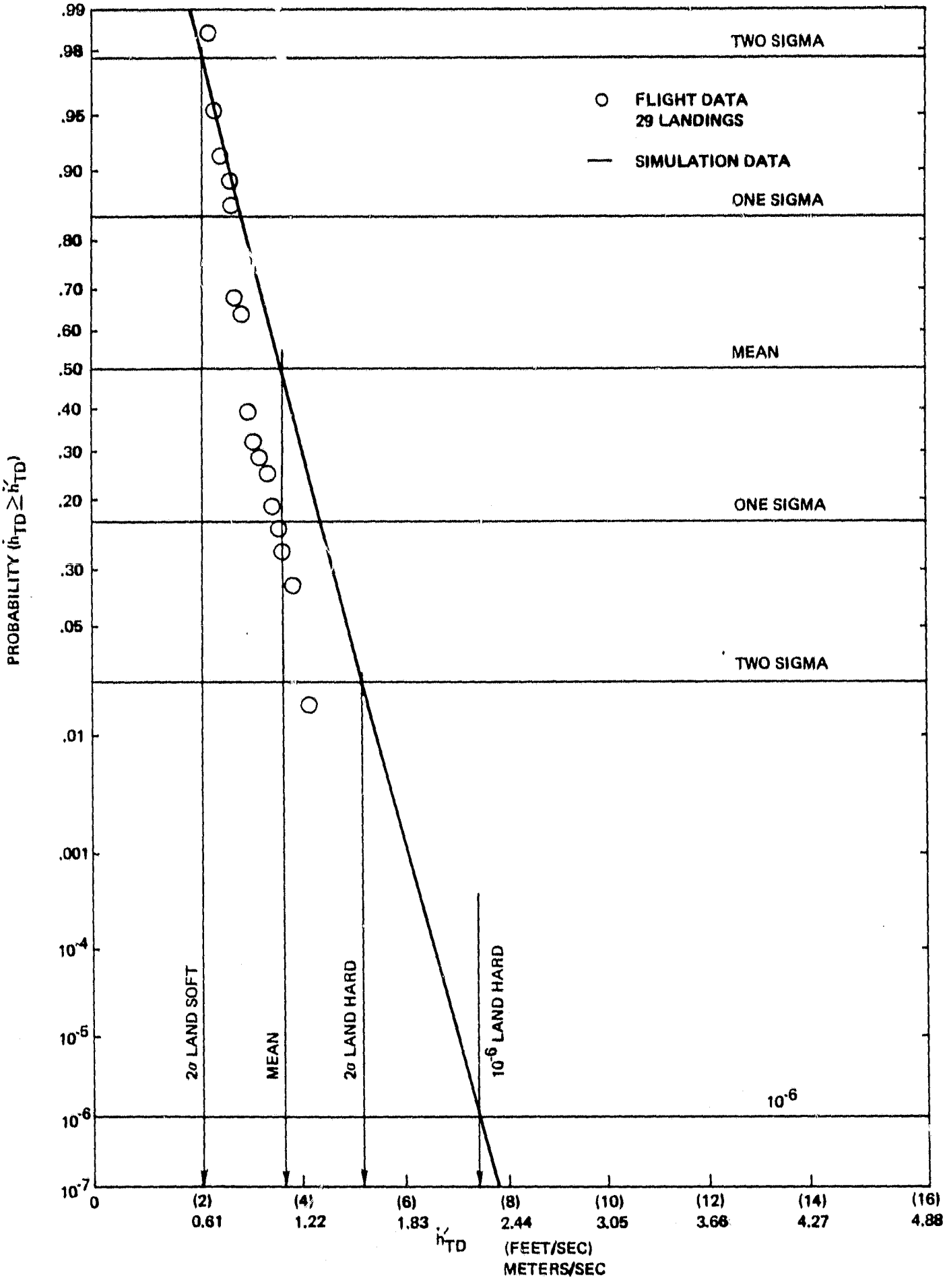

FIGURE 7-2. TOUCHDOWN SINK RATE DISTRIBUTION COMPARISON, THREE CONTROLS

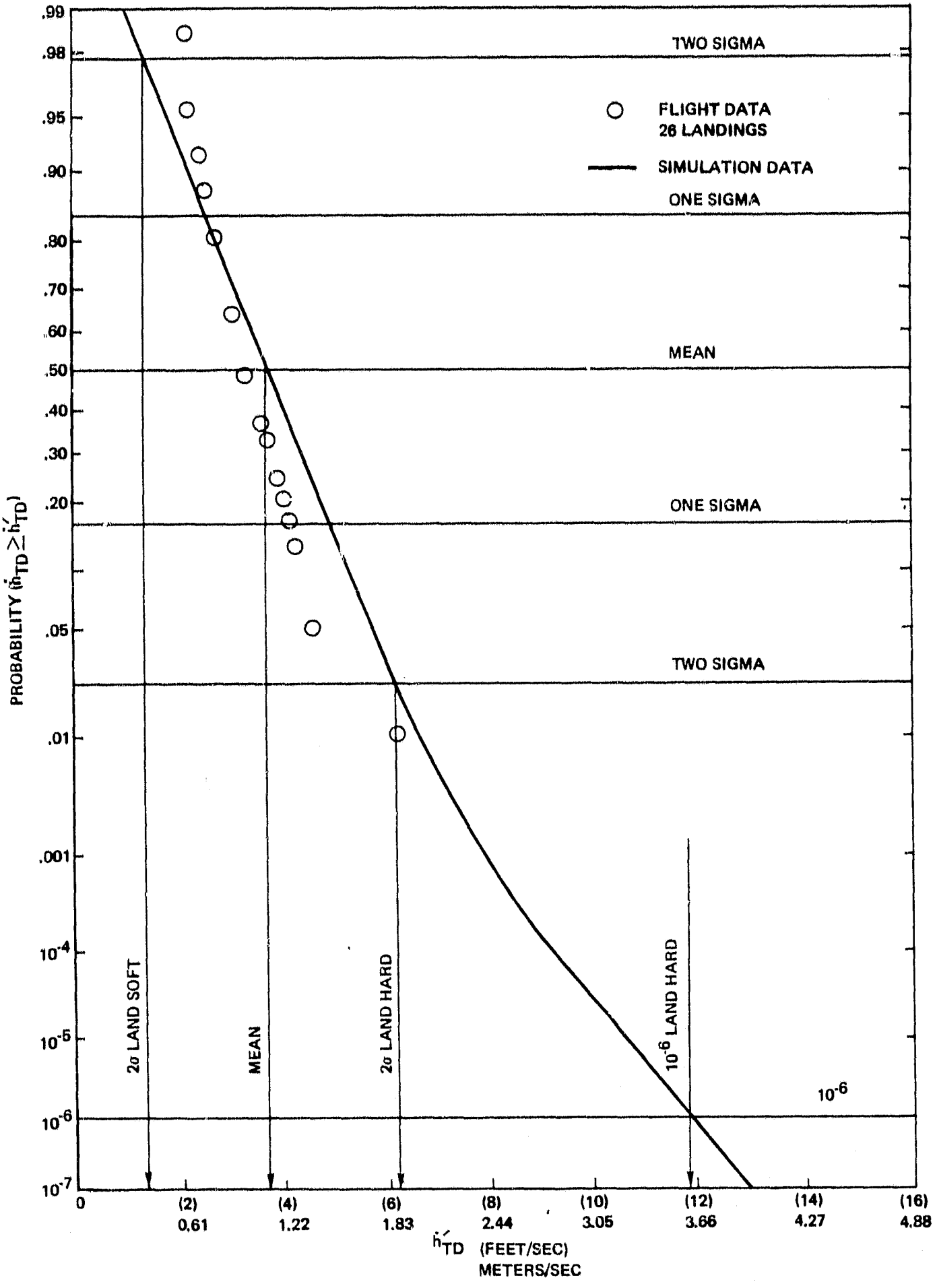

FIGURE 7-3. TOUCHDOWN SINK RATE DISTRIBUTION COMPARISON, TWO CONTROLS

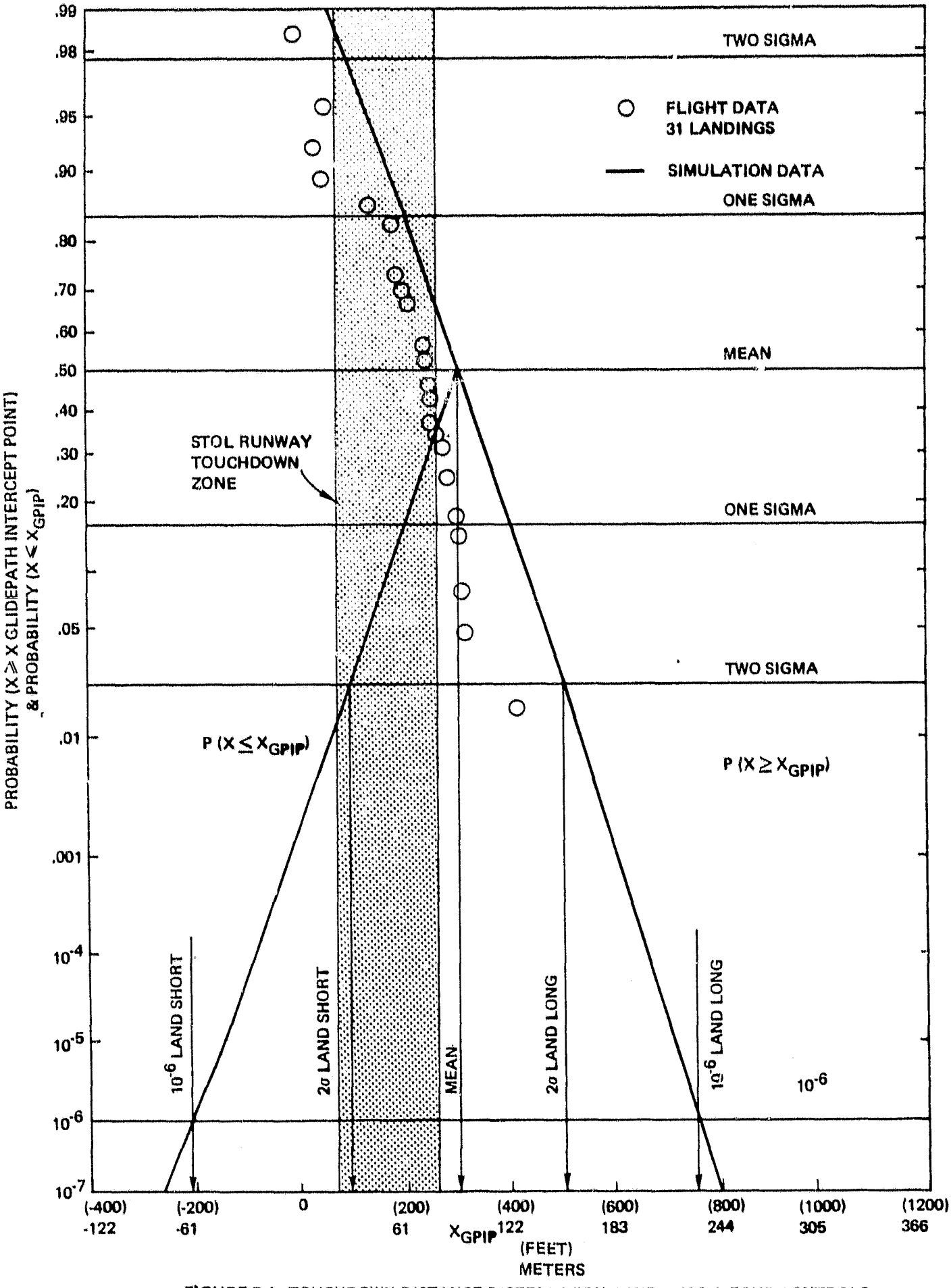

FIGURE 7-4. TOUCHDOWN DISTANCE DISTRIBUTION COMPARISON, FOUR CONTROLS

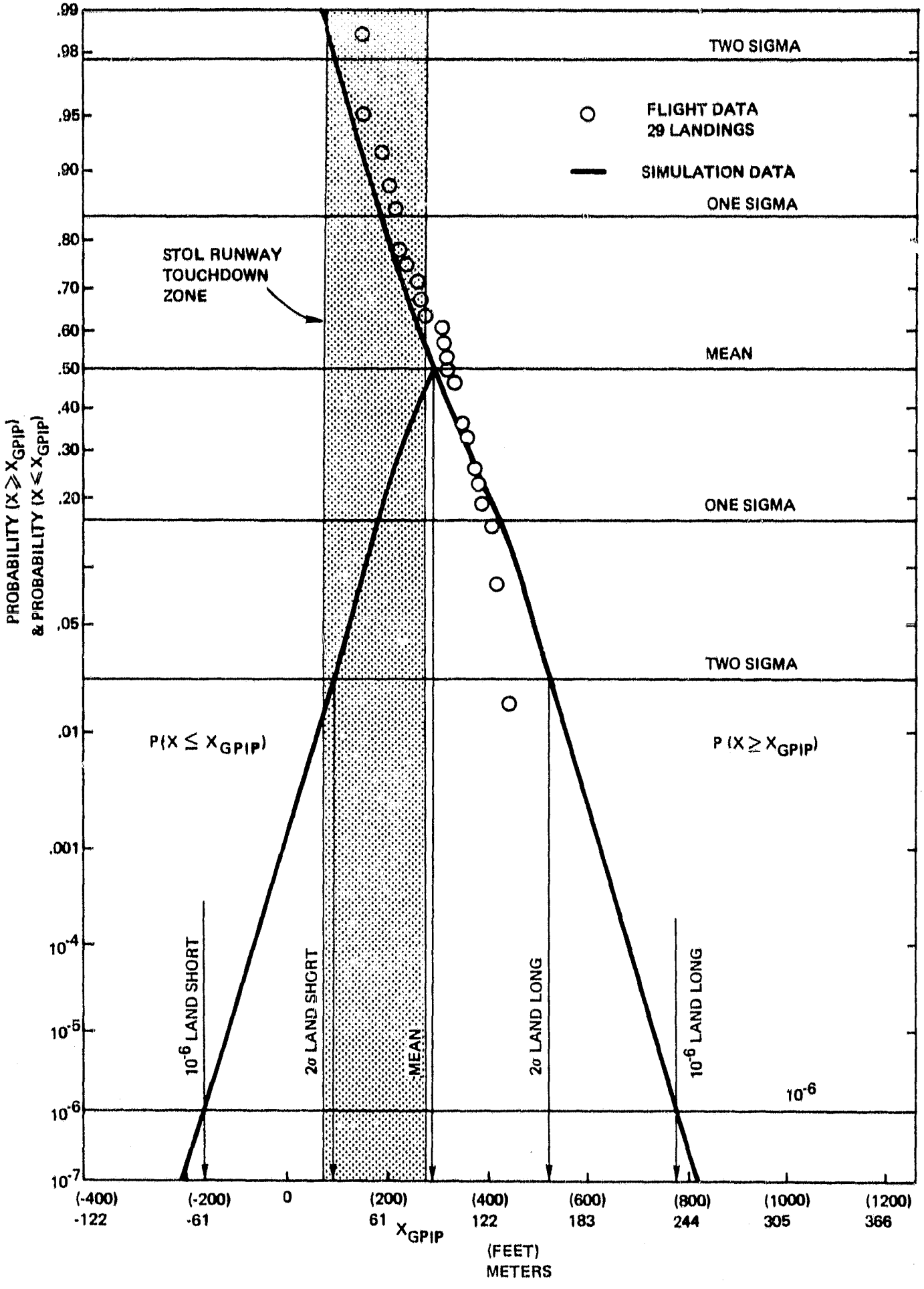

FIGURE 7-5. TOUCHDOWN DISTANCE DISTRIBUTION COMPARISON, THREE CONTROLS

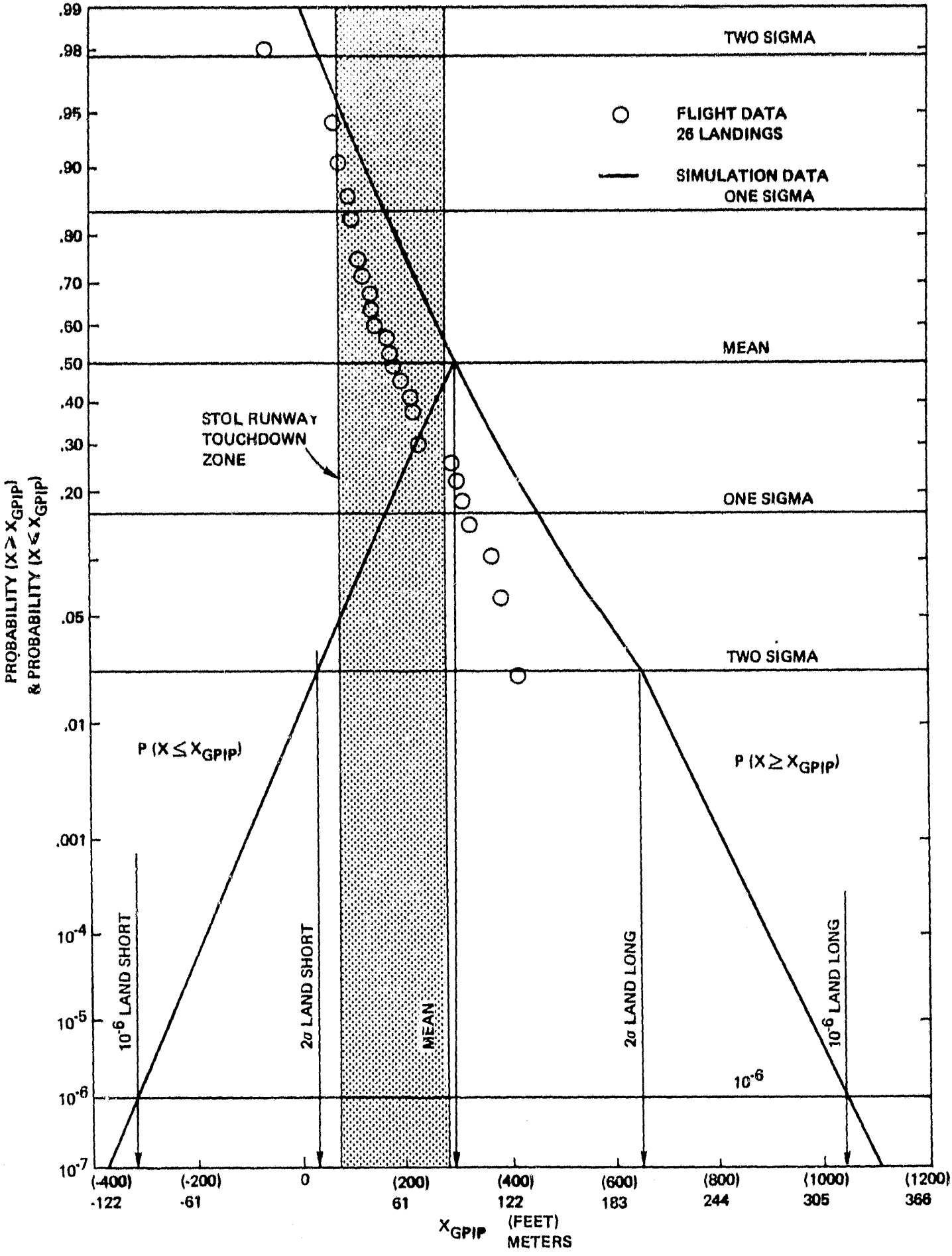

FIGURE 7-6. TOUCHDOWN DISTANCE DISTRIBUTION COMPARISON, TWO CONTROLS

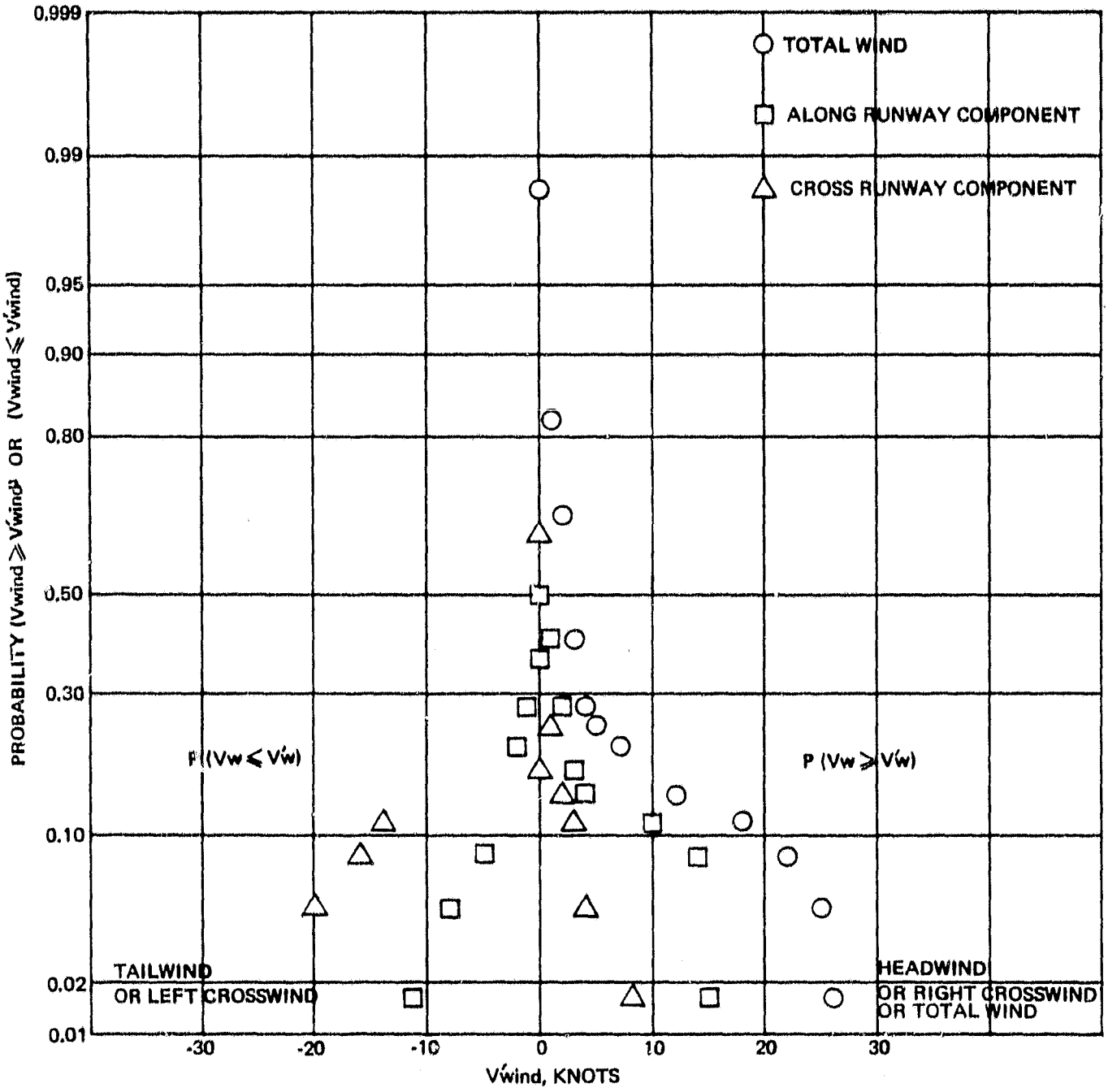

FIGURE 7-7. WIND DISTRIBUTION FOR LANDINGS WITH FOUR CONTROLS

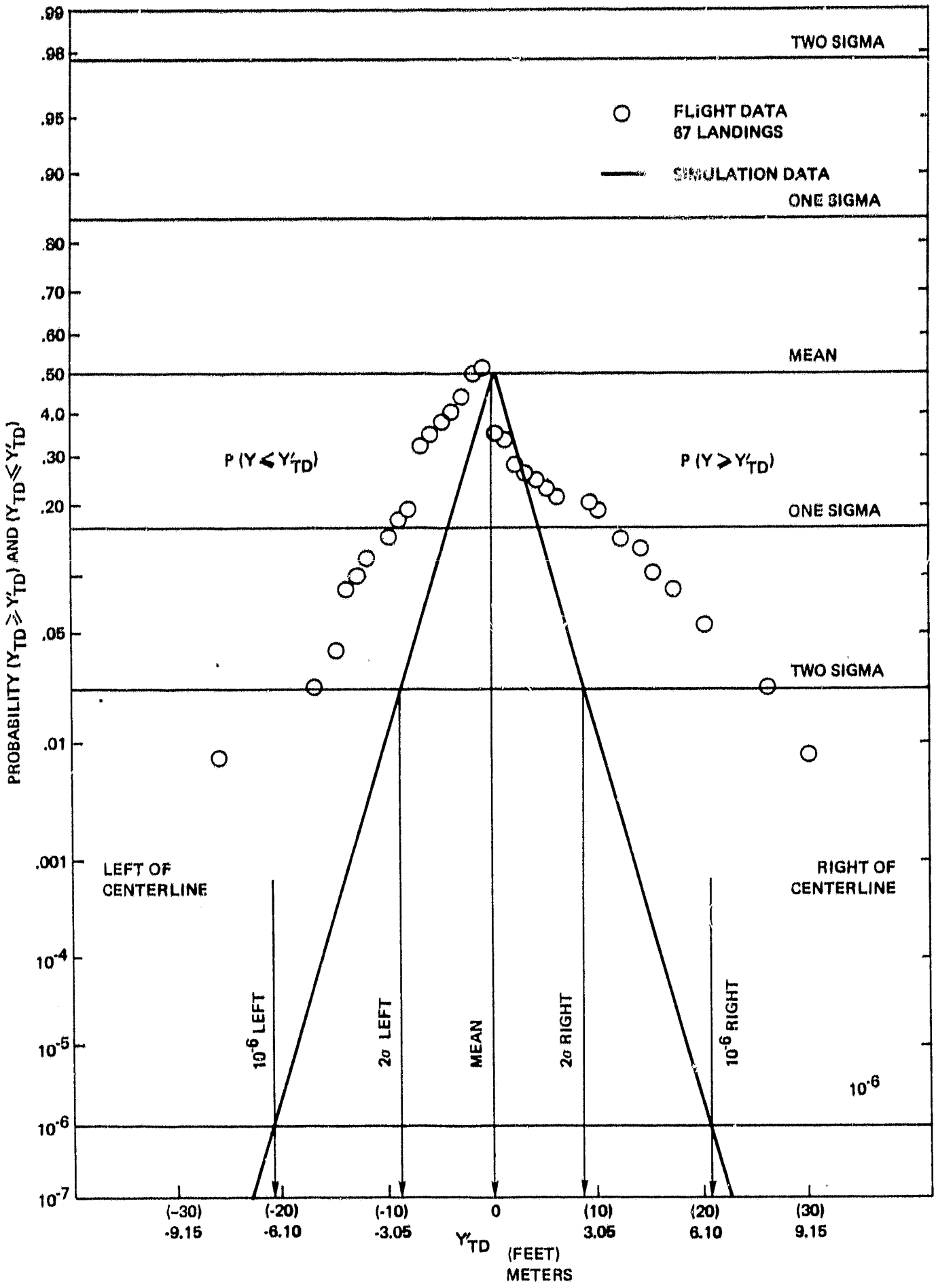

FIGURE 7-8. LATERAL TOUCHDOWN DISTANCE DISTRIBUTION COMPARISON

8.0 Conclusions

The conclusions of this powered lift STOL aircraft automatic landing study are given here. General conclusions based on the results of flight test and simulation are given first, followed by results that were derived mainly from simulation studies.

8.1 General Conclusions

1. For powered lift STOL aircraft that operate on the backside of the power curve, good normal acceleration control is needed for flight path control. This establishes requirements on both amplitude and bandwidth. For the Augmenter Wing airplane both the engine response and the throttle servo rate limits were marginal. These limitations were partially overcome through the use of the direct lift control chokes.

2. With these automatic landing control laws, the longitudinal distance dispersion of the Augmenter Wing airplane is consistent with STOL port requirements as defined in Reference 11. These control laws also provide excellent sink-rate control.

3. The primary requirement placed on the STOL autoland control law development was that precise and soft sink-rate control be achieved. This is consistent with the current practice for CTOL Category III autoland systems. Better touchdown range control may be possible if the allowable touchdown sink-rate is increased through landing gear design or if the emphasis in the control law design is shifted from primarily sink-rate control to a combination of sink-rate and range control.

4. Good correlation was obtained in the touchdown range and sink-rate data between flight and simulation results through an iterative process of refining mathematical models and control laws per flight test results.

Under these conditions, the fast time simulation is effective for extrapolating the limited amount of flight data to account for low probability events. Additional work is needed to obtain similar correlation in the lateral axis.

8.2 Simulation Studies Conclusions

1. Equivalent landing performance was obtained with the four and three control configurations. The performance of the two control configuration was not as good. Therefore, the three control configuration offers a good tradeoff between performance and complexity if the increased pitch activity is acceptable for passenger comfort.

2. In the longitudinal axis, winds and turbulence are the major contributor to landing dispersions and the impact of MLS noise is insignificant. Two sigma dispersions are approximately proportional to turbulence level and the major effect of deterministic winds and shears is to shift the mean touchdown range. Excellent sink-rate control and acceptable range control were obtained with linear shears of up to 50 kt/100 ft. Using the CAA rather than FAA vertical turbulence model resulted in some increase in activity, but had very little impact on landing performance.

3. The effect of weight and temperature variations on landing dispersions is small.

4. Sink-rate control is approximately proportional to the system bandwidth as controlled by throttle and choke command gain. Touchdown range and glide slope deviation are less sensitive to variations of this gain.

5. The RPM and chokes complementation scheme that was used allows each one of these controllers to compensate for some reduction in authority of the other without a significant degradation in performance.

6. Increasing the touchdown sink-rate from 1.16 m/sec (3.8 fps) to 1.77 m/sec (5.8 fps) resulted in a modest reduction in range dispersion.

7. Rejecting approaches outside the approach window at the 30.5 m (100 ft) decision height had very little impact on landing dispersions.

8. MLS noise does contribute significantly to lateral activity and landing dispersions.

9. Precise wing down compensation plays an important role in the minimization of lateral deviations during runway alignment.

APPENDIX A

SIMULATION DEFINITION

LIST OF FIGURES AND TABLES

APPENDIX A

Simulation Definition

The nonpiloted simulation of the Augmentor Wing airplane and its automatic landing system are defined in this appendix. This simulation definition includes:

1. Airframe Dynamics
2. Control Dynamics
3. Geometry and Sensors
4. MLS Noise Model
5. Wind Models

This appendix is patterned after the simulation definition of Reference 5. It has been revised, however, to include model refinements that were included as a result of flight tests.

A-1 Airframe Dynamics

The normal set of uncoupled, linearized, small perturbation aerodynamic equations of motion as documented in Tables A-I and A-III were used as a starting point. Non-linearities associated with the propulsive lift system were added to improve correlation with flight results. Figure A-1 shows the variation of drag, lift and hot thrust as a function of engine RPM. Actually, hot thrust varies with the high rotor speed (N_H) and lift and drag vary with the low rotor speed (N_L) but statically they can all be expressed as function of the high rotor speed. Dynamically, the engine model includes two separate paths for N_H and N_L. Lift and hot thrust variations are computed as functions of engine RPM:

$$\frac{L_{WB}}{m} = f_1 (N_L)$$

$$\frac{T_H}{m} = f_2 (N_H)$$

A linear approximation is used for drag variation with RPM. The hot thrust is resolved to its longitudinal and normal components as a function of nozzle angle. Thus, the following modifications are made in the drag and lift equations:

i) $X_{\delta RPM}\delta_{RPM}$ replaced with $X_{\delta NL}\delta_{NL}$

$X_{\delta N}\delta_N$ replaced with

$$\frac{T_H(N_H)}{m}\cos\delta_N - \frac{T_H(N_{HO})}{m}\cos\delta_{NO}$$

where N_{HO}, δ_{NO} are the trim values.

ii) $Z_{\delta RPM}\delta_{RPM} + Z_{\delta N}\delta_N$ replaced with

$$-\left[\frac{L_{WB}}{m}(N_L) - \frac{L_{WB}}{m}(N_{LO})\right] - \left[\frac{T_H}{m}(N_H)\sin\delta_N - \frac{T_H}{m}(N_{HO})\sin\delta_{NO}\right]$$

iii) The term $U_o q$ in the lift equation was replaced by $U_1 q$ in order to account for the large variation in ground speed associated with variations in headwind.

The resulting $\dot{u}$ and $\dot{w}$ equations are:

$$\dot{u} = X_u u_A + X_w w_A - g\cos\gamma_o \cdot \theta + \left[\Delta X_{GE} + \Delta X_{\alpha GE}\alpha\right] HF$$

$$+X_{\delta e}\delta_e + X_{\delta NL}\delta_{NL} + \frac{T_H(N_H)}{m}\cos\delta_N - \frac{T_H(N_{HO})}{m}\cos\delta_{NO} + X_{\delta CH}\delta_{CH}$$

$$\dot{w} = Z_u u_A + Z_{\dot{w}}\dot{w} + Z_w w_A + (U_I + Z_q)\cdot q - g \cdot \sin\gamma_o \cdot \theta + \left[\Delta Z_{GE} + \Delta Z_{\alpha GE}\cdot\alpha\right]\cdot HF$$

$$+Z_{\delta e}\delta_e - \left[\frac{L_{wb}(N_L)}{m} - \frac{L_{wb}(N_{LO})}{m}\right] - \left[\frac{T_H(N_H)}{m}\sin\delta_N - \frac{T_H(N_{HO})}{m}\sin\delta_{NO}\right] + Z_{\delta CH}\delta_{CH}$$

Four longitudinal and two lateral/directional flight conditions were studied. The stability axes dimensional derivatives and other pertinent data are included in Tables A-II and A-IV. Data was obtained from References A-1 and A-2 and from the NASA ARC simulation.

Longitudinal free aircraft responses for the nominal flight condition are shown in Figures A-2 and A-3 for elevator, choke, engine RPM and nozzle step inputs and in Figure A-4 for u and α gust steps. Lateral directional free airframe responses at the 65 knot flight conditions are shown in Figure A-5 for rudder and wheel step inputs and in Figure A-6 for roll rate and yaw rate initial conditions.

TABLE A-I. LONGITUDINAL EQUATIONS OF MOTION (LINEAR)

$$\dot{u} = X_u \cdot u_A + X_w \cdot w_A - g\cos\gamma_o \cdot \theta + \left[\Delta X_{GE} + \Delta X_{\alpha GE} \cdot \alpha\right] \cdot HF$$

$$+X_{\delta e} \cdot \delta_e + X_{\delta RPM} \cdot \delta_{RPM} + X_{\delta N} \cdot \delta_N + X_{\delta CH} \cdot \delta_{CH}$$

$$\dot{w} = Z_u \cdot u_A + Z_{\dot{w}} \cdot \dot{w} + Z_w \cdot w_A + (U_o + Z_q) \cdot q - g\sin\gamma_o \cdot \theta + \left[\Delta Z_{GE} + \Delta Z_{\alpha GE} \cdot \alpha\right] \cdot HF$$

$$+Z_{\delta e} \cdot \delta_e + Z_{\delta RPM} \cdot \delta_{RPM} + Z_{\delta N} \cdot \delta_N + Z_{\delta CH} \cdot \delta_{CH}$$

$$\dot{q} = M_u \cdot u_A + M_{\dot{w}} \cdot \dot{w} + M_w \cdot w_A + M_q \cdot q + \left[\Delta M_{GE} + \Delta M_{\alpha GE} \cdot \alpha\right] \cdot HF$$

$$+M_{\delta e} \cdot \delta e + M_{\delta RPM} \cdot \delta_{RPM} + M_{\delta N} \cdot \delta_N + M_{\delta CH} \cdot \delta_{CH}$$

$$\dot{h} = U_I(q - \dot{\alpha}) + \sin\gamma_o \cdot \dot{u}$$

$$\dot{h} = U_I \cdot \gamma_I$$

$$\dot{\alpha} = \dot{w}/U_o \quad , \alpha_A = w_A/U_o$$

$$U_I = U_o + u_A - u_{wind}$$

$$\gamma_I = \theta_T - \alpha_T$$

$$\alpha_T = \alpha_o + \alpha_A - \alpha_{WIND}$$

$$\theta_T = \theta_o + \theta$$

$$HF = e^{-(h_g/h_{GE})}$$

u_A, w_A, a_A are incremental aerodynamic values about trim

θ is incremental pitch attitude about trim.

The subscripts o and T indicate trim and total values respectively.
The subscript I indicates inertial quantity.

TABLE A-11B. FLIGHT CONDITIONS AND LONGITUDINAL STABILITY DERIVATIVES
(ENGLISH UNITS)

γ_{c_0}=65° γ_{CH0}=30 , γ_0 = -7.5°, h=1400 ft

	NOM.	HEAVY	LIGHT	HOT
τ(°c)	15.	15.	15.	33.
W(lb)	43000.	40000.	40000.	43000.
U_0(kt)	72.	72.	66.	75.
γ_0(deg)	4.48	5.686	4.809	6.494
γ_{NO}(deg)	75.	73.	78.	62.
η_H(%)	95.16	94.61	94.57	95.59
X_u(1/s)	- 0.07069	- 0.06769	- 0.07010	- 0.06986
X_w(1/s)	0.09007	0.08907	0.07978	0.09664
$X_{\delta N}$(fps²/rad)	- 6.158	- 6.070	- 6.791	- 4.308
$X_{\eta H}$(fps²/%)	0.04513	0.06145	0.02310	0.1475
$X_{\delta CH}$(fps²/%)	0.003783	0.004499	0.005698	0.005148
Z_u(1/s)	- 0.2617	- 0.2633	- 0.3097	- 0.2775
Z_w(1/s)	- 0.5191	- 0.5131	- 0.5345	- 0.5210
$Z_{\dot{w}}$(1/s)	- 0.013	- 0.012	- 0.014	- 0.013
Z_q(fps²/rps)	- 3.859	- 3.691	- 3.789	- 3.739
$Z_{\delta e}$(fps²/rad)	- 3.575	- 3.411	- 3.296	- 3.545
$Z_{\delta N}$(fps²/rad)	- 1.207	- 1.279	- 0.9198	- 1.736
$Z_{\eta H}$(fps²/%)	- 1.264	- 1.381	- 1.330	- 1.237
$Z_{\delta CH}$(fps²/%)	0.1331	0.1274	0.1347	0.1326
M_u(rps²/fps)	0.001437	0.001218	0.001440	0.001395
M_w(rps²/fps)	- 0.008095	- 0.005837	- 0.006187	- 0.004970
$M_{\dot{w}}$(rps²/fps²)	- 0.0037	- 0.0037	- 0.0037	- 0.0037
M_q(1/s)	- 1.168	- 1.179	- 1.0706	- 1.146
$M_{\delta e}$(1/s²)	- 1.082	- 1.089	- 0.9313	- 1.086
$M_{\delta N}$(1/s²)	- 0.09488	- 0.09509	- 0.1011	- 0.05426
$M_{\eta H}$(rps²/%)	- 0.001219	0.002374	0.001292	0.003447
$M_{\delta CH}$(rps²/%)	0	0	- 0.000238	0
X_{GE}(fps²)	0	0	0	0
$X_{\delta GE}$(fps²/rad)	3.91	3.74	3.532	4.243
Z_{GE}(fps²)	$[-3.185]^{*}_{1.932}$	$[-3.043]_{1.846}$	$[-2.877]_{-1.745}$	$[-3.456]_{-2.096}$
$Z_{\delta GE}$(fps²/rad)	9.22	8.81	8.33	10.00
M_{GE}(rps²)	- 0.0524	- 0.0624	-0.0473	- 0.0569
$M_{\delta GE}$(1/s²)	- 1.064	- 1.064	-0.9638	- 1.158
h_{GE}(ft)	15.	15.	15.	15.

* $Z_{GE} = -3.185e^{-h_G/h_{GE}}$ limited to $Z_{GE} \geq -1.932$

NOTE: All derivatives are in stability axes.

TABLE AIIA FLIGHT CONDITIONS AND LONGITUDINAL STABILITY DERIVATIES

γ_0=-5°, θ_{NO}=30°, γ_0=-7.5°, h=427m

	NOM	HEAVY	LIGHT	HOT
t(°C)	15.	15.	15.	38.
W(N)	191264.	200160.	177320.	191264.
U_0(kt)	72.	72.	66.	75.
α_0 (deg)	4.48	5.686	4.809	6.494
θ_{NO}(deg)	75.	73.	73.	62.
NH (%)	95.16	94.61	94.57	95.59
X_u(1/s)	-0.07069	-0.06769	-0.07010	-0.06986
X_w(1/s)	0.09007	0.08907	0.07978	0.09664
$X_{\delta N}$(m/sec²/rad)	-1.877	-1.851	-2.070	-1.313
X_{NH}(m/sec²/%)	0.01376	0.01873	0.007043	0.04497
$X_{\delta CH}$(m/sec²/%)	0.001153	0.001372	0.001737	0.001570
Z_u(1/s)	-0.2617	-0.2633	-0.3097	-0.2775
Z_w(1/s)	-0.5191	-0.5131	-0.5345	-0.5210
$Z_{\dot{w}}$(1/s)	-0.013	-0.012	-0.014	-0.013
Z_q(m/sec²/rps)	-1.177	-1.125	-1.155	-1.140
$Z_{\delta e}$(m/sec²/rad)	-1.090	-1.040	-1.005	-1.081
$Z_{\delta N}$(m/sec²/rad)	-0.3680	-0.3899	-0.2804	-0.5293
Z_{NH}(m/sec²/%)	-0.3854	-0.4210	-0.4207	-0.3771
$Z_{\delta CH}$(m/sec²/%)	0.04058	0.03884	0.04107	0.04043
M_u(rps²/m/sec)	0.004713	0.003995	0.004723	0.004576
M_w(rps²/m/sec)	0.02655	-0.01915	-0.02029	0.01630
$M_{\dot{w}}$(rps²/m/sec)	-0.0121	-0.0121	-0.0121	-0.0121
M_q(1/s)	-1.168	-1.179	-1.0706	-1.146
$M_{\delta e}$(1/s²)	-1.082	-1.089	-0.9313	-1.086
$M_{\delta N}$(1/s²)	-0.09488	-0.09509	-0.1011	-0.05426
M_{NH}(rps²/%)	-0.001219	0.002874	0.001292	0.003447
$M_{\delta CH}$(rps²/%)	0	0	-0.000238	0
X_{GE}(m/sec²)	0	0	0	0
$X_{\alpha GE}$(m/sec²/rad)	1.192	1.140	1.077	1.294
Z_{GE}(m/sec²)	[-0.971]* -0.589	[-0.928] -0.563	[-0.877] -0.532	[-1.054] -0.639
$Z_{\alpha GE}$(m/sec²/rad)	2.81	2.69	2.54	3.05
M_{GE} (rps²)	-0.0524	-0.0524	-0.0473	-0.0569
$M_{\alpha GE}$(1/s²)	-1.164	-1.164	-0.9638	-1.153
h_{GE}(m)	4.573	4.573	4.573	4.573

*Z_{GE} = $-0.971e^{-h/b_{GE}}$ Limited to Z_{GE}= -0.589

NOTE: All derivatives are in stability axes.

TABLE A-III. LATERAL DIRECTIONAL EQUATIONS OF MOTION

$$U_o \cdot \dot{\beta} = Y_p \cdot P_A + \alpha_o \cdot U_o \cdot p + Y_r \cdot r_A - U_o \cdot r + Y_\beta \cdot \beta_A + g\cos\theta_o \cdot \phi$$

$$+ Y_{\delta R} \cdot \delta_R + Y_{\delta A} \cdot \delta_A + Y_{\delta SP} \delta_{SP} + Y_{\delta CH} \cdot \delta_{CH}$$

$$\dot{p} = L_p \cdot P_A + \frac{I_{xz}}{I_x} \cdot \dot{r} + L_r \cdot r_A + L_{\dot{\beta}} \cdot \dot{\beta} + L_\beta \cdot \beta_A$$

$$+ L_{\delta R} \cdot \delta_R + L_{\delta A} \cdot \delta_A + L_{\delta SP} \cdot \delta_{SP} + L_{\delta CH} \cdot \delta_{CH}$$

$$\dot{r} = N_p \cdot p_A + \frac{I_{xz}}{I_z} \cdot \dot{p} + N_r \cdot r_A + N_\beta \cdot \beta + N_\beta \cdot \beta_A$$

$$+ N_{\delta R} \cdot \delta_R + N_{\delta A} \cdot \delta_A + N_{\delta SP} \cdot \delta_{SP} + N_{\delta CH} \cdot \delta_{CH}$$

$$\begin{bmatrix} p \\ r \end{bmatrix}_B = \begin{bmatrix} \cos\alpha_o & -\sin\alpha_o \\ \sin\alpha_o & \cos\alpha_o \end{bmatrix} \begin{bmatrix} p \\ r \end{bmatrix}_S \quad \text{Body axes rates}$$

$$\dot{\phi} = p_B + \tan\theta_o \cdot r_B \quad \text{Euler rates}$$

$$\dot{\psi} = r_B$$

$$a_y = U_o (\dot{\beta} + r_B) - g\phi \quad \text{Lateral acceleration}$$

$$\dot{Y}_R = \cos\Delta\psi \cdot (a_y + g\phi) \quad \text{Runway crosstrack acceleration}$$

$$\beta_A = \beta + \beta_{WIND}$$

$$\Delta\psi = \psi - \psi_{RUNWAY}$$

δ_A, δ_{SP}, and δ_{CH} indicate differential deflections, with chokes given in %.

The A and o subscripts denote aerodynamic and trim quantities respectively.
The B subscript denotes body axes quantities.
The subscript I indicates inertial quantity.

TABLE A-IV. LATERAL DIRECTIONAL STABILITY DERIVATIVES

Parameter	Units	Nominal Flight Condition	Fast Flight Condition
U_o	m/sec (kts)	33.5 (65.)	36.0 (70.)
α_o	rad (deg)	.0906 (5.19)	.0541 (3.1)
RPM		91.0	90.8
I_X	kg-m^2 (slug-ft^2)	352448. (259950.)	355227. (262000.)
I_Z	kg-m^2 (slug-ft^2)	603412. (445050.)	601175. (443400.)
I_{XZ}	kg-m^2 (slug-ft^2)	26642. (19650.)	35712. (26340.)
Y_p/U_o		-.0141	-.0136
Y_r/U_o		.0236	.0240
Y_β/U_o	1/sec	-.1216	-.124
L_p	1/sec	-.612	-.6504
L_r	1/sec	.363	.842
L_β	1/sec	-.0068	-.0089
$L_{\dot\beta}$	1/sec^2	0.0	0.0
N_p	1/sec	-.2064	-.1907
N_r	1/sec	-.285	-.256
N_β	1/sec	.0255	.0272
$N_{\dot\beta}$	1/sec^2	.510	.596
$Y_{\delta R}/U_o$	1/sec	.0593	.064
$L_{\delta R}$	1/sec^2	.206	.293
$N_{\delta R}$	1/sec^2	-.7754	-.895
$Y_{\delta A}/U_o$	1/sec	-.0052	-.0055
$L_{\delta A}$	1/sec^2	.695	.677
$N_{\delta A}$	1/sec^2	-.060	-.060
$Y_{\delta SP}/U_o$	1/sec	-.0095	-.010
$L_{\delta SP}$	1/sec^2	.280	.321
$N_{\delta SP}$	1/sec^2	-.0058	0.0
$Y_{\delta CH}/U_o$	1/sec^2-%	-.0000559	-.0000524
$L_{\delta CH}$	1/sec^2-%	.00428	.00337
$N_{\delta CH}$	1/sec^2-%	.000063	.00014

NOTE: 1. All derivatives and inertias are given in stability axes.
2. All angles are in radians unless otherwise noted.

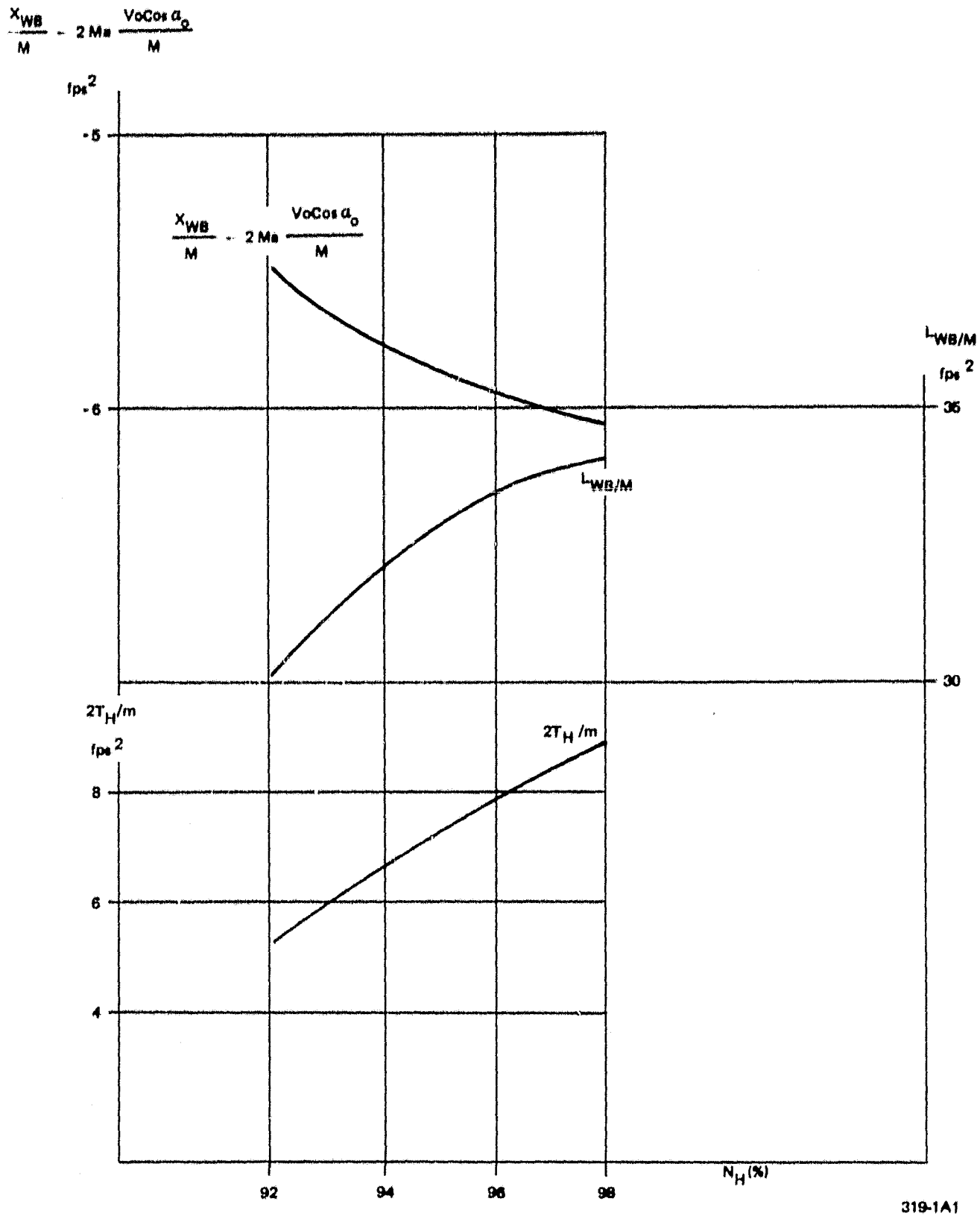

FIGURE A-1. VARIATION OF PROPULSIVE FORCES WITH ENGINE RPM

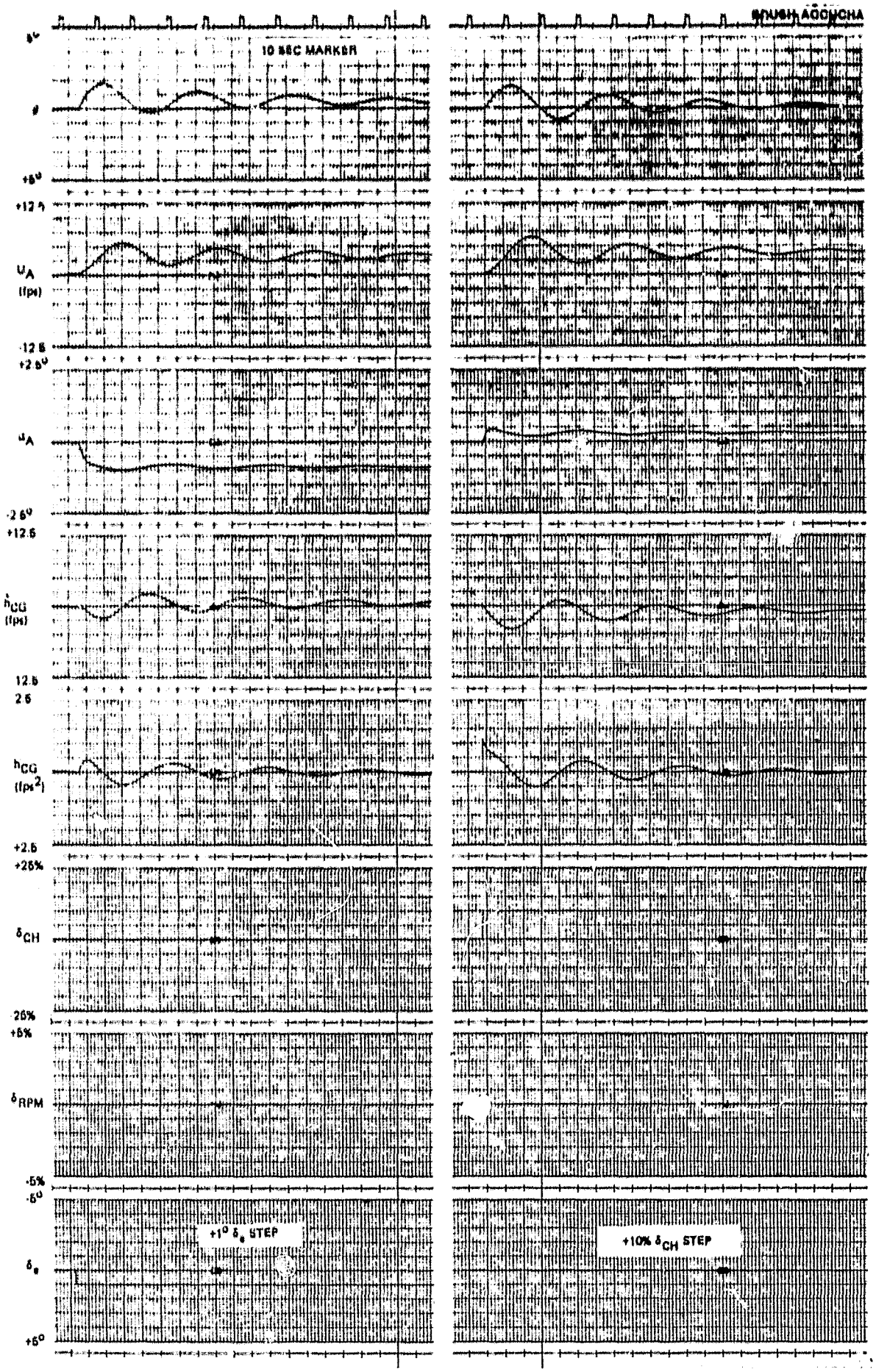

FIGURE A-2 LONGITUDINAL AIRFRAME STEP RESPONSES

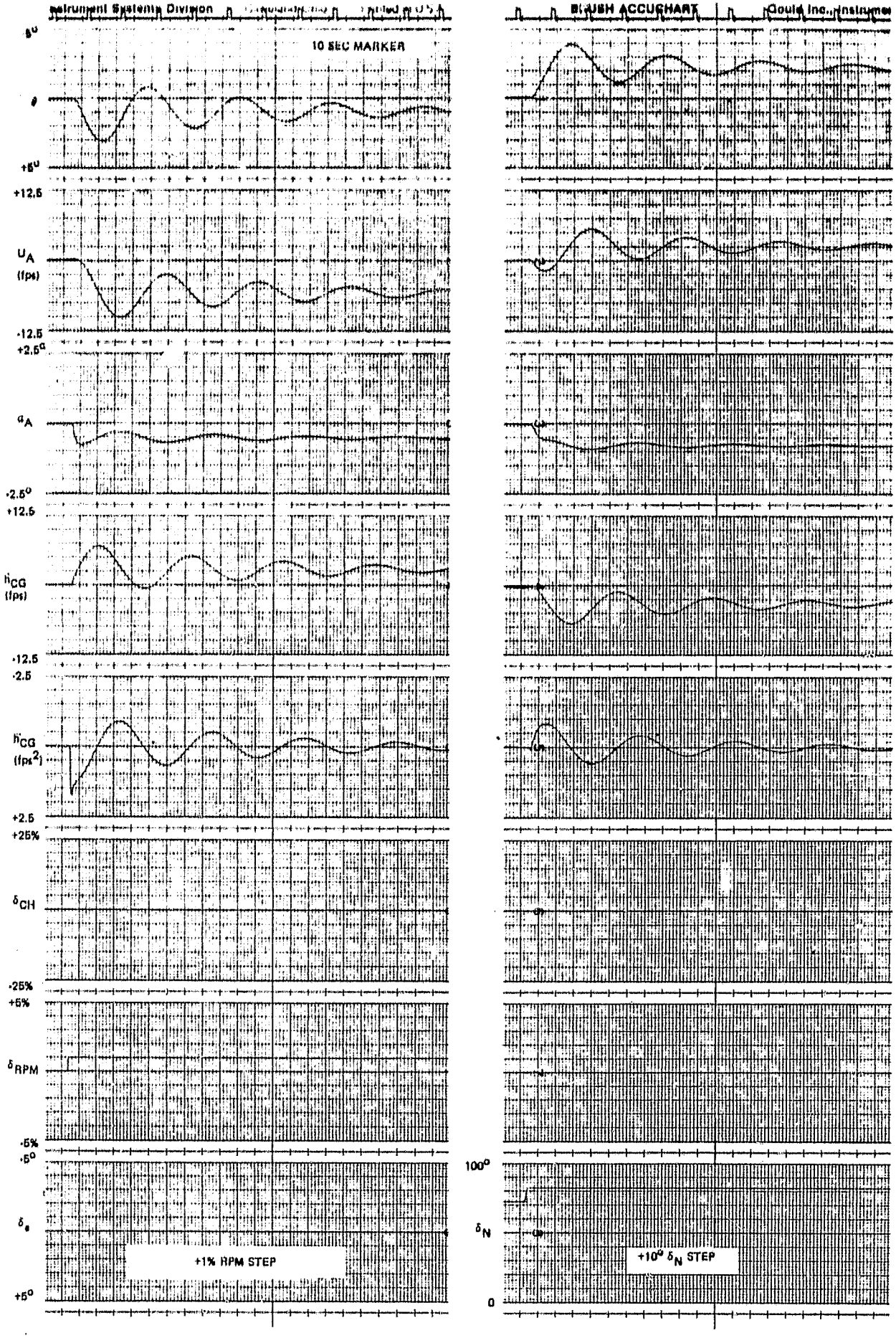

FIGURE A-3. LONGITUDINAL AIRFRAME STEP RESPONSES

Aug Wing 26 March 80

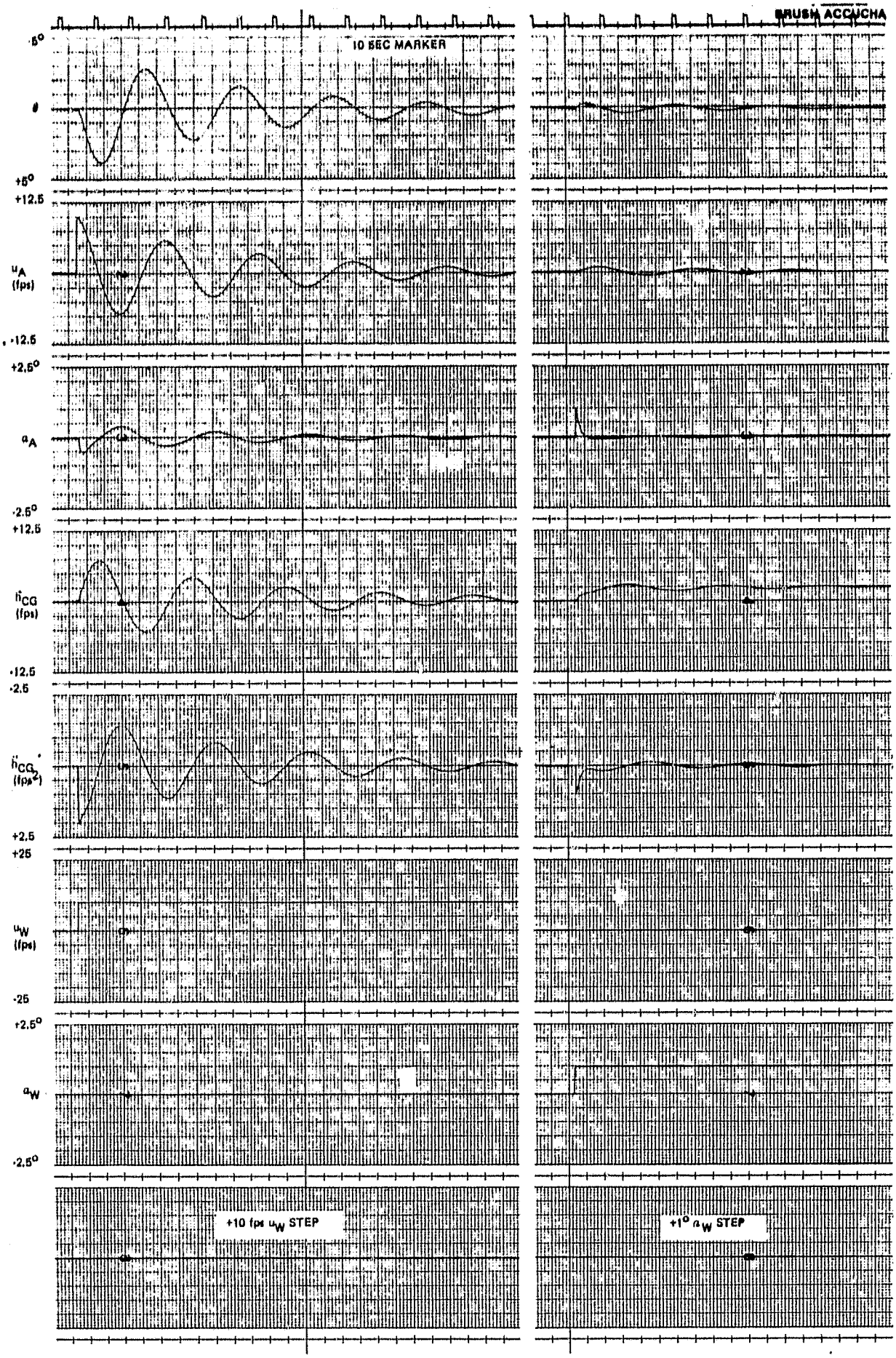

FIGURE A-4. FREE AIRFRAME RESPONSES, STEP GUST

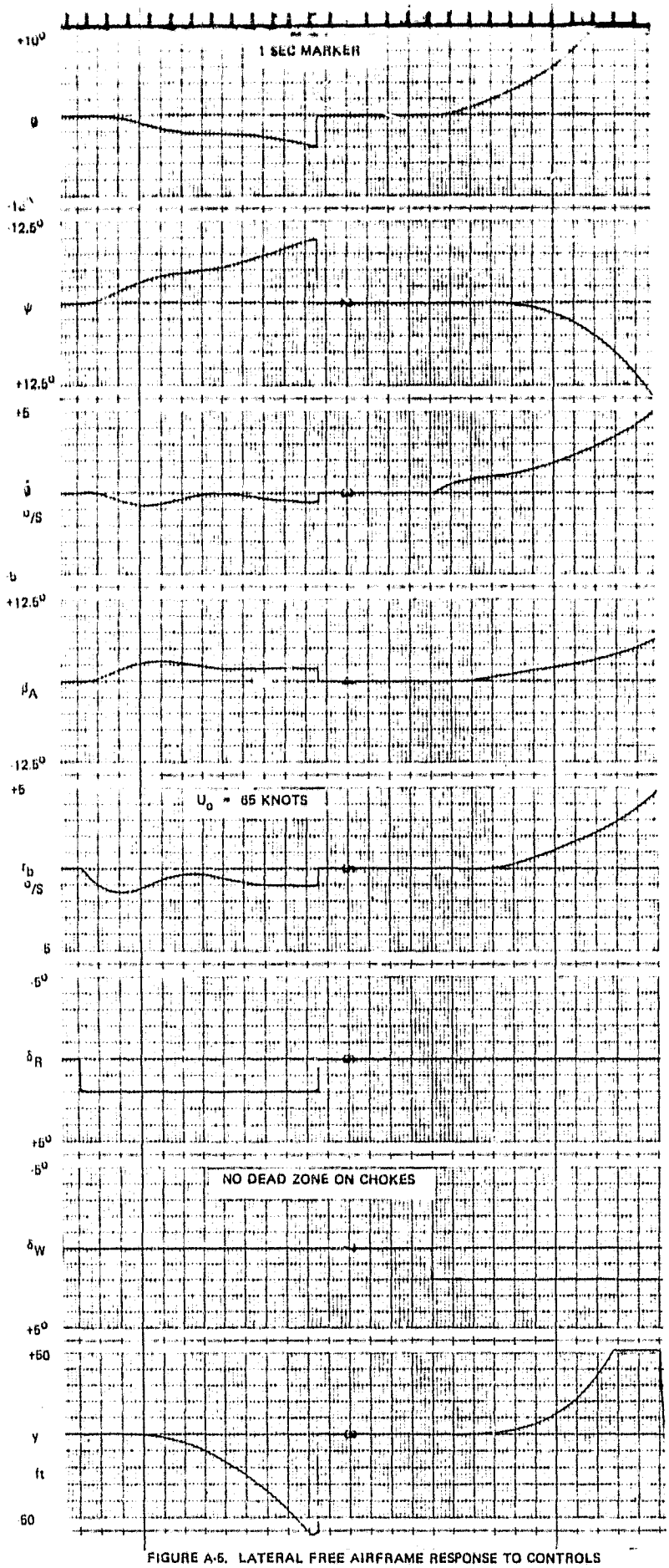

FIGURE A-5. LATERAL FREE AIRFRAME RESPONSE TO CONTROLS

AUG WING 1 MAR 79

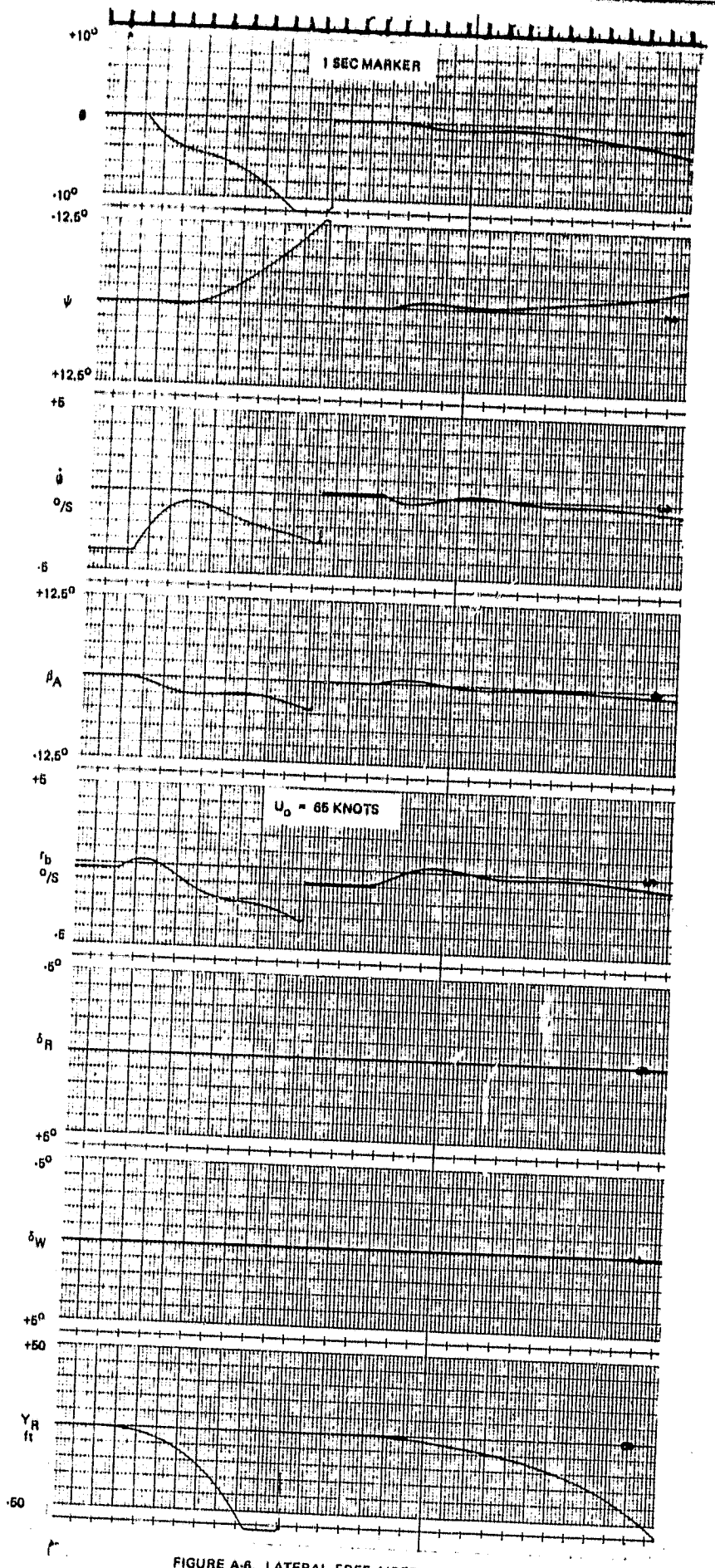

FIGURE A-6. LATERAL FREE AIRFRAME RESPONSE TO I.C.

A-2 Control System Dynamics

The engine is the main flight path controller in this airplane and as a result, landing performance turned out to be sensitive to the details of the engine dynamics model. Therefore, a model as accuracte as practically possible was used and is described here.

For the other controllers, control surface aerodynamic and inertia loads were sufficiently small that acceleration limits and detailed actuator models were not required. Thus only important nonlinearities as hysteresis and rate and position limits were included in this study. The simplified actuator models are described in this section.

A-2.1 Longitudinal Control System

The details of the throttle servo were defined in the longitudinal control law block diagram of Figure 4-1. The engine model is based on Reference 10 and is shown in Figure A-7. The model includes throttle hysteresis, different time constants for power increase or reduction and separate paths for the high speed rotor RPM and low speed rotor RPM. This is a simplified model which is valid for the 92% to 98% N_H speed region at which the engine operates during the STOL approach. Figure A-8 shows throttle and RPM responses to throttle command steps with throttle loop gains that were computed to produce a second order overall response with a natural frequency of 2 rps and a damping ratio of 0.7 and with no throttle hysteresis.

The elevator, choke, and nozzle actuator models are presented as Figure A-9. Spoilers and flaps were not used as control elements in longitudinal landing studies. A 30% choke bias is used, to give a ±0.1 g direct lift capability.

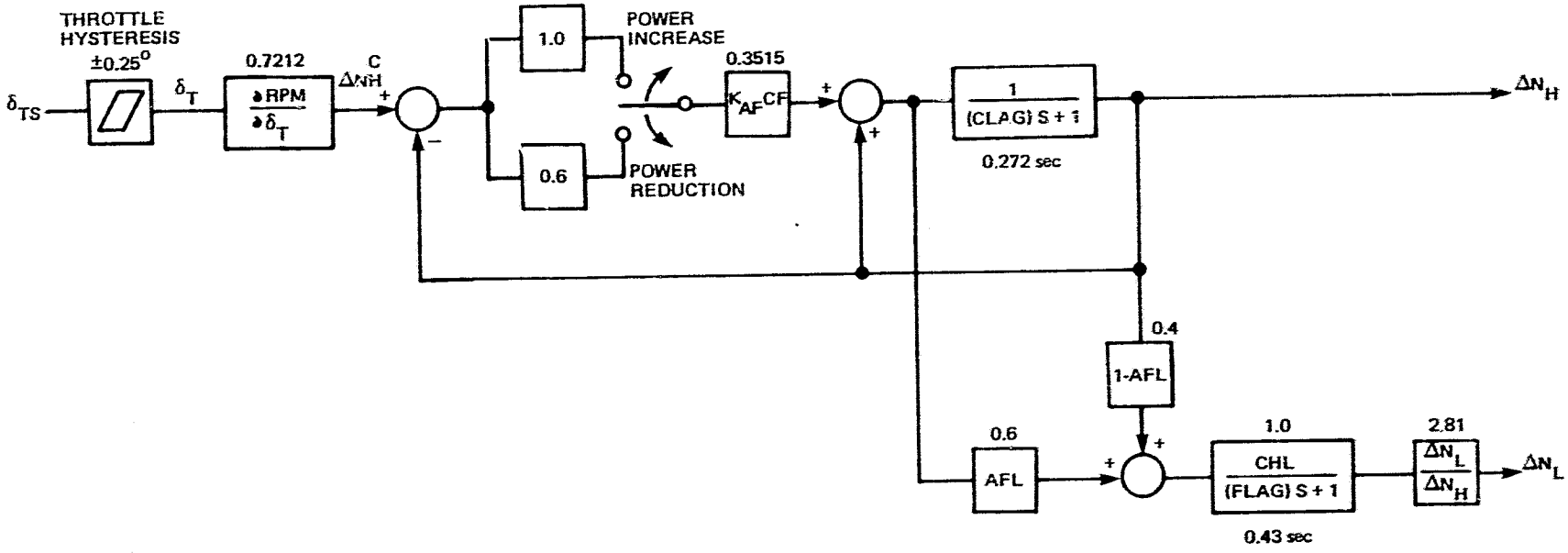

FIGURE A-7. ENGINE MODEL BLOCK DIAGRAM

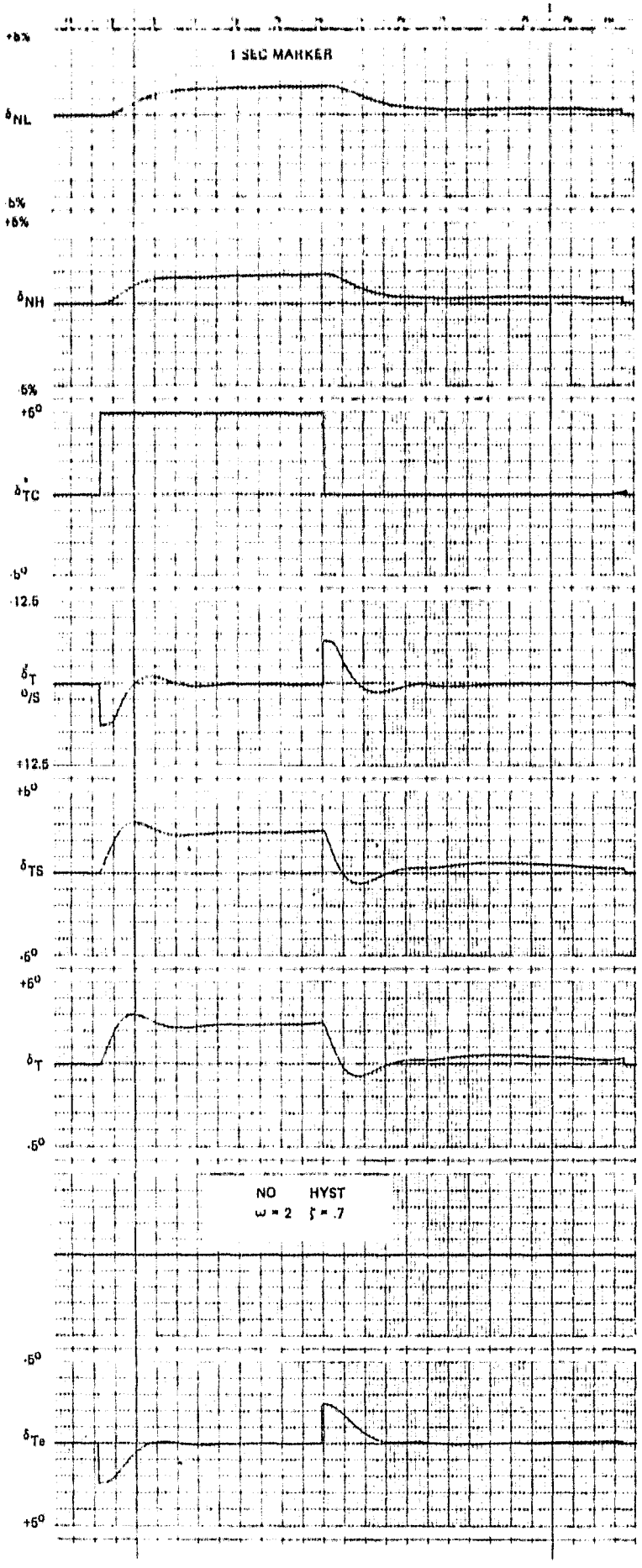

FIGURE A-8. THROTTLE STEP RESPONSES

AJG WINC 17 July 79

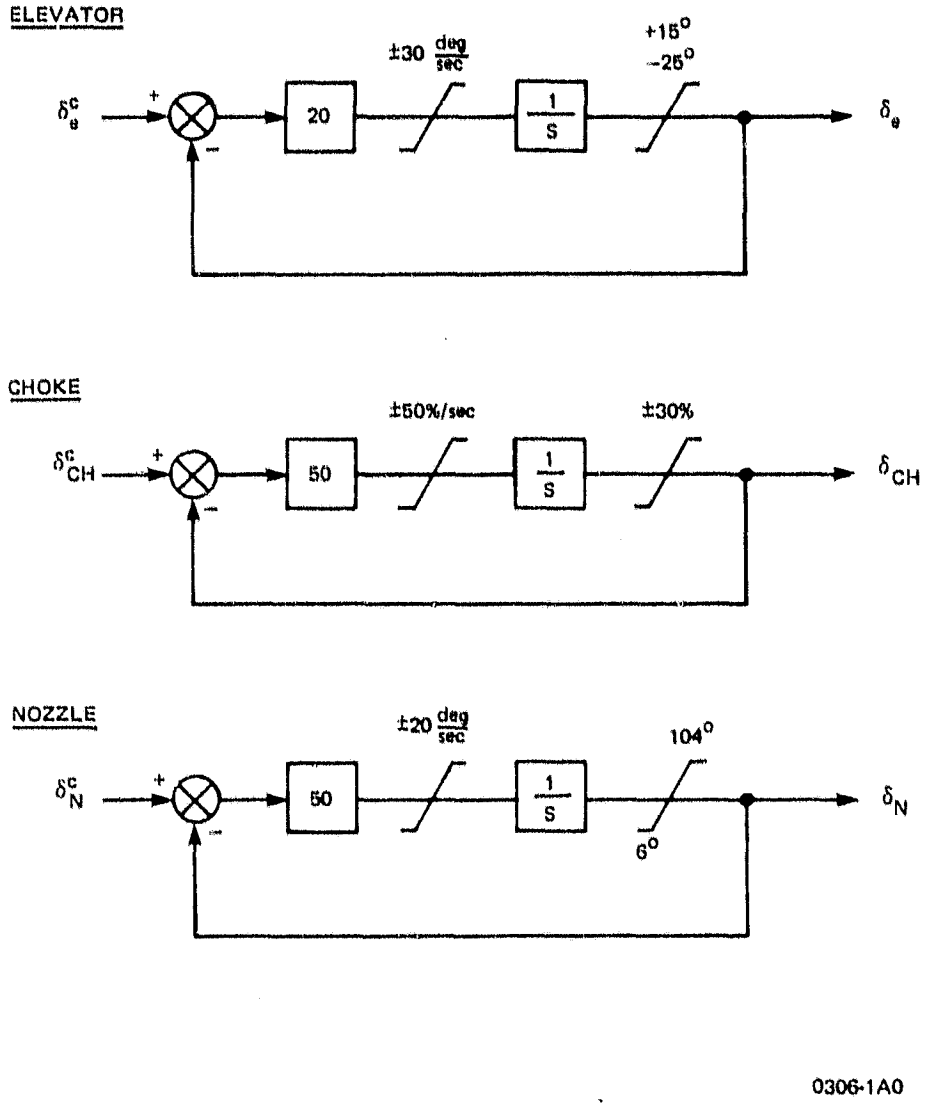

0306-1A0

FIGURE A-9. LONGITUDINAL ACTUATOR MODELS

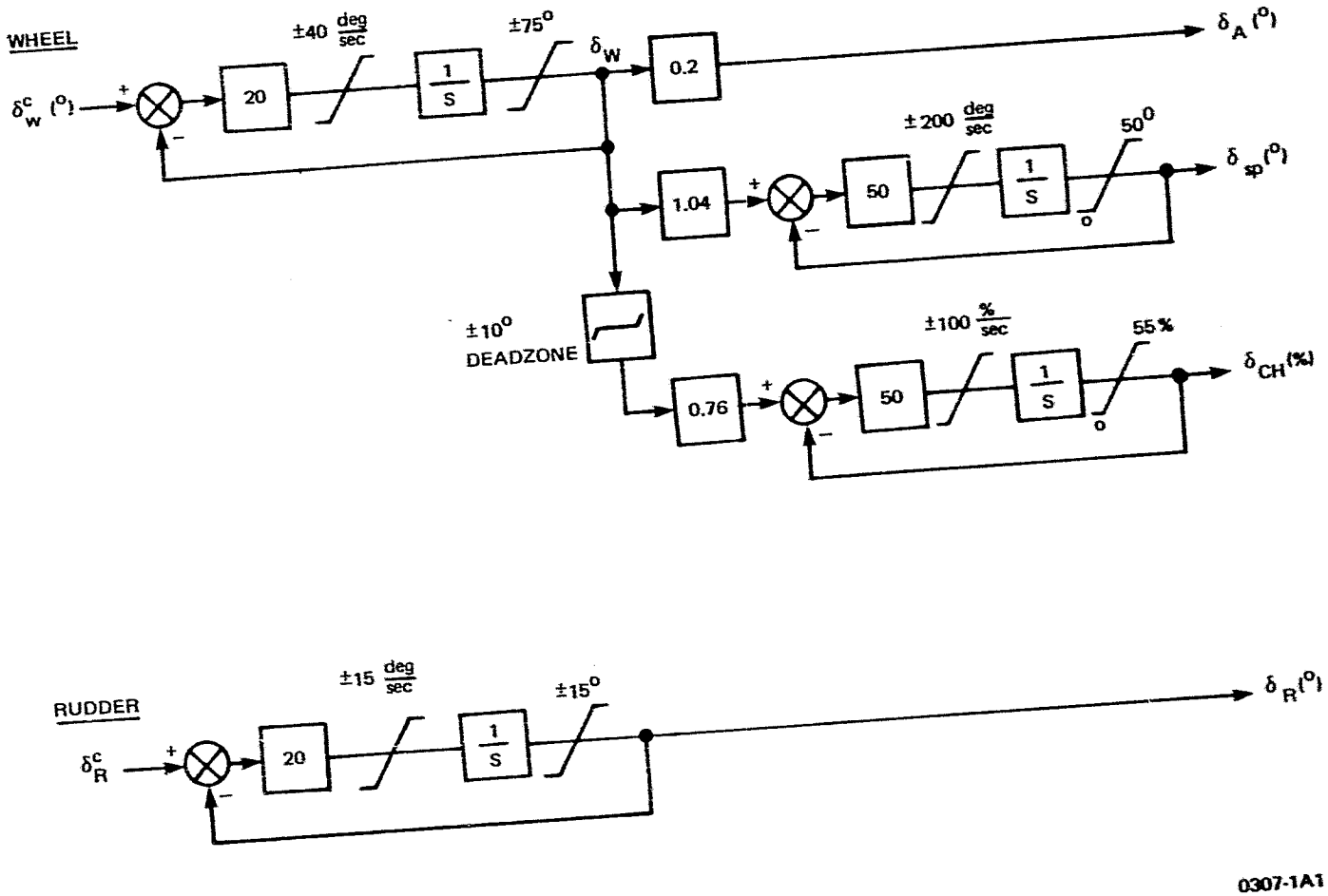

FIGURE A-10. LATERAL-DIRECTIONAL ACTUATOR MODELS

A-2.2 Lateral/Directional Control System

The wheel, rudder, aileron, spoiler, and choke models are shown in Figure A-10, along with the roll control nonlinearities. The spoiler and choke actuator dynamics were omitted during these simulation studies with negligible loss of fidelity since the wheel actuator dynamics and limits are more constraining.

A-3 Geometry and Sensors

A-3.1 Sensor Geometry

The relative geometry of the gear, c.g., and MLS antenna are illustrated in Figure A-11. The gear and MLS receiver location are expressed in terms of cg height above the runway by the expressions:

$$h_G = h_{cg} - Z_G \cos\theta + X_G \sin\theta \qquad X_{REC} = 7.62\text{m (25.0 ft)}$$

$$h_{REC} = h_{cg} - Z_{REC} \cos\theta + X_{REC} \sin\theta \qquad Z_{REC} = 1.524\text{m (5.0 ft)}$$

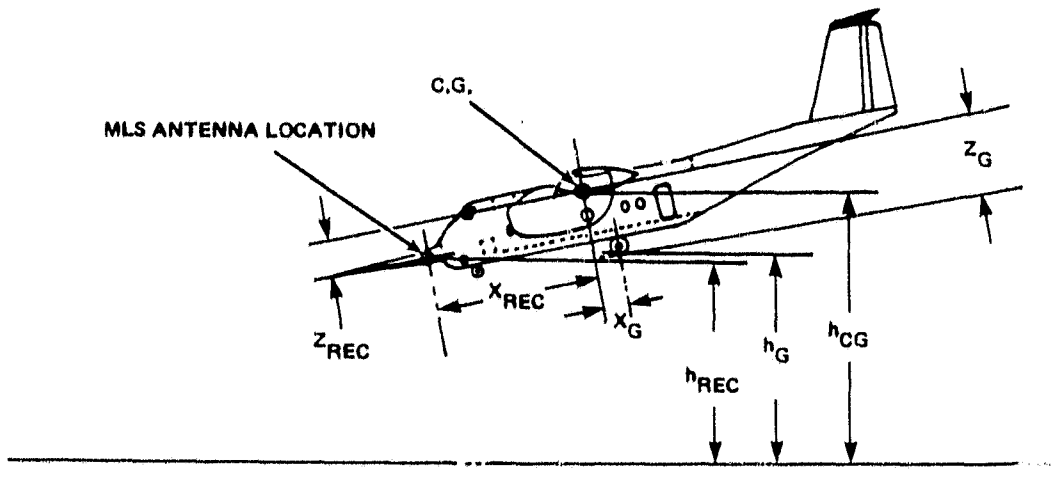

317-1A1

FIGURE A-11. AIRPLANE GEOMETRY

The three axis accelerometers are located near the cg. Since offset location corrections are included in the acceleration signal processing, the sensors were assumed to be cg mounted for this study. The radar altimeter antennas are located very near the gear fuselage station and calibrated for the gear length. The rate gyros were assumed to be oriented with the fuselage reference line. Barometric altitude and rate are not used in the landing control laws and thus were not included in the simulation.

A-3.2 Physical Data

The weight, inertia, and dimensions of the Aug Wing vehicle in landing configuration are given in Table A-V. The gear geometry is also presented. This geometry defines the following absolute touchdown constraints for the Aug Wing vehicle:

$\theta_{min} = -1^{o}$ $\quad \theta_{MAX} = +15.1^{o}$ gear compressed $\quad \phi_{MAX_{\text{gear compressed}}} = 28^{o}$

$= +17.0^{o}$ gear extended

A-3.3 Sensor Models

Only those sensors whose dynamics or errors impact landing performance are discussed in this section. Also, only the errors which affect landing performance are included - e.g. accelerometer biases are not included since the signals are complementary filtered and therefore biases are washed out. The properties of the sensors which impact landing performance are summarized in Table A-VI.

Although MLS yields discrete information at 5 scans per second for elevation 1 and azimuth guidance, and 40 per second for DME, we used continuous position inputs were used during these studies. During the previous glide slope and localizer track MLS studies reported in Reference A-3, it was determined that these update rates provided control activity and landing performance identical to a continuous guidance signal, especially if beam filtering is used. Although continuous

TABLE A-V. PHYSICAL DATA FOR LANDING CONFIGURATION

GEAR GEOMETRY

	NOSE	RIGHT	LEFT
X_G	7.285 (23.9)	-1.183 (-3.88)	-1.183 (-3.88)
Y_G	0.0	4.648 (15.25)	-4.648 (-15.25)
Z_G	3.383 (11.1)	3.383 (11.1)	3.383 (11.1)
$Z_{Compression}$	.253 (0.83)	.311 (1.02)	.311 (1.02)

AIRCRAFT DIMENSIONS

W	177929 N	(40,000. lb)
I_X	359295 Kg $-m^2$	(265,000. slug-ft^2)
I_Y	280656 Kg $-m^2$	(207,000. slug-ft^2)
I_Z	596565 Kg $-m^2$	(440,000. slug-ft^2)
I_{XZ}	48810 Kg $-m^2$	(36,000. slug-ft^2)
S_{wing}	80.36m^2	(865. ft^2)
$S_{Hor.Tail}$	21.65m^2	(233. ft^2)
$S_{Vert. Tail}$	14.12m^2	(152. ft^2)
b	24.00 m	(78.75 ft)
$\bar{C}$	3.78 m	(12.4 ft)
FSCG	866.65 cm.	(341.2 in)
WLCG	454.66 cm.	(179.0 in)

NOTE; Gear Geometry is expressed in meters (feet).

TABLE A-VI. SENSOR CHARACTERISTICS

Sensor	Dynamics	Errors
Radar Altimeter	$\frac{1}{.1S + 1}$	Bias - ±1.03 m (3.4 ft)
GS/LOC Receiver	$\frac{1}{.1S + 1}$	Figure A-12
Vertical Gyro		Verticality - ± .6°
		False erection - ±1.0°
Accelerometers		Cross axis sensitivity .01
Course Datum		Equivalent Bias - ±4.0°

NOTE: All errors are given as 4.5 σ values.

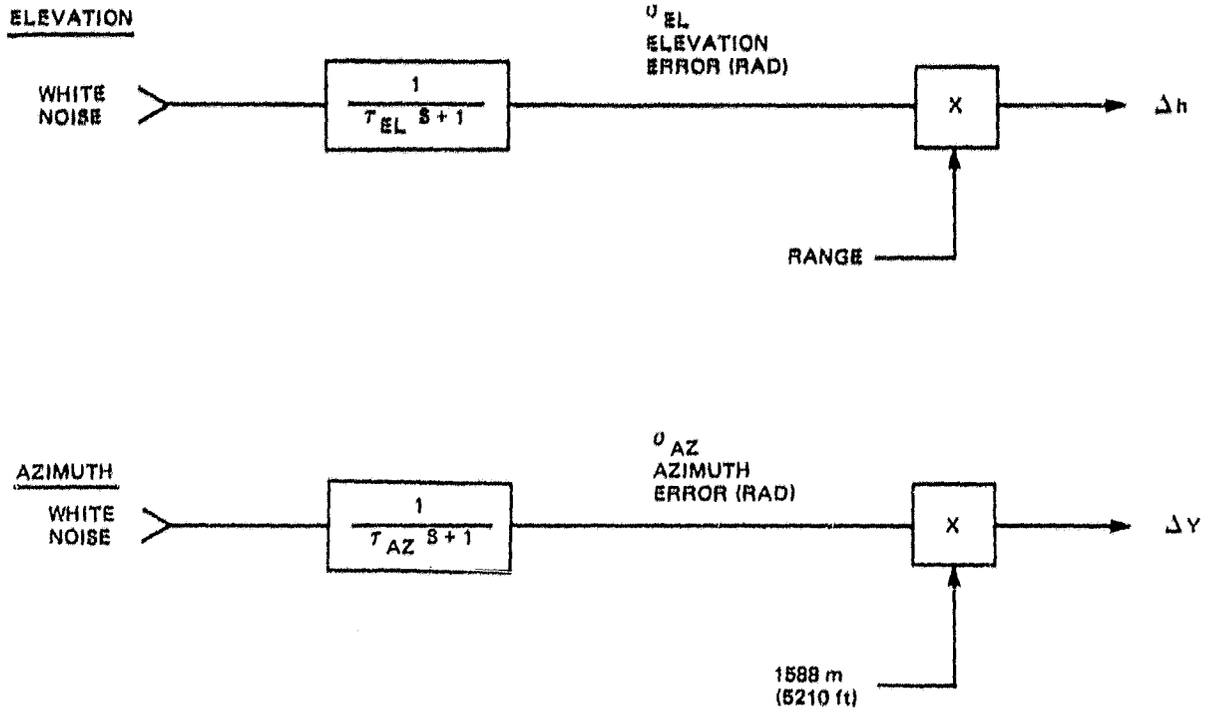

	τ	σ NOISE	σ BIAS
ELEVATION	0.5 sec	0.0625°	0.0375°
AZIMUTH	0.5 sec	0.105°	0.0935°
DME	0.5 sec	12.2m (40.0 ft)	15.2m (50.0 ft)

0308-1A1

FIGURE A-12. MLS ERROR MODELS

position signals were used to limit simulation complexity, the actual MLS error models defined below were included to maintain fidelity in the results.

A-4 MLS Disturbance Models

In this study MLS error models were used with data obtained from NASA. The azimuth, elevation, and DME error amplitudes and spectral characteristics are given in Figure A-12. It should be noted that the effect of DME inaccuracies is small with respect to the angular errors during the final approach.

A-5 Atmospheric Disturbance Models

A standard atmospheric disturbance model, patterned after the FAA wind model of AC-20-57A (Reference 4), was used for the bulk of the simulation work done in these landing studies. Some data were also taken with a vertical turbulence model patterned after the British Civil Aviation Authority (CAA). Both these models are described here. Data were also taken with non-standard deterministic wind shears and these, along with the results, are described in Section 5.2.1.

A-5.1 Standard Wind Model

The basic wind model used for approach and landing is closely patterned after the standard FAA wind model specified in AC-20-57A (Reference 4) and described more fully in Reference 1 and 2. The total wind level also determines the turbulence amplitudes, while the shear corresponds to the headwind and crosswind components. A summary of the standard wind model is shown as Figure A-13.

For this study, winds were assumed to be in earth local level axes and transformed into aircraft axes. Probability distribution curves that were plotted for the total atmospheric environment were computed assuming a 70% probability of encountering a 25 knot shearing headwind and a 30% probability of encountering a 10 knot shearing tailwind. Random turbulence with an intensity of 3.73 knot (6.3 fps) RMS for the horizontal and lateral components and 1.5 knots (2.54 fps) RMS for the vertical component was used as the design condition. No pitch rate gusts were used, since their effects are negligibly small compared to horizontal and vertical turbulence. Uncorrelated white noise generators were used for longitudinal, lateral, vertical, and roll rate gusts.

A-5.2 CAA Vertical Turbulence Model

The same Dryden model is used as with the FAA vertical turbulence model, but the scale length in the CAA model is a function of altitude rather than a constant. Also, the intensity of the CAA vertical turbulence is proportional to the total wind speed as shown in Table A-VII. In this study, a total wind velocity of 25 knots was used, resulting in a CAA vertical turbulence intensity of 2.25 knots.

TABLE A-VII VERTICAL TURBULENCE MODEL COMPARISON

	FAA	CAA
L_w m (ft)	9.15 (30)	$0.5\Delta h$ for $9.15 \underset{(30)}{<} h \underset{(1000)}{<} 305$
		4.57 (15) for $h < \underset{(30)}{9.15}$
σ_w kt	1.5	0.09 WINDV

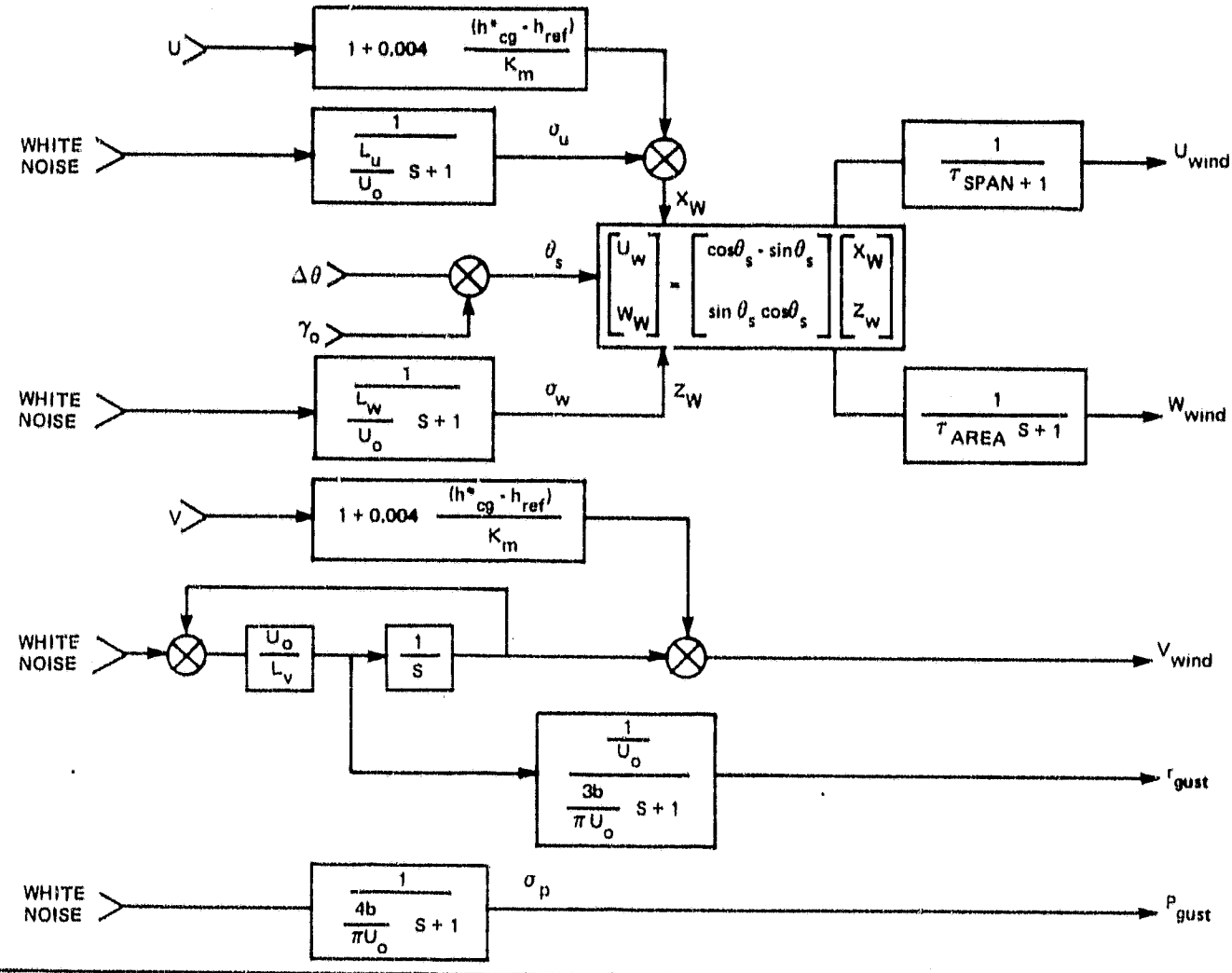

	U	V	W	P
$L_{(SCALE\ LENGTH)}$	182.88m (600 ft)	182.88m (600 ft)	9.14m (30 ft)	———
$\tau_{SPAN, AREA}$	$\frac{27.65K_m}{U_o}$	———	$\frac{17.78K_m}{U_o}$	———
σ	0.15WINDV	0.15V	$0.773\frac{m}{sec}$ (1.5 kt)	$.00853\frac{\sigma_w}{K_m}\frac{RAD}{sec}$
Mean Wind Limit	+12.88 +25kt -5.15 m/sec -10kt	± 7.73 m/sec (± 15kt)	———	———
Prob of Exceedance	1%	4.5%	———	———

h_{cg} = CG Height (200 ft maximum)

h_{ref} = Wind Reference Altitude = 7.62m (25 ft)

K_M = Metric Constant = 0.34m (1.0 ft) for metric (English) units

b = Wing Span = 19.81m (65 ft)

U_o = Approach speed = 38.61m/sec (126.7 fps)

U = Down Wind Speed; V = Crosswind Speed; WINDV = Total Wind Speed (25 kt Limit)

0309-1A1

FIGURE A-13. WIND AND TURBULENCE MODEL

A-5.3 Altitude Profiles for Lateral Landings

Since the time between align initiate and touchdown can have a significant impact on landing performance, the effect of longitudinal winds and shears on lateral performance was included in the simulation.

A simplified flare model was constructed, with the altitude trajectory varying with inertial velocity and flare time constant in a manner very similar to the actual pitch approach and flare control system. The altitude profile generator block diagram is given as Figure A-14, with sample profiles for limiting headwind and tailwind shown in Figure A-15.

This altitude trajectory is used to drive the sidewind shear and the align model, and to indicate touchdown. Thus the proper relationship is maintained between altitude and time for all downwind conditions to allow realistic determination of lateral landing performance.

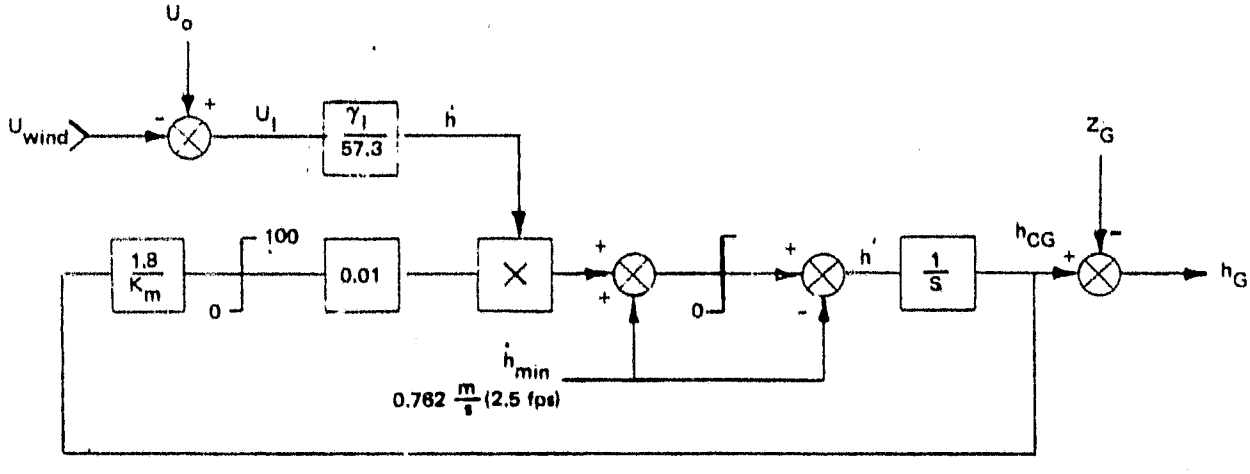

K_m = metric constant = 0.3048 (1.0) for metric (English) units.
Z_G = 3.383m (11.1 ft)

FIGURE A-14. ALTITUDE PROFILE GENERATION

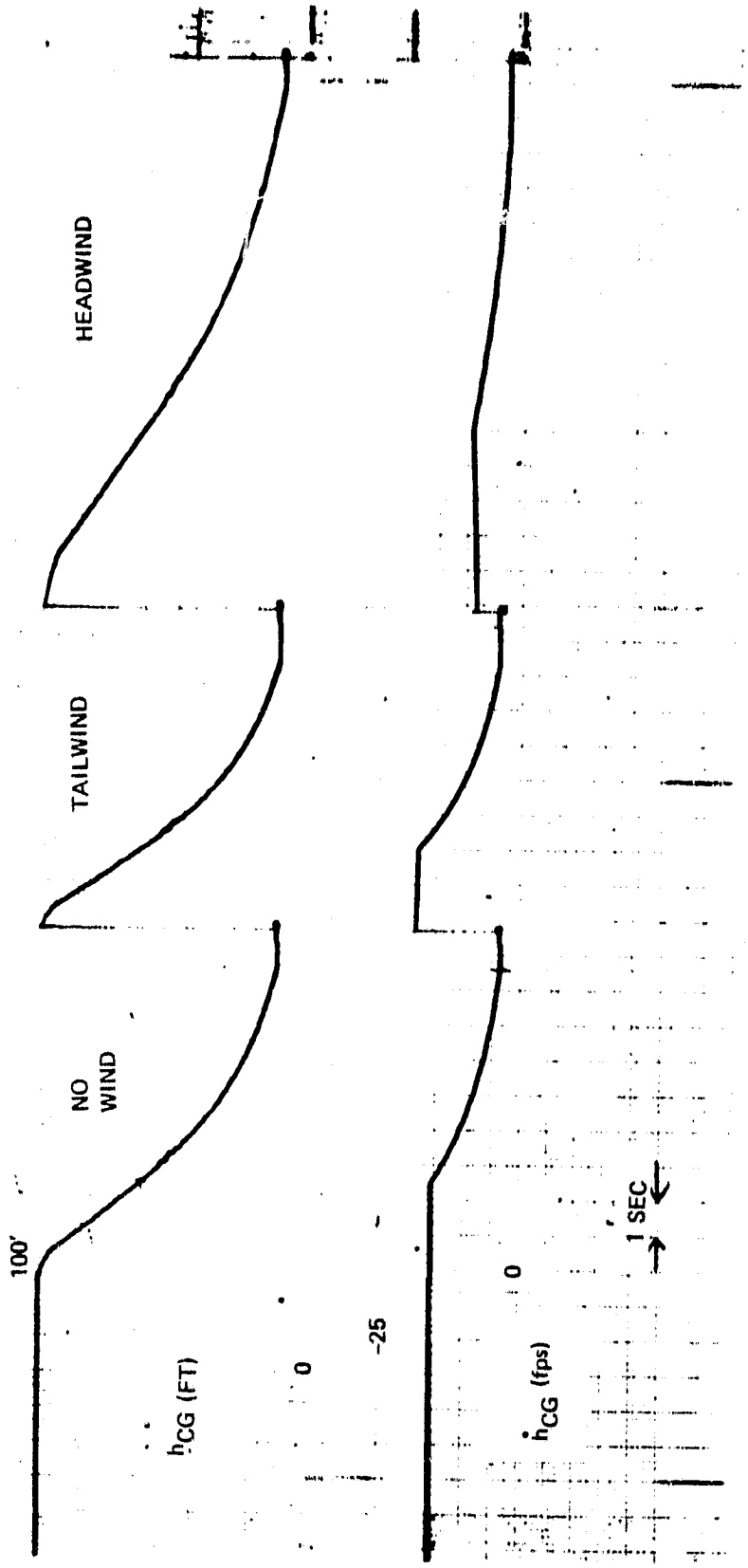

FIGURE A-15. TYPICAL ALTITUDE PROFILES

APPENDIX B

SUPPLEMENTARY SIMULATION DATA

LIST OF FIGURES

Landing Performance Summaries

Landing Time Histories

*See explanation in Section 5.4.3

Probability Distributions

APPENDIX B

SUPPLEMENTARY SIMULATION DATA

This Appendix contains landing performance summaries, landing time histories and probability distributions from which the results presented in the main body of the report were drawn. The material given here was mainly used in Sections 5 and 7.

Figures B-1 and 2 are landing performance summaries showing the effects of headwind and turbulence on landing dispersions for the four controls configuration. Similar results with the three controls configuration were included as Figures 5-5 and 5-6 in Section 5.2.2. Similarly, the effects of weight and temperature on landing performance with the three controls configuration are shown in Figures 5-7 and 5-8 in Section 5.3, whereas the equivalent data for the four controls configuration is given here as Figures B-3 and B-4.

Figures B-5 through B-20 are landing time histories. Landing time histories of the four controls configuration with the standard deterministic winds and shears is given in Section 5.1, Figure 5-2. The equivalent time histories for the three and two controls configuration are given here as Figures B-5 and B-6. Figures B-7 through B-10 show the landing time histories with the non-standard wind shear profiles that are discussed in Section 5.2.1. Figures B-11 through B-16 give the landing time histories for the airframe weight and temperature variations that are discussed in Section 5.3. Section 5.4.1 summarizes the effects of throttle command gain variations and Figure B-17 shows landing time histories with reduced throttle command gain. The results of an increased throttle feedback gain, $k_{\delta TF}$, are discussed in Section 5.4.3; landing time histories with the increased value of $k_{\delta TF}$ are given in Figure B-18. Figures B-19 and 20 are landing time histories with an increased touchdown sink-rate command and they supplement Section 5.4.4.

Figures B-21 through B-108 contain the probability distribution curves that were used to obtain the summaries presented in Section 5 and 7 of this report. Figures B-21 through B-32 are the probability distributions obtained with the nominal four, three and two controls configurations. Three curves are given in each figure, labeled "HW", "TW" and "Combined". The headwind curve was obtained with 25 knot shearing headwind, 3.7 knots RMS horizontal turbulence, 1.5 knots RMS vertical turbulence and beam noise. The tailwind curve was obtained with 10 knots shearing tailwind and the same levels of turbulence and beam noise as in the headwind case. The combined curve was obtained by combining the headwind and tailwind curves and associating a 70% occurrence probability with the headwind and 30% with the tailwind. The landing performance summary results that are given in Table 5-II of Section 5.1 are based on these figures. Also, the simulation curves of Figures 7-1 through 7-6 are taken from Figures B-21, 22, 25, 26, 29 and 30.

Probability distributions for the four and three controls configurations (with $k_{\delta TF}$ of 2.53) with various wind and turbulence levels are given in Figures B-33 through B-56. This data was used in Section 5.2. The three curves here were obtained with 25 or 12.5 knots of shearing headwind, as indicated in the list of figures, with zero headwind and with 10 knots of shearing tailwind. Data was taken with 3.7, 1.9 or 0 knots RMS horizontal turbulence as indicated in the list of figures. In each set of runs, one turbulence level was used with all three deterministic wind conditions. Vertical turbulence per the FAA model with an intensity of 1.5 knots RMS was included in most runs as indicated in the list of figures. Beam noise is the only disturbance included in Figures B-49 through B-51 and the CAA vertical turbulence is used in B-52 through B-56.

Probability distributions with weight and temperature variations are given in Figures B-57 through B-80. The summaries presented in Section 5.3, Figures 5-7 and 5-8, as well as Figures B-3 and 4 are based on these probability distributions.

Figures B-81 through B-108 are probability distributions with various system variations. These distributions are the source of the data that is summarized in Section 5.4.

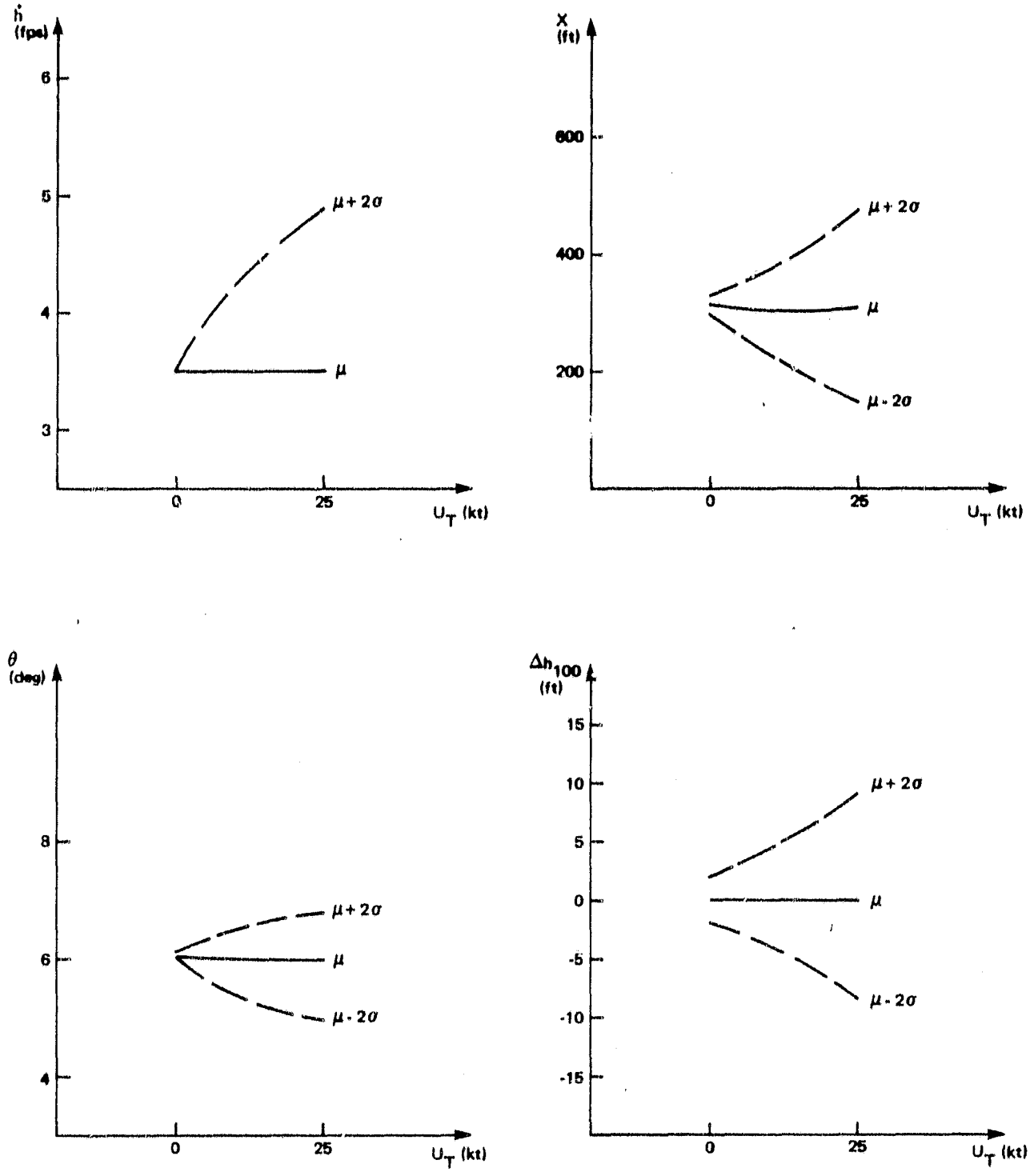

ZERO HEADWIND; TURBULENCE PROPORTIONAL TO U_T

326-1A1

FIGURE B-1. THE EFFECT OF TURBULENCE ON LANDING DISPERSIONS
4 CONTROLS, ($k_{\delta TF}$ = 2.53)

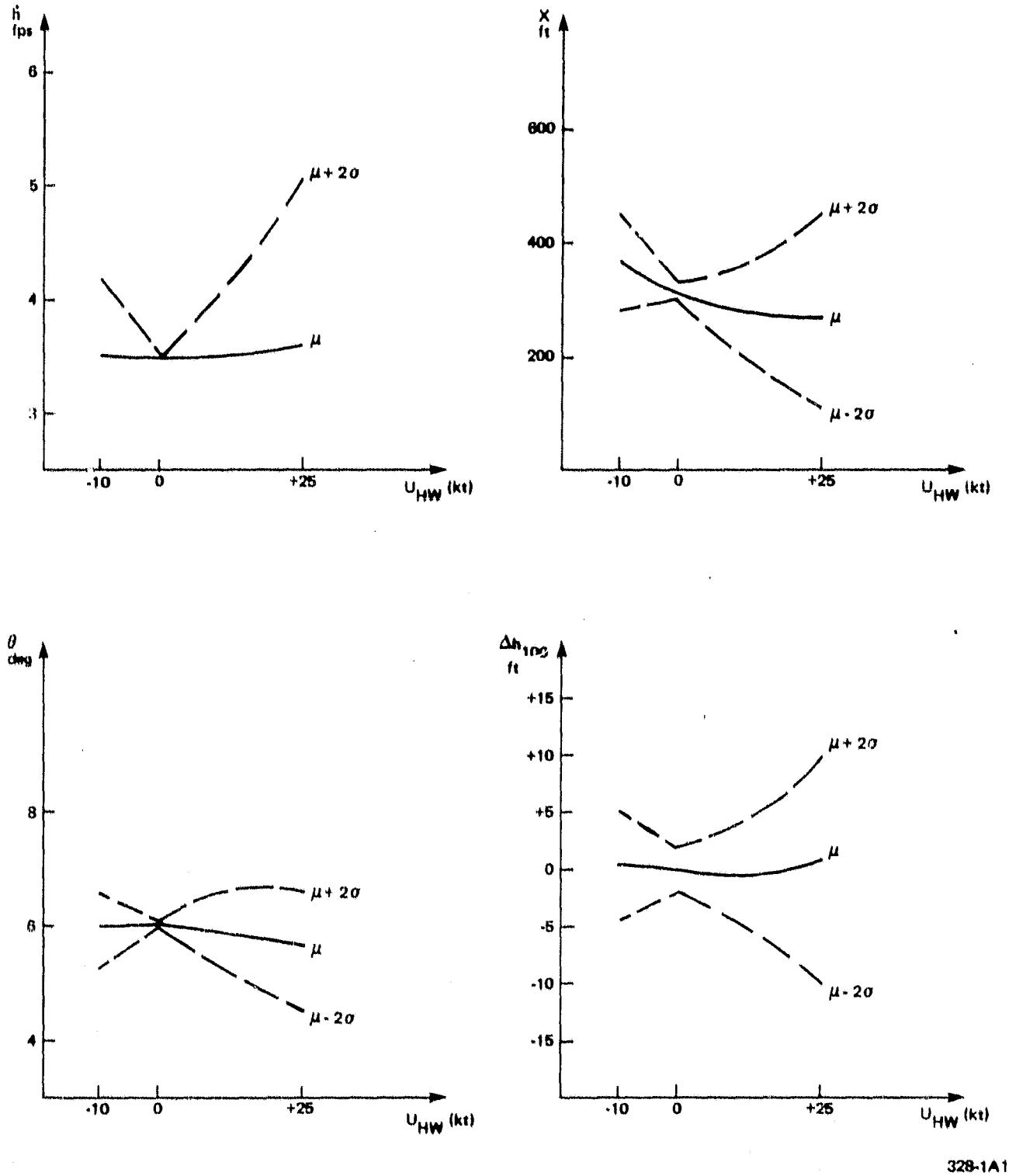

TURBULENCE PROPORTIONAL TO HEADWIND; σ_u = 3.7 kt FOR U_W = 25 kt

FIGURE 8-2. THE EFFECT OF HEADWIND AND TURBULENCE ON LANDING DISPERSIONS
4 CONTROLS, ($k_{\delta TF}$ = 2.53)

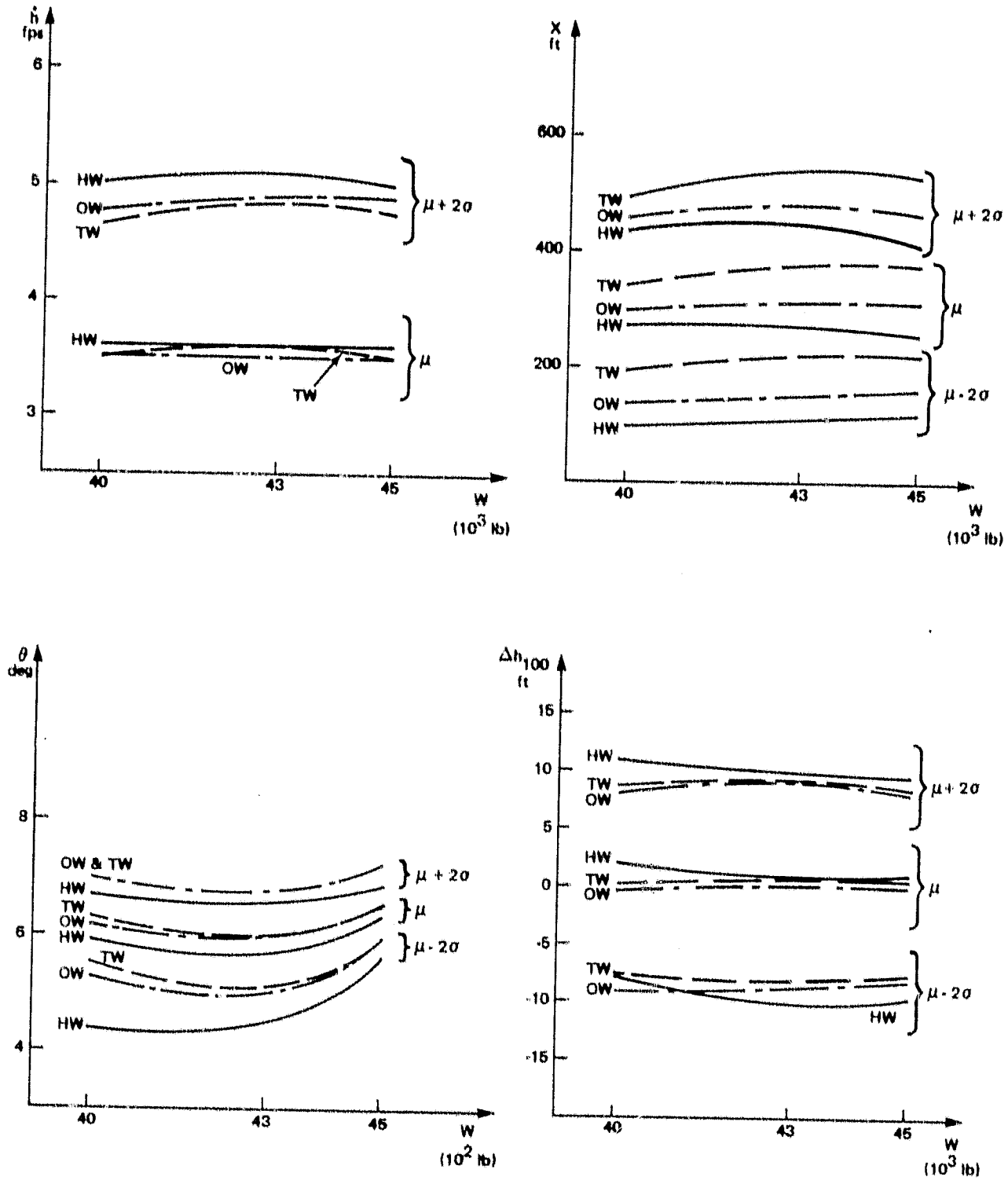

329-1A1

FIGURE B-3. THE EFFECT OF WEIGHT ON LANDING DISPERSIONS
4 CONTROLS ($k_{\delta TF}$ = 2.53)

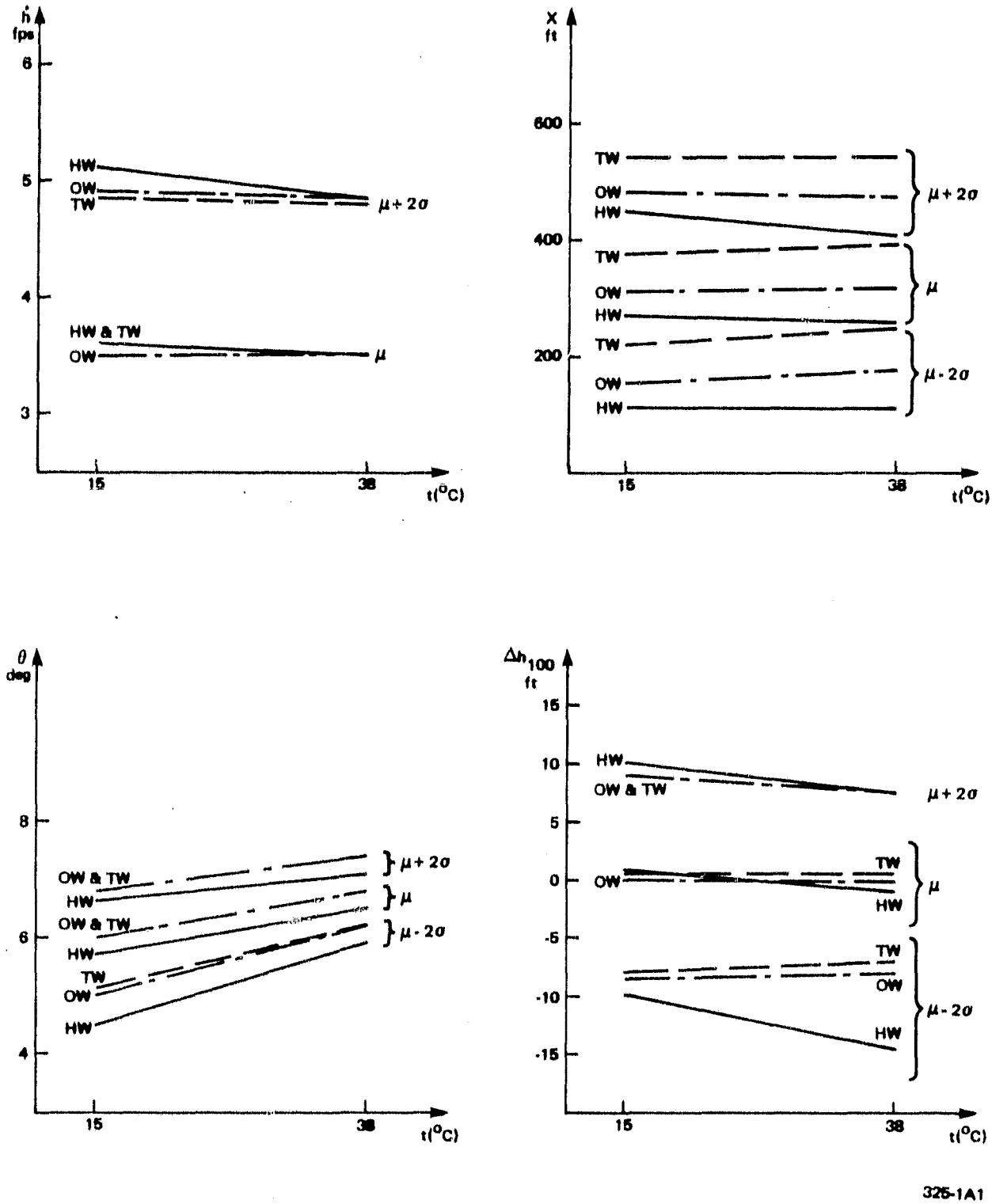

FIGURE B-4. THE EFFECT OF TEMPERATURE ON LANDING DISPERSIONS
4 CONTROLS, ($k_{\delta TF}$ = 2.53)

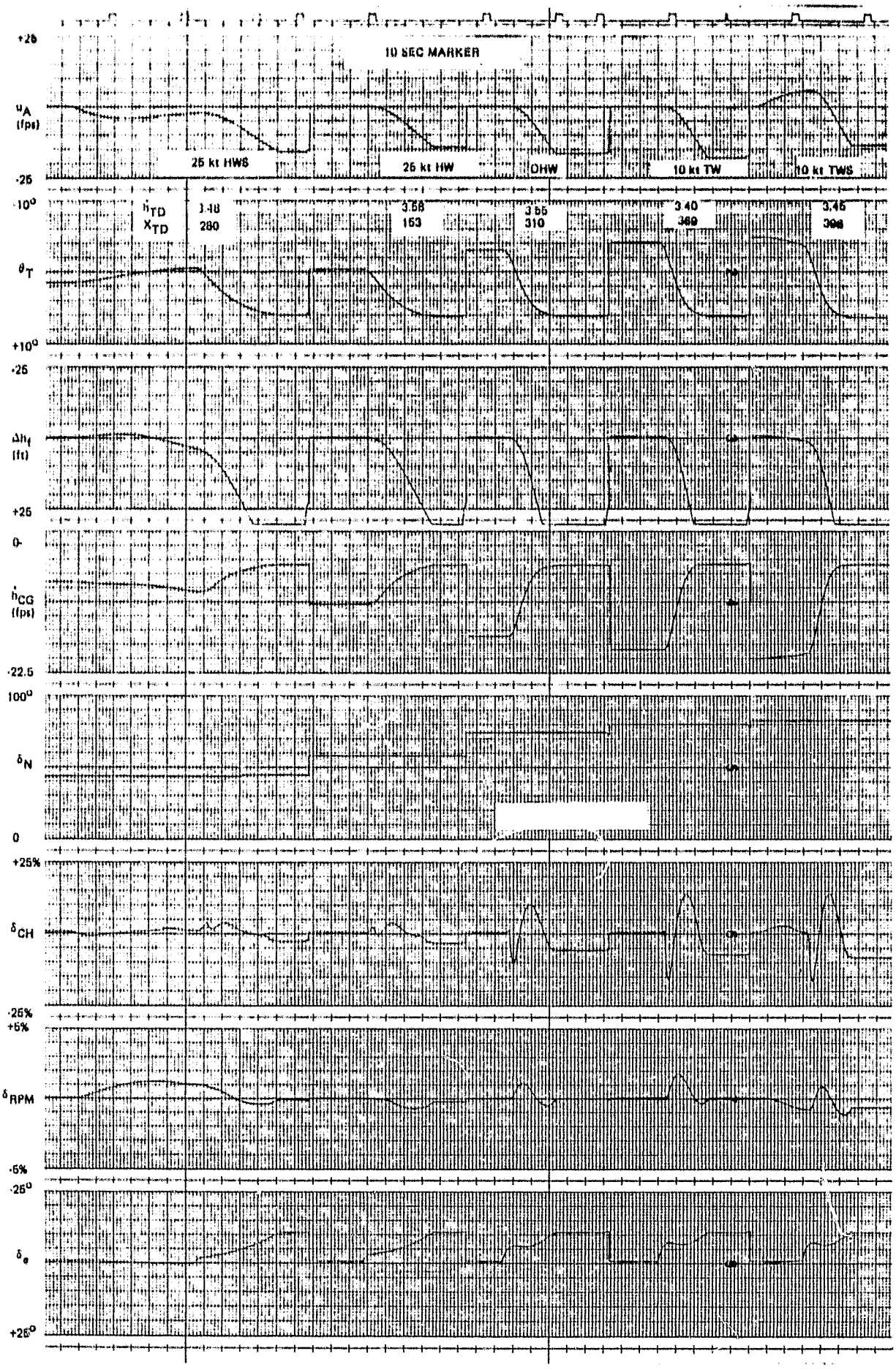

FIGURE B-5. THREE CONTROLS, NOMINAL GAINS

Aug Wing 21 March 80

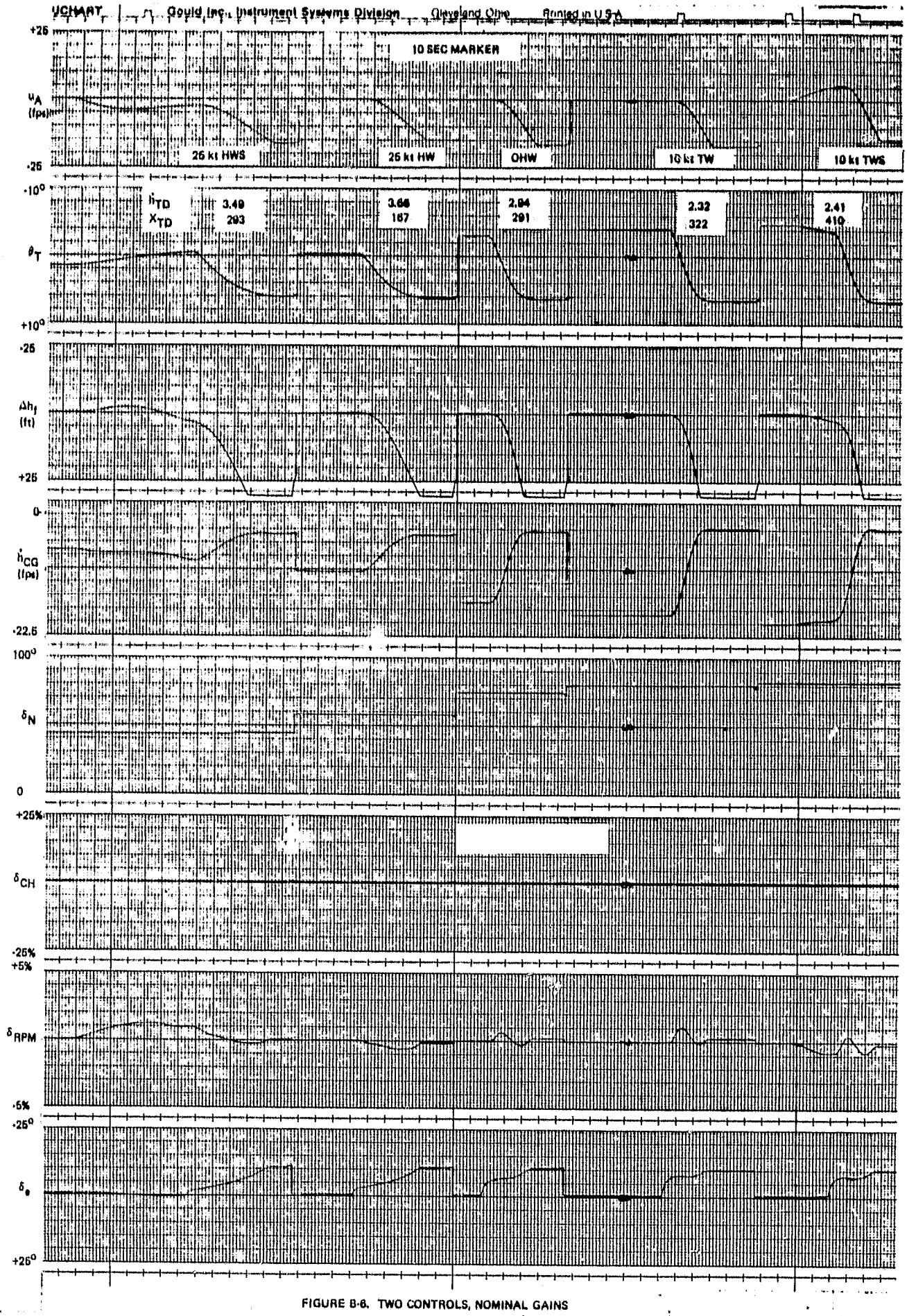

FIGURE 8-6. TWO CONTROLS, NOMINAL GAINS

Aug Wing 21 March 80

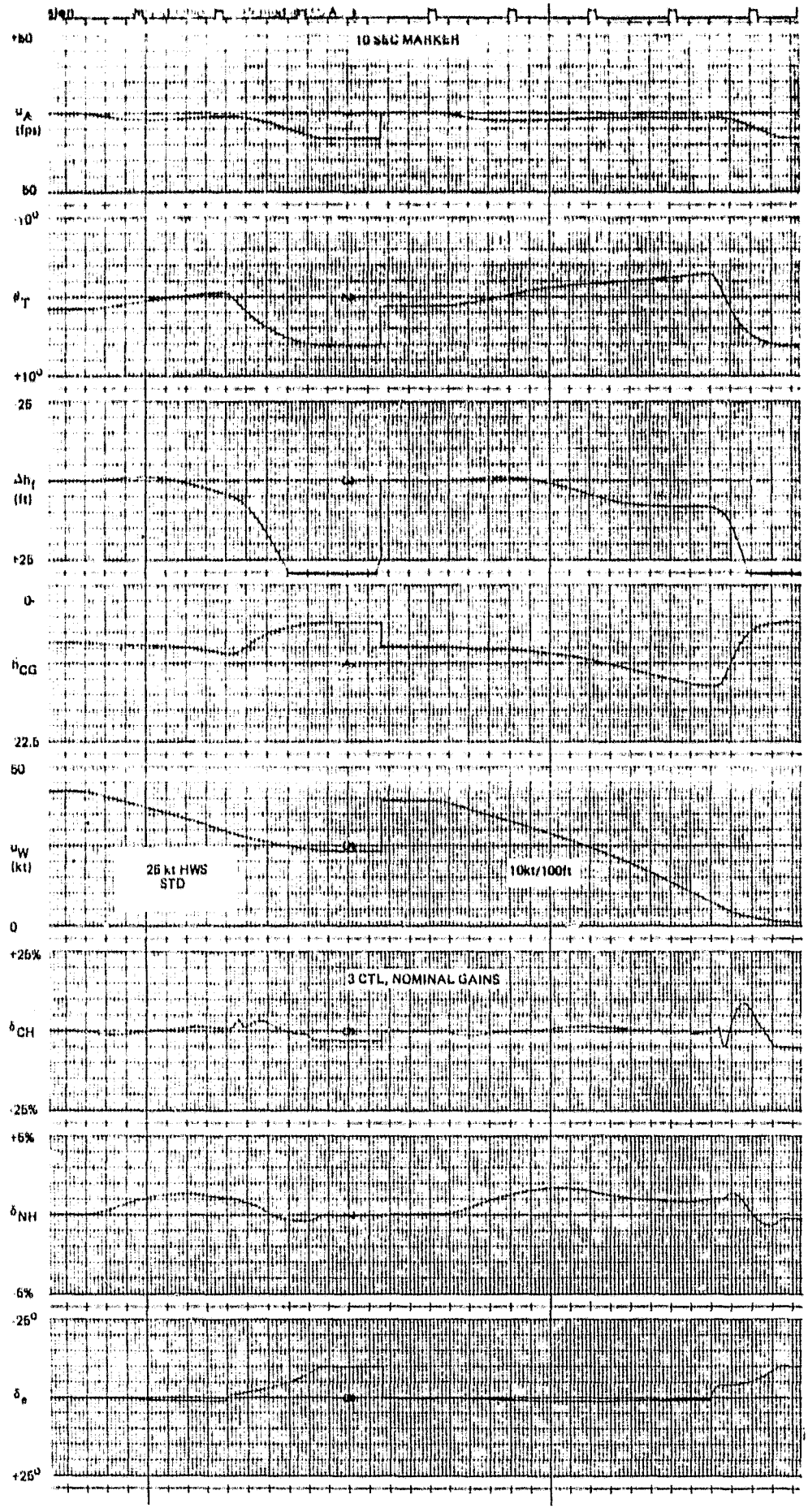

FIGURE 8-7. NONSTANDARD HEADWIND SHEAR PROFILES

AW 23 Feb 80

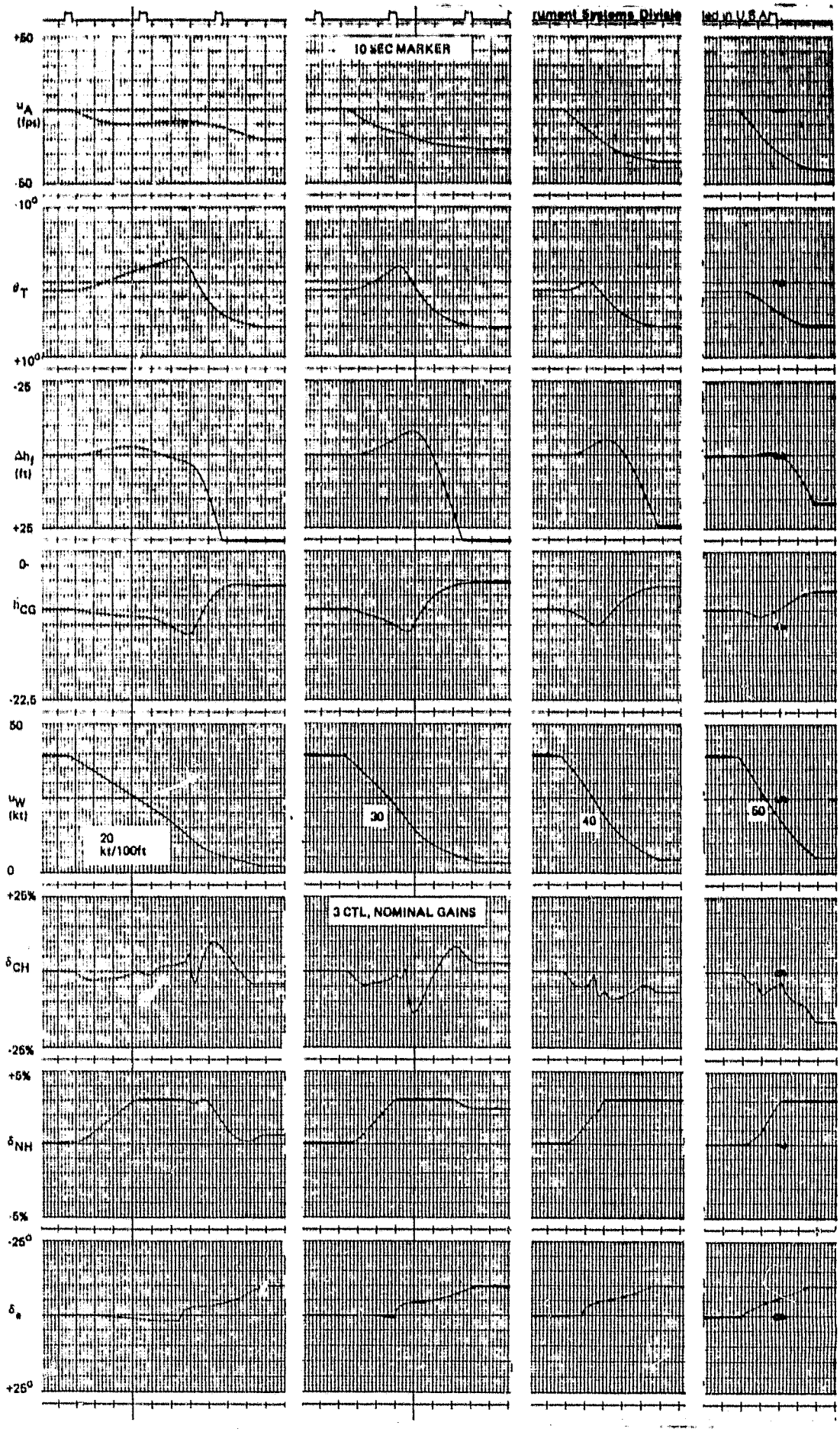

FIGURE B-8. NONSTANDARD HEADWIND SHEAR PROFILES

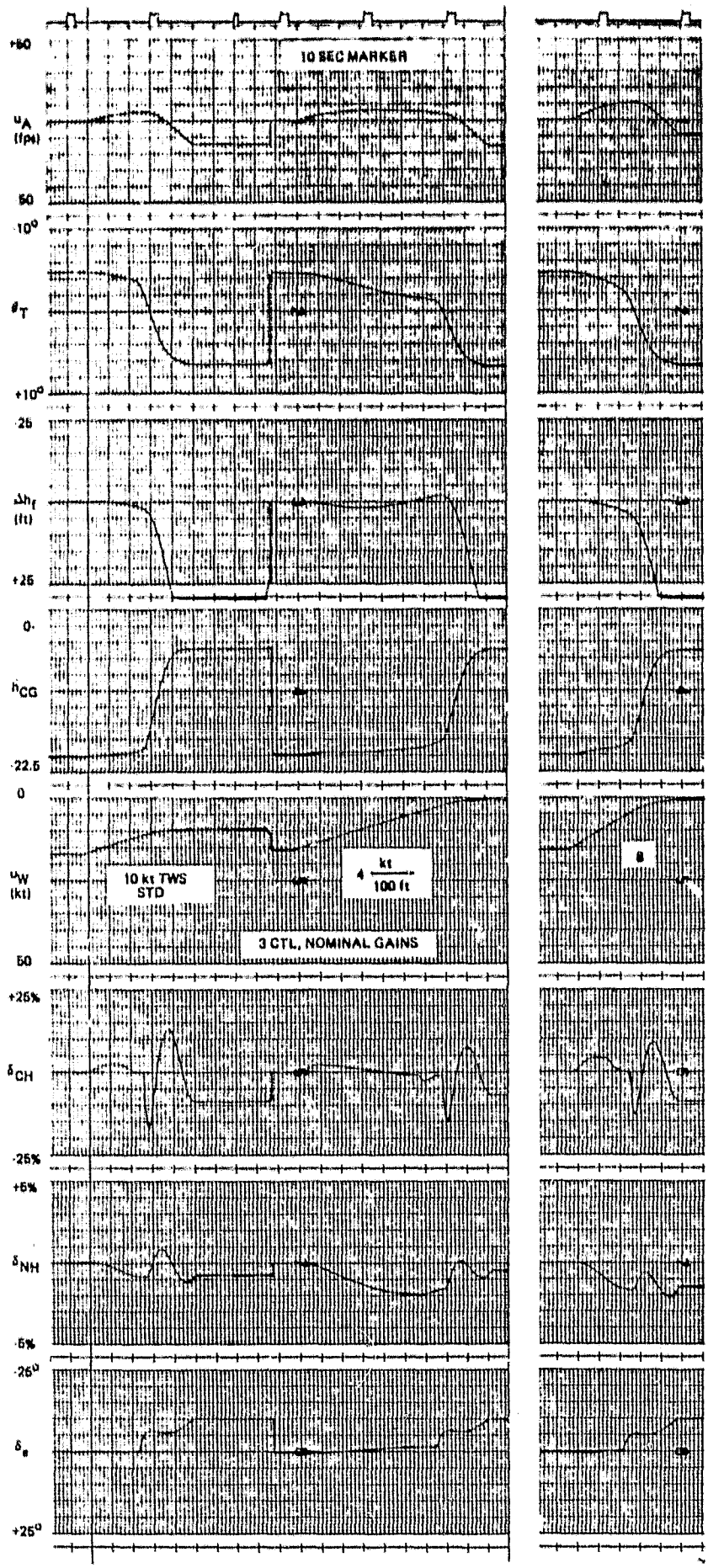

FIGURE 8-9. NONSTANDARD TAILWIND SHEAR PROFILES

AW 23 Feb 80

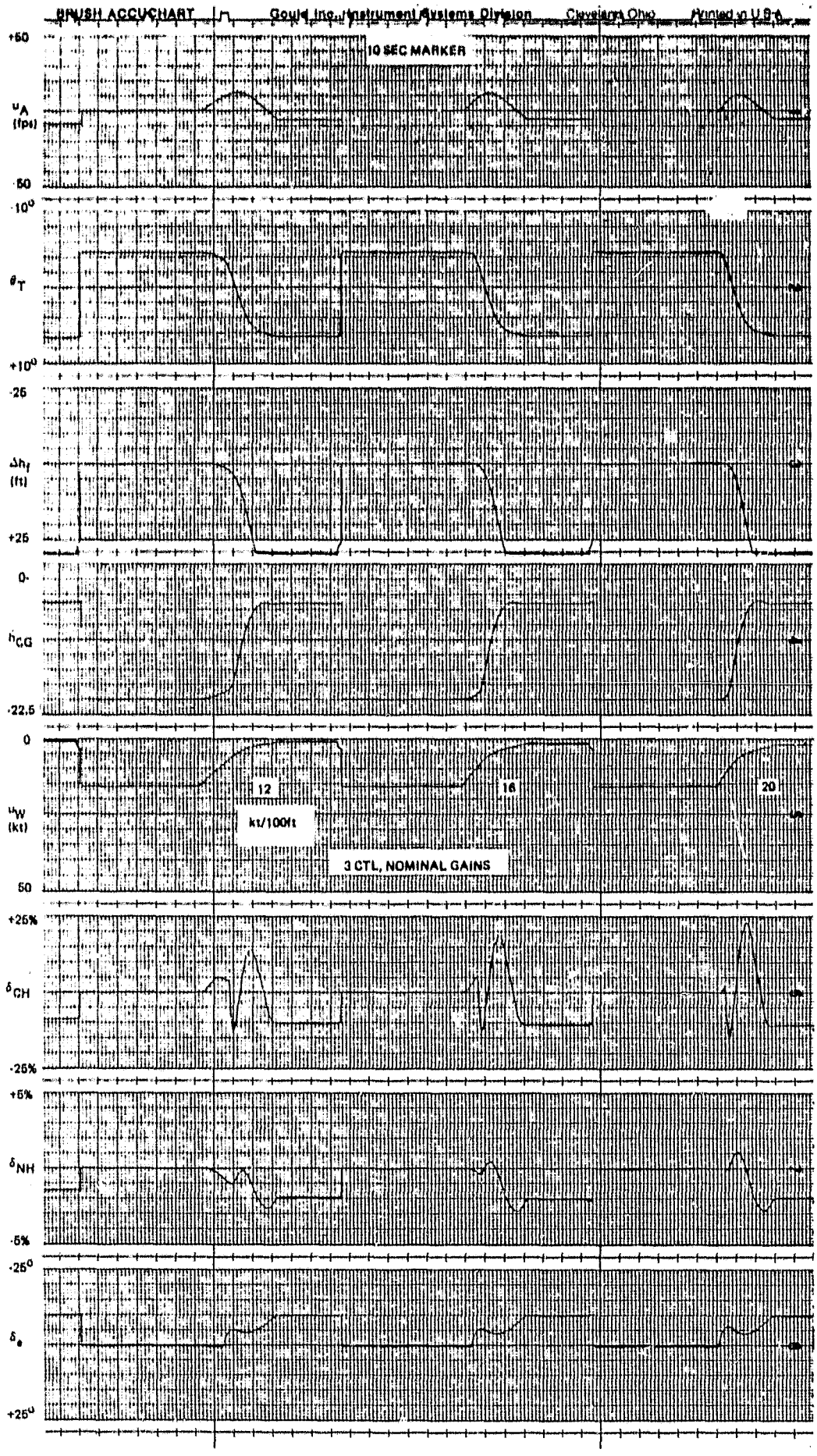

FIGURE B-10. NONSTANDARD TAILWIND SHEAR PROFILES

AW 23 FGL Ro

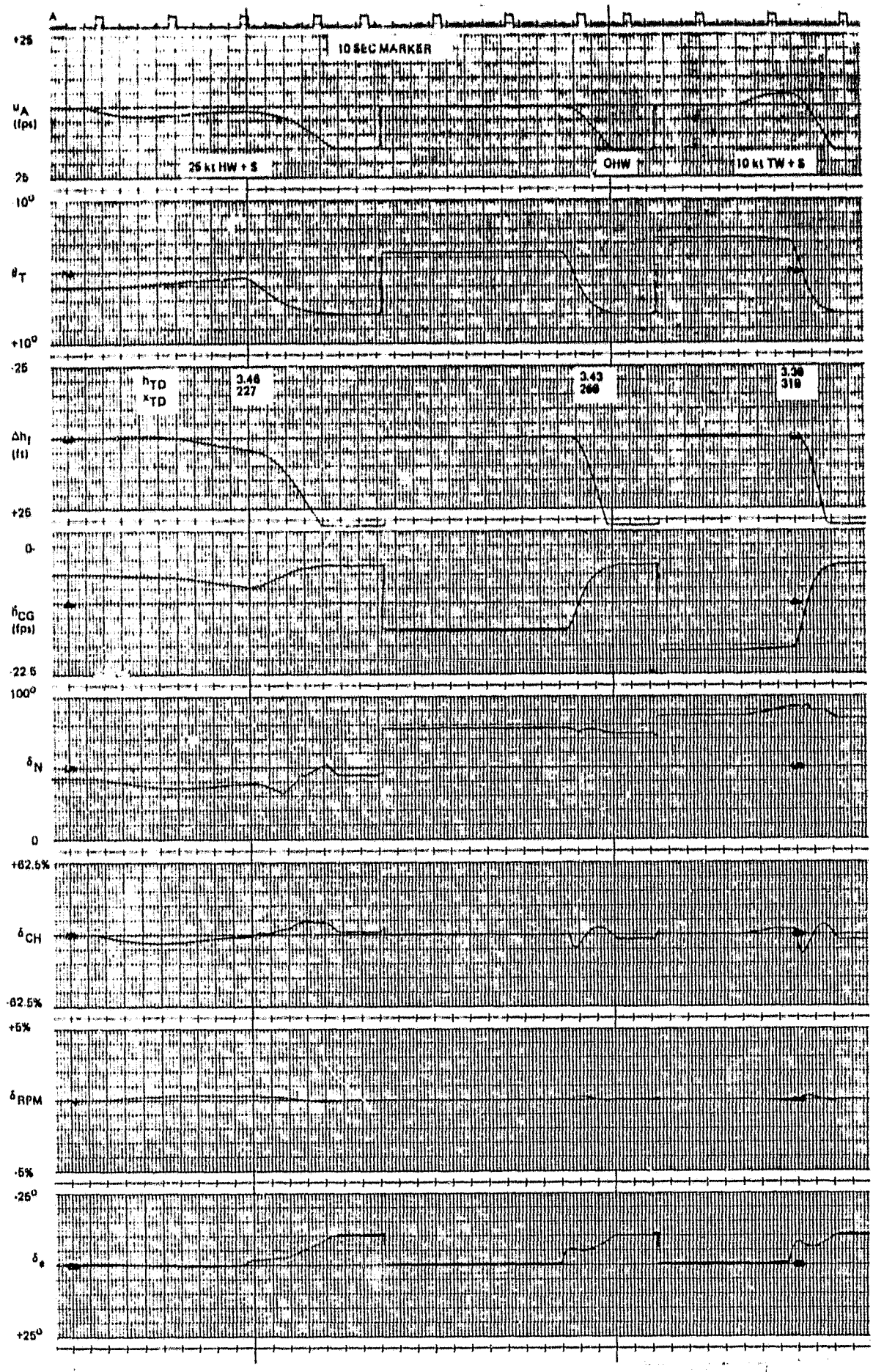

FIGURE B-11. LIGHT WEIGHT FLIGHT CONDITION; 4 CONTROLS, ($k_{\delta TF}$ = 2.53)

AUG WING 21 DEC 79

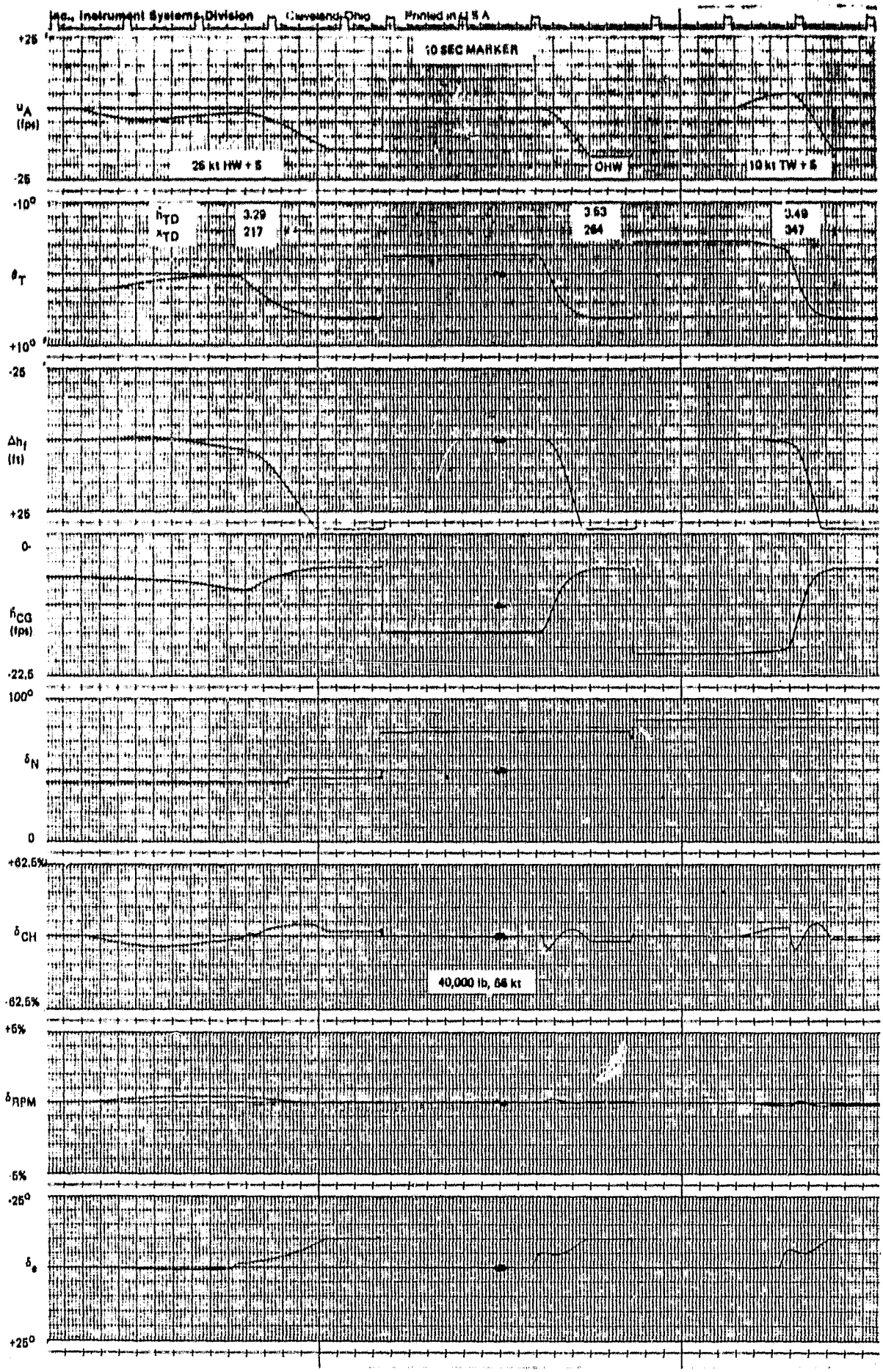

FIGURE B-12. LIGHT WEIGHT FLIGHT CONDITION; 3 CONTROLS, ($k_{\delta TF}$ = 2.53)

AU4 WING 24 DEC '77

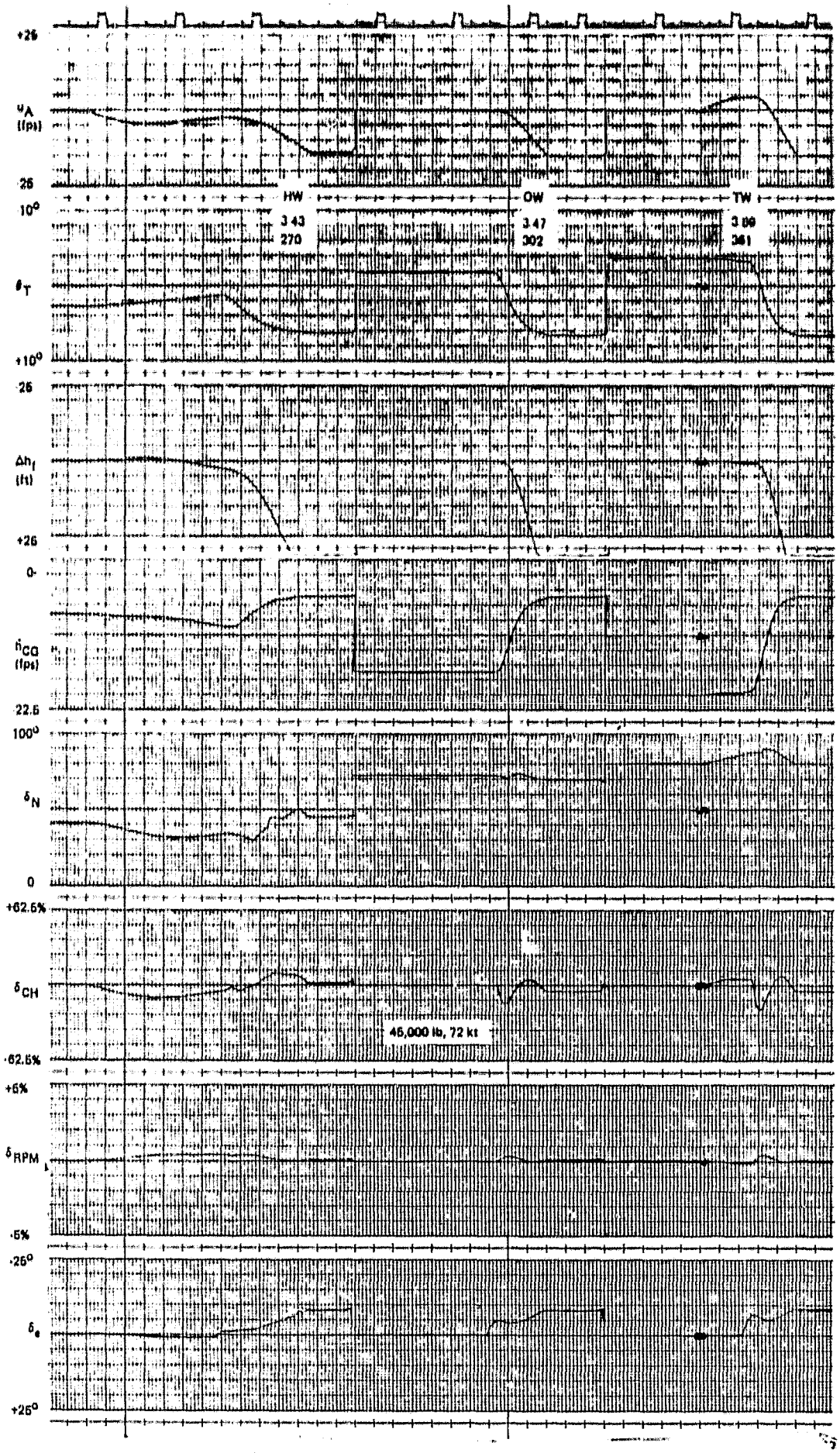

FIGURE B-13. HEAVY WEIGHT FLIGHT CONDITION; 4 CONTROLS, ($k_{\delta TF}$ = 2.53)

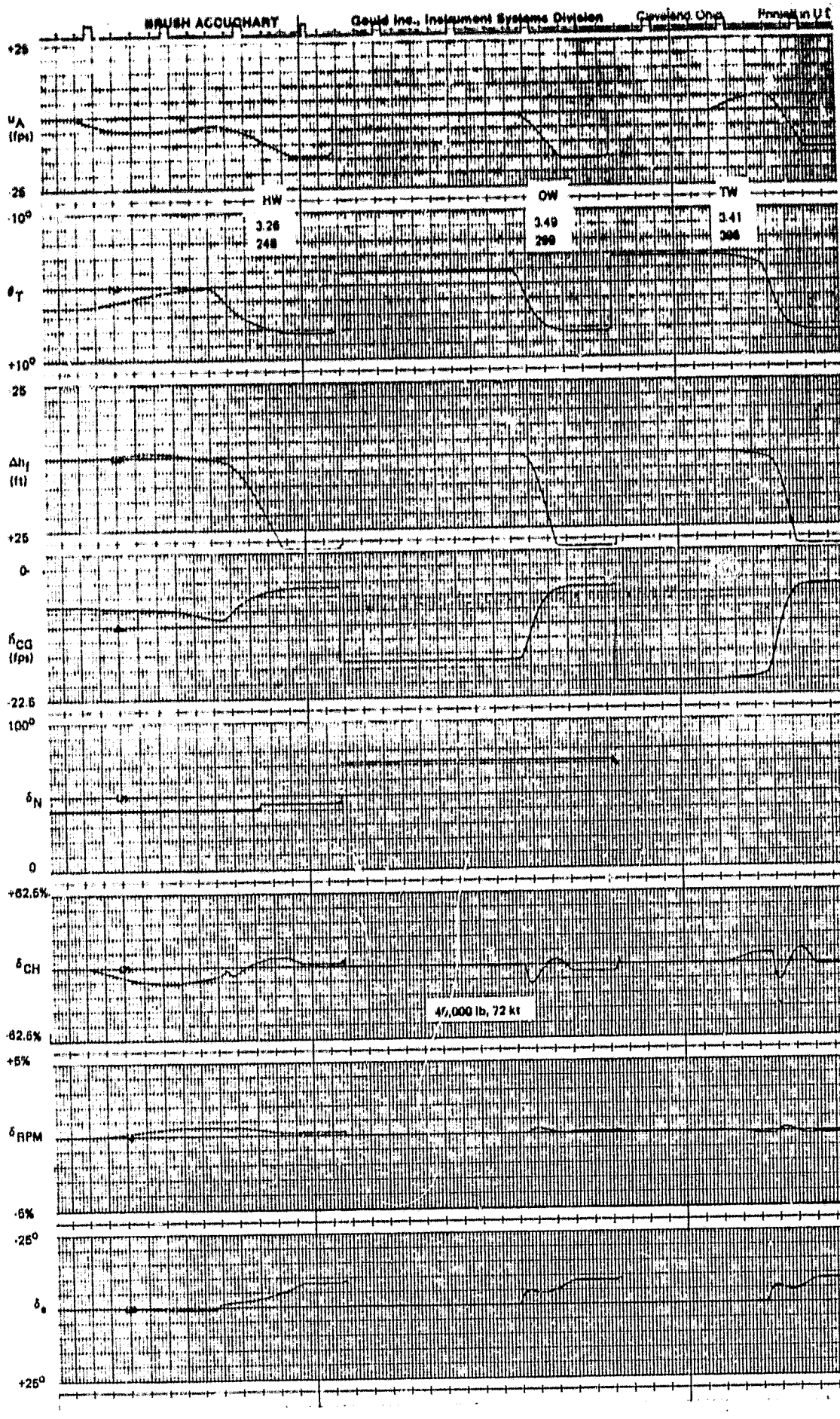

FIGURE B-14. HEAVY WEIGHT FLIGHT CONDITION; 3 CONTROLS, ($k_{\delta TF}$ = 2.53)

AW 2 JAN 60

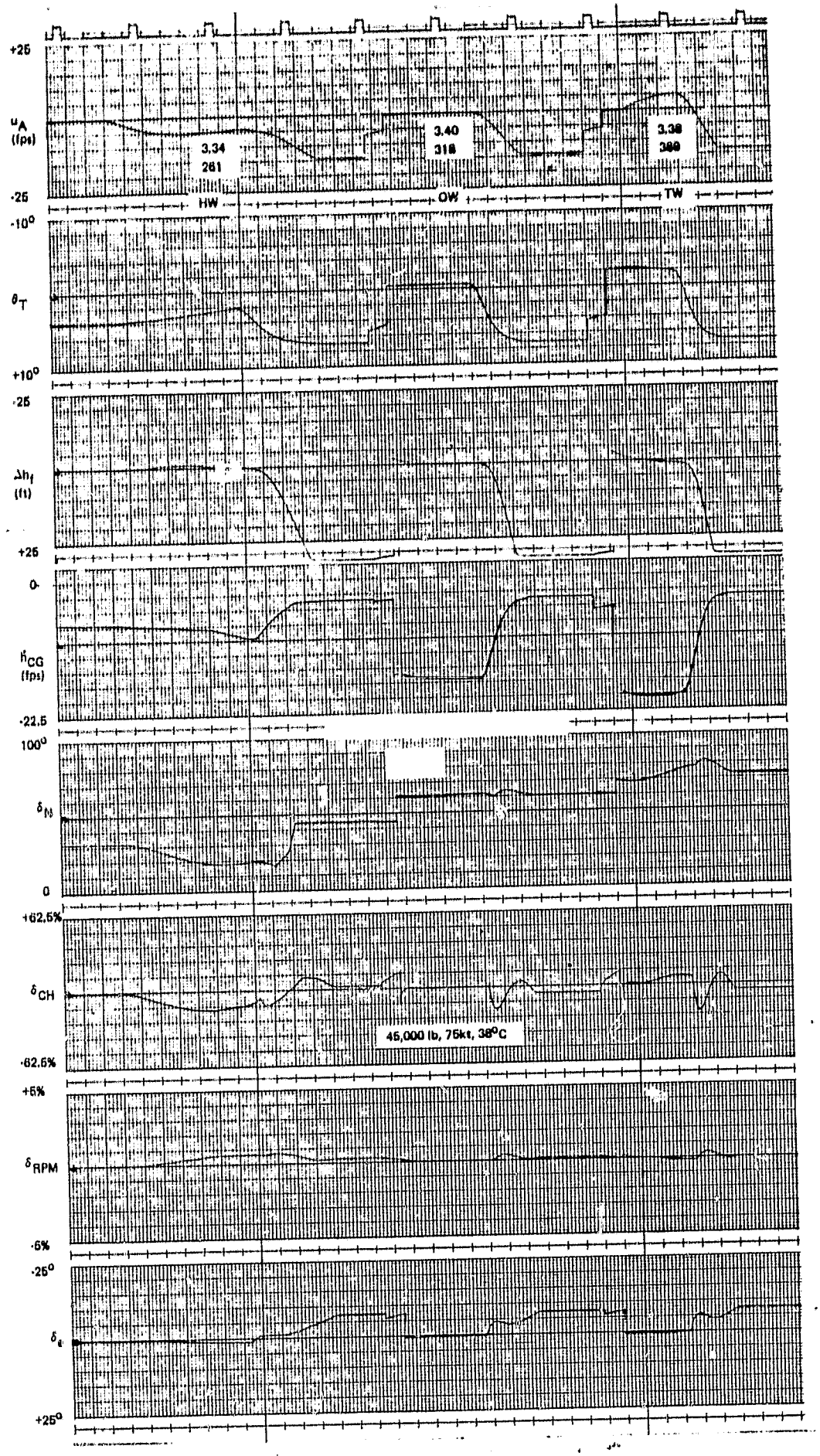

FIGURE B-15. HIGH TEMPERATURE FLIGHT CONDITION 4 CONTROLS; ($k\delta_{TF}$ = 2.53)

AW 28 DEC 79

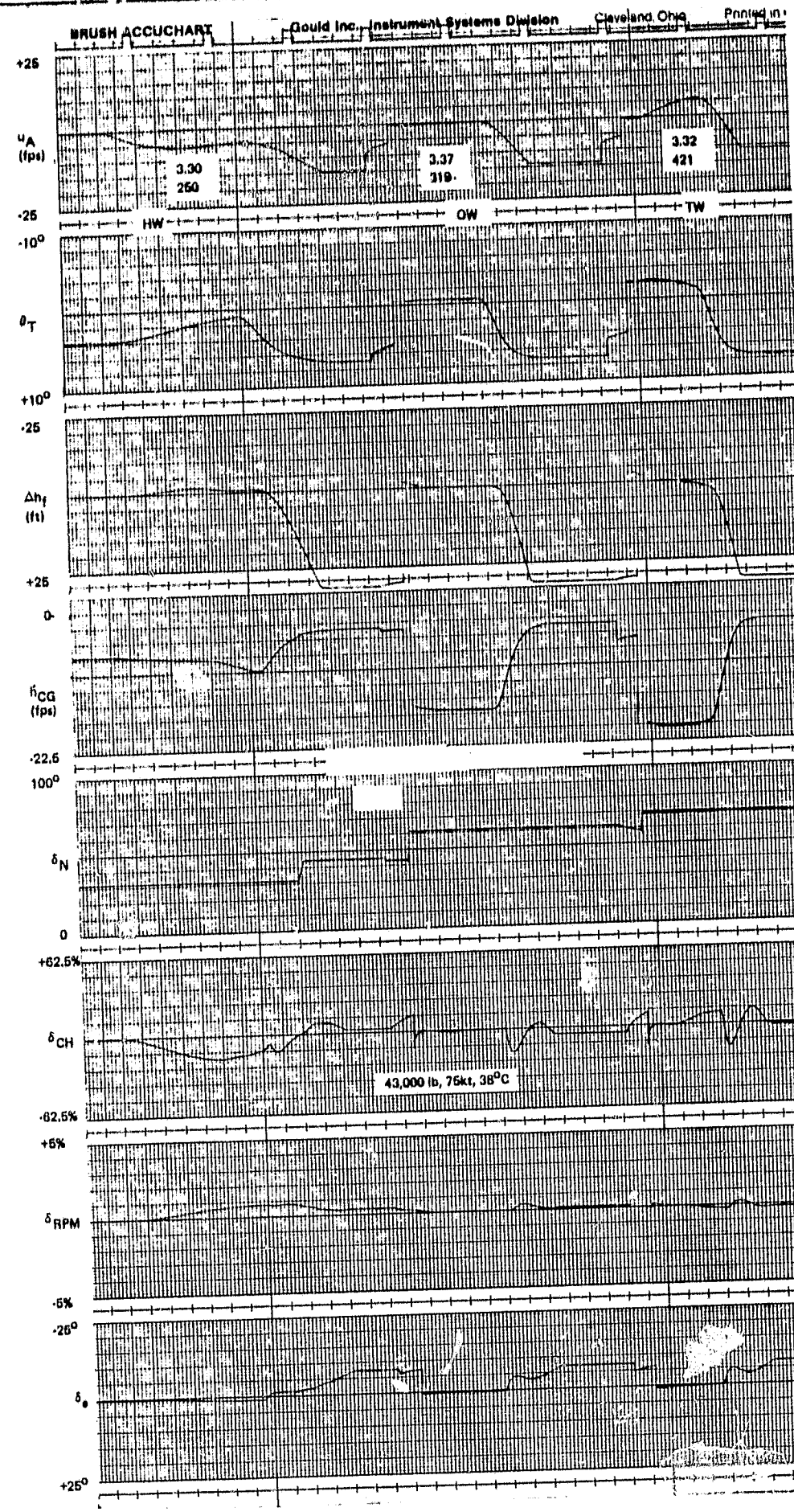

FIGURE B-16. HIGH TEMPERATURE FLIGHT CONDITION
3 CONTROLS, ($k_{\delta TF}$ = 2.53)

AW 28 DEC 79

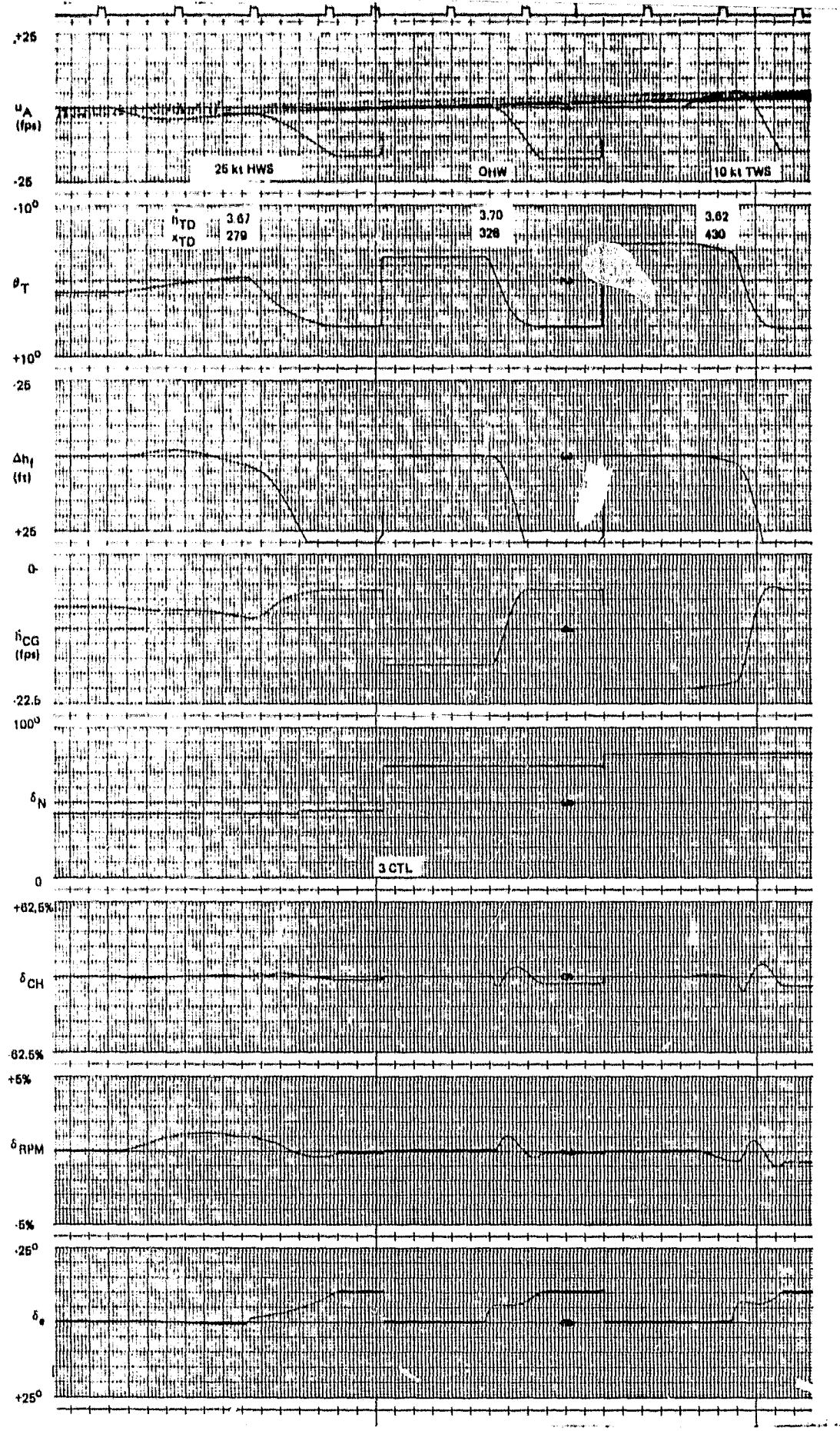

FIGURE B-17. REDUCED THROTTLE COMMAND GAIN ($k_{\delta TC}$ = 2.3 deg/m/sec)

AUG WING 14 FEB 80

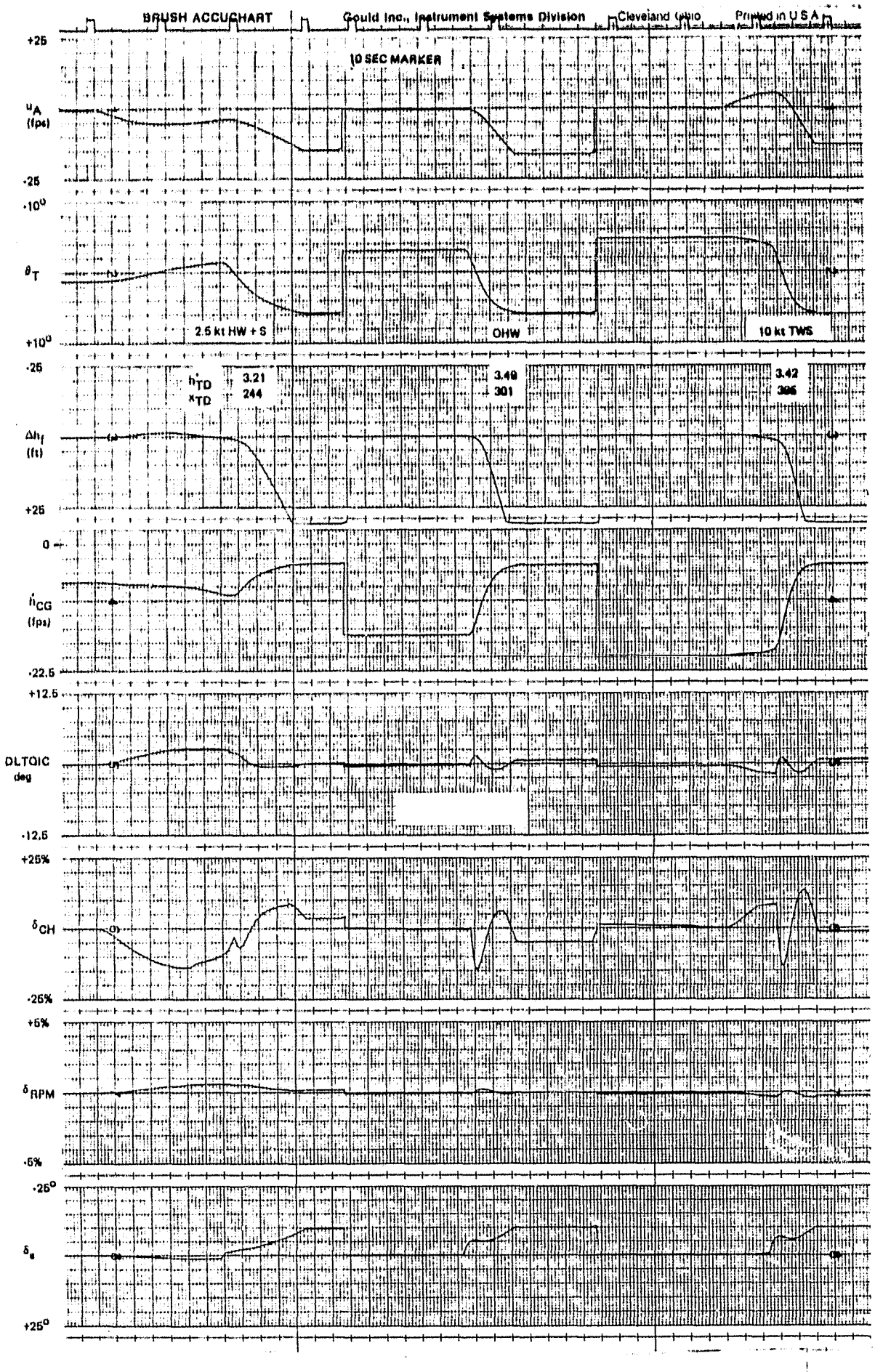

FIGURE B-18. THREE CONTROLS, ($k_{\delta TF}$ = 2.53)

16 oct '78

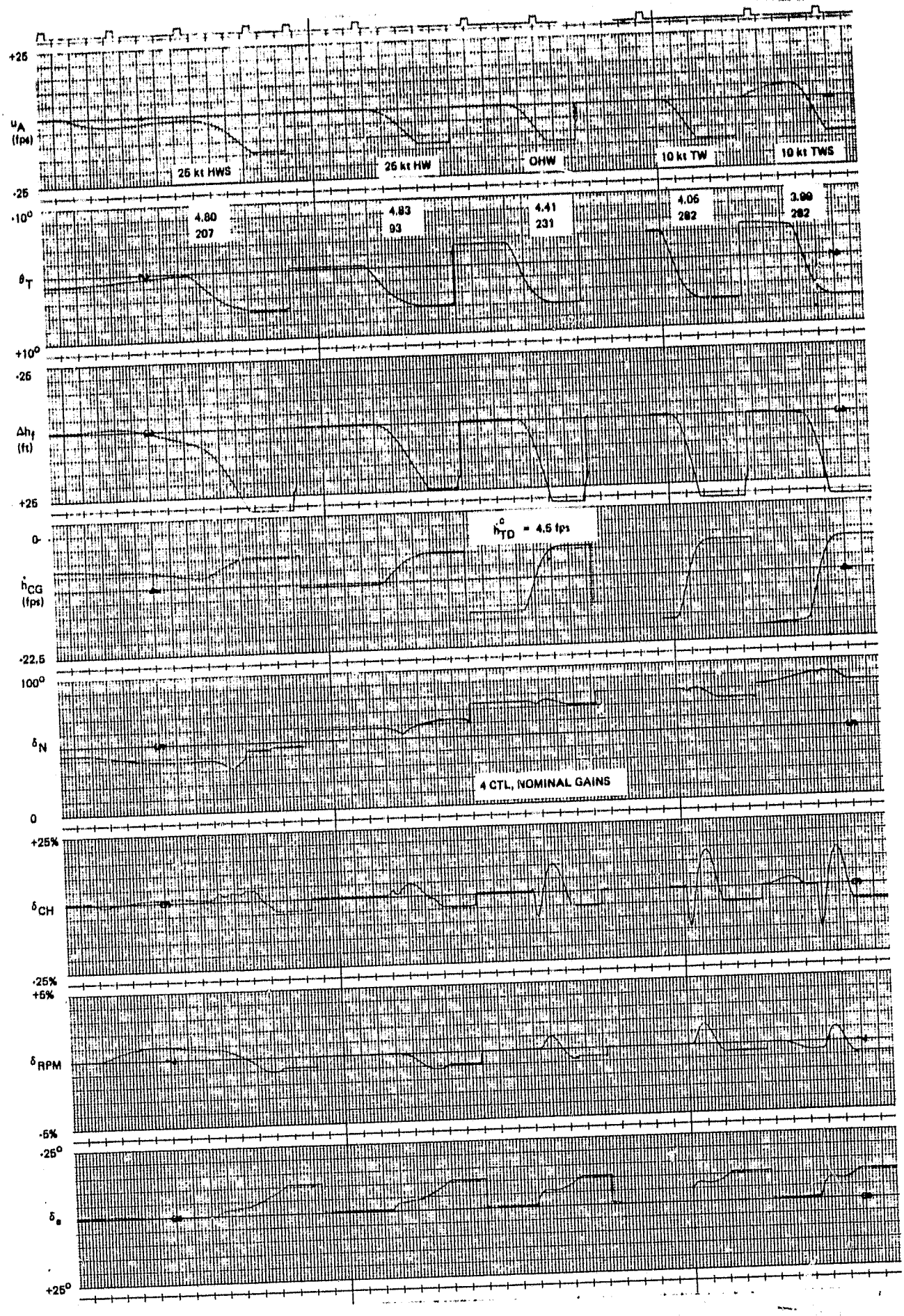

FIGURE B-19. INCREASED TOUCHDOWN SINK RATE COMMAND

Aug Wing 21 March 80

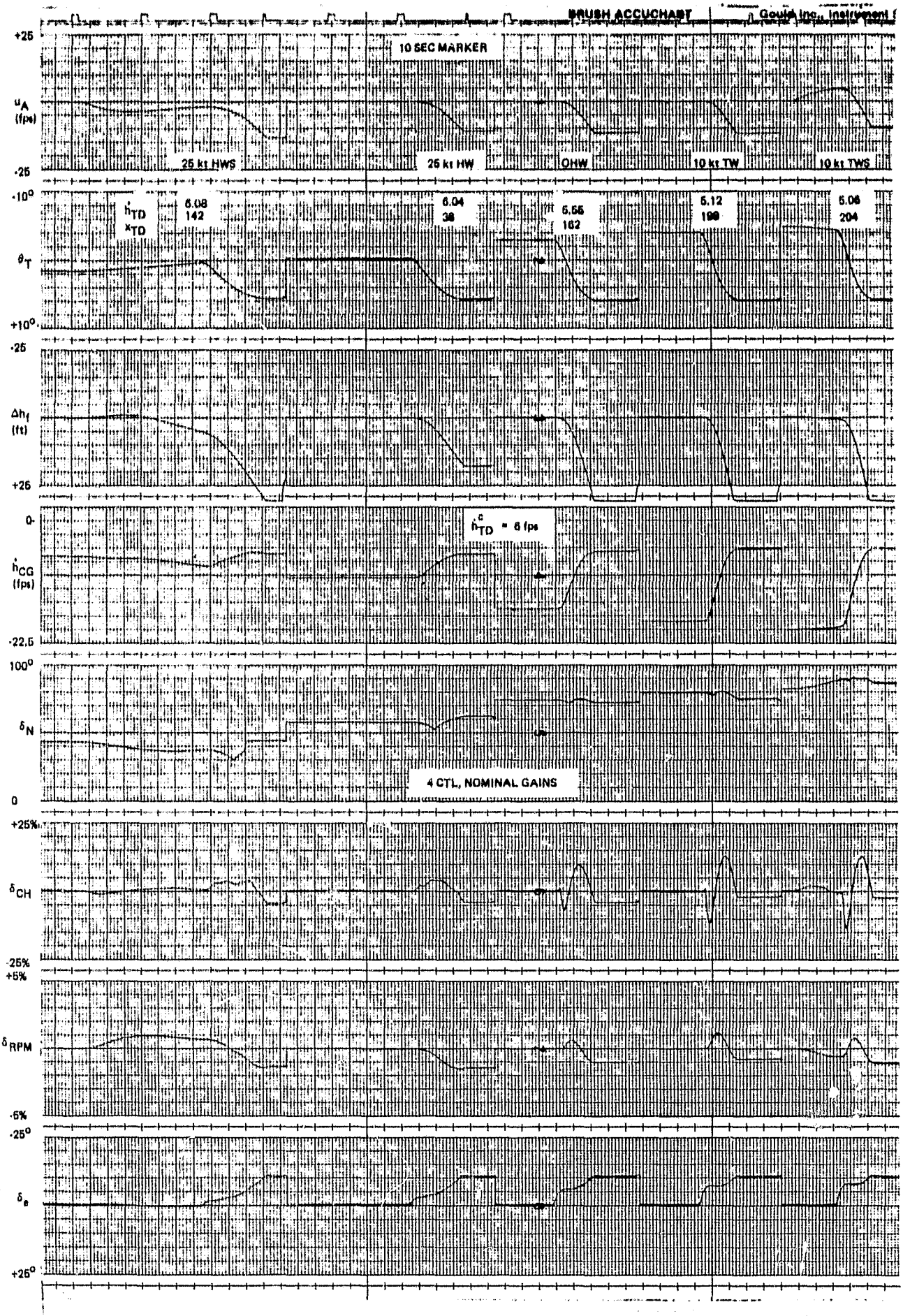

FIGURE B-20. INCREASED TOUCHDOWN SINK RATE COMMAND

Andy Wing 21 March 80

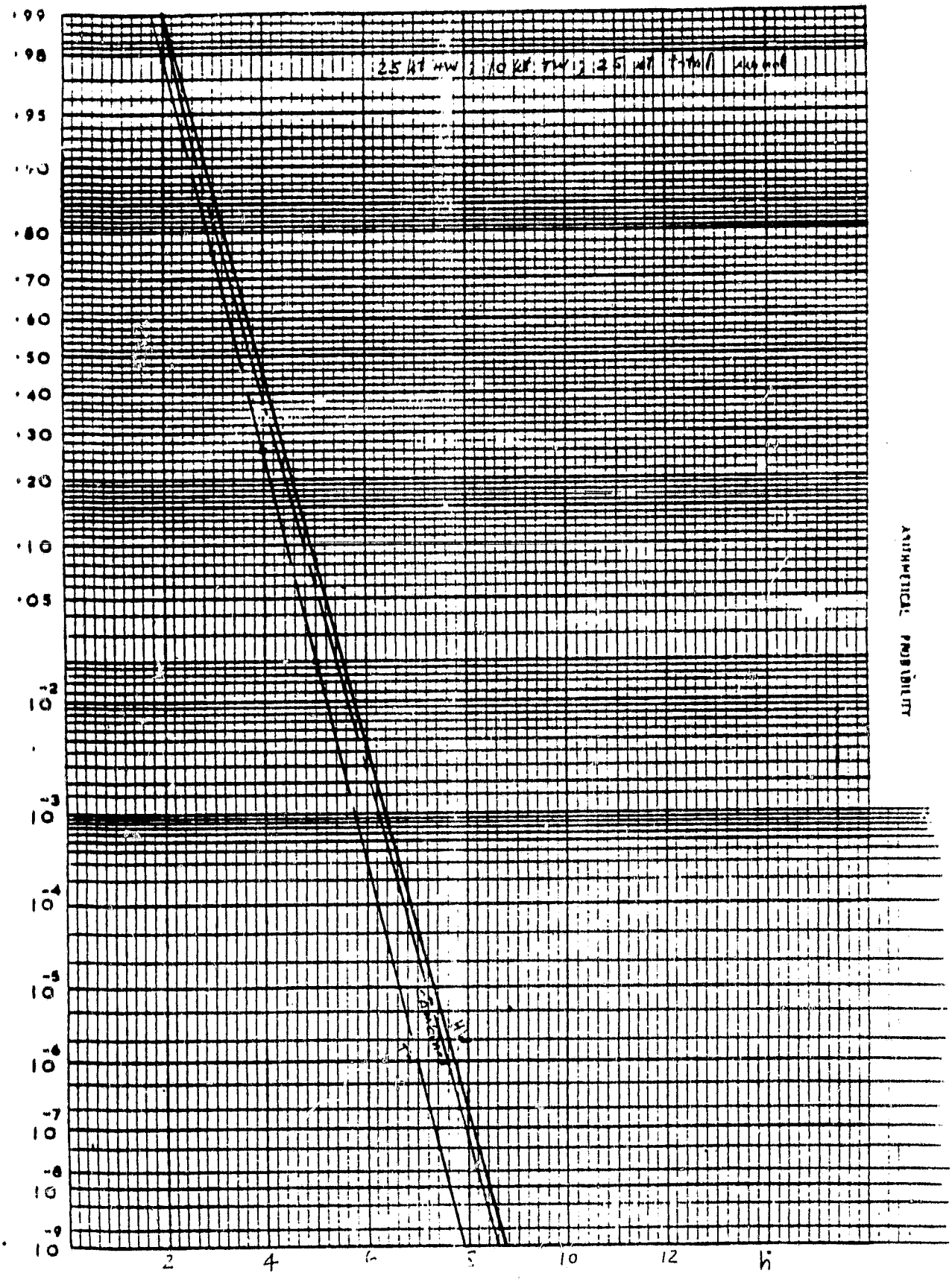

FIGURE B-21. FOUR CONTROLS, NOMINAL

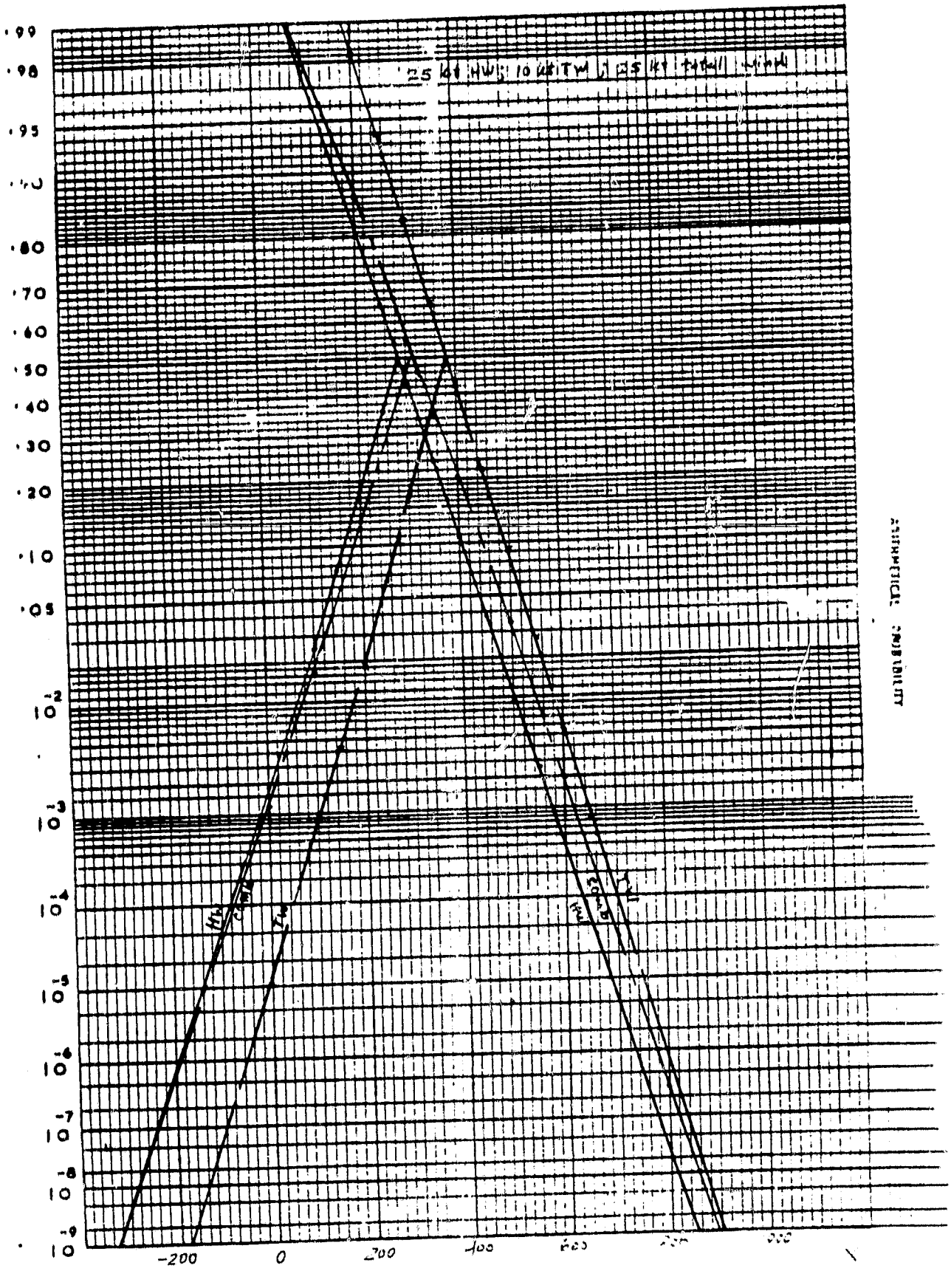

FIGURE B-22. FOUR CONTROLS, NOMINAL

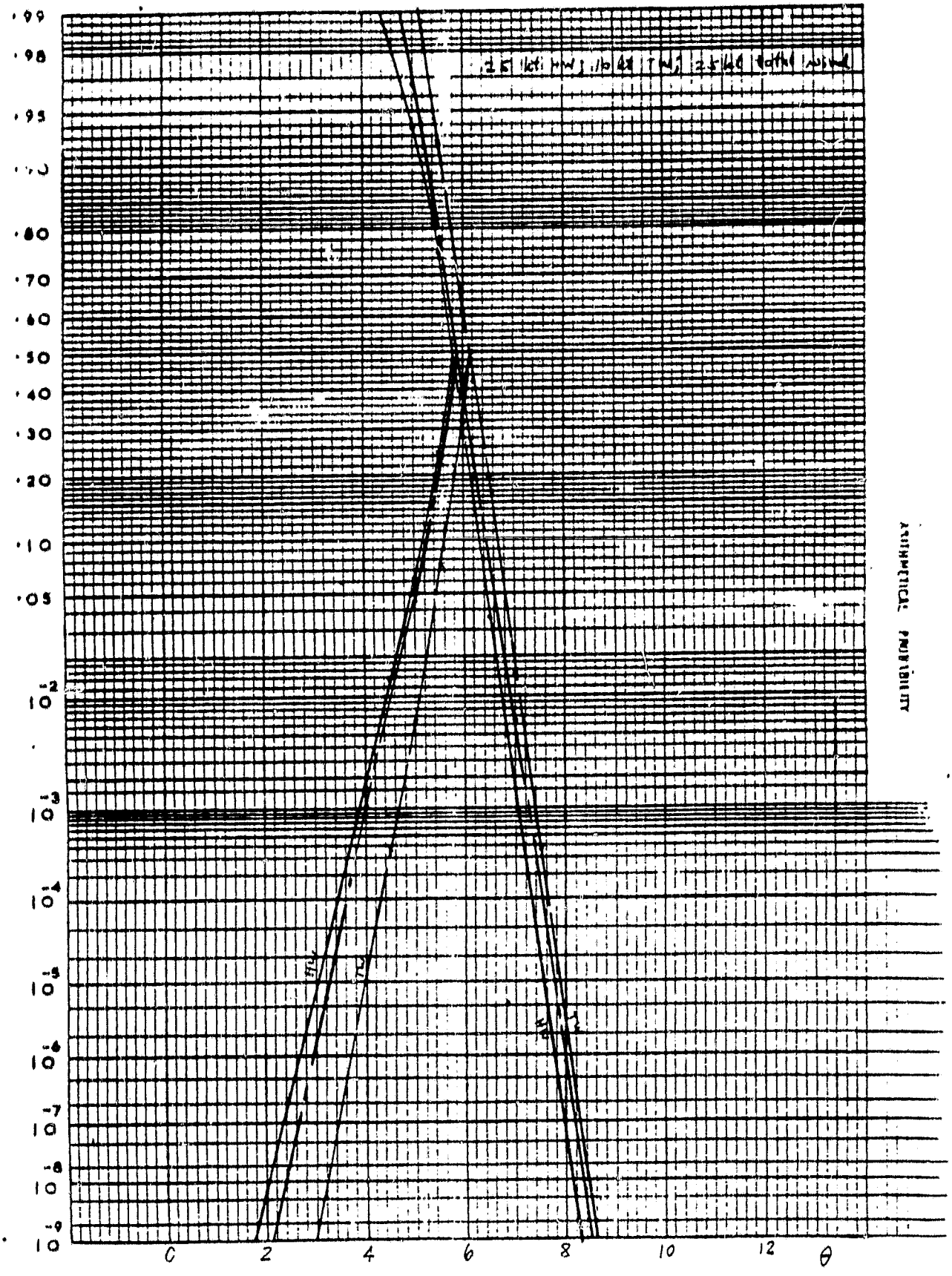

FIGURE B-23. FOUR CONTROLS, NOMINAL

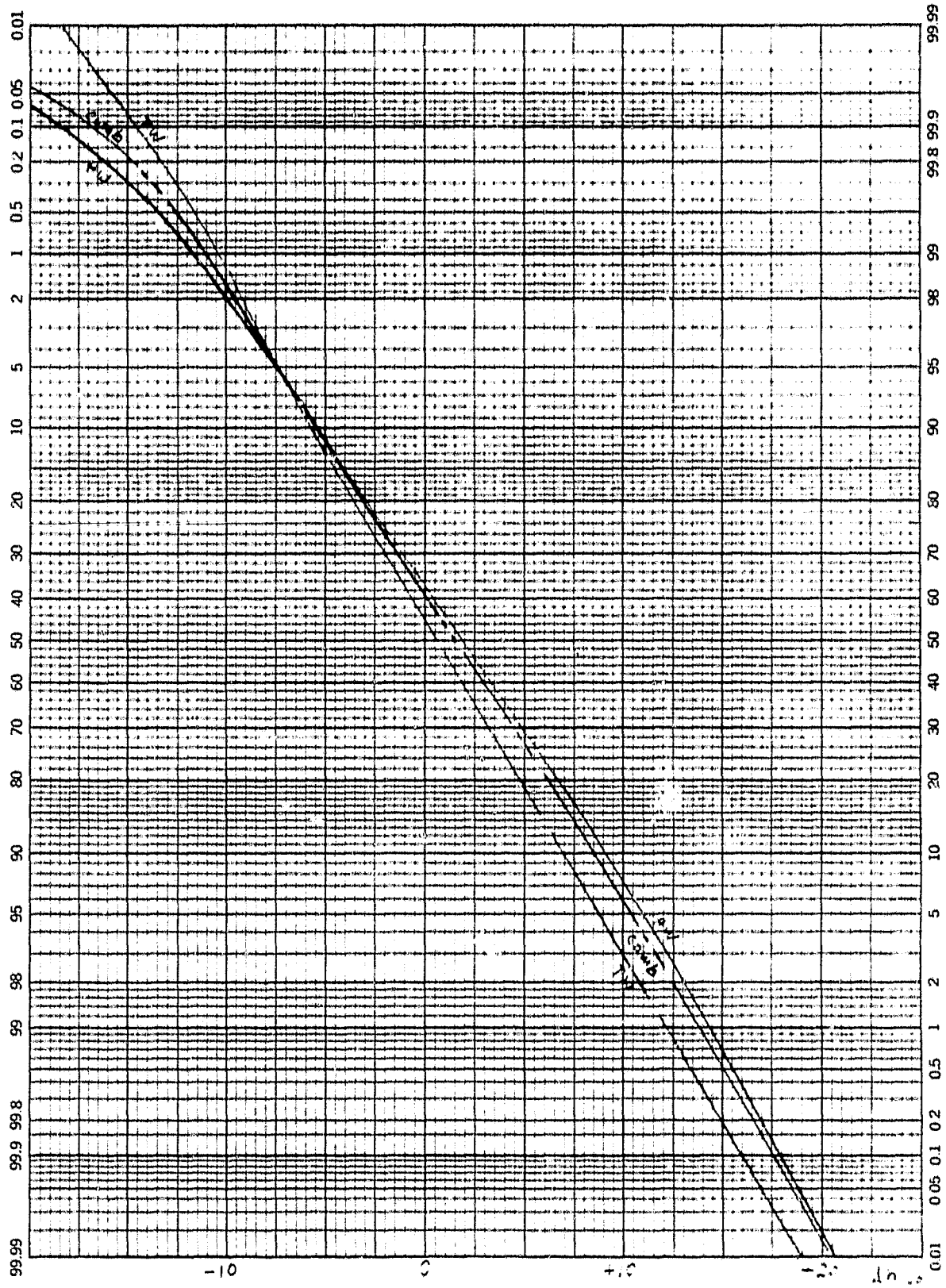

FIGURE B-24. FOUR CONTROLS, NOMINAL

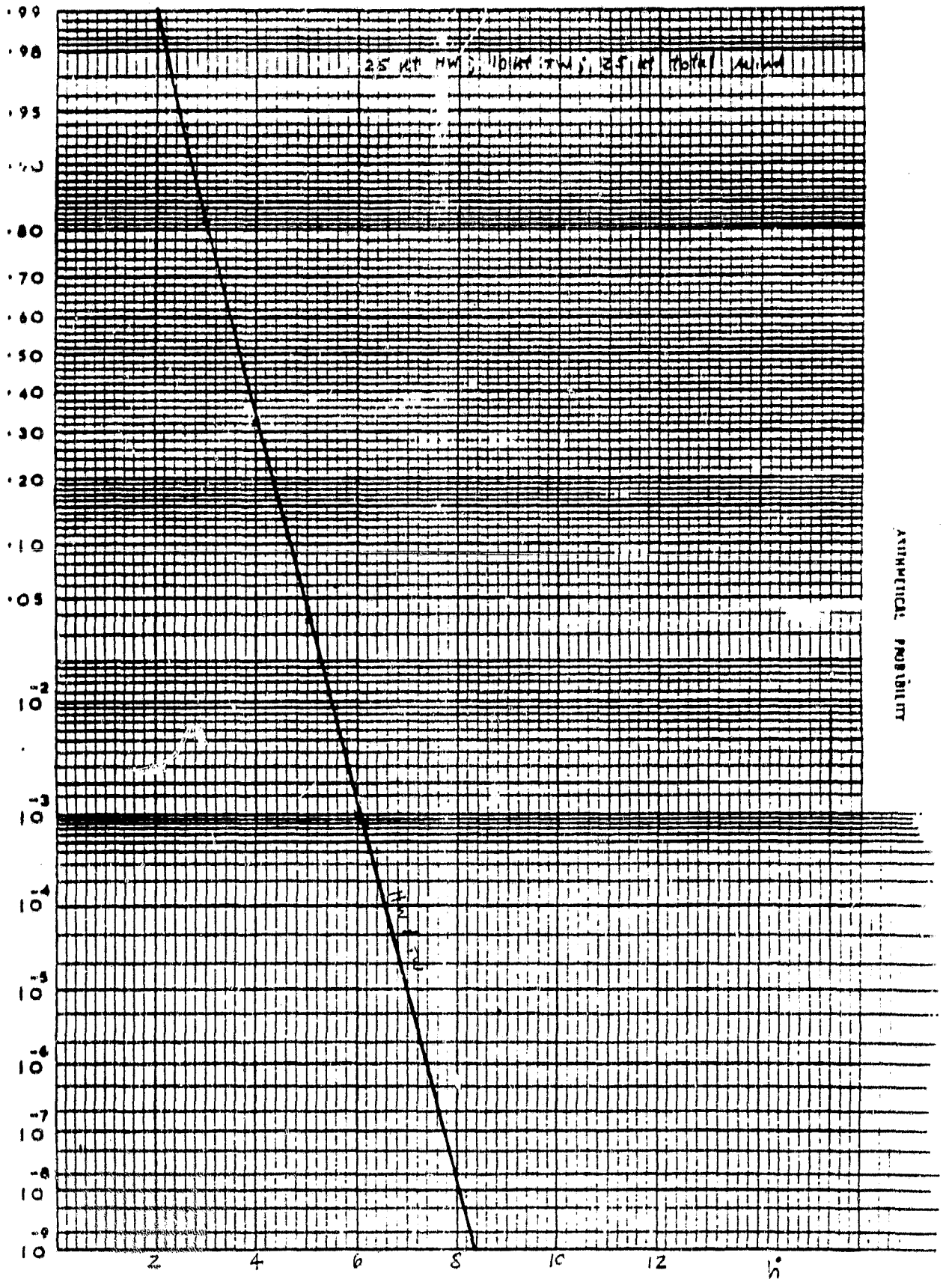

FIGURE B-25. THREE CONTROLS, NOMINAL

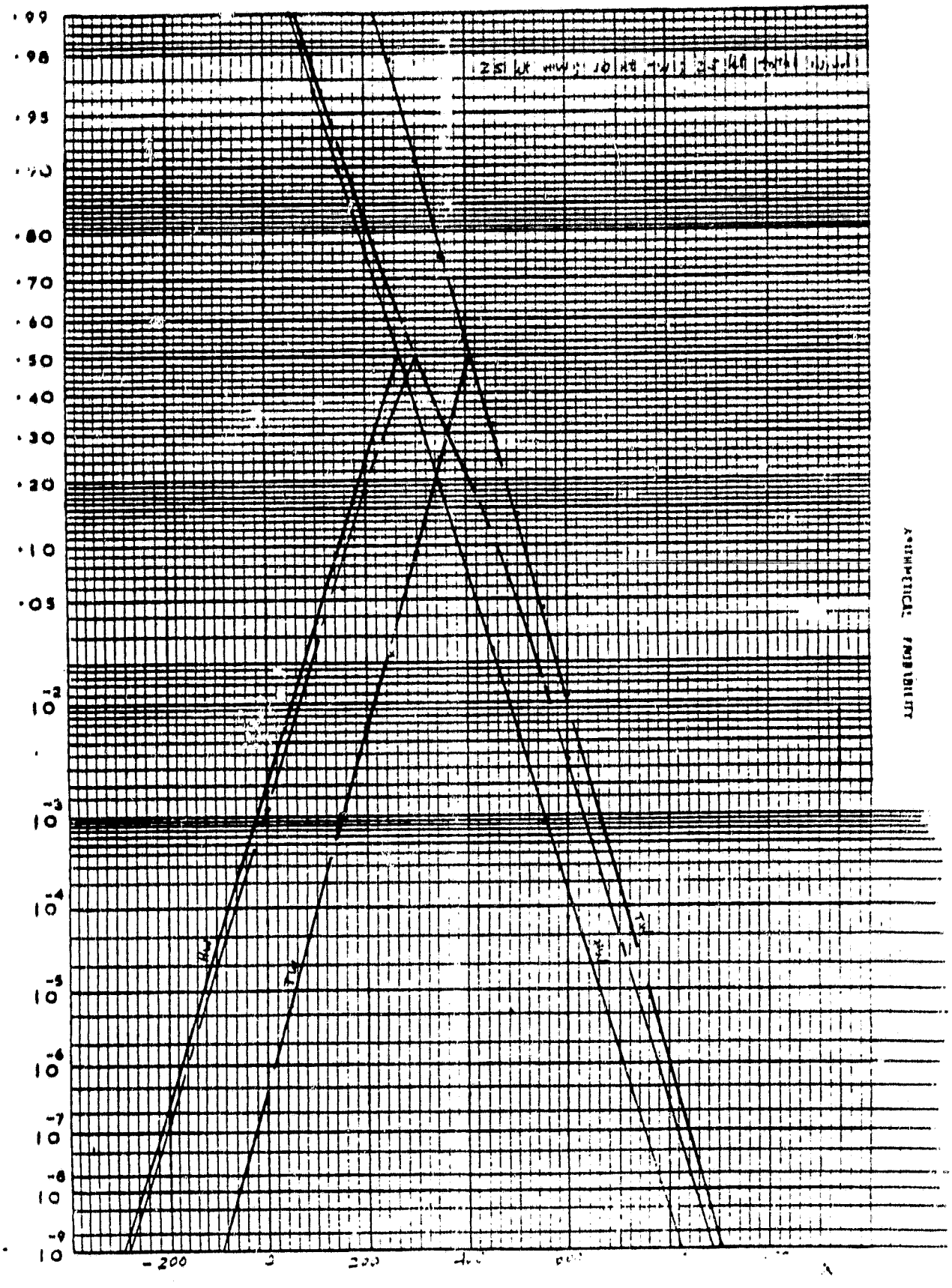

FIGURE B-28. THREE CONTROLS, NOMINAL

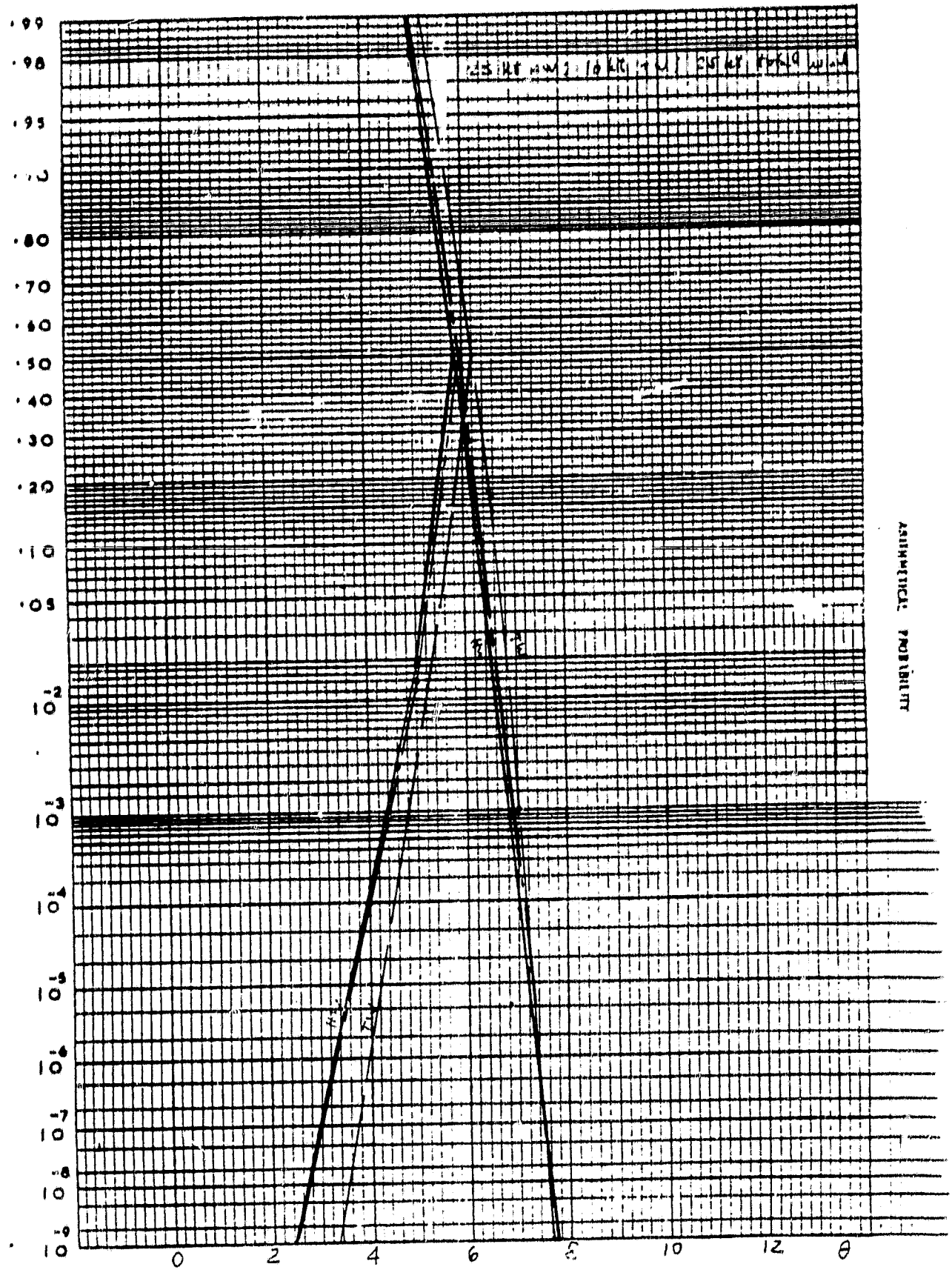

FIGURE B-27. THREE CONTROLS, NOMINAL

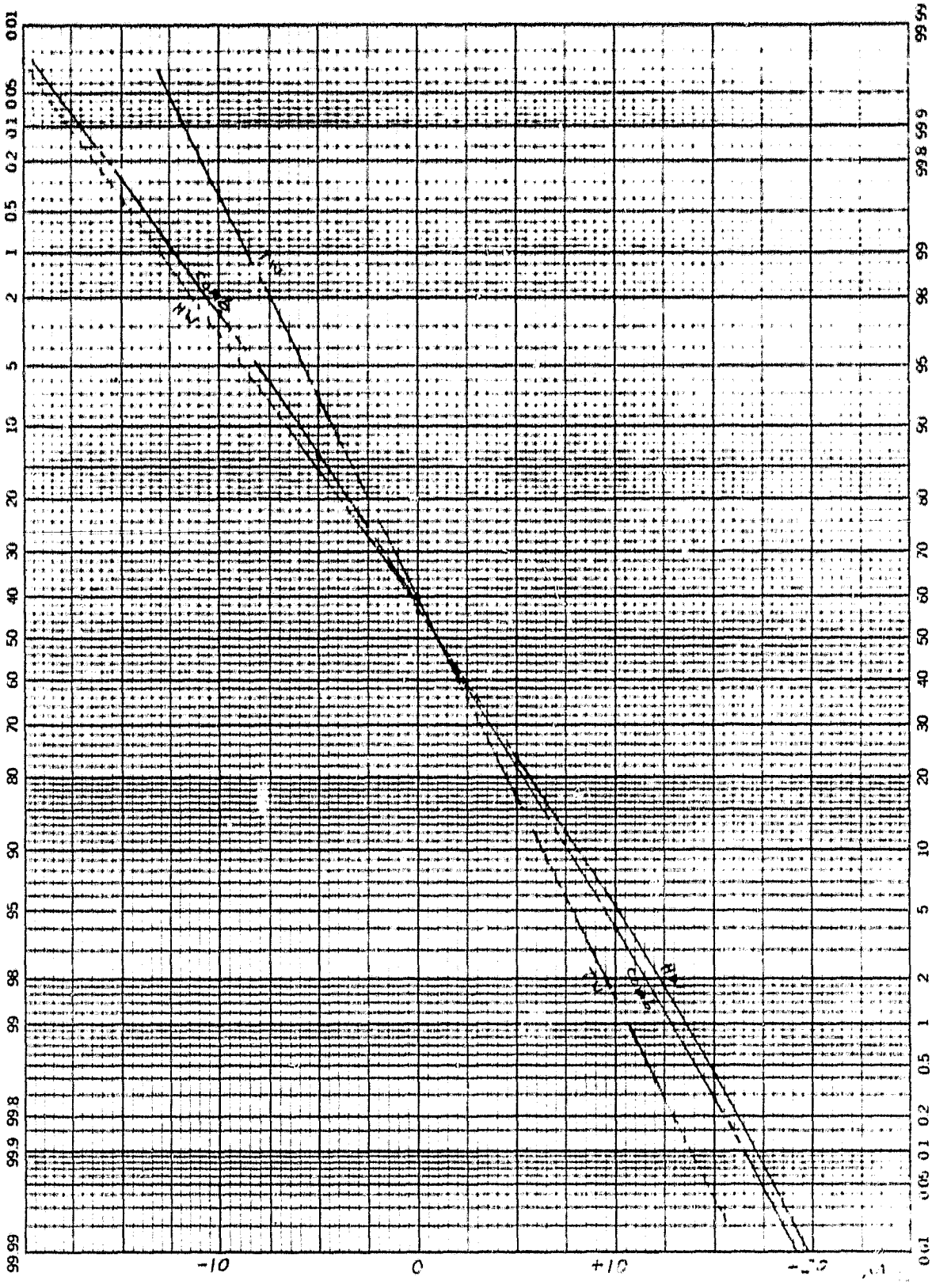

FIGURE B-28. THREE CONTROLS, NOMINAL

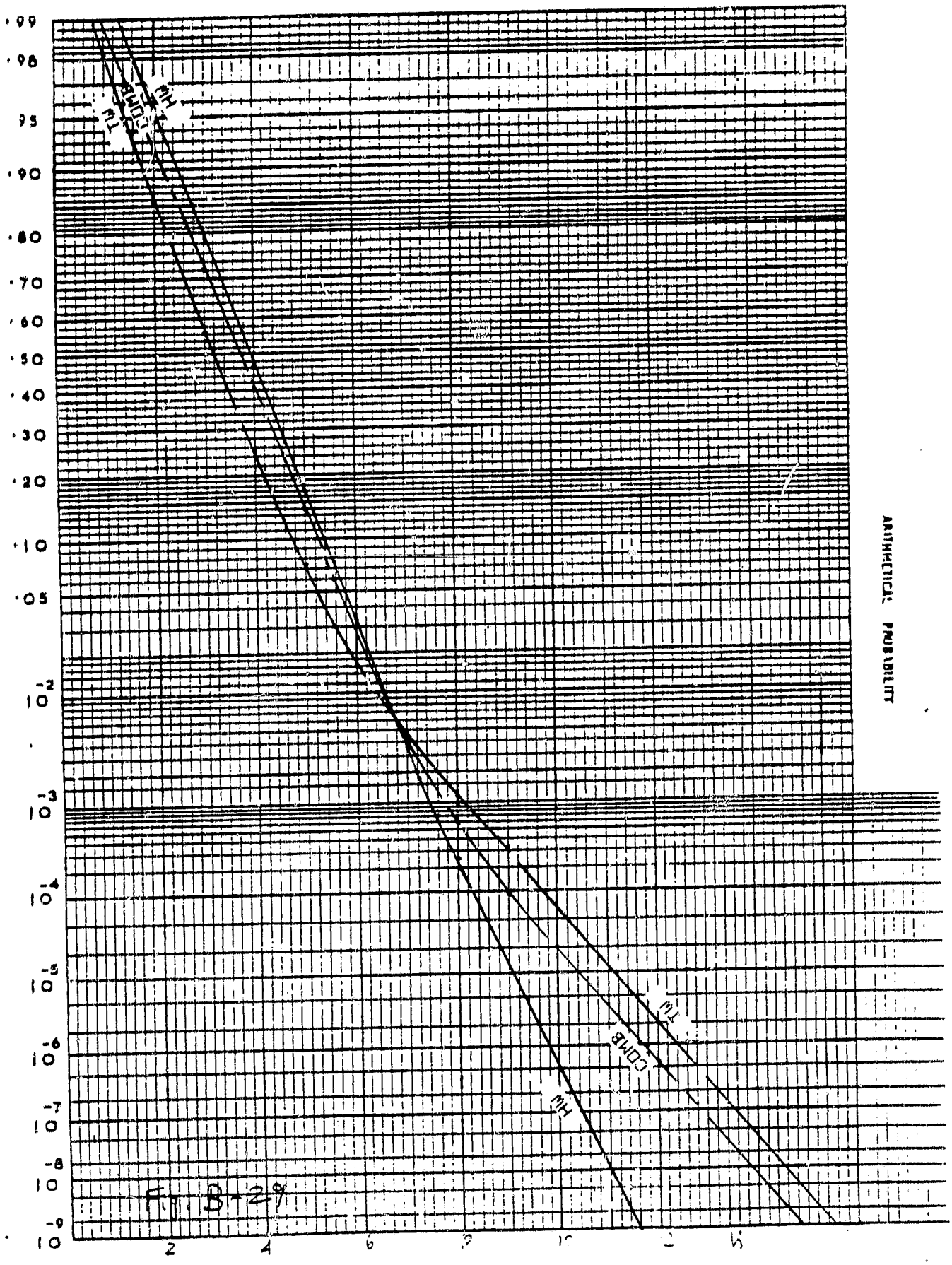

Fig. B-29

FIGURE B-29. TWO CONTROLS, NOMINAL

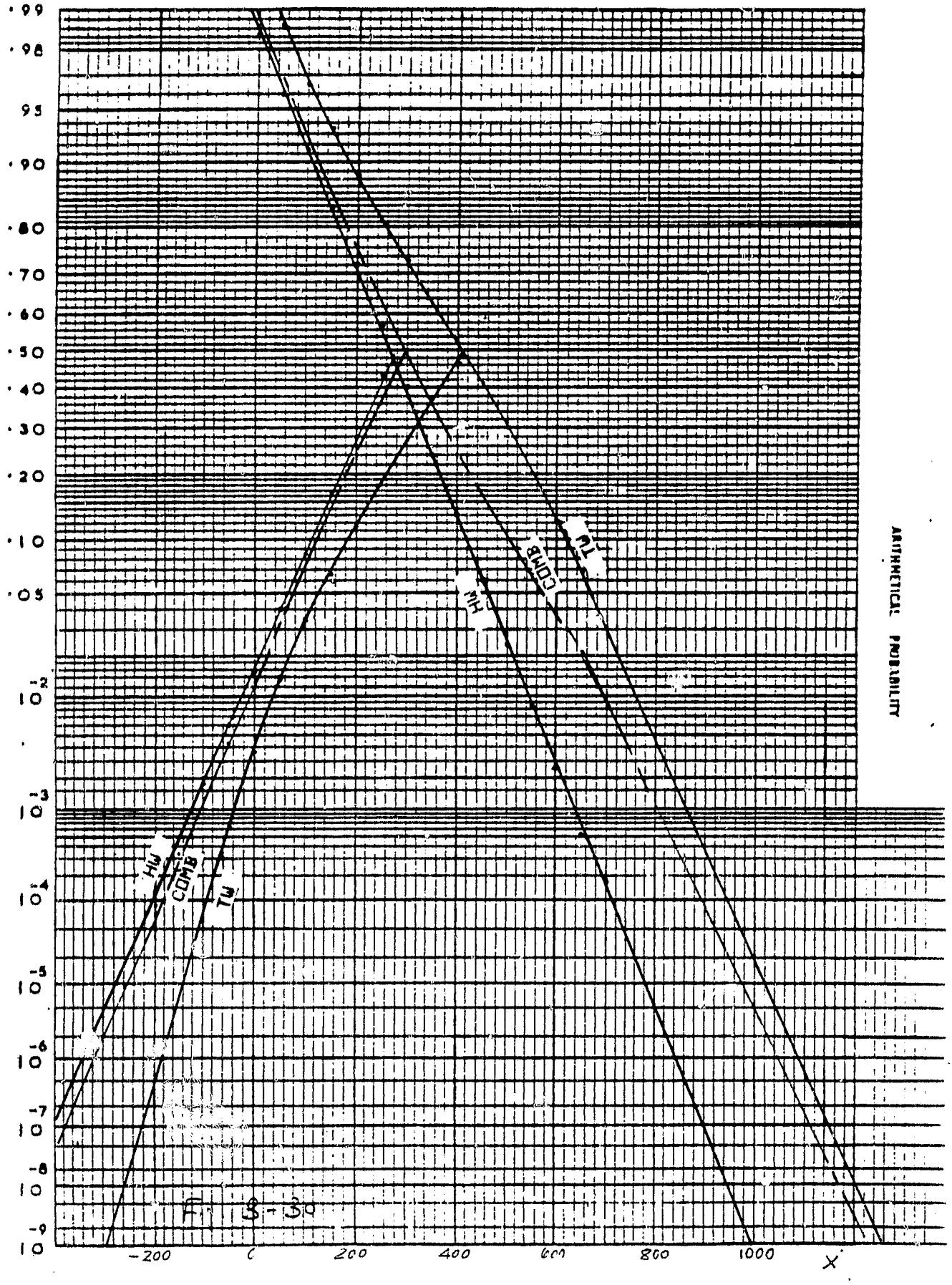

FIGURE B-30. TWO CONTROLS, NOMINAL

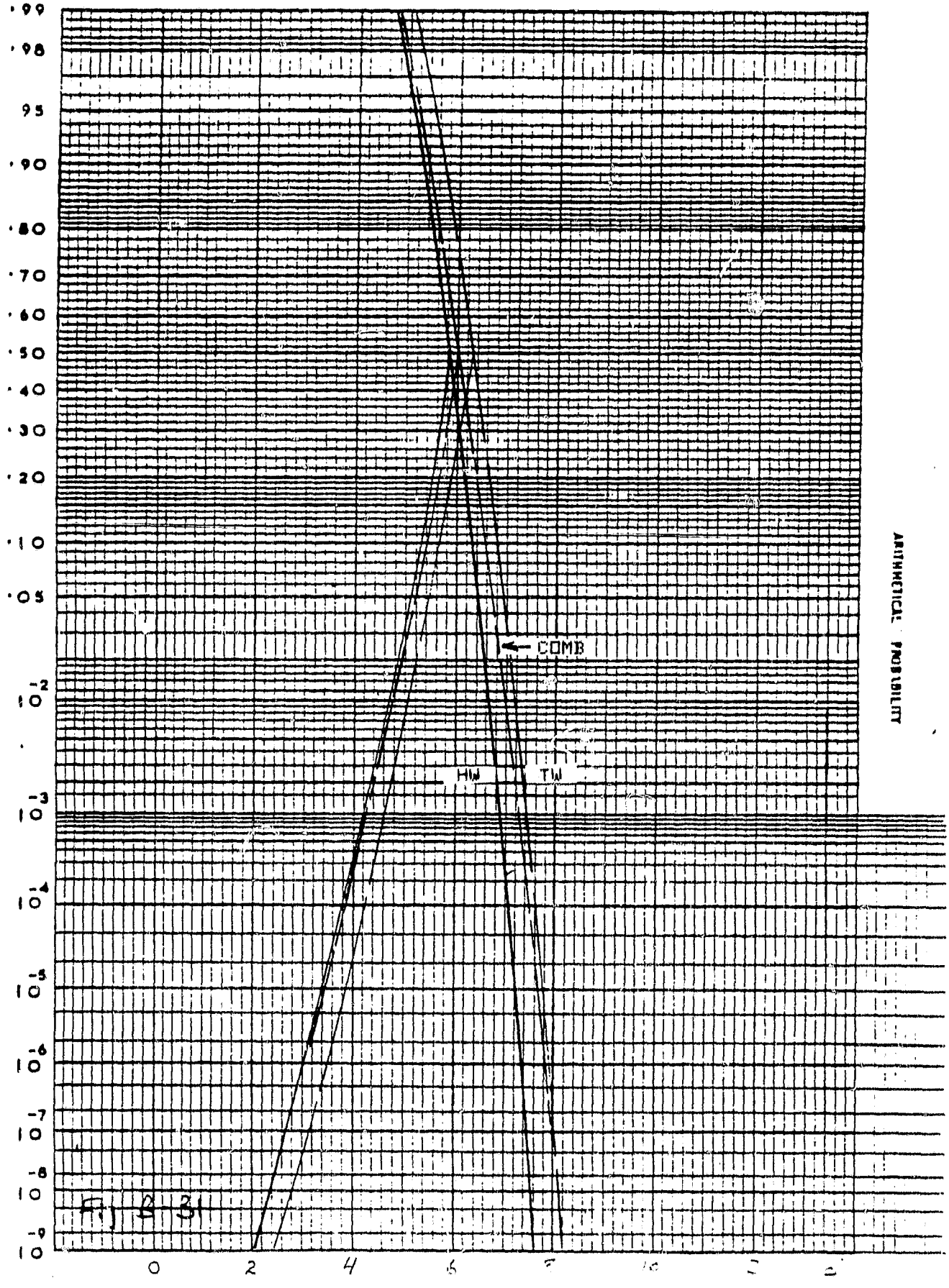

FIGURE B-31. TWO CONTROLS, NOMINAL

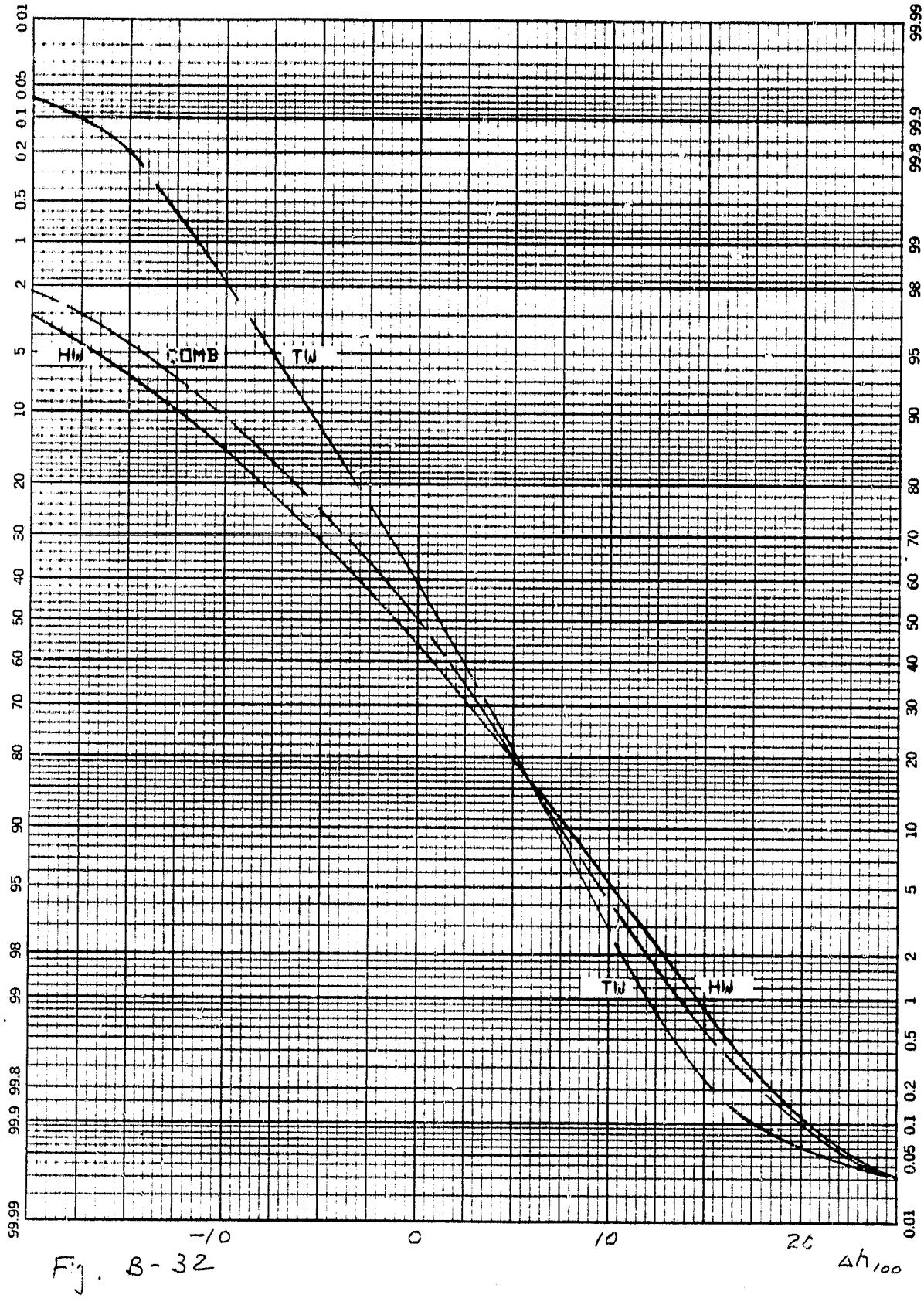

Fig. B-32

46 8003

K&E PROBABILITY X 90 DIVISIONS KEUFFEL & ESSER CO MADE IN U.S.A.

FIGURE B-32. TWO CONTROLS, NOMINAL

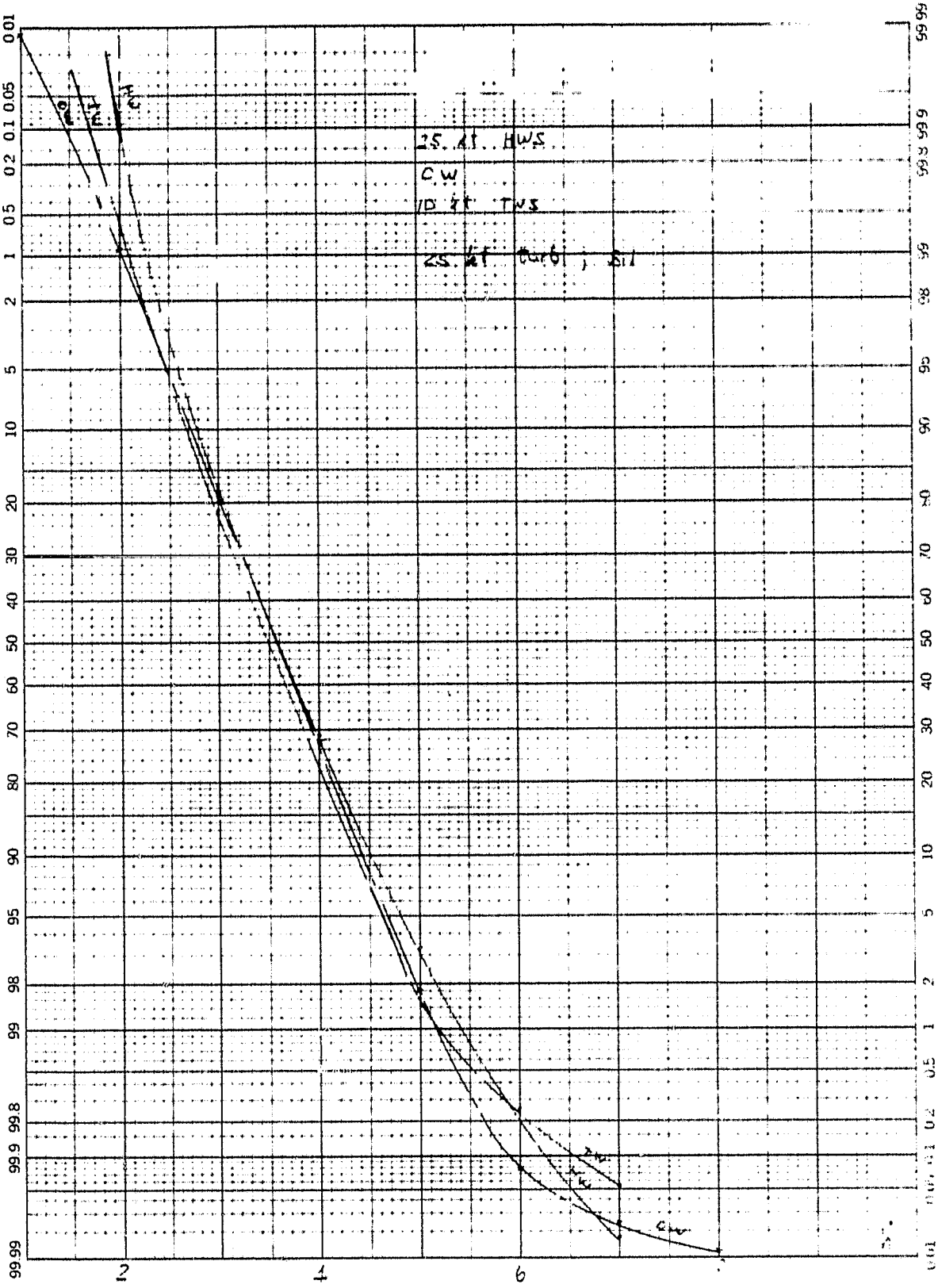

46 8003

K&E PROBABILITY X 90 DIVISIONS
KEUFFEL & ESSER CO

FIGURE B-33. FOUR CONTROLS, $k\delta_{TF}$ = 2.53

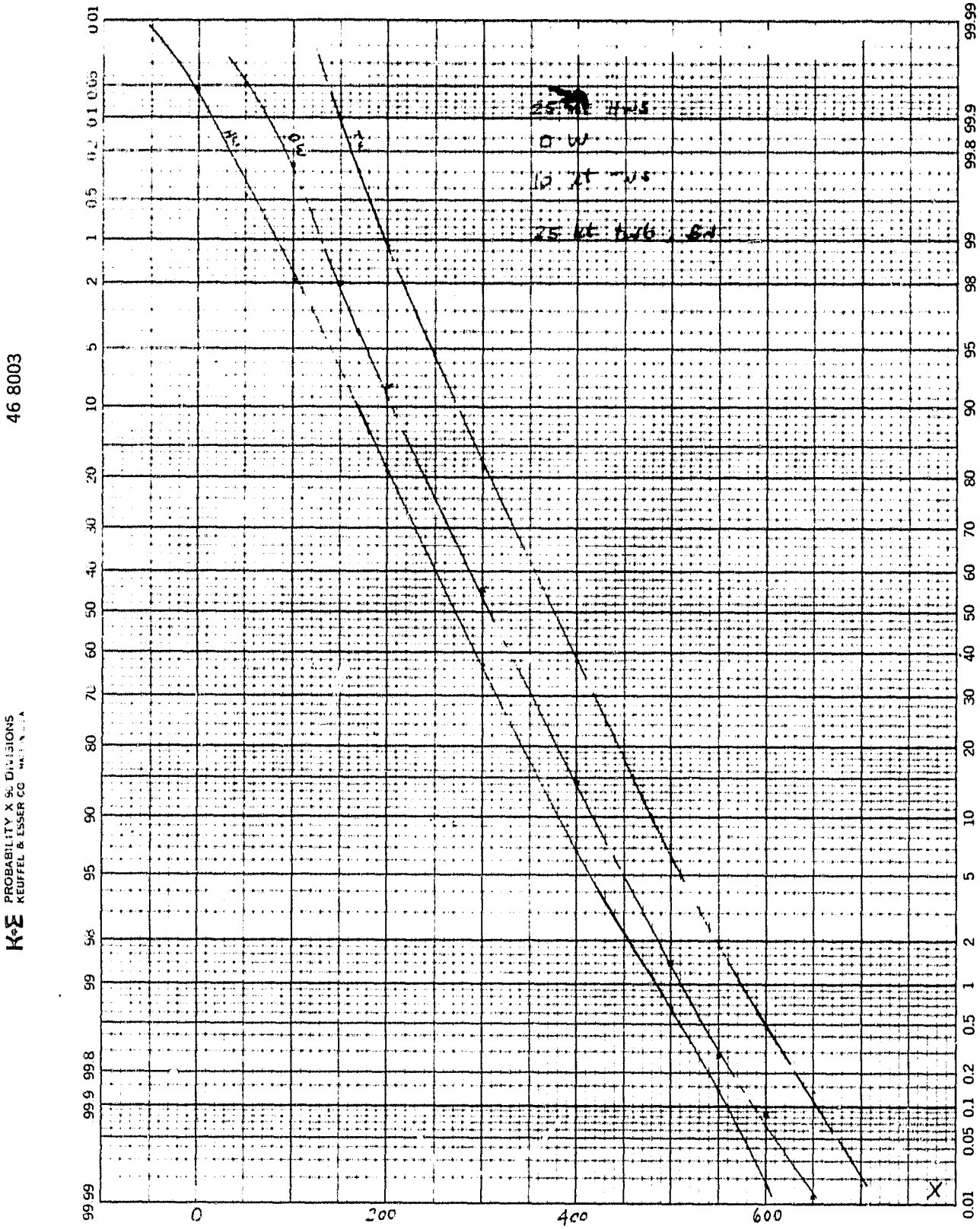

FIGURE B-34. FOUR CONTROLS, $k\delta_{TF}$ = 2.53

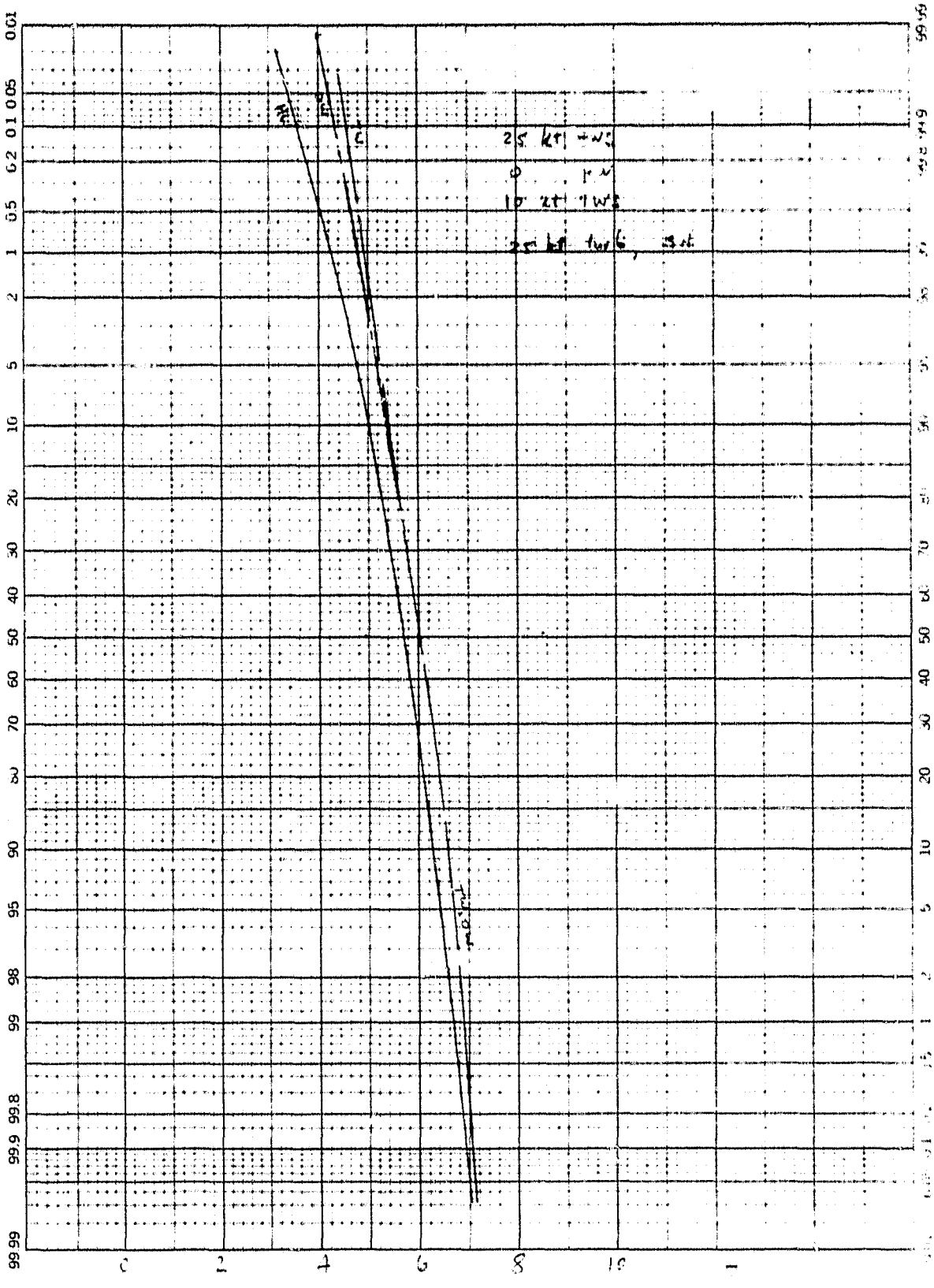

FIGURE B-35. FOUR CONTROLS, $k\delta_{TF}$ = 2.53

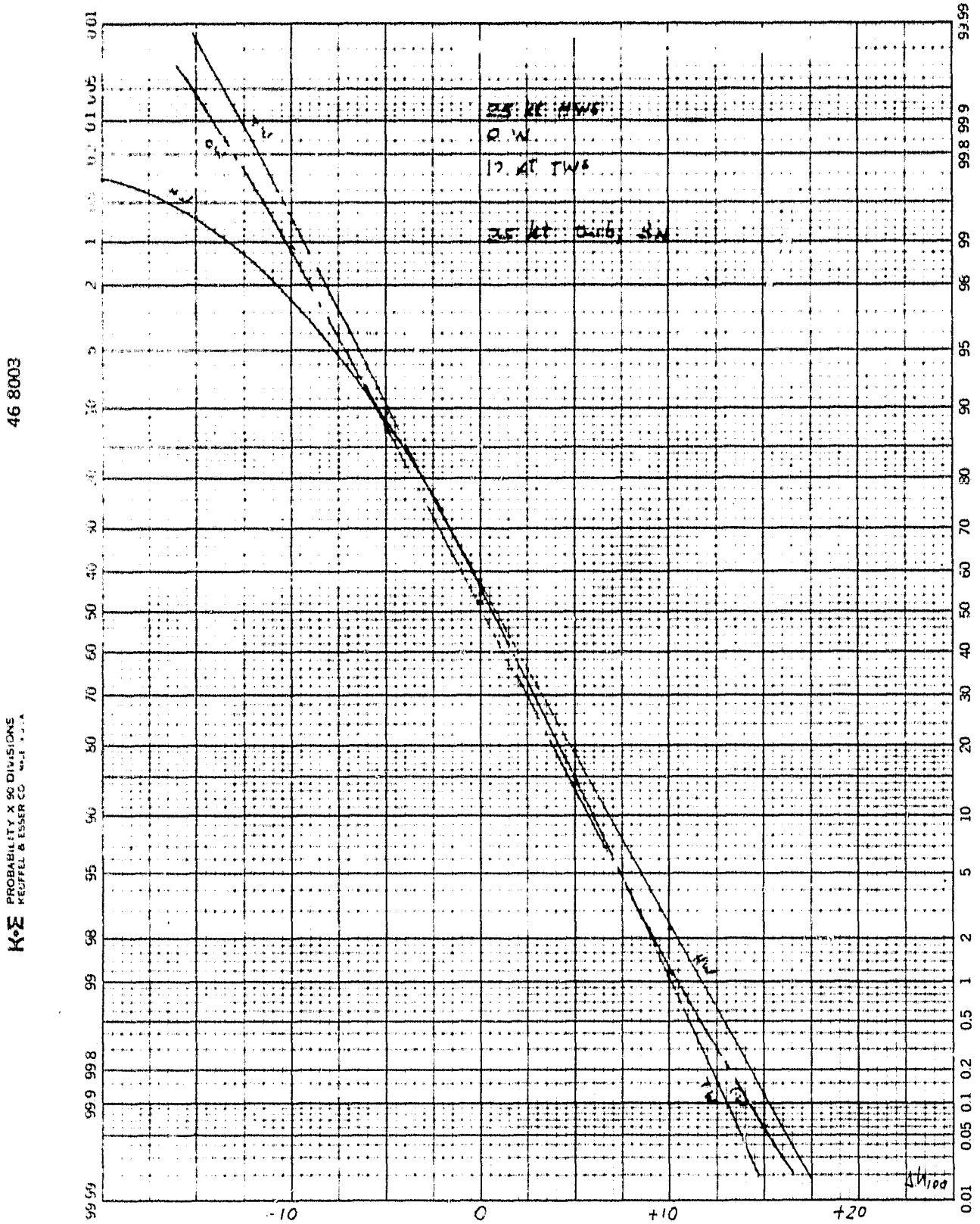

FIGURE B-36. FOUR CONTROLS, $k\delta_{TF}$ = 2.53

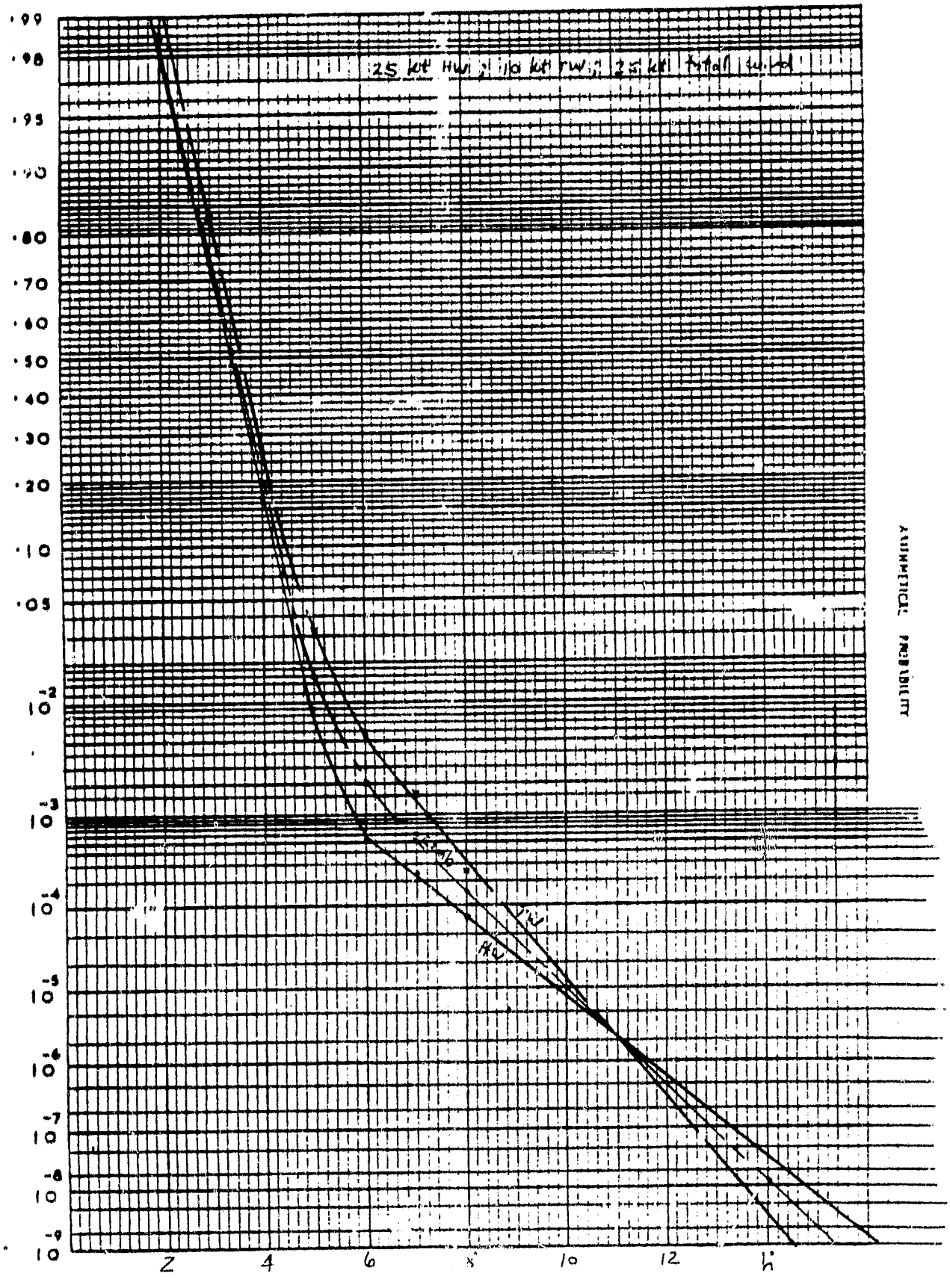

FIGURE B-37. THREE CONTROLS, $K_{\delta TF}$ = 2.53

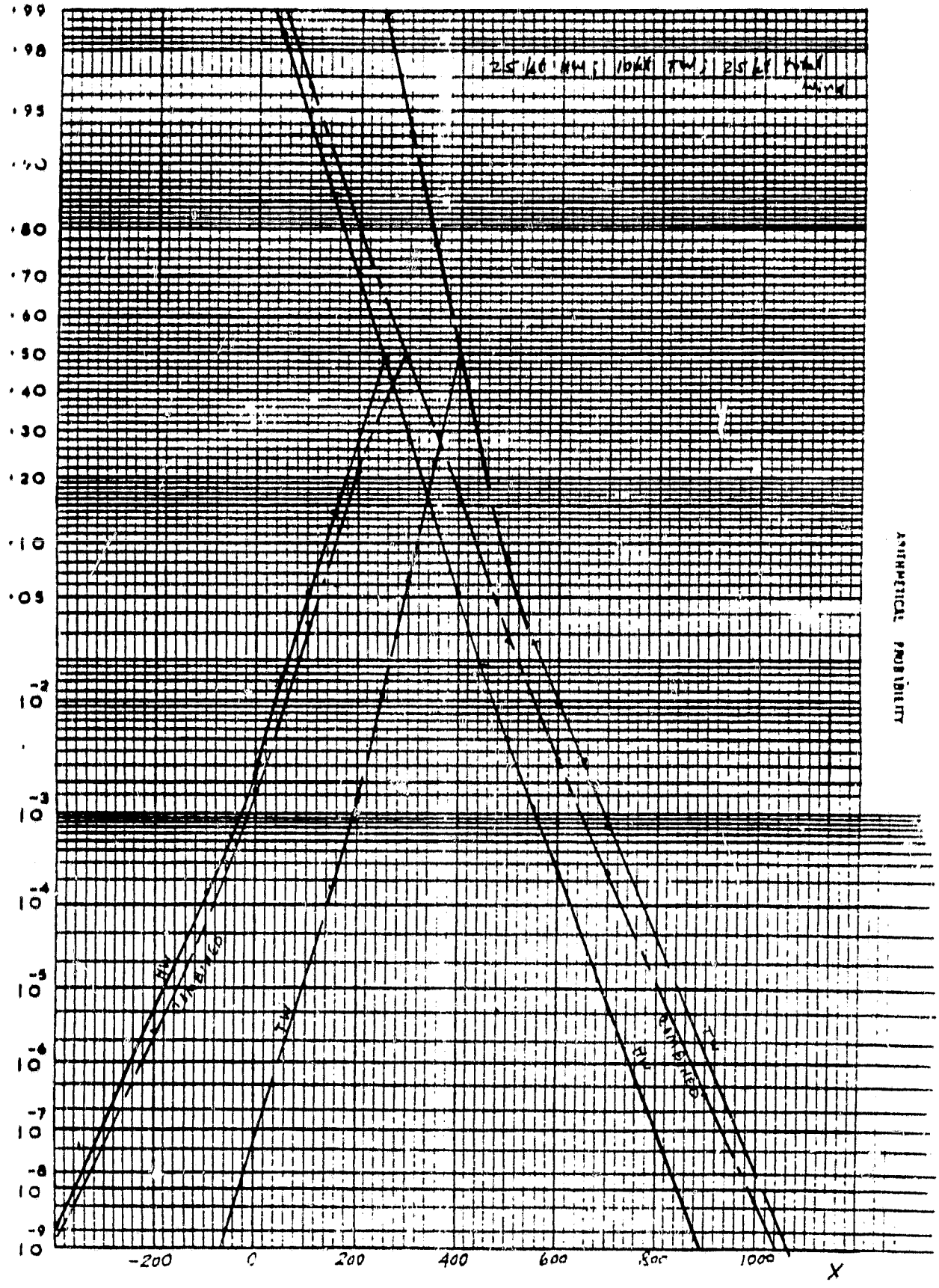

FIGURE B-38. THREE CONTROLS, $k\delta_{TF} = 2.53$

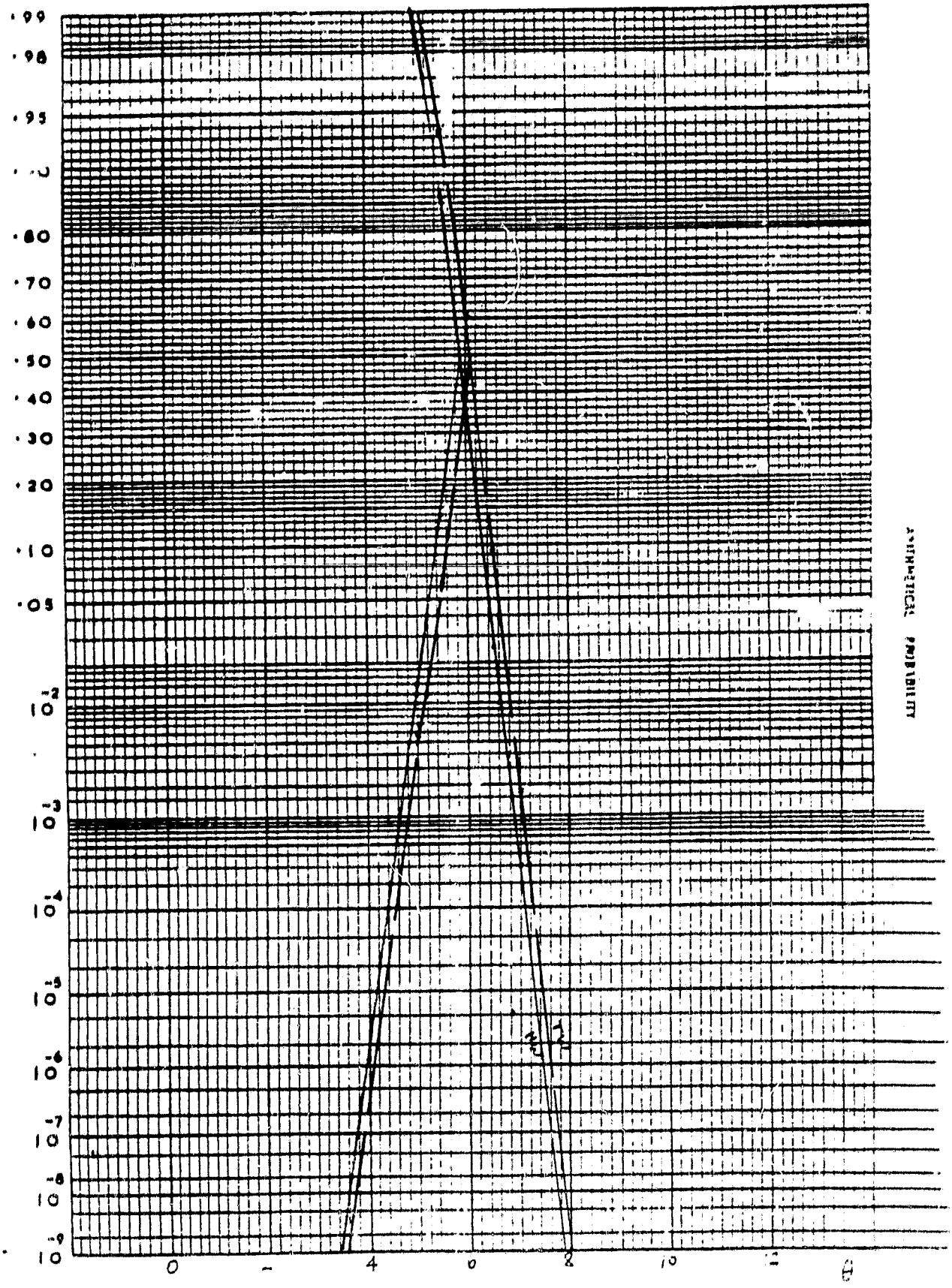

FIGURE B-39. THREE CONTROLS, $k\delta_{TF}$ = 2.53

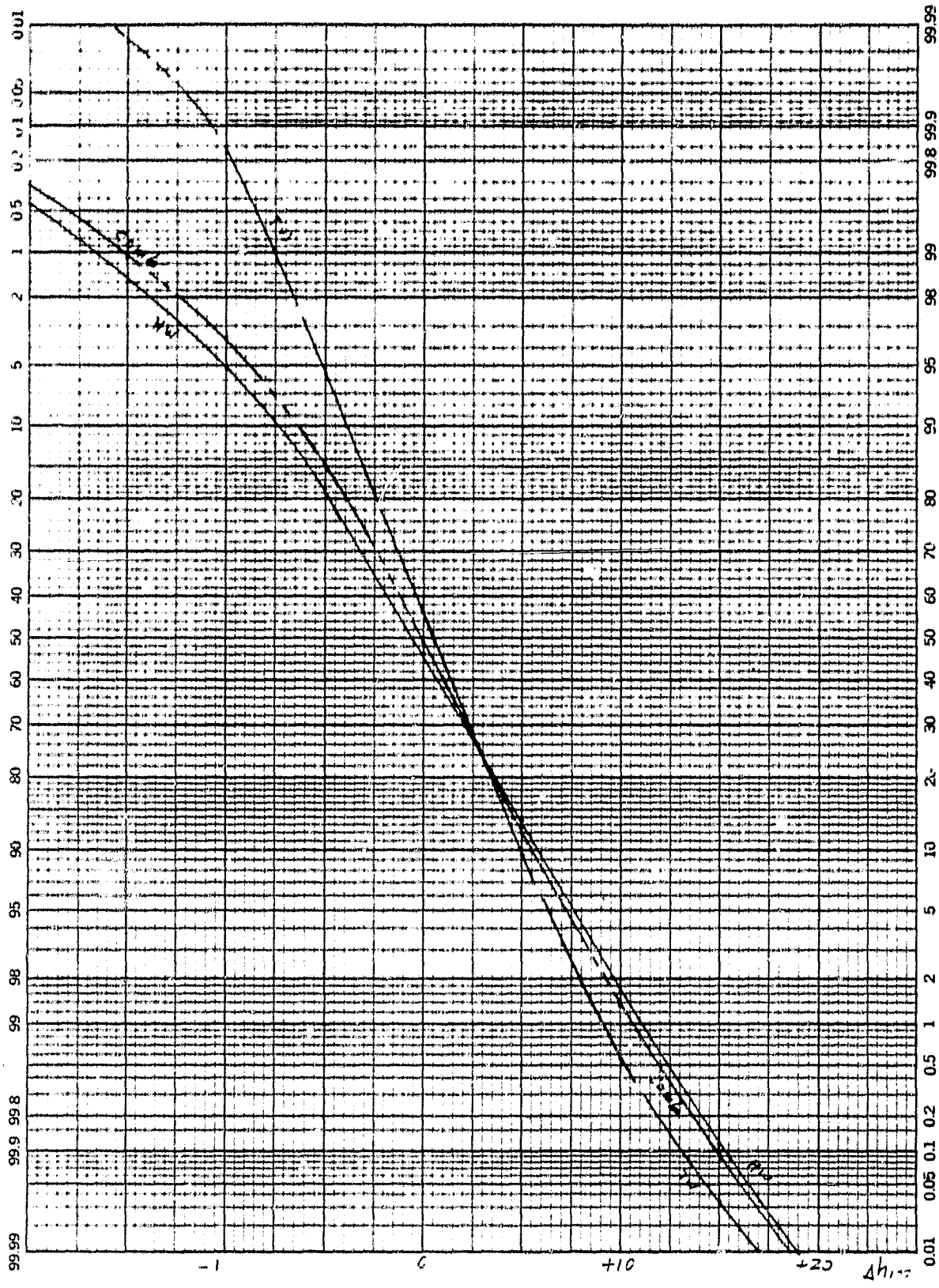

FIGURE B-40. THREE CONTROLS, $k\delta_{TF}$ = 2.53

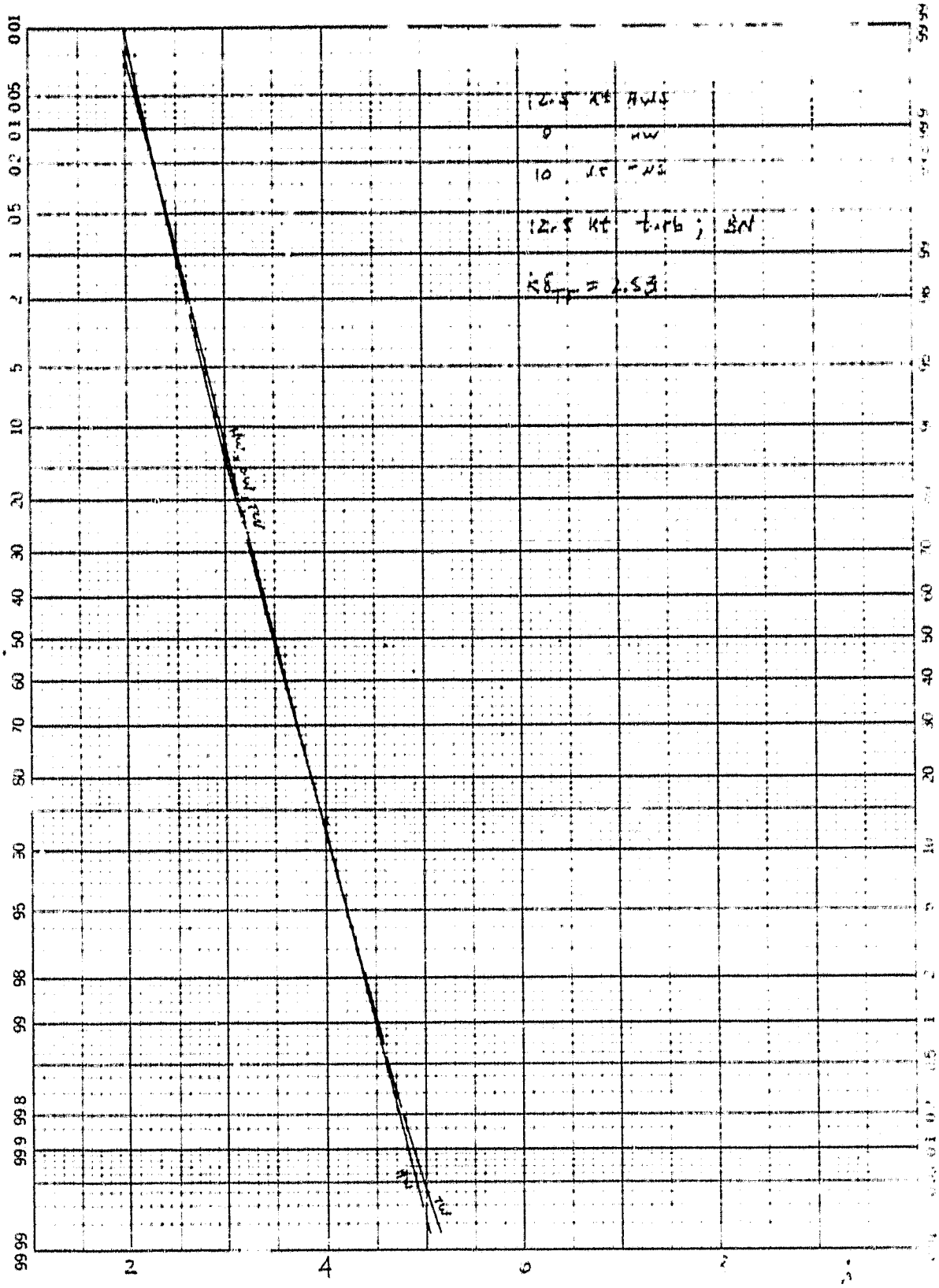

FIGURE B-41. FOUR CONTROLS, REDUCED WIND LEVEL

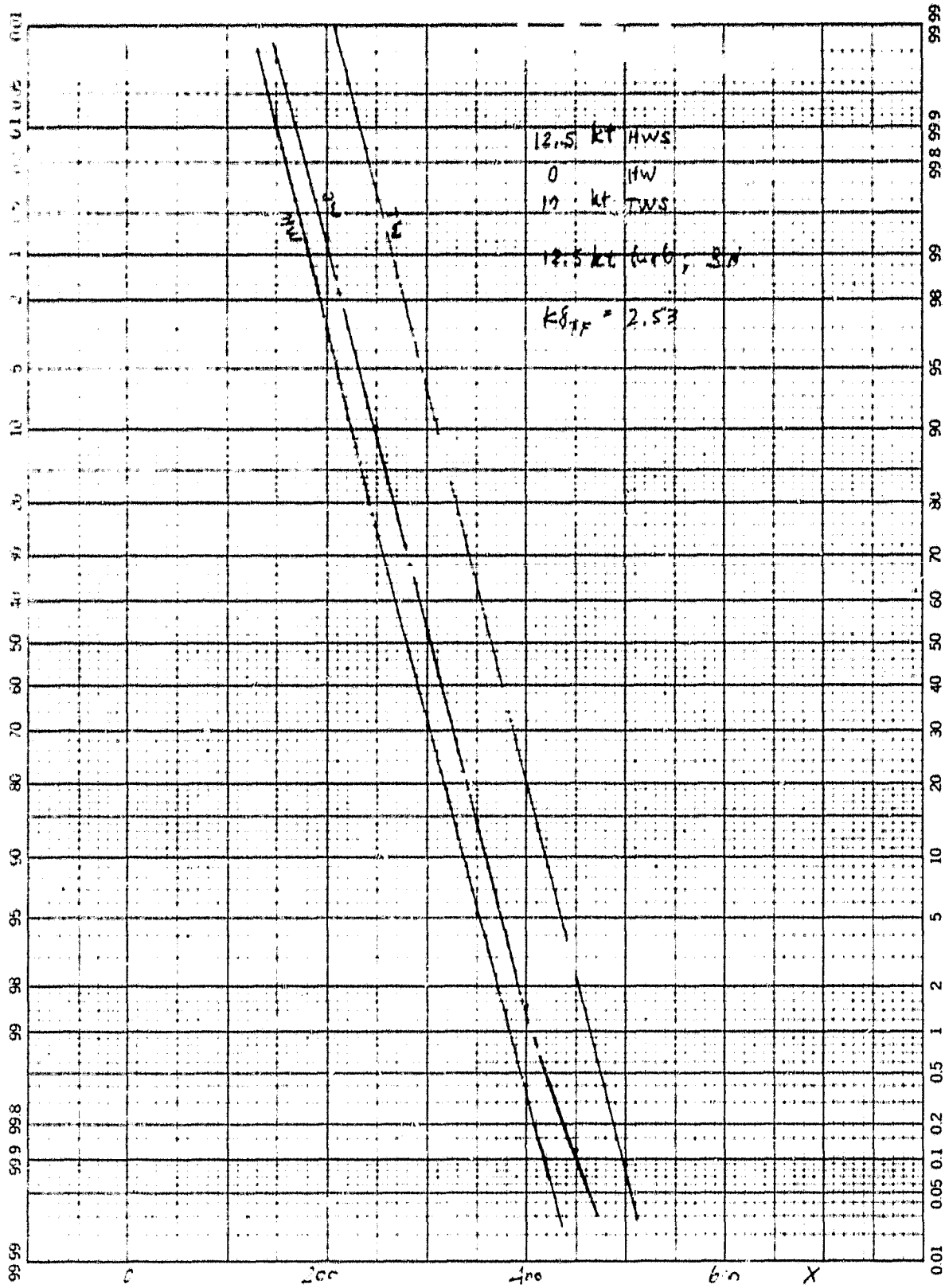

46 8003

K&E PROBABILITY X & LOGARITHMIC
KEUFFEL & ESSER CO

FIGURE B-42. FOUR CONTROLS, REDUCED WIND LEVEL

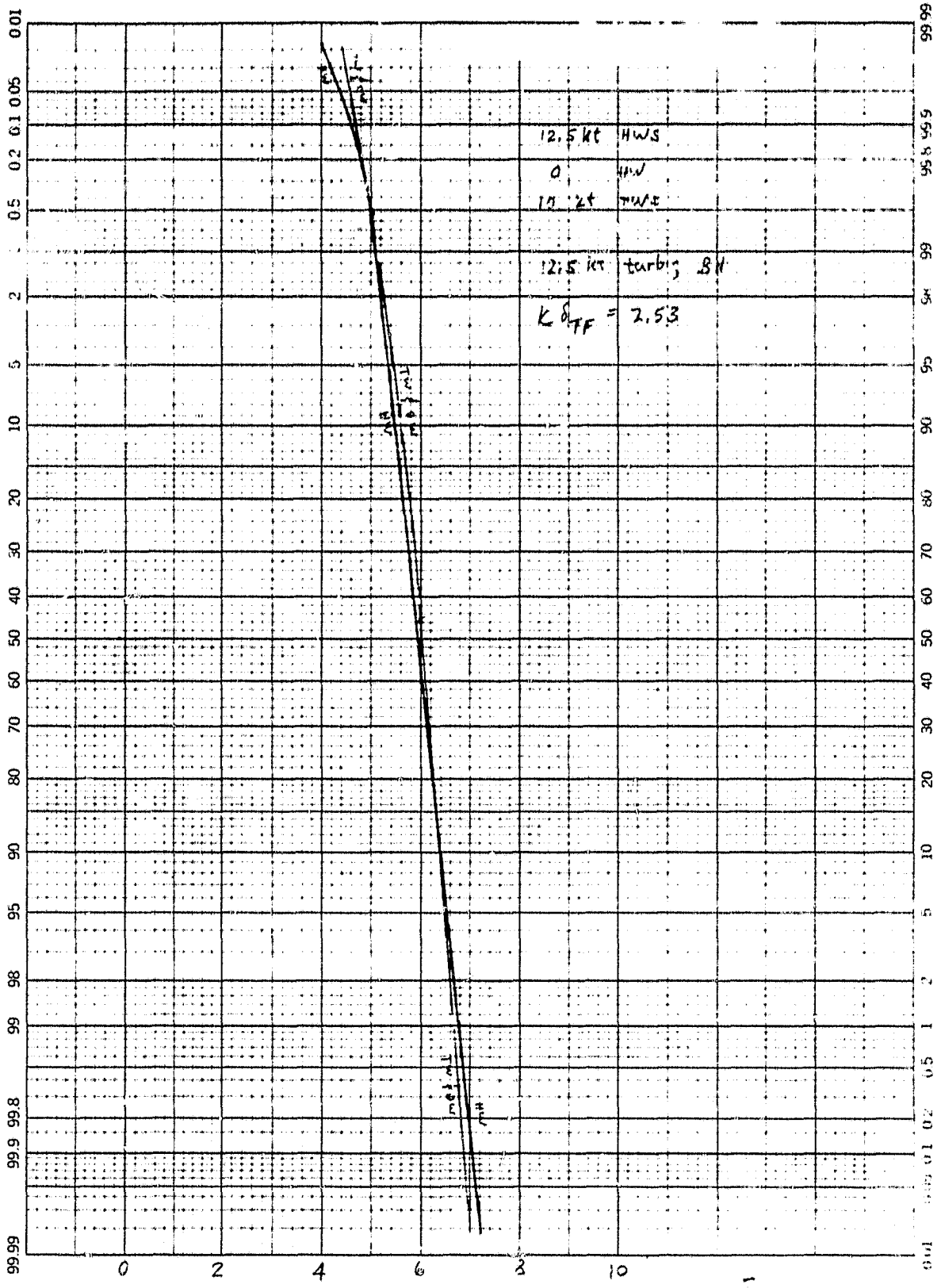

46 8003

PROBABILITY X 90 VISIONS
KEUFFEL & ESSER CO

FIGURE B-43. FOUR CONTROLS, REDUCED WIND LEVEL

C-3

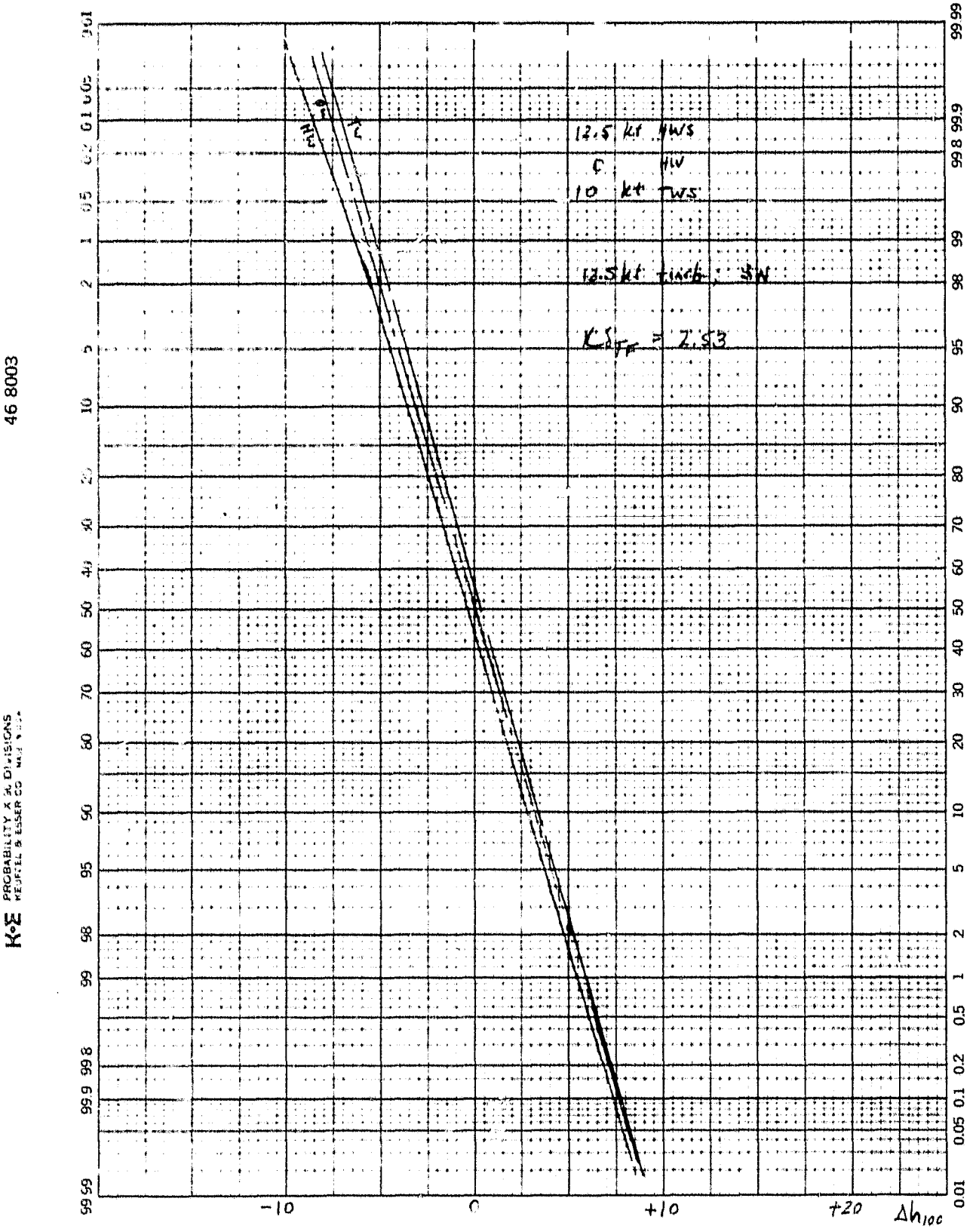

46 8003

K·E PROBABILITY X & Y DIVISIONS
KEUFFEL & ESSER CO.

FIGURE B-44. FOUR CONTROLS, REDUCED WIND LEVEL

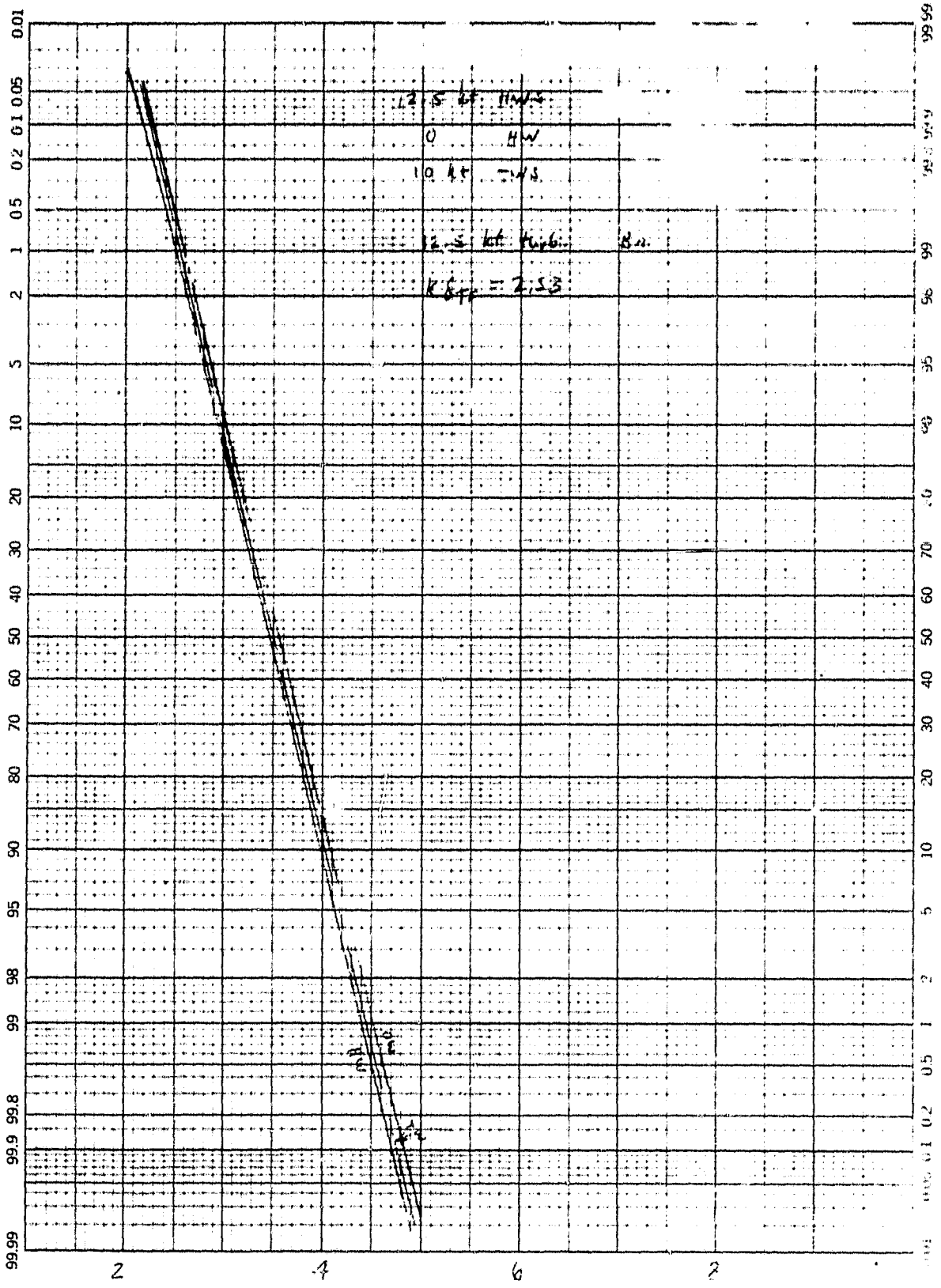

PROBABILITY X BY IVISIONS
KEUFFEL & ESSER CO

46 8003

FIGURE B-45. THREE CONTROLS, REDUCED WIND LEVEL

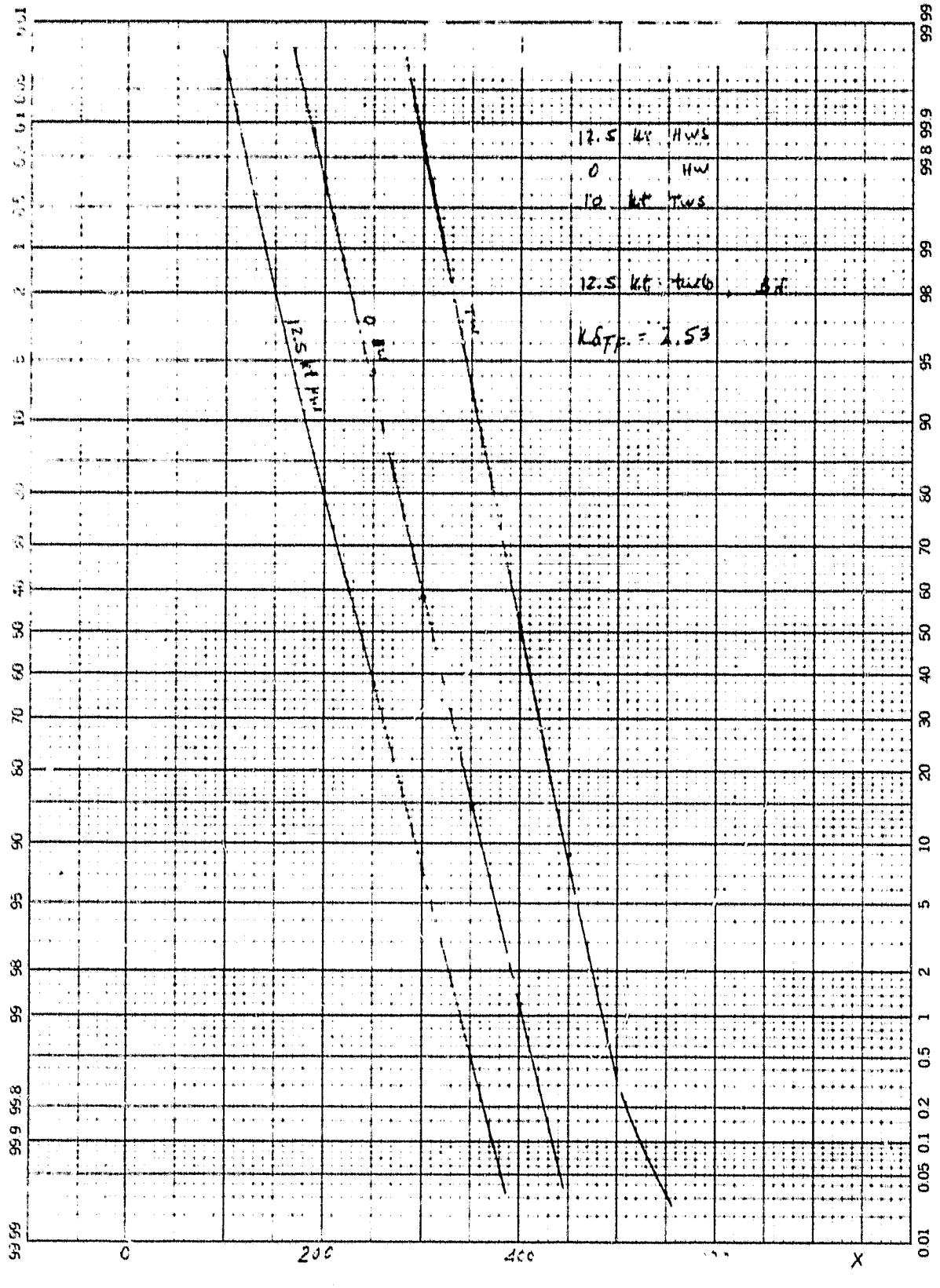

FIGURE B-46. THREE CONTROLS, REDUCED WIND LEVELS

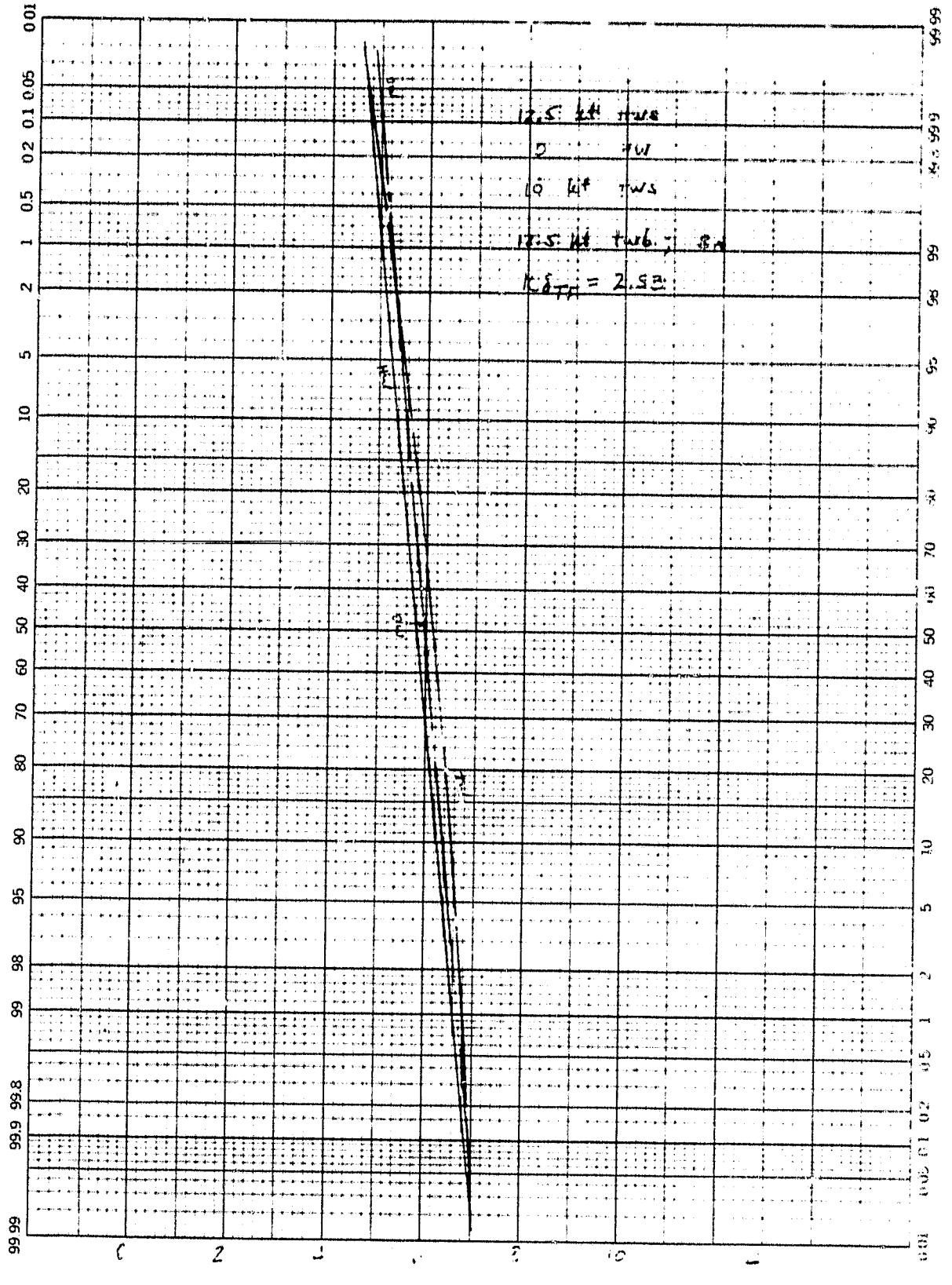

46 8003

K&E PROBABILITY X-Y DIVISIONS
KEUFFEL & ESSER CO.

FIGURE B-47. THREE CONTROLS, REDUCED WIND LEVELS

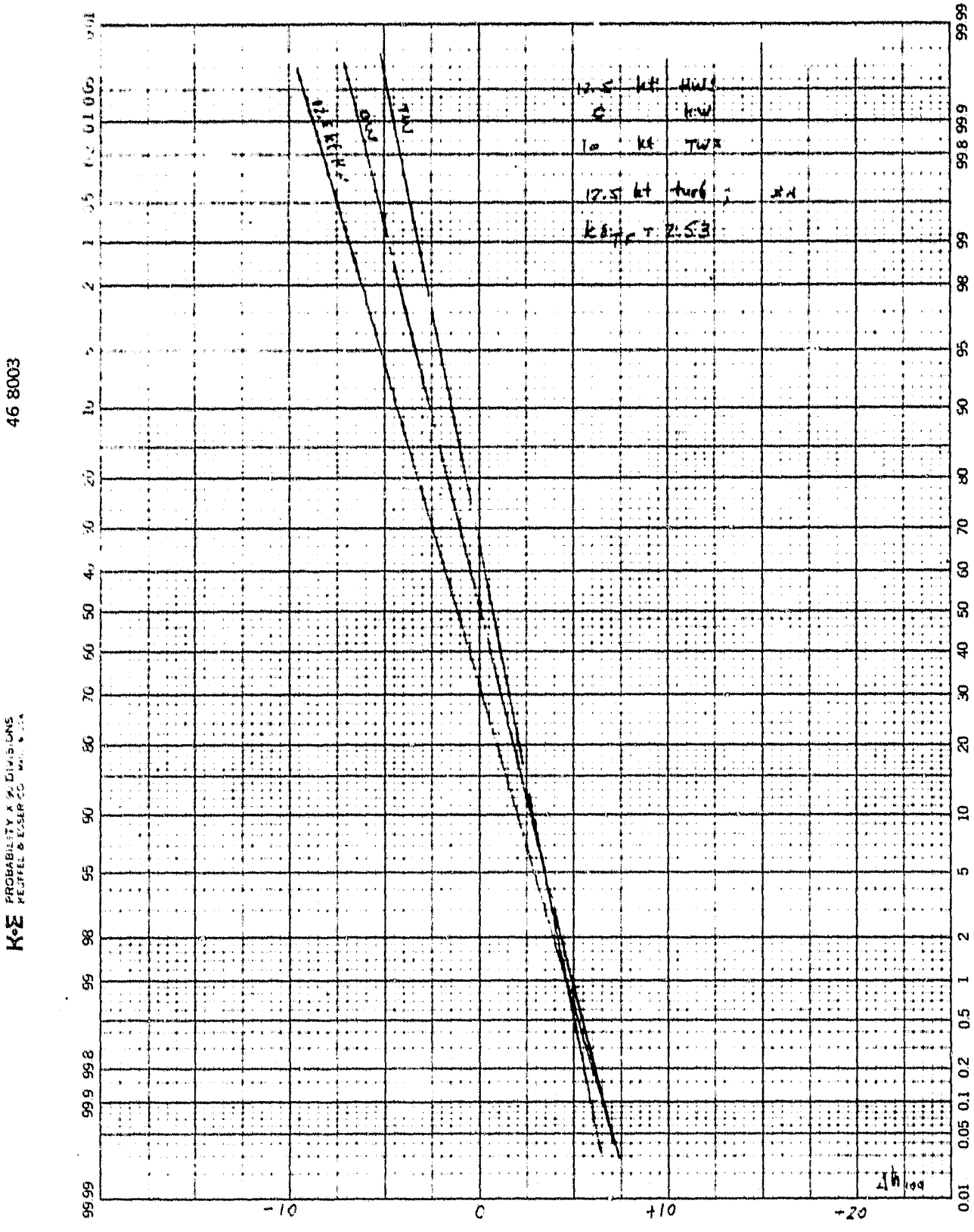

FIGURE B-48. THREE CONTROLS, REDUCED WIND LEVEL

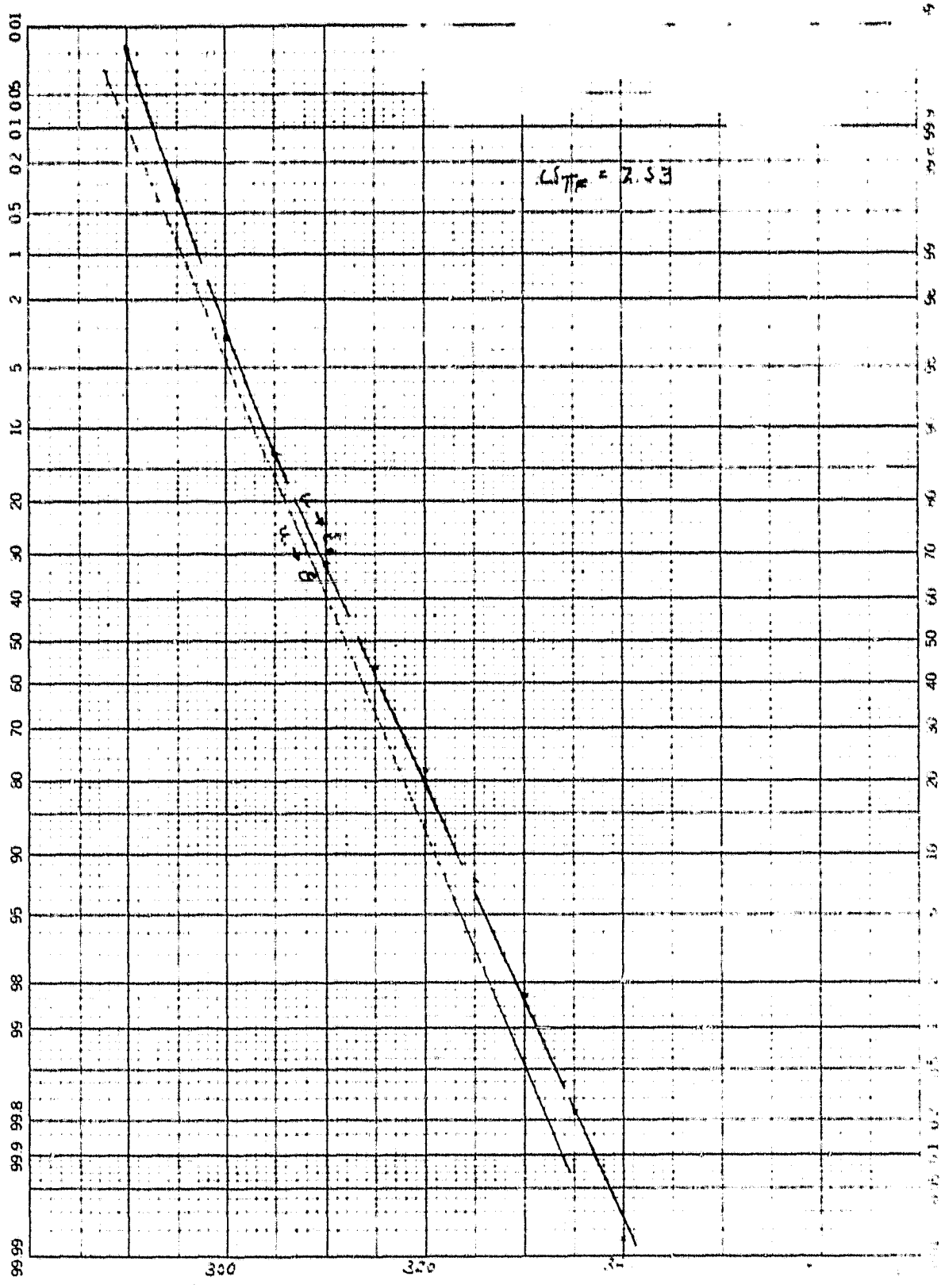

FIGURE B-49. FOUR AND THREE CONTROLS, BEAM NOISE ONLY

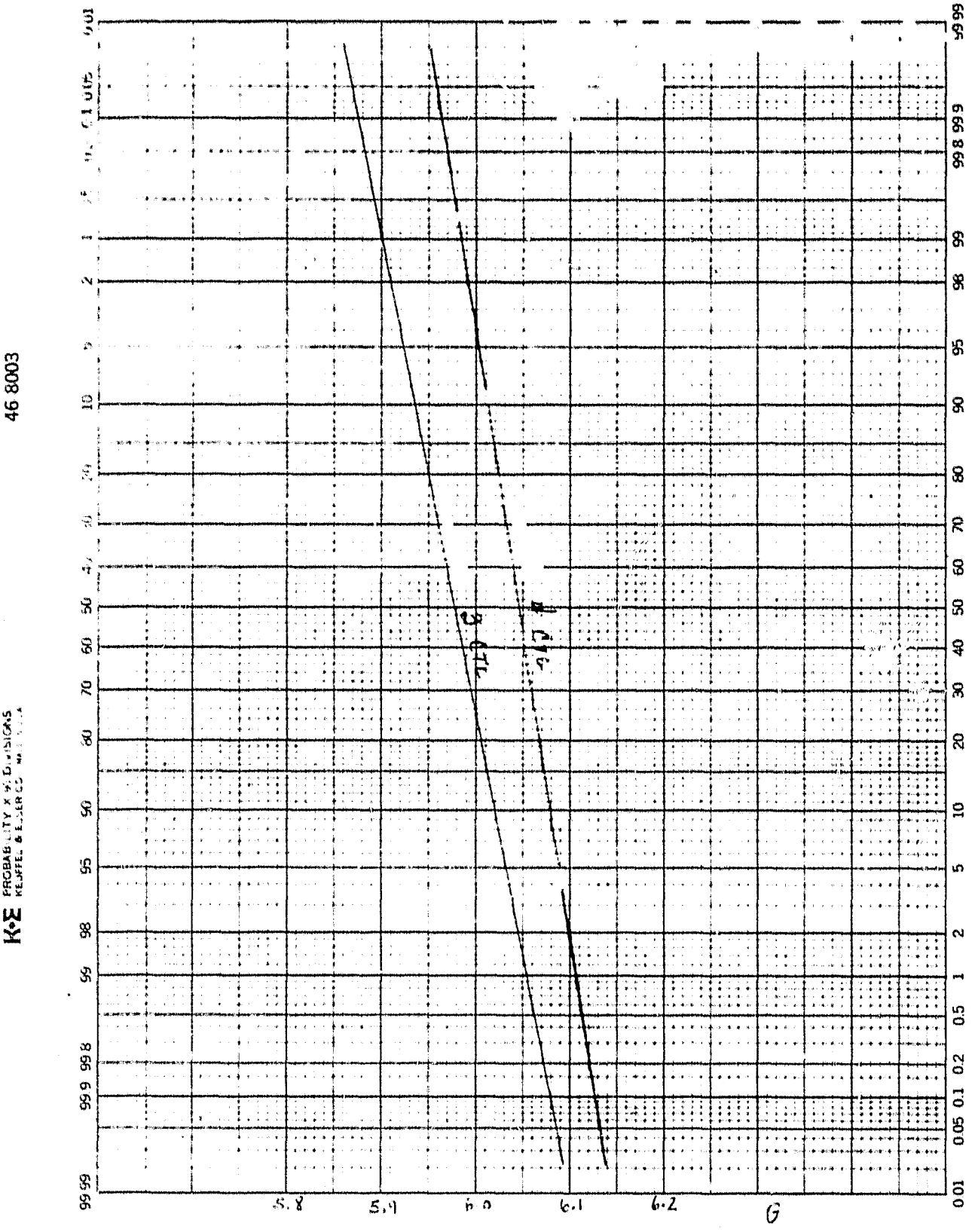

FIGURE B-50. FOUR AND THREE CONTROLS, BEAM NOISE ONLY

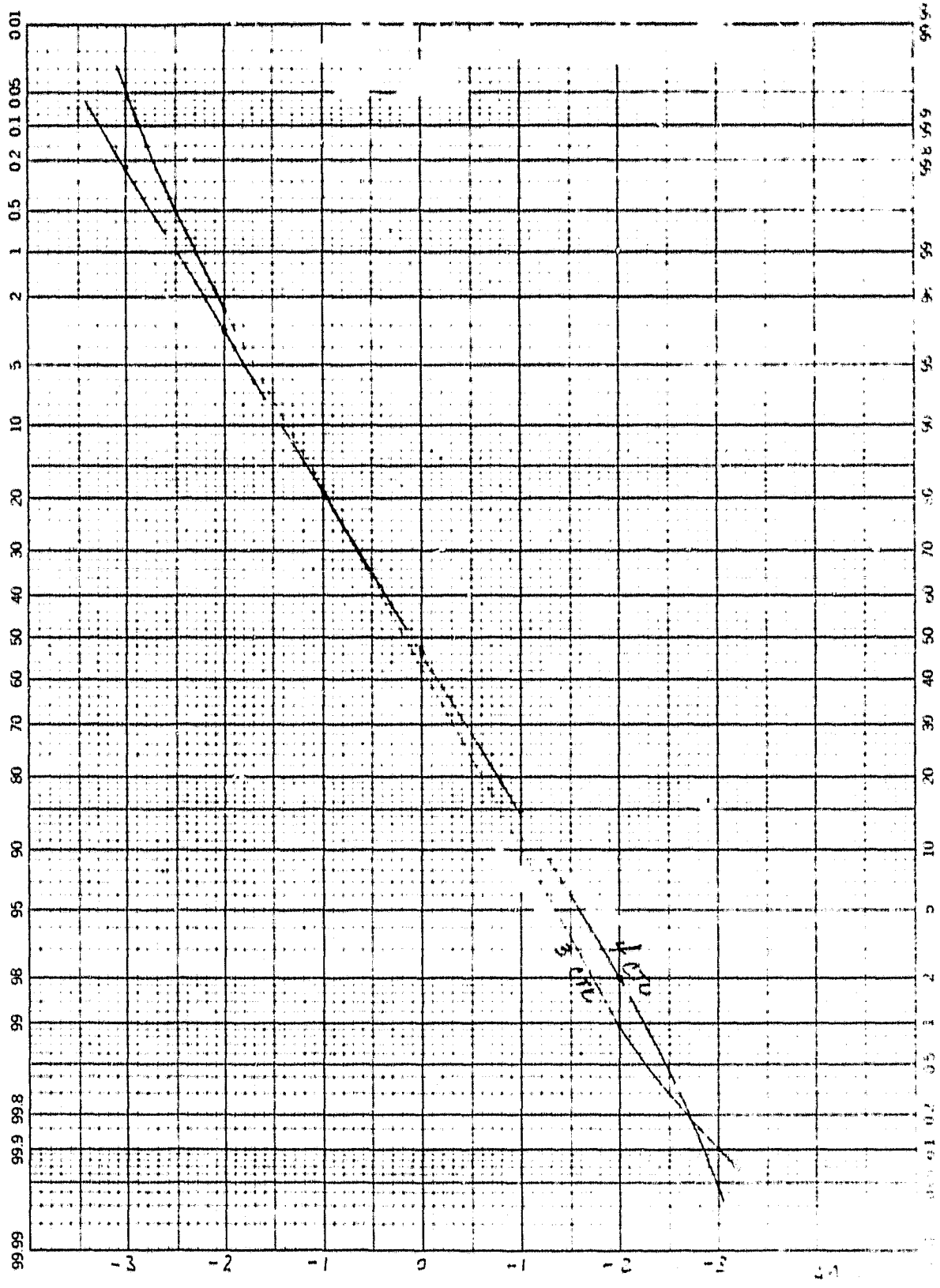

FIGURE B-51. FOUR AND THREE CONTROLS, BEAM NOISE ONLY

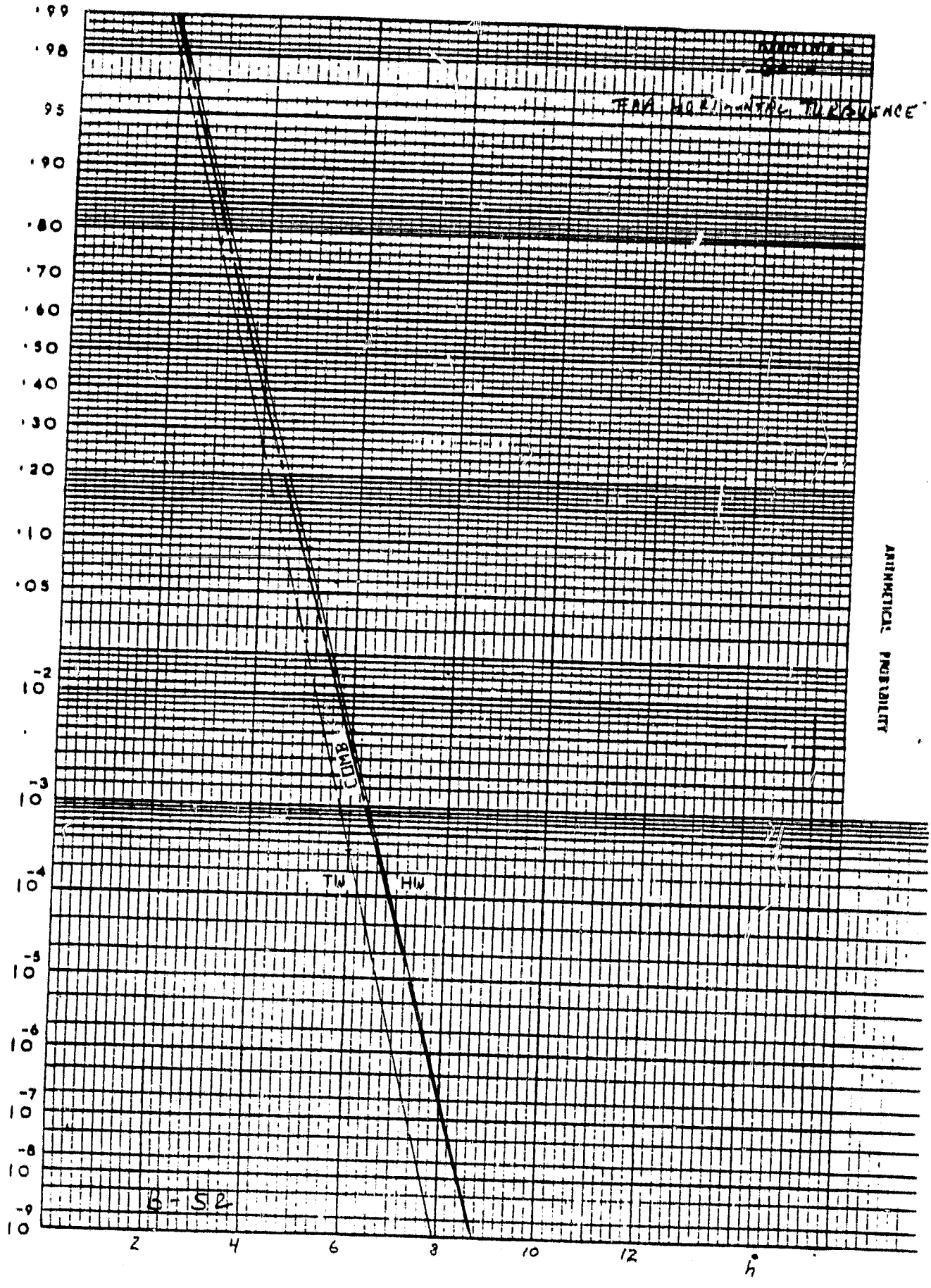

FIGURE B-52. FOUR CONTROLS, CAA VERTICAL TURBULENCE

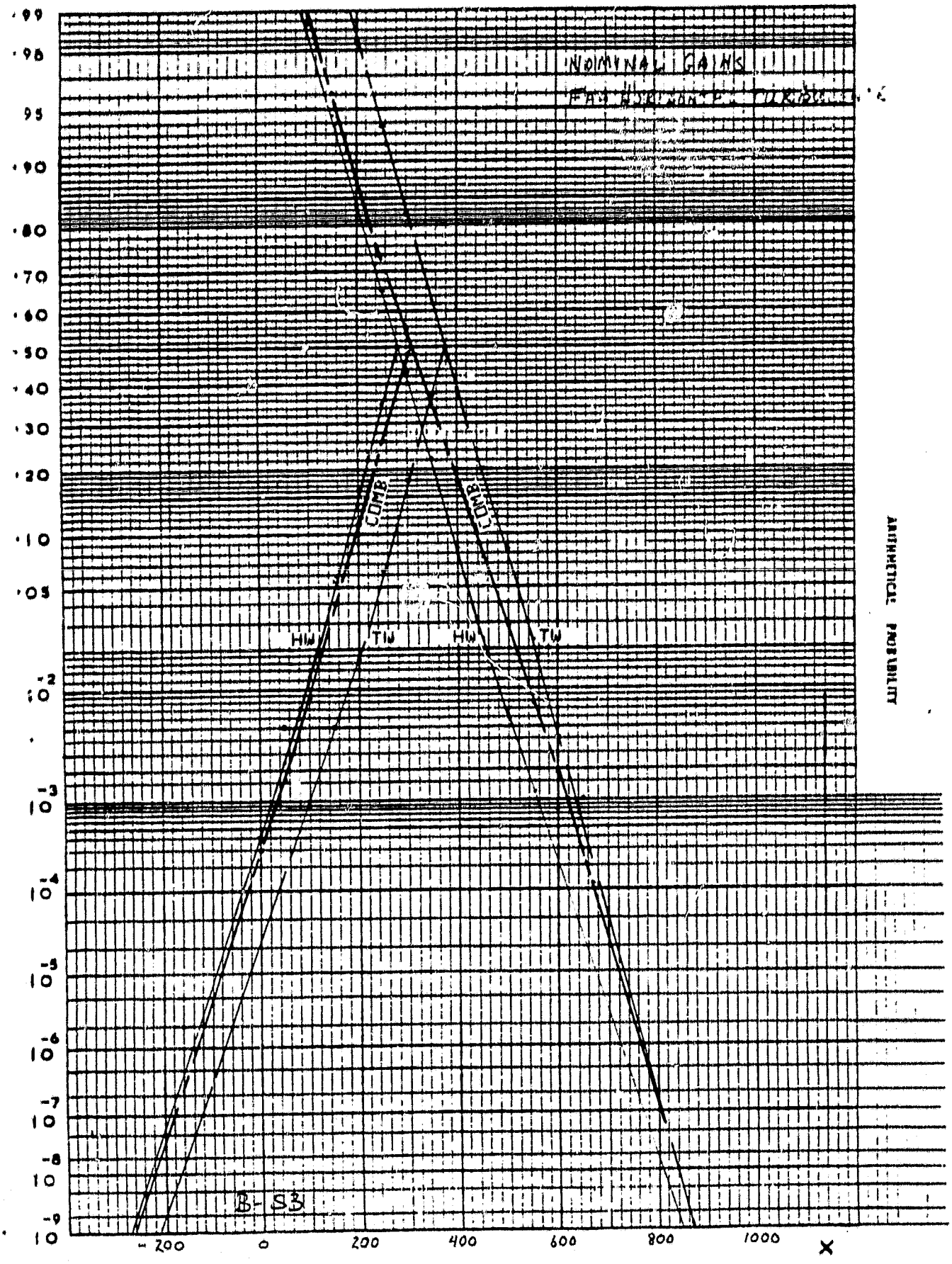

FIGURE B-53. FOUR CONTROLS, CAA VERTICAL TURBULENCE

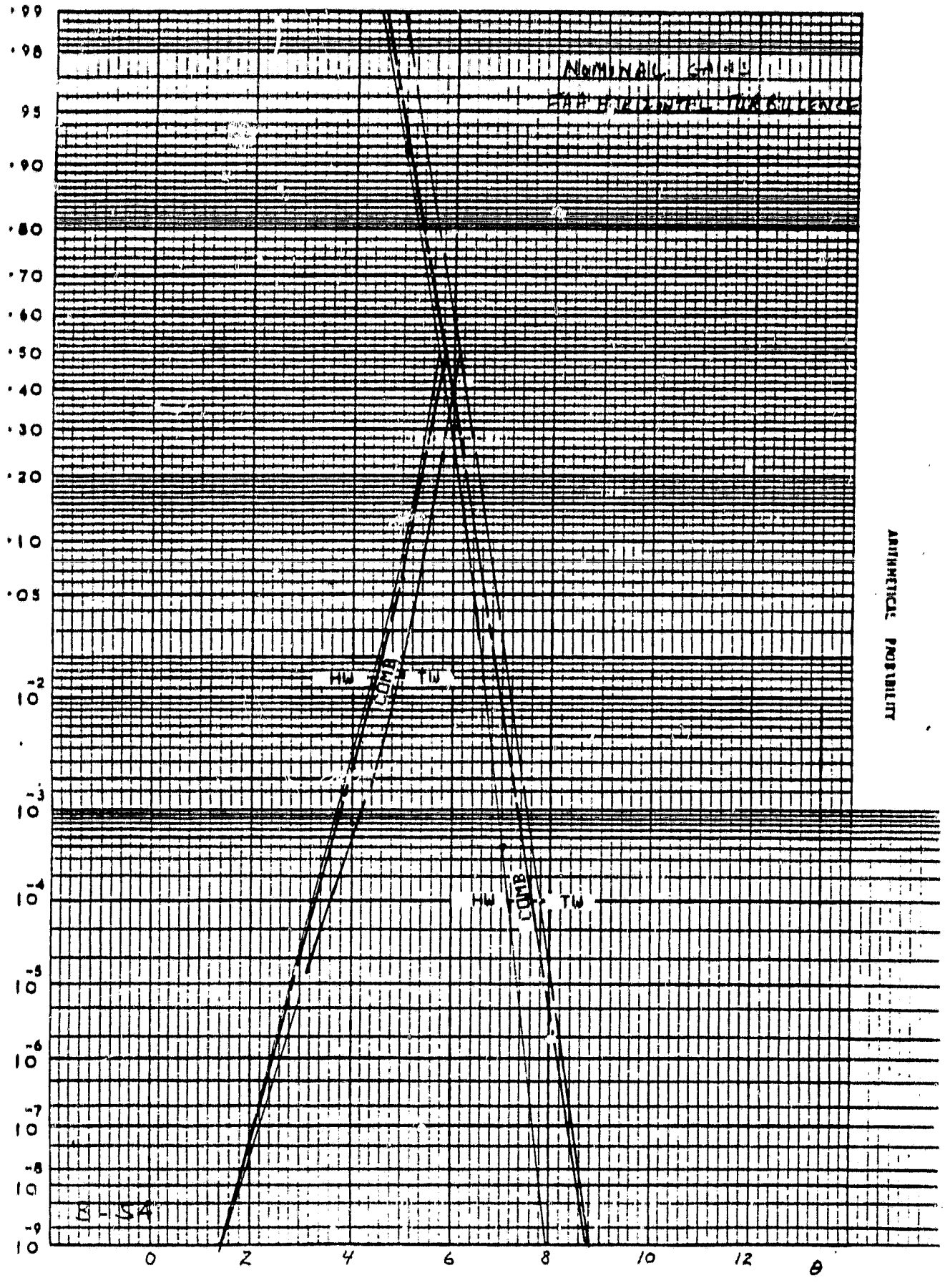

FIGURE B-54. FOUR CONTROLS, CAA VERTICAL TURBULENCE

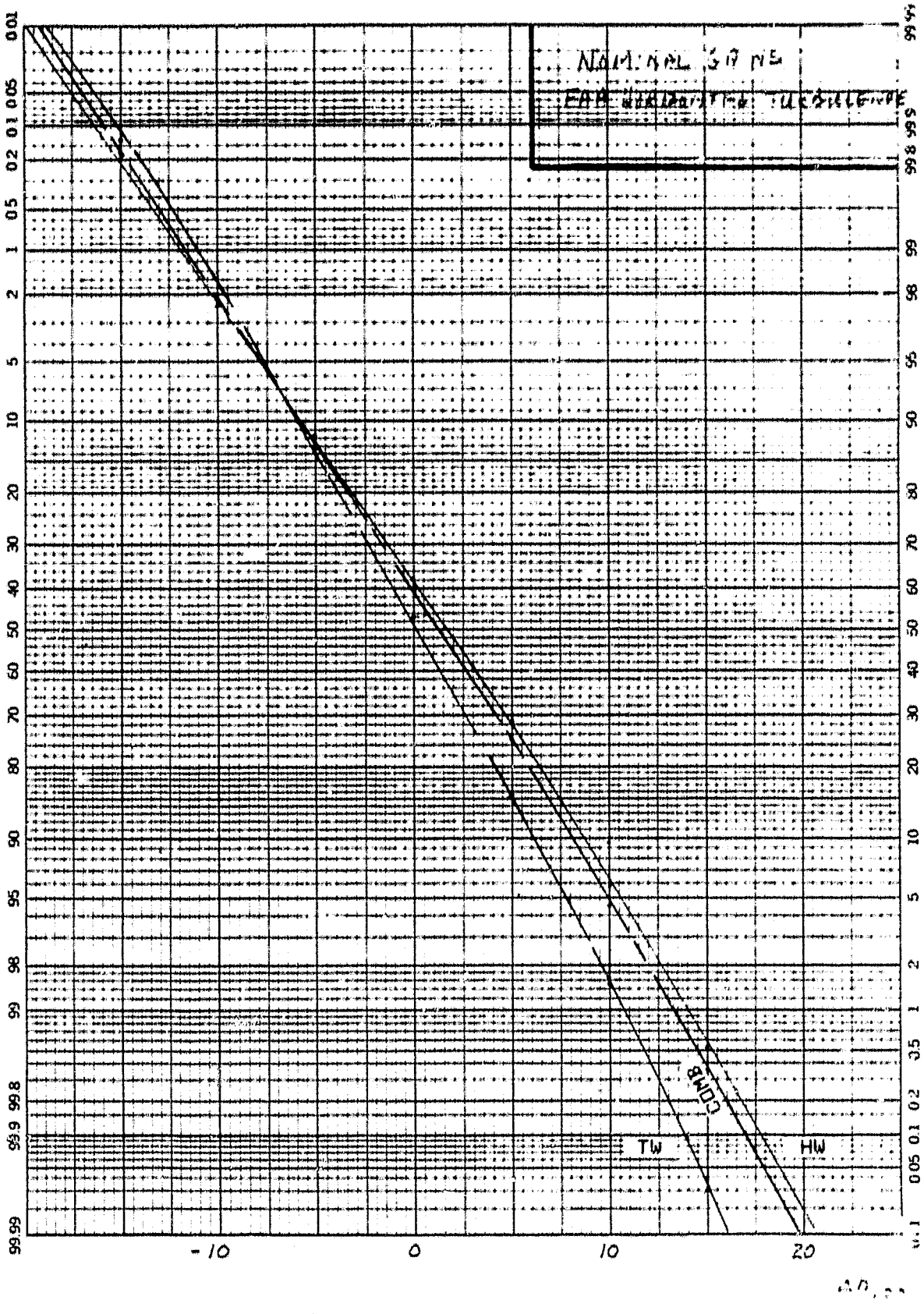

FIGURE B-55. FOUR CONTROLS, CAA VERTICAL TURBULENCE

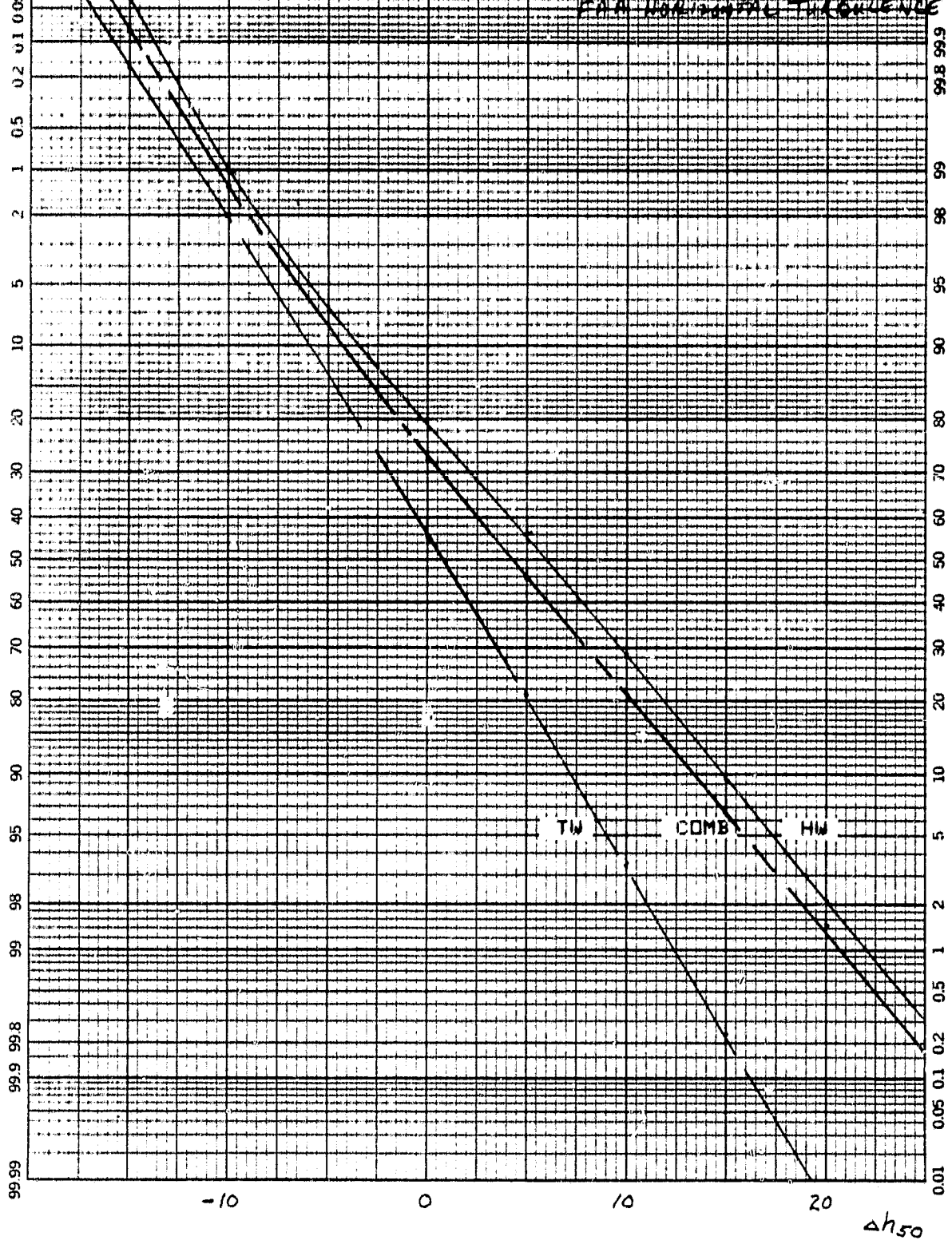

46 8003

K&E PROBABILITY X 90 DIVISIONS
KEUFFEL & ESSER CO MADE IN U.S.A.

FIGURE B-56. FOUR CONTROLS, CAA VERTICAL TURBULENCE

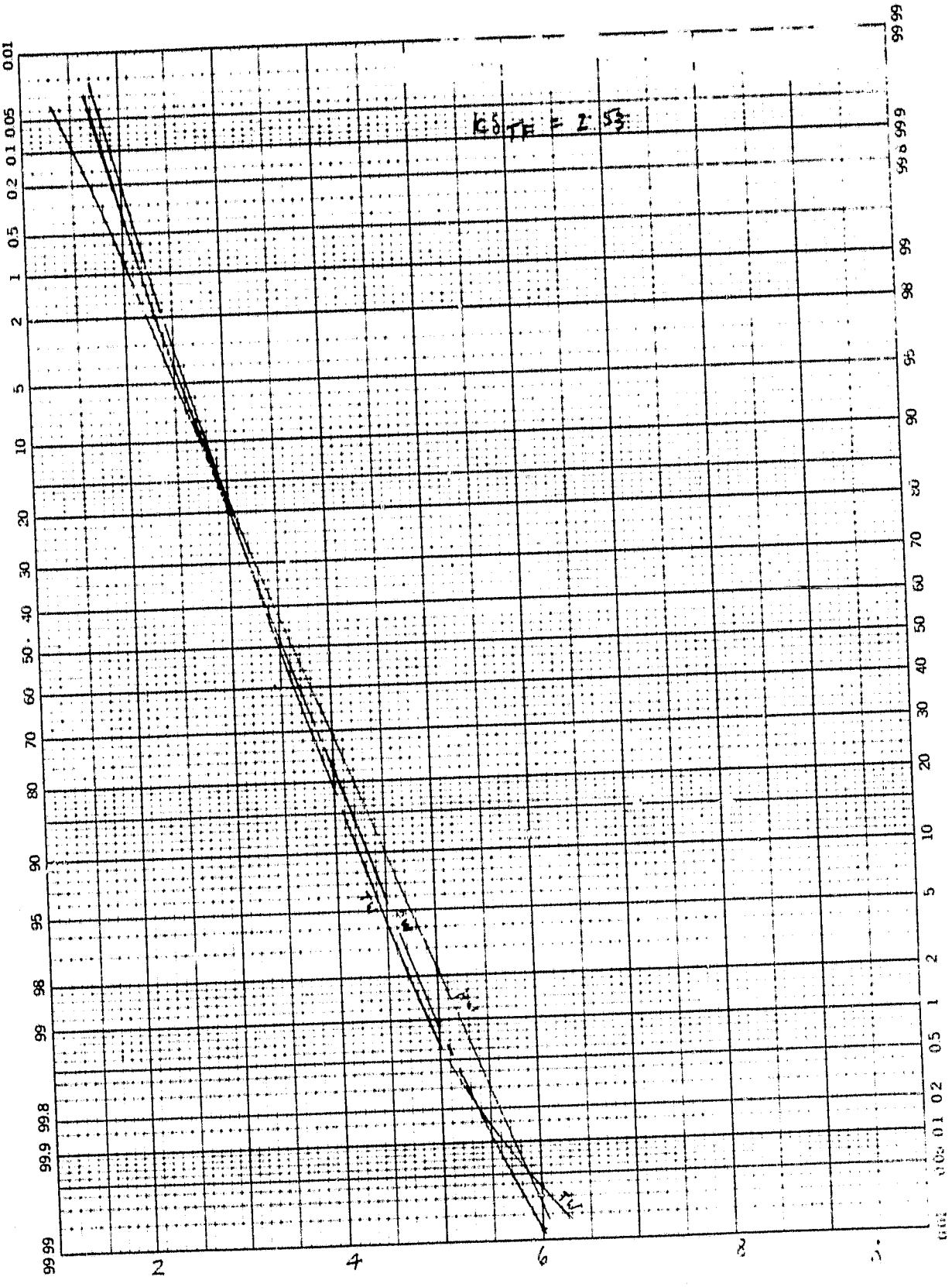

FIGURE B-57. LIGHT WEIGHT, FOUR CONTROLS

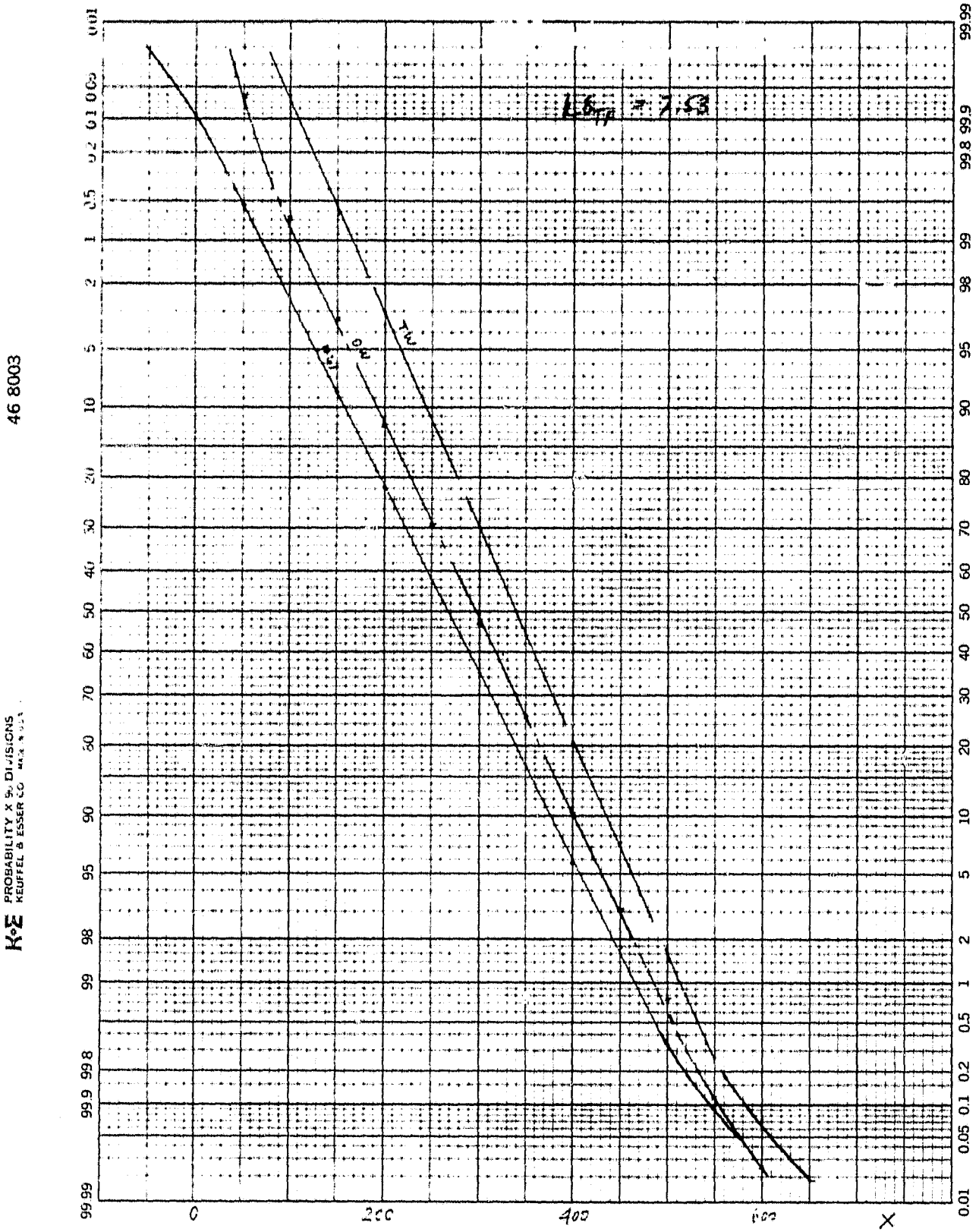

FIGURE B-58. LIGHT WEIGHT, FOUR CONTROLS

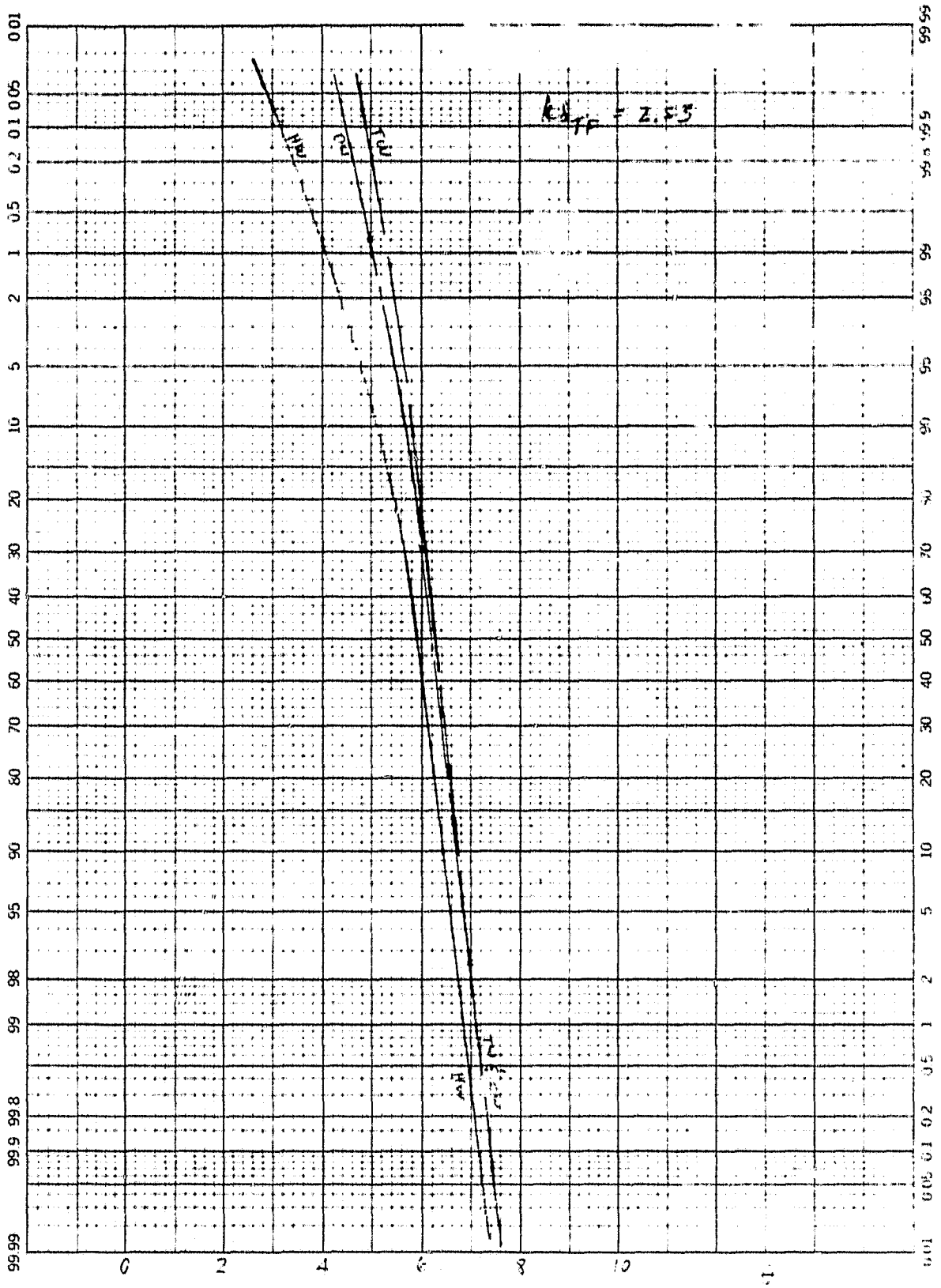

46 8003

FIGURE B-59. LIGHT WEIGHT, FOUR CONTROLS

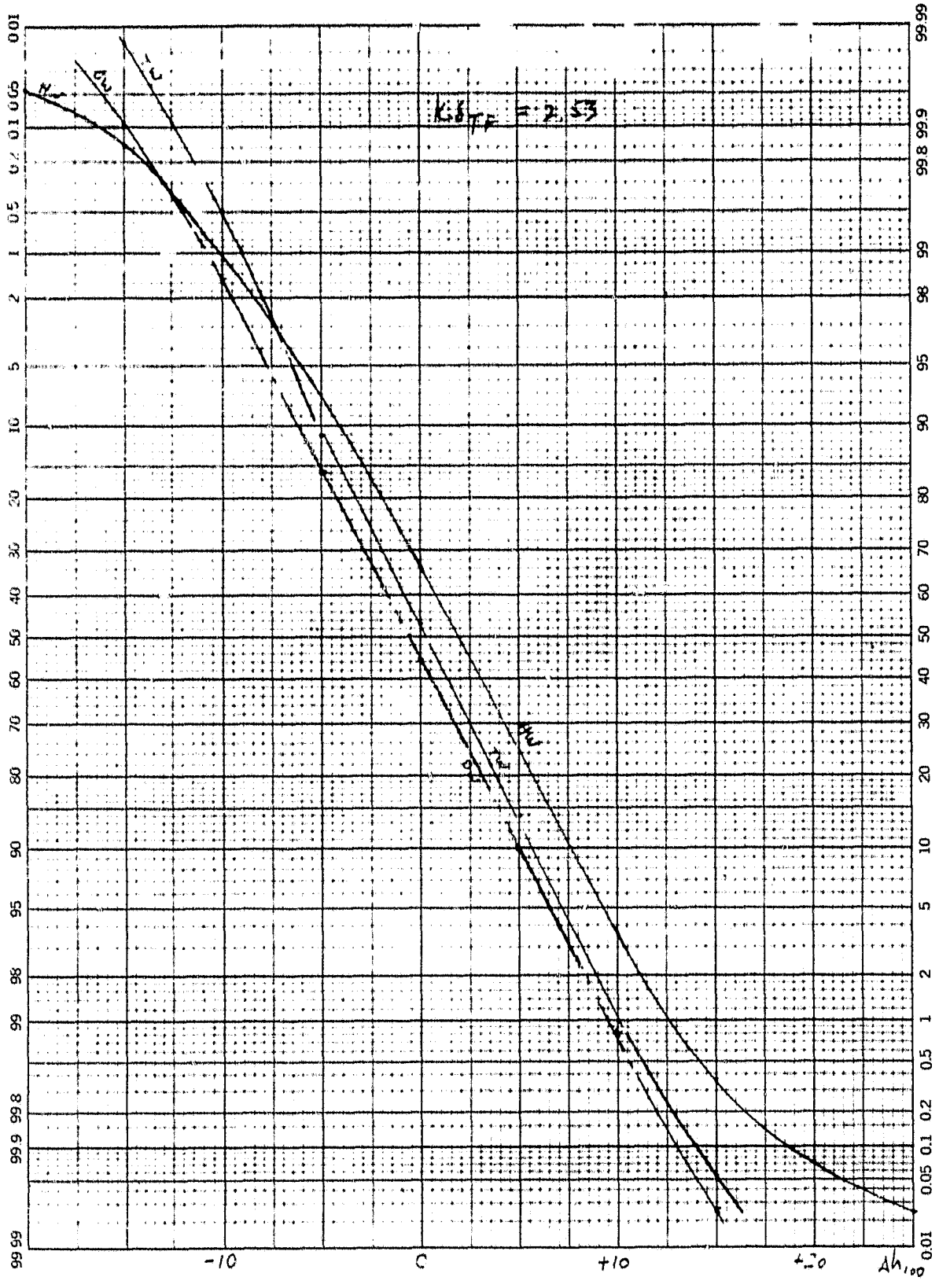

FIGURE B-60. LIGHT WEIGHT, FOUR CONTROLS

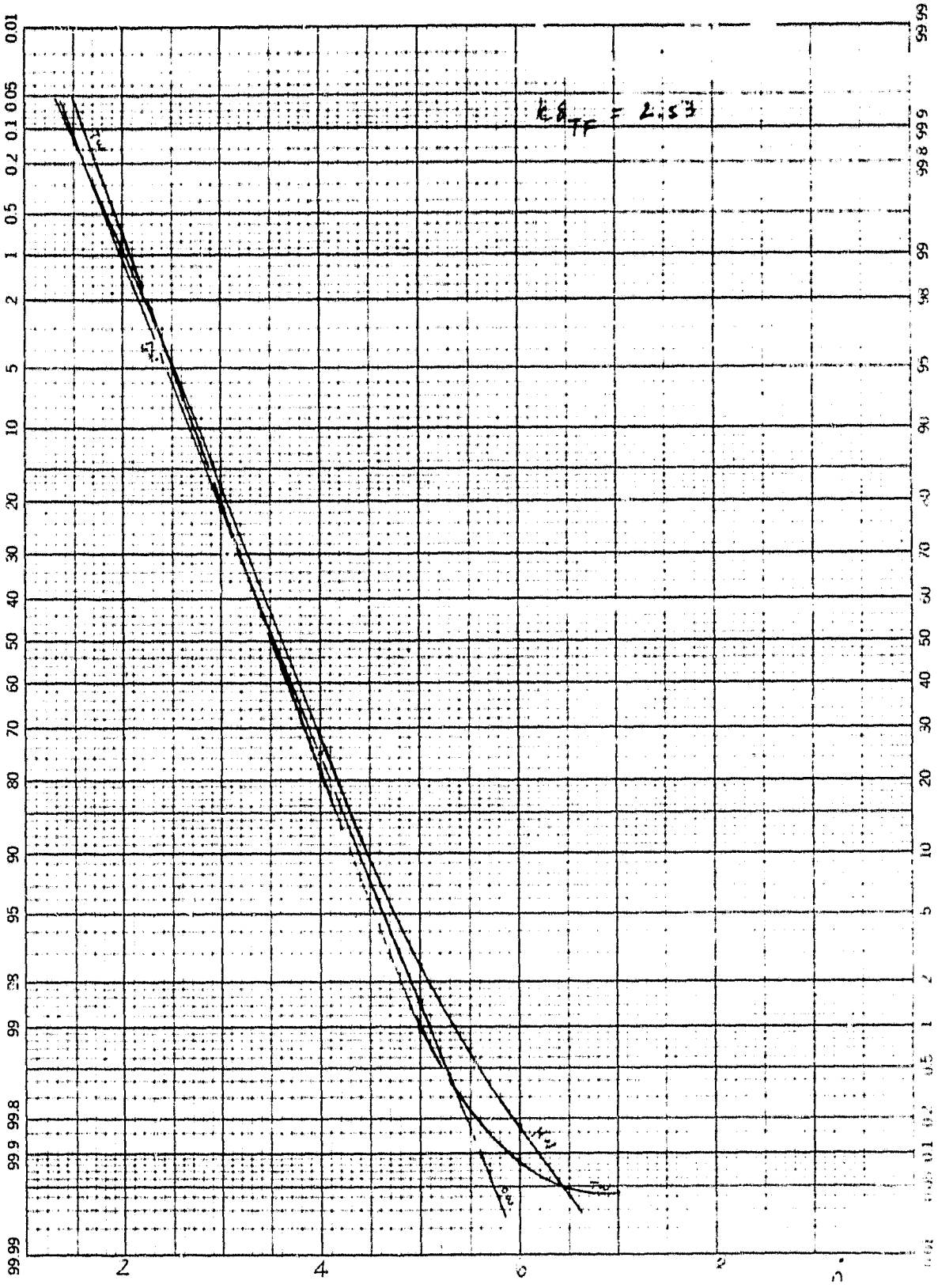

46 8003

KEUFFEL & ESSER CO. PROBABILITY X 96 DIVISIONS

FIGURE B-61. HEAVY WEIGHT, FOUR CONTROLS

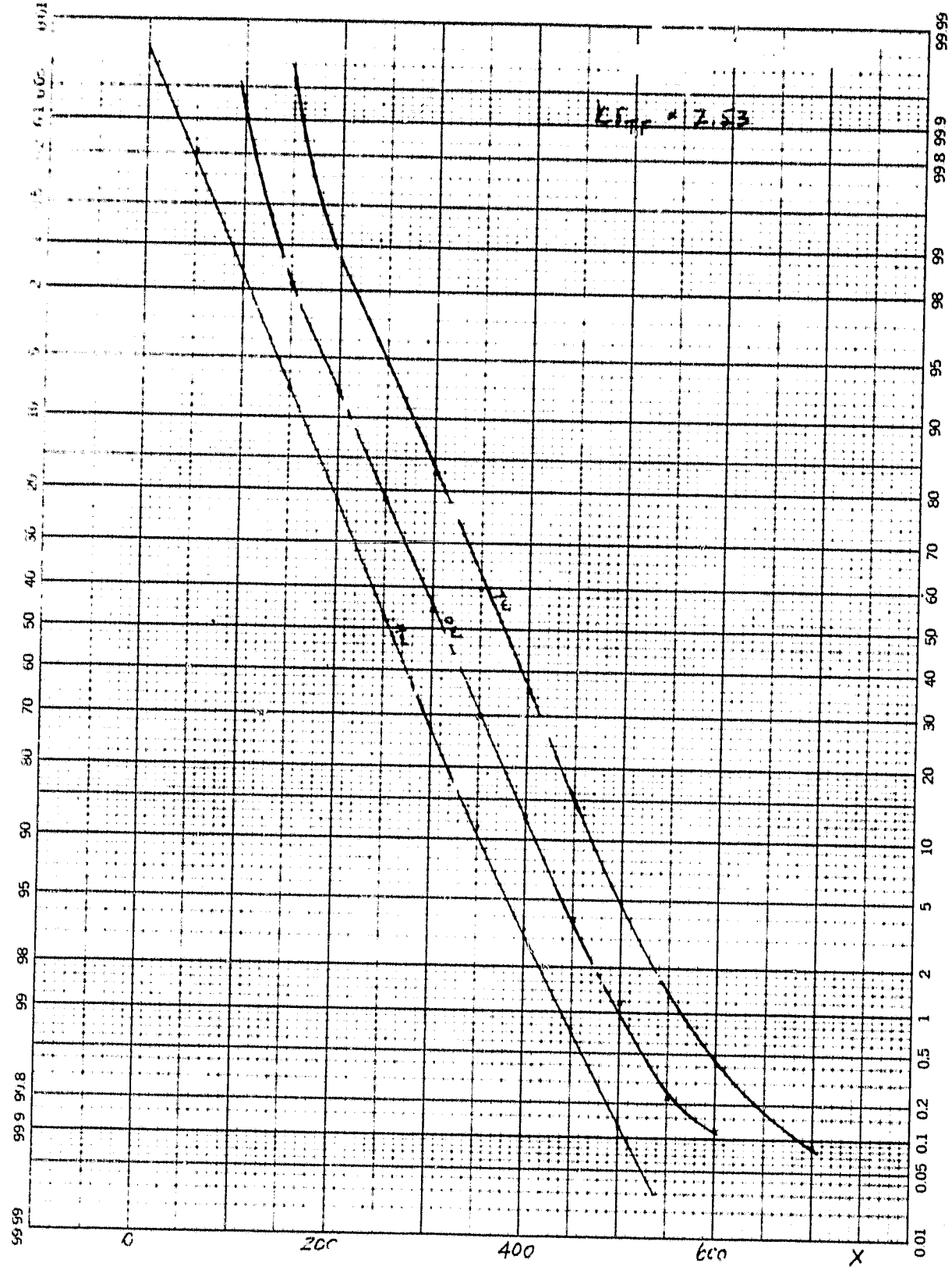

FIGURE B-62. HEAVY WEIGHT, FOUR CONTROLS .

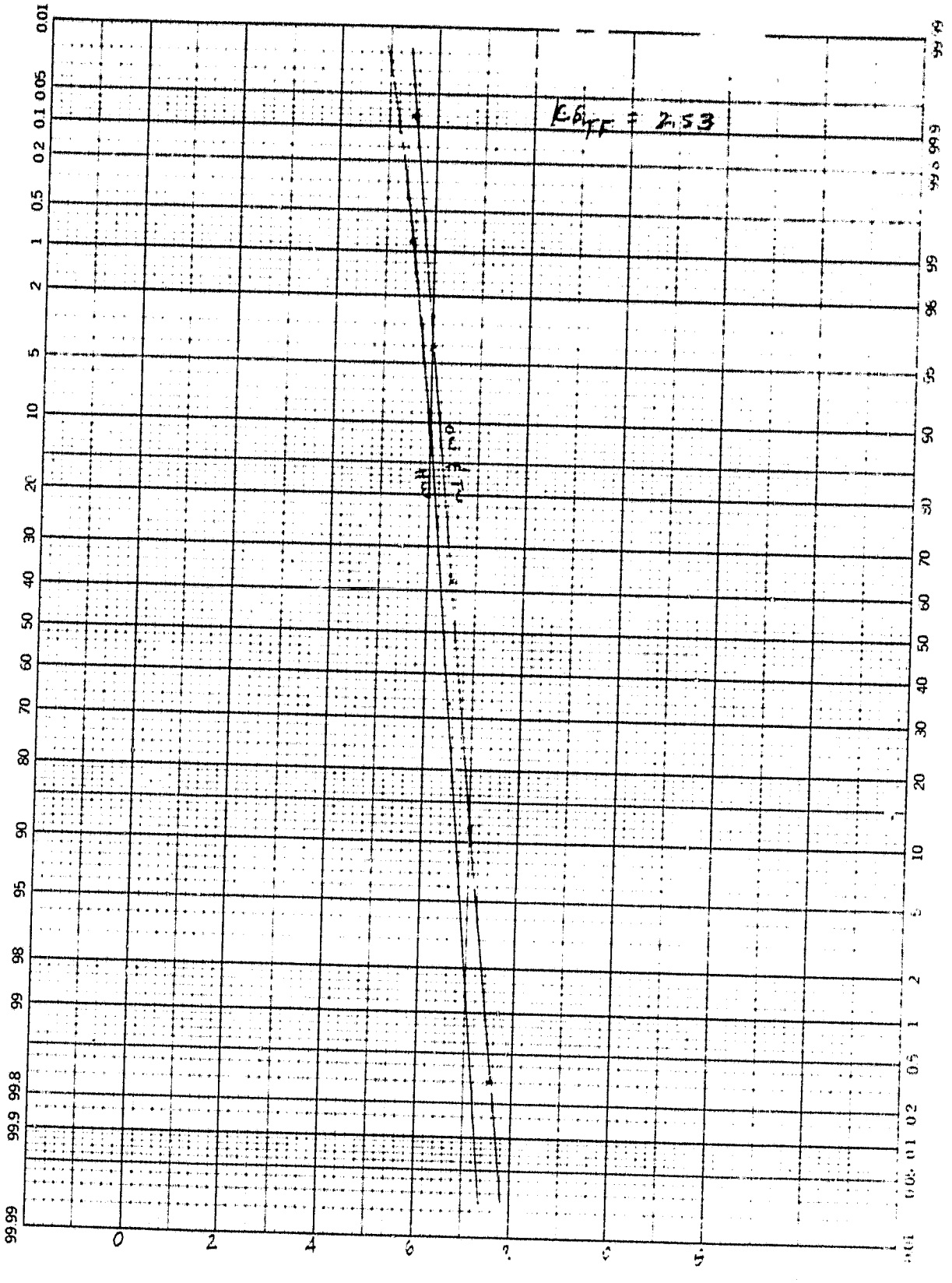

FIGURE B-63. HEAVY WEIGHT, FOUR CONTROLS

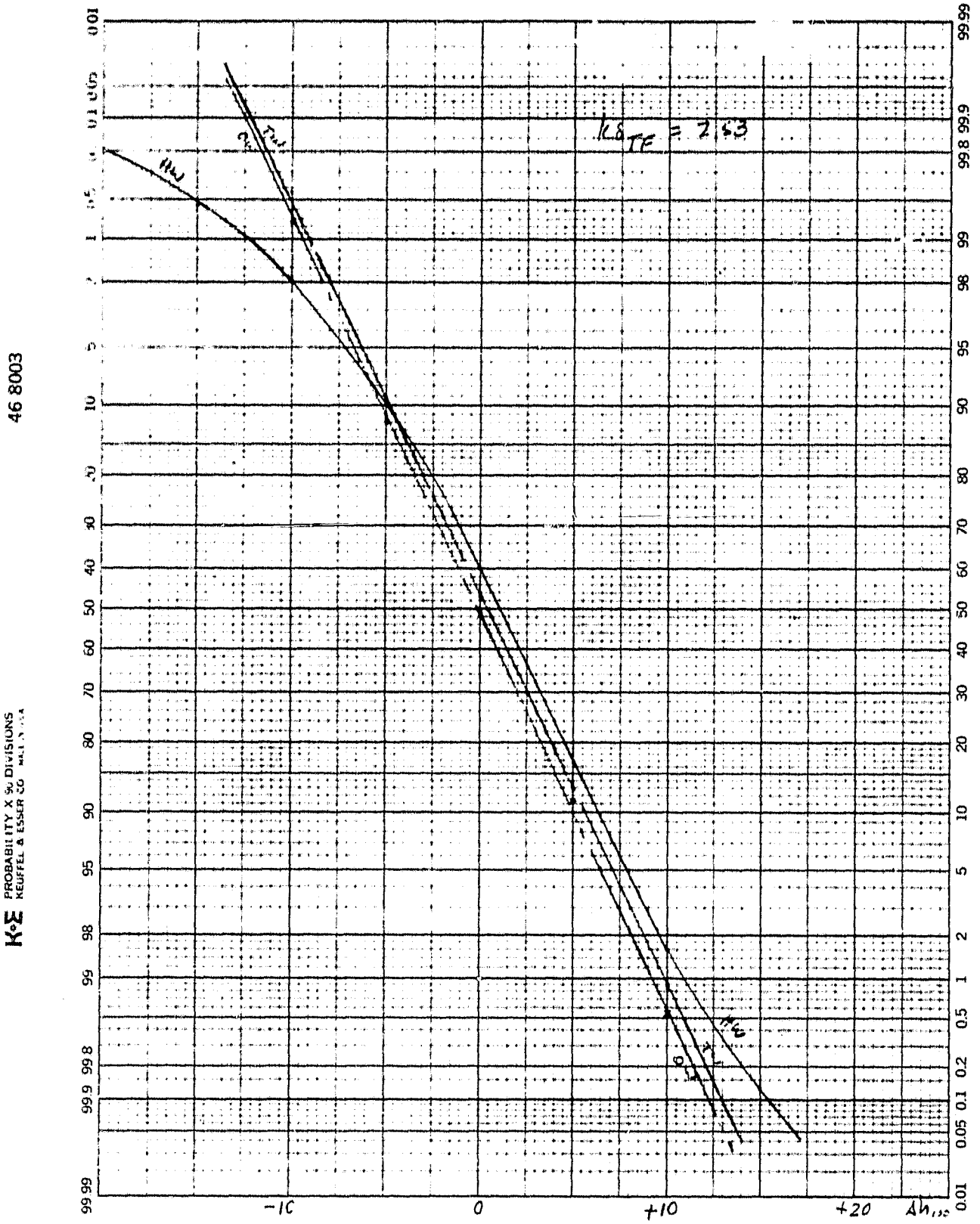

FIGURE B-64. HEAVY WEIGHT, FOUR CONTROLS

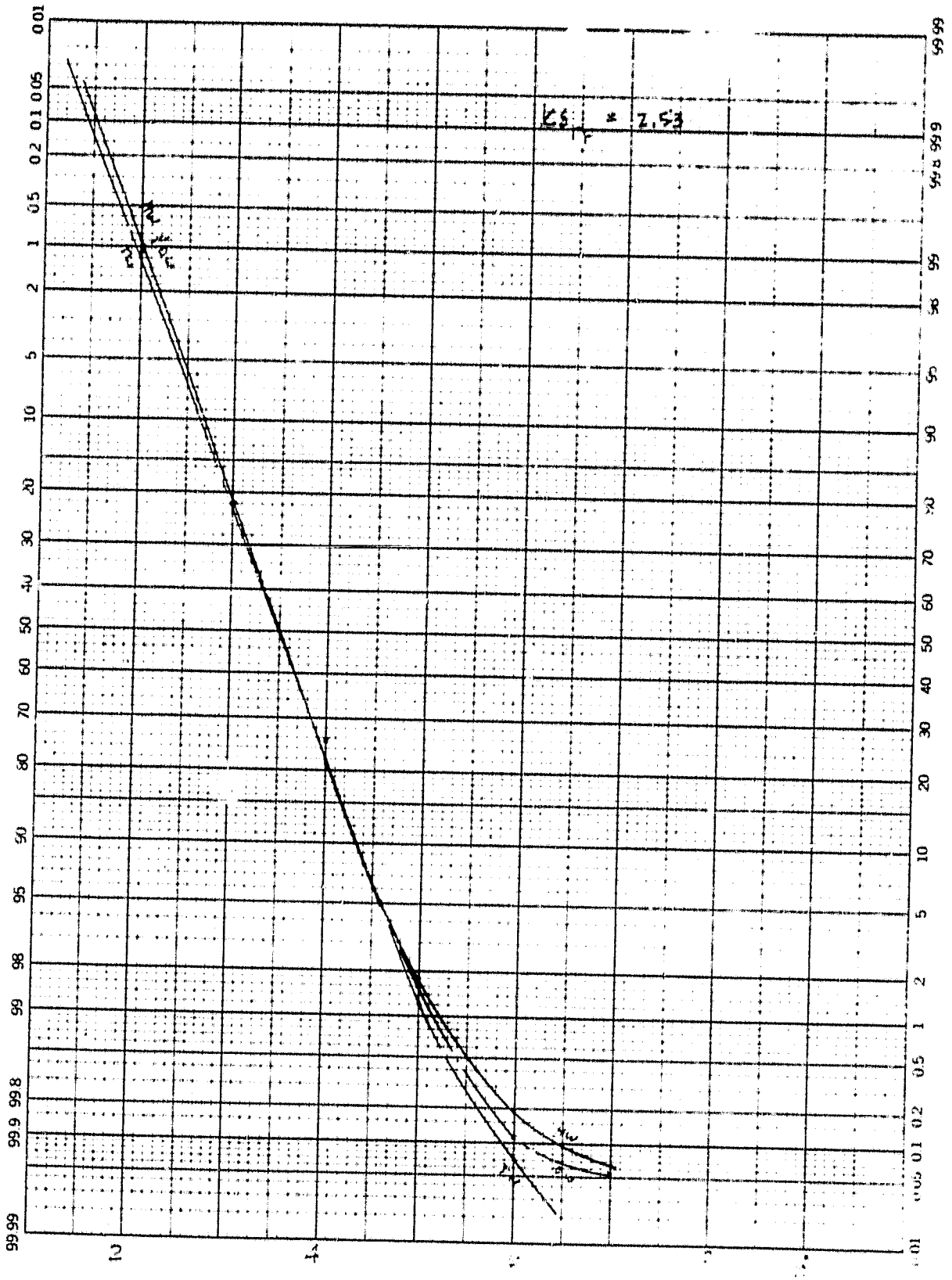

FIGURE B-65. HOT, FOUR CONTROLS

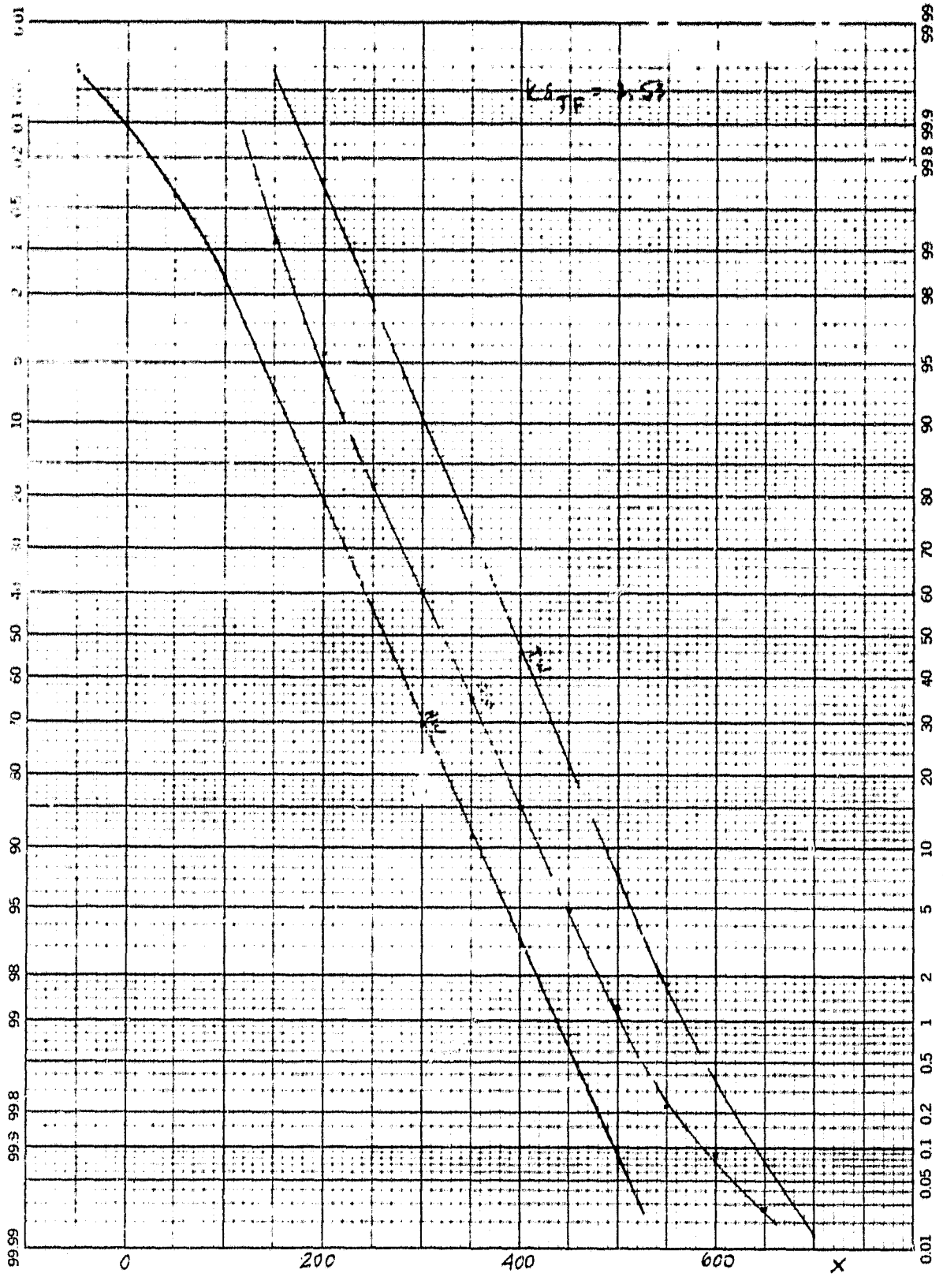

FIGURE B-66. HOT, FOUR CONTROLS

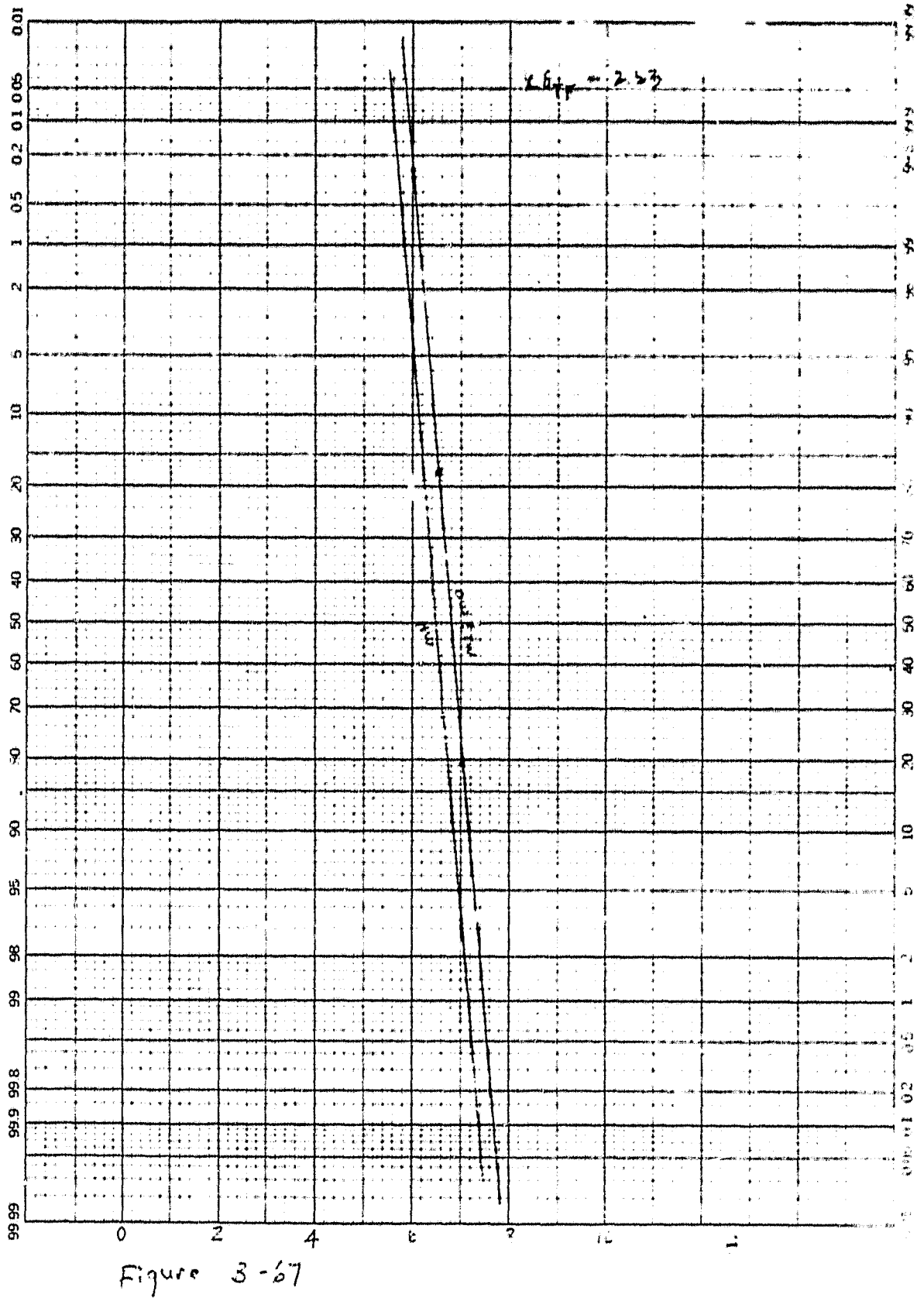

FIGURE B-67. HOT, FOUR CONTROLS

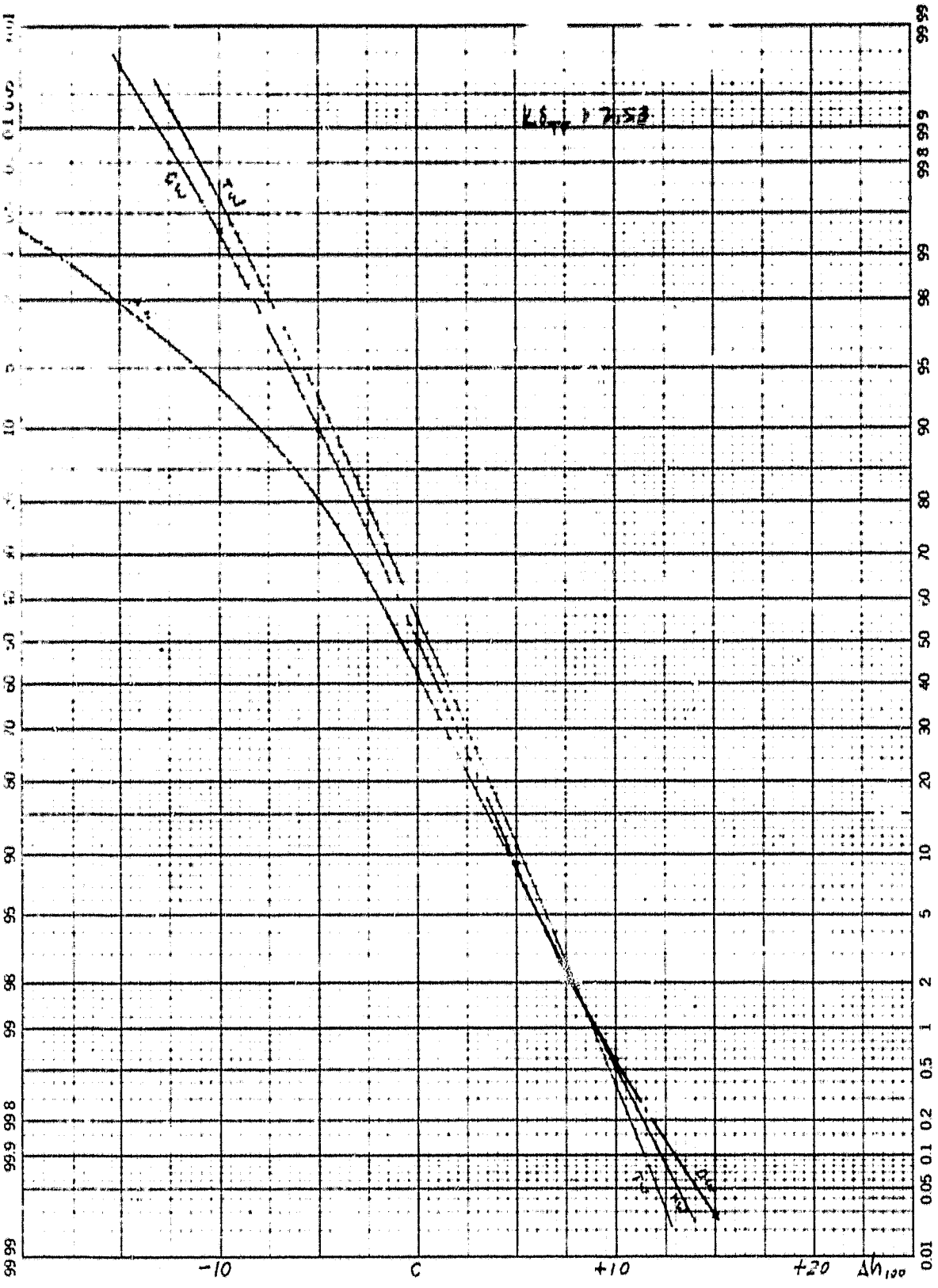

Figure B-67

FIGURE B-68. HOT, FOUR CONTROLS

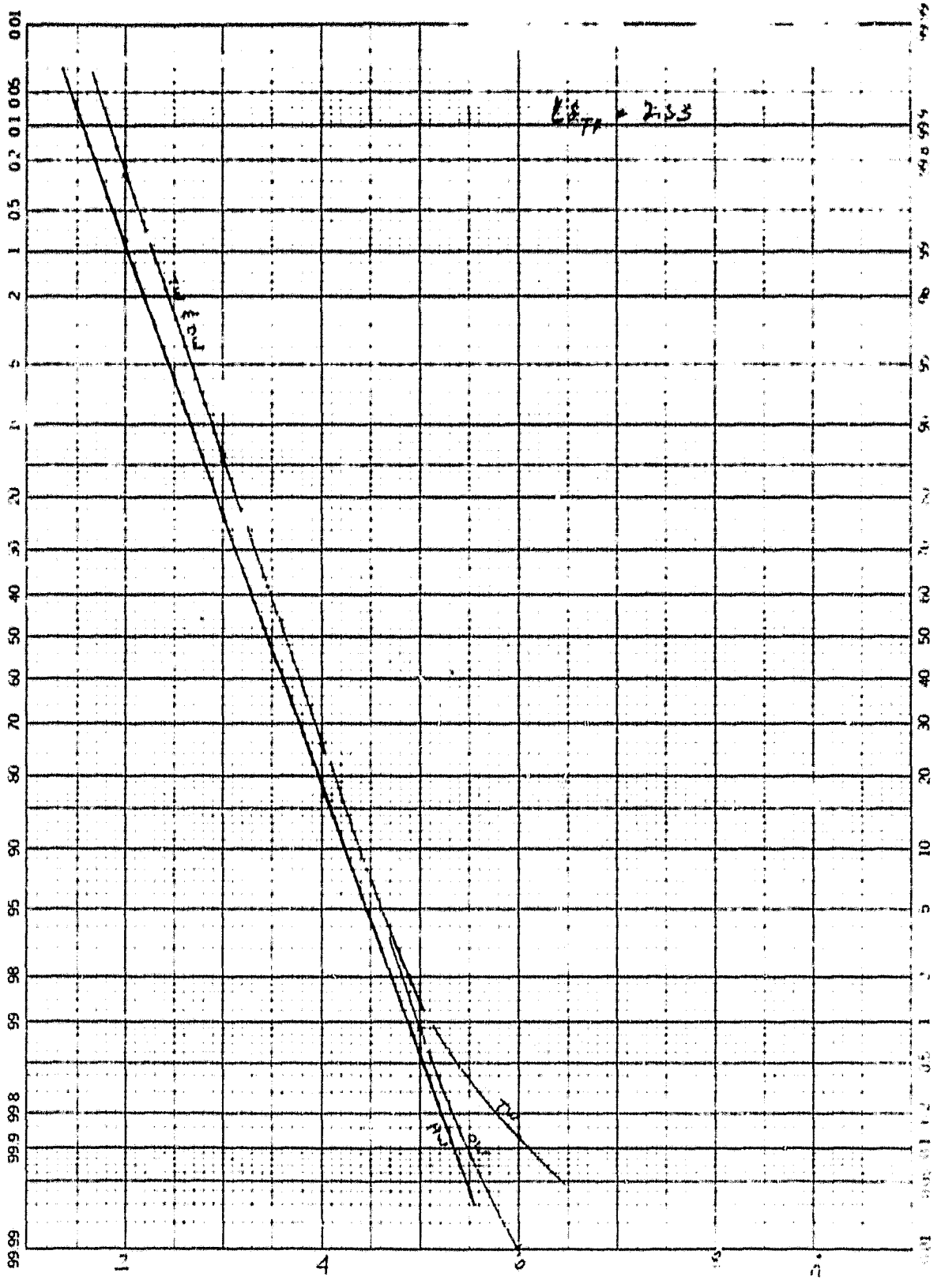

FIGURE B-69. LIGHT WEIGHT, THREE CONTROLS

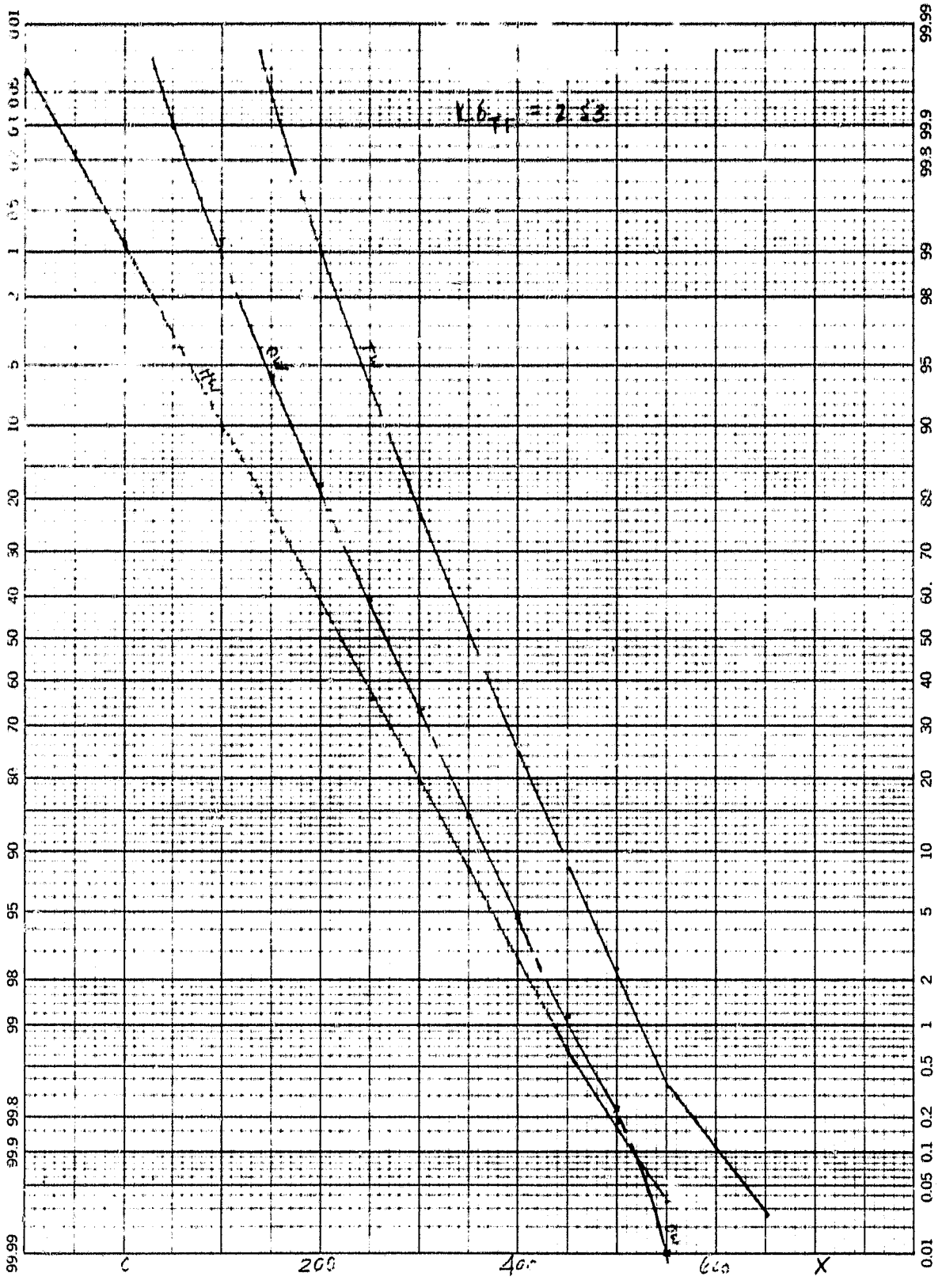

FIGURE B-70. LIGHT WEIGHT, THREE CONTROLS

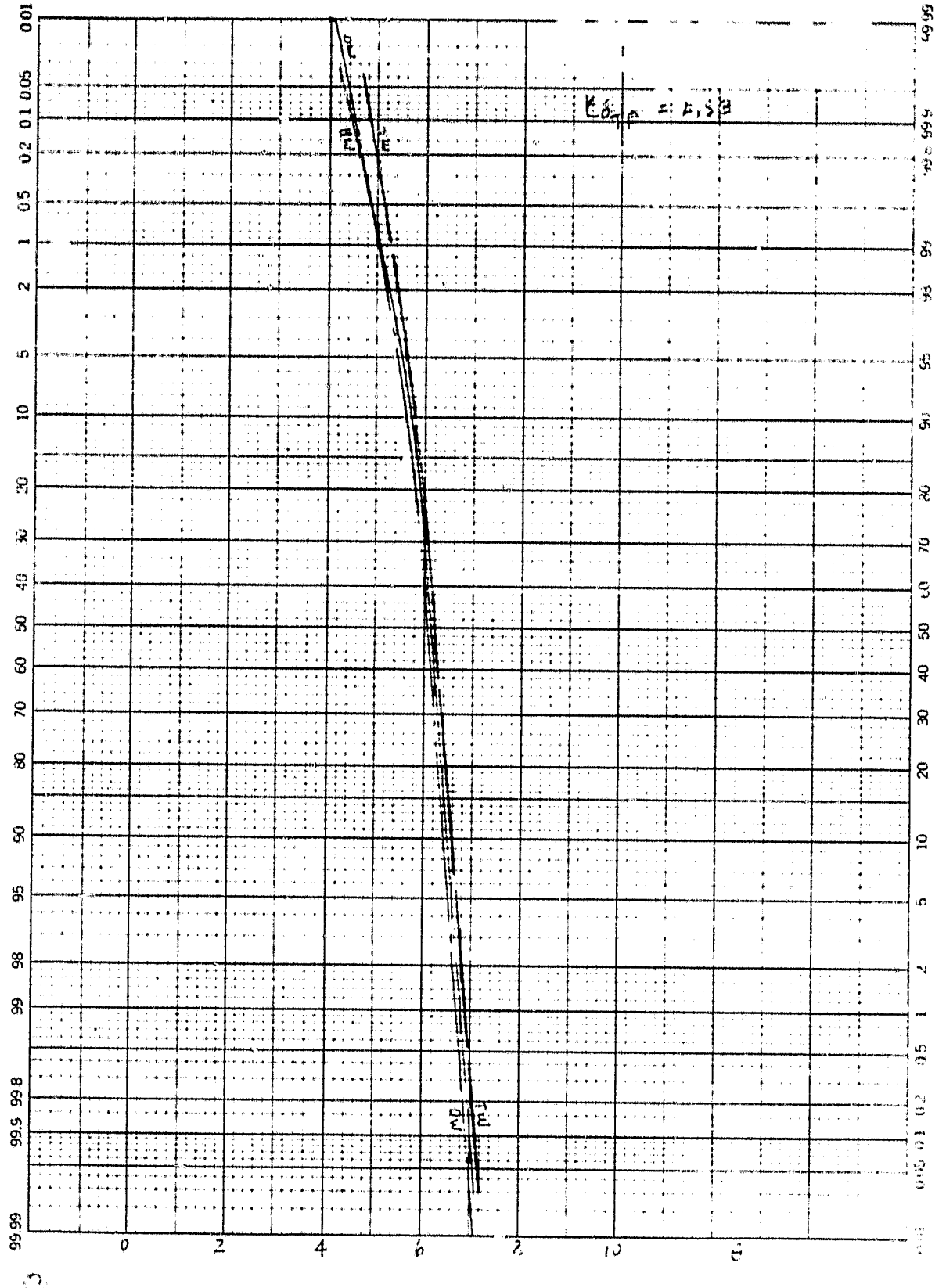

FIGURE B-71. LIGHT WEIGHT, THREE CONTROLS

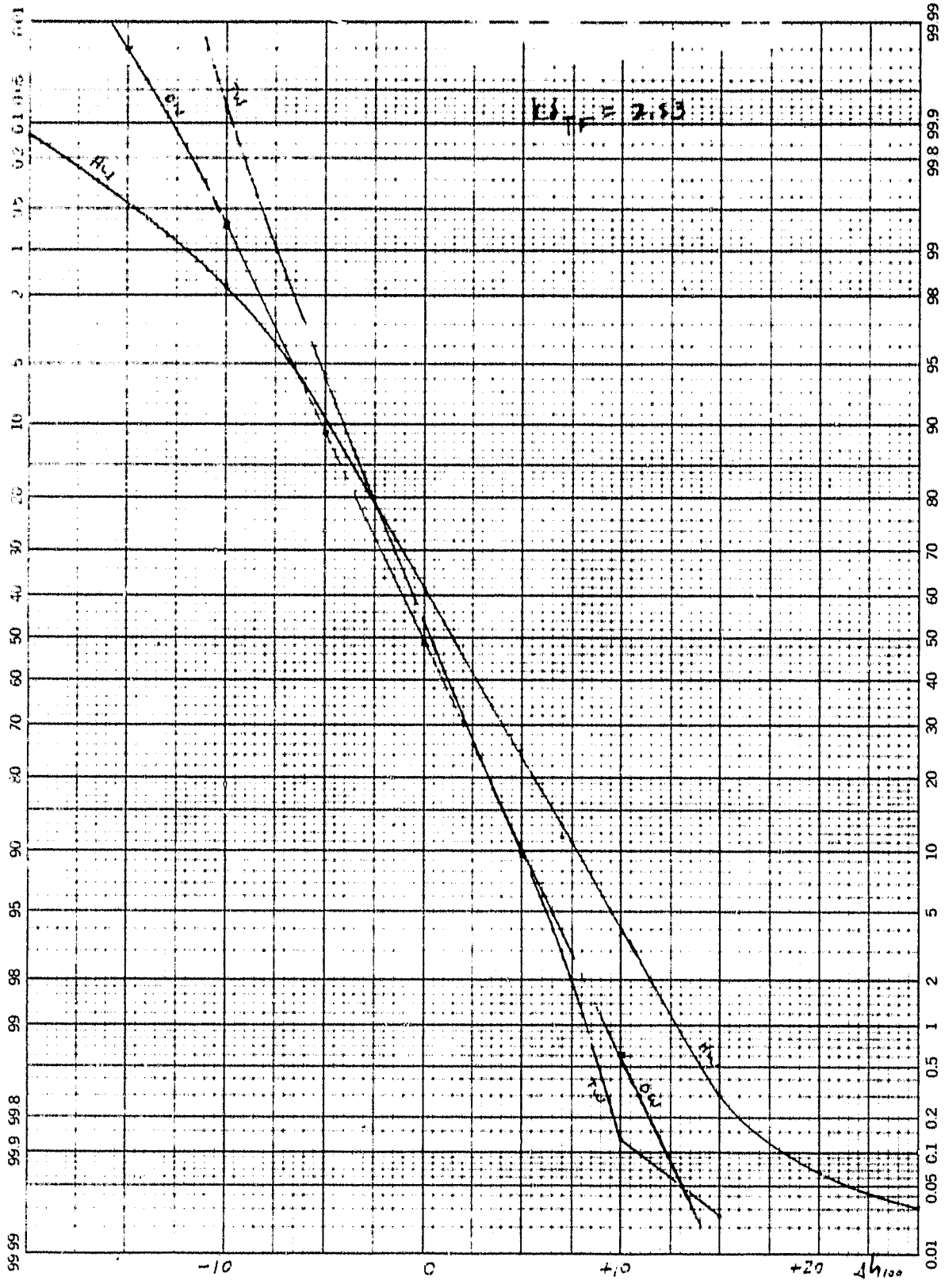

FIGURE B-72. LIGHT WEIGHT, THREE CONTROLS

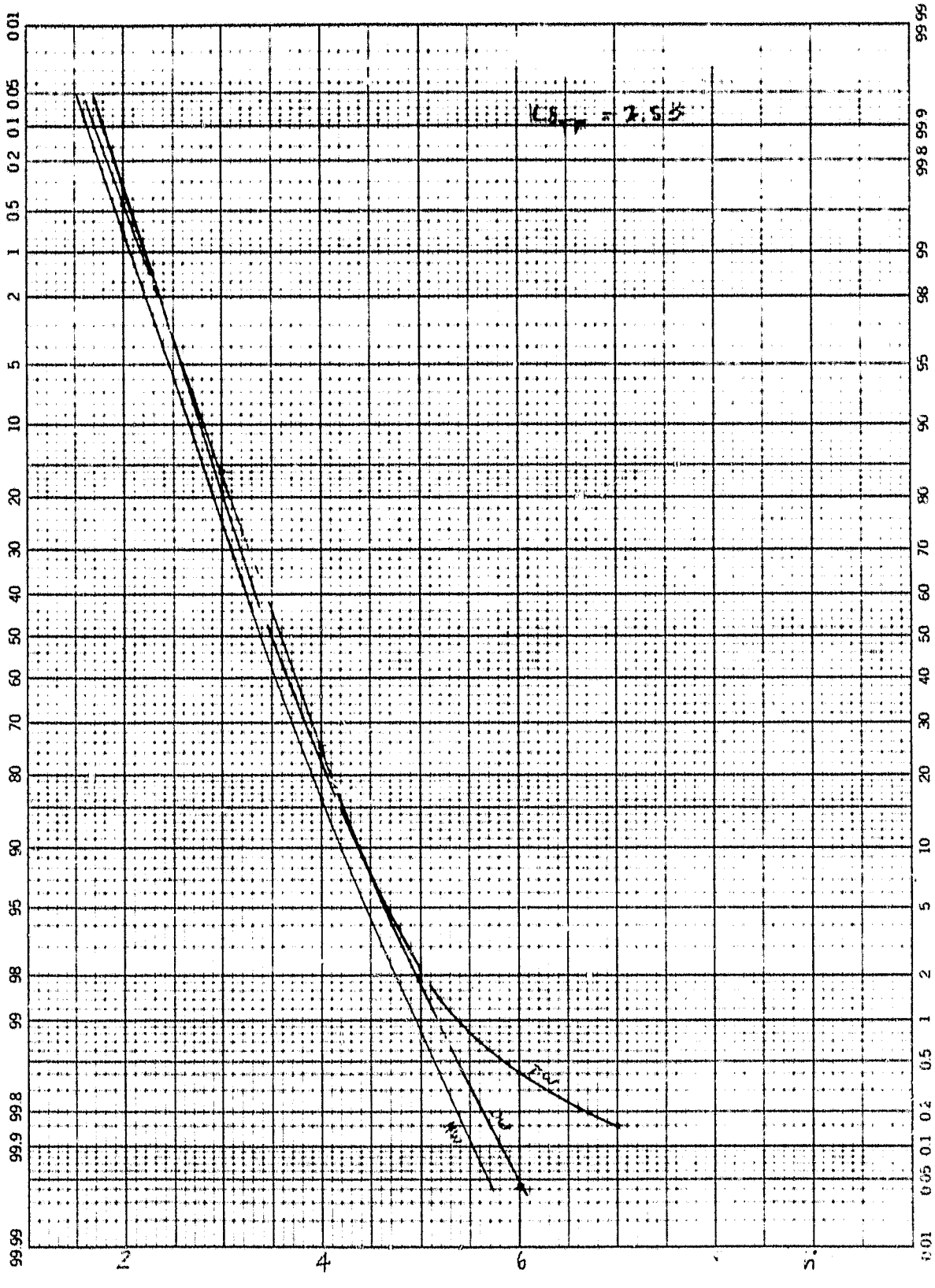

FIGURE B-73. HEAVY WEIGHT, THREE CONTROLS

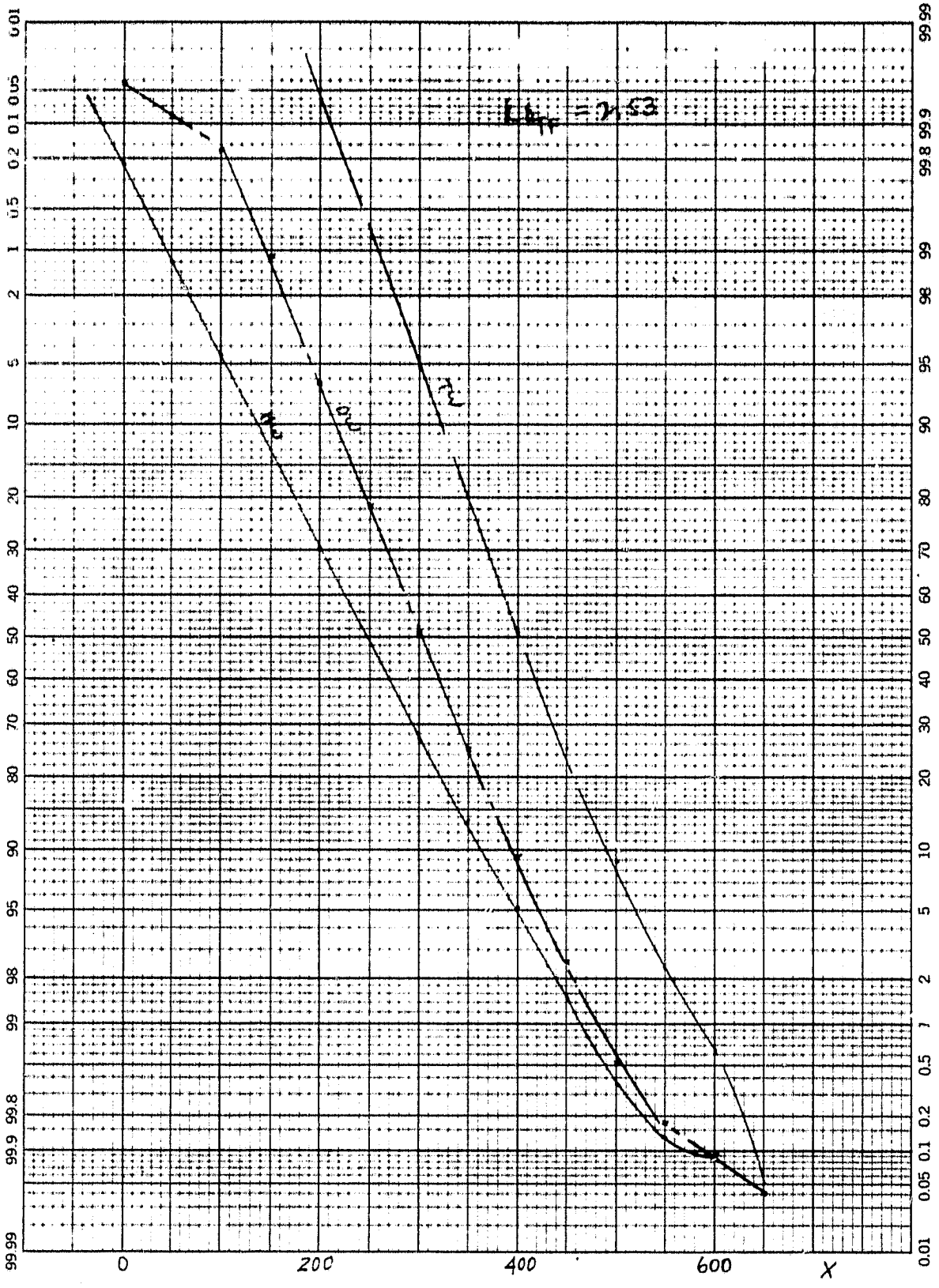

FIGURE B-74. HEAVY WEIGHT, THREE CONTROLS

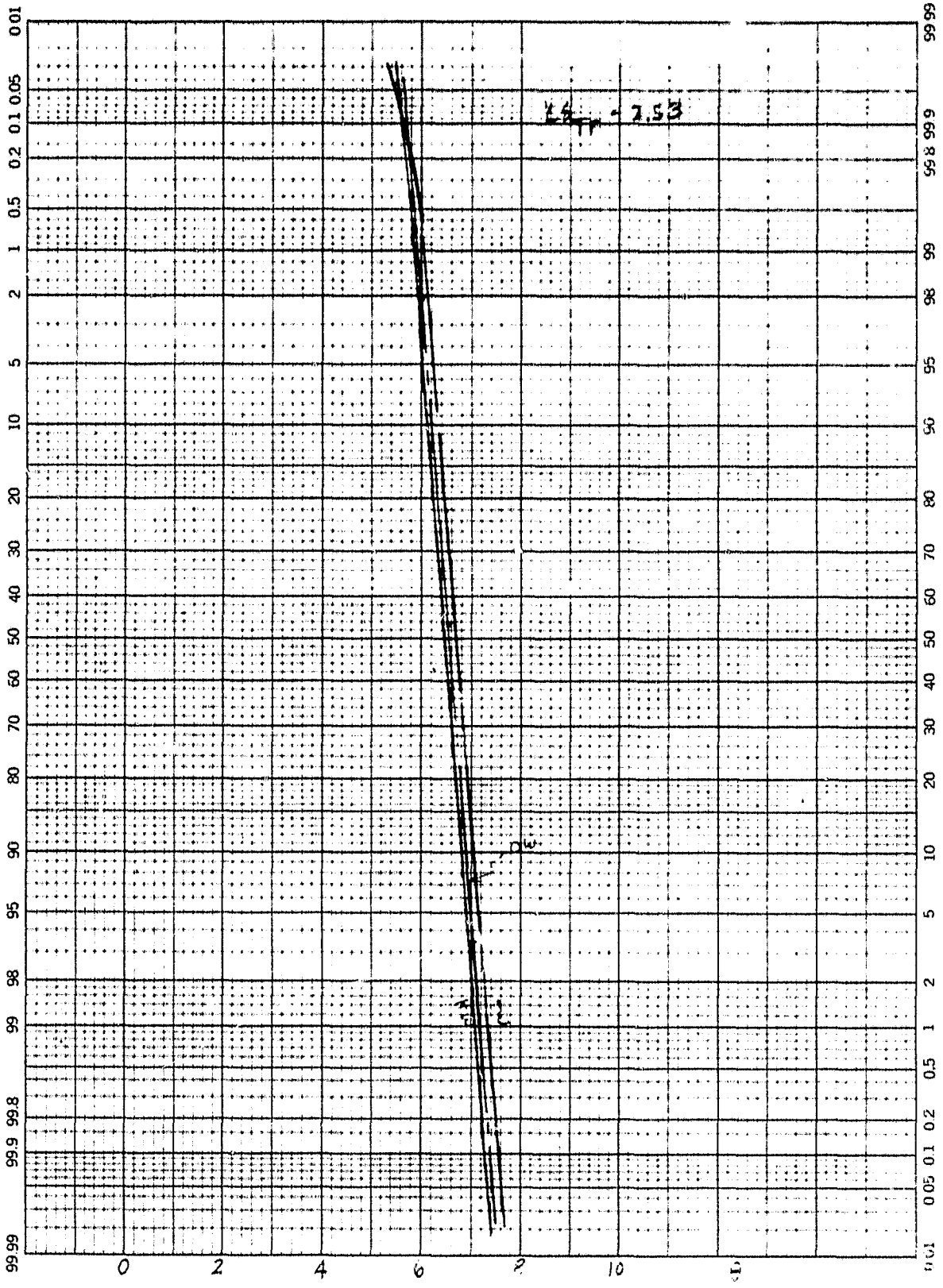

FIGURE B-75. HEAVY WEIGHT, THREE CONTROLS

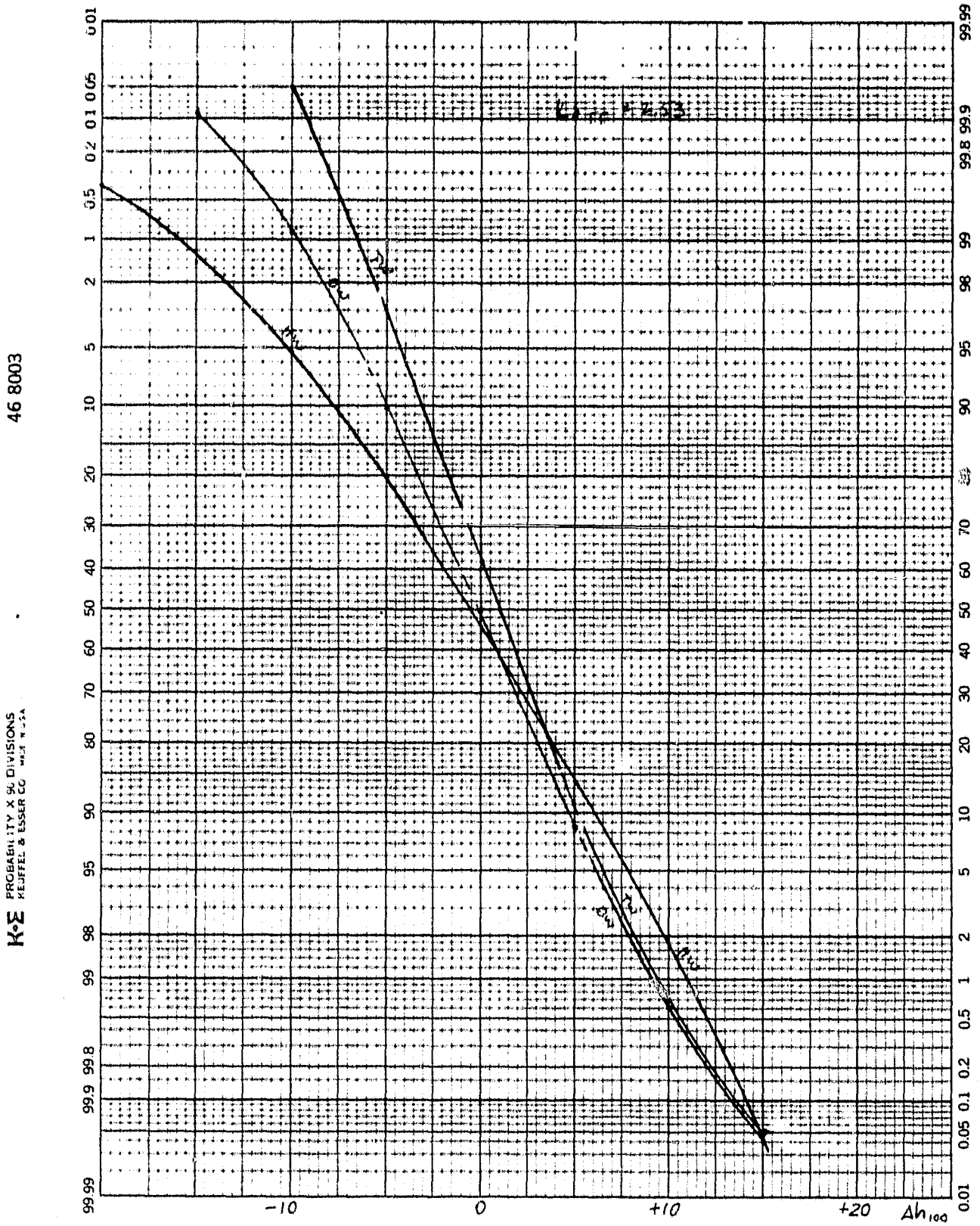

FIGURE B-76. HEAVY WEIGHT, THREE CONTROLS

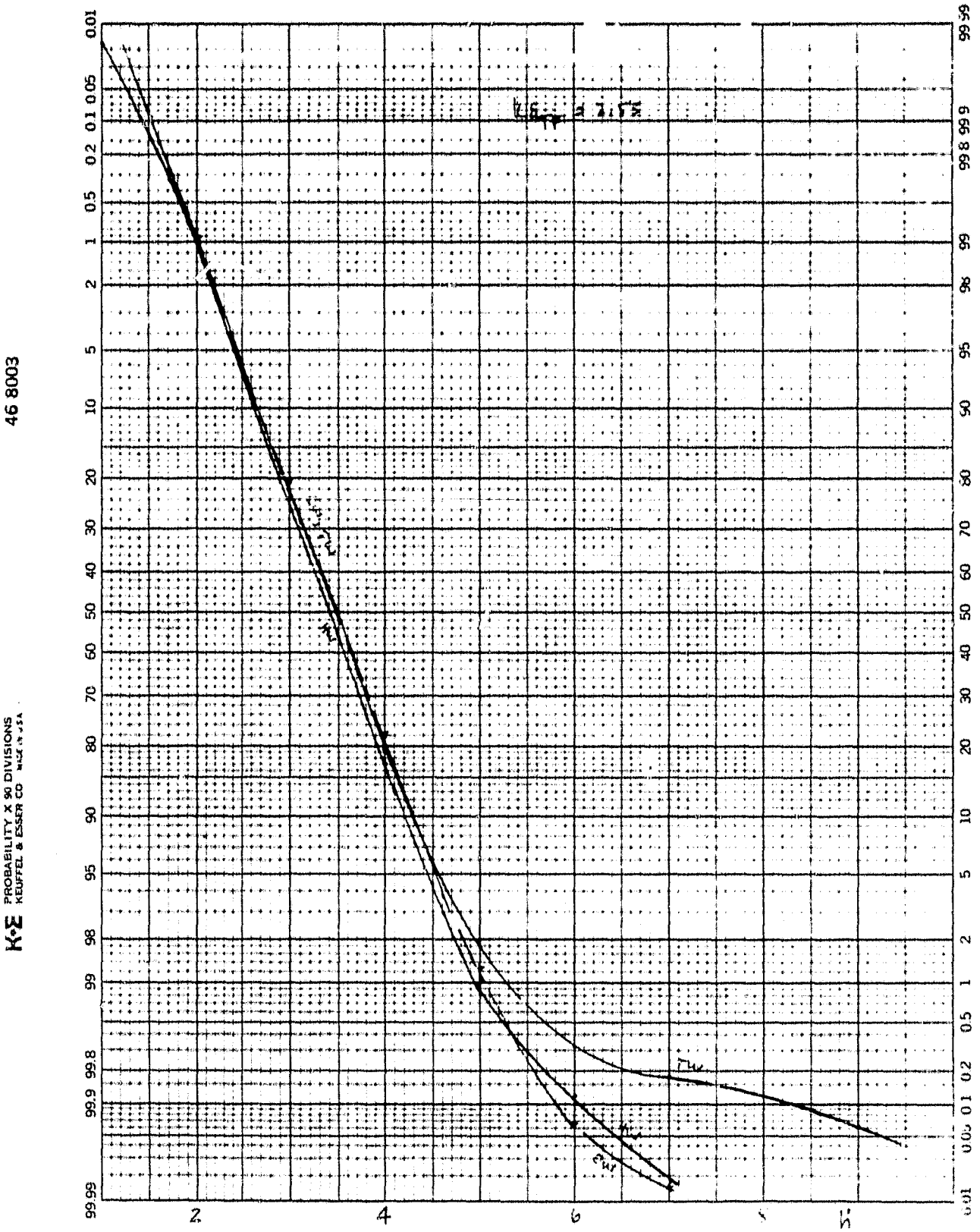

FIGURE B-77. HOT, THREE CONTROLS

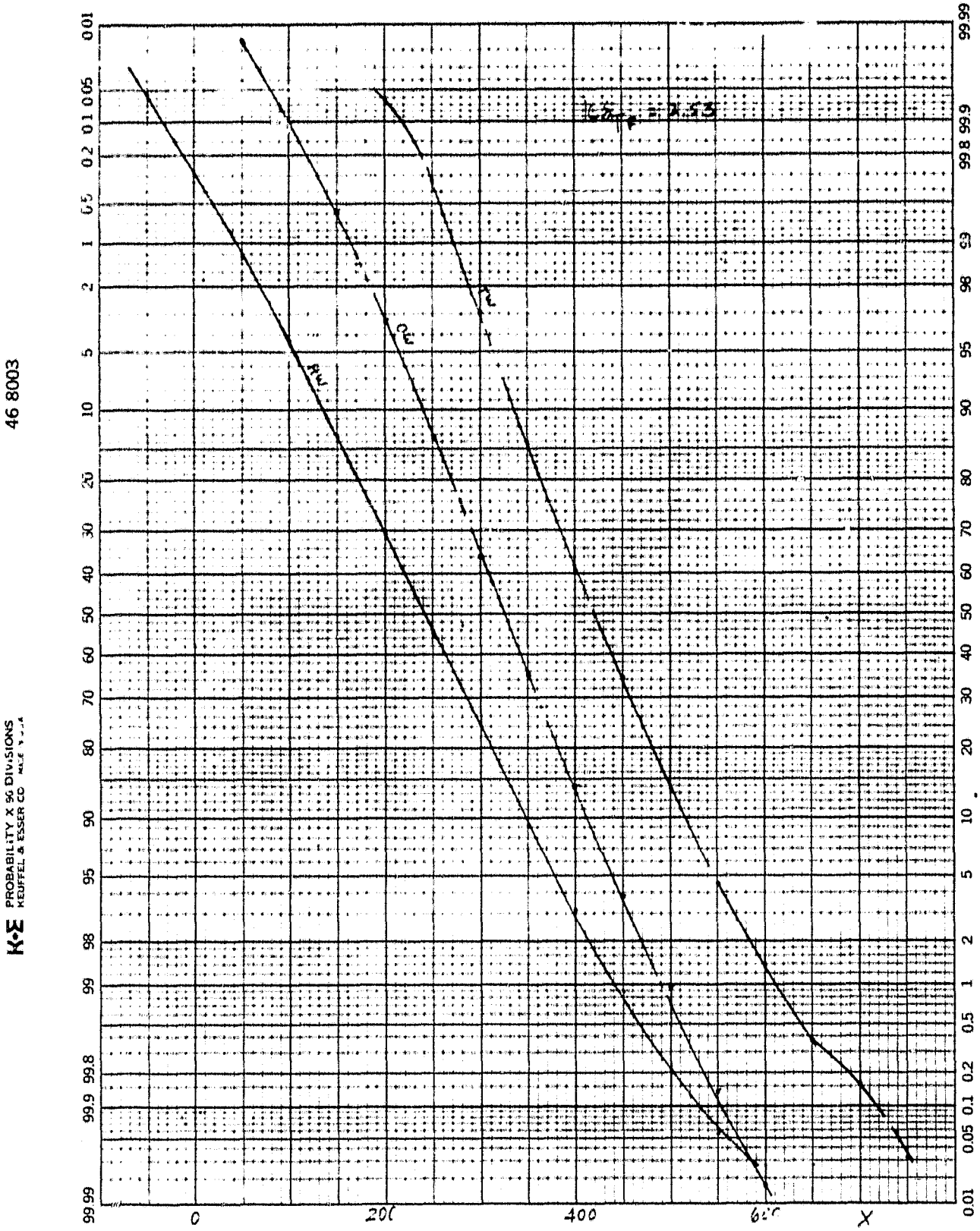

FIGURE B-78. HOT, THREE CONTROLS

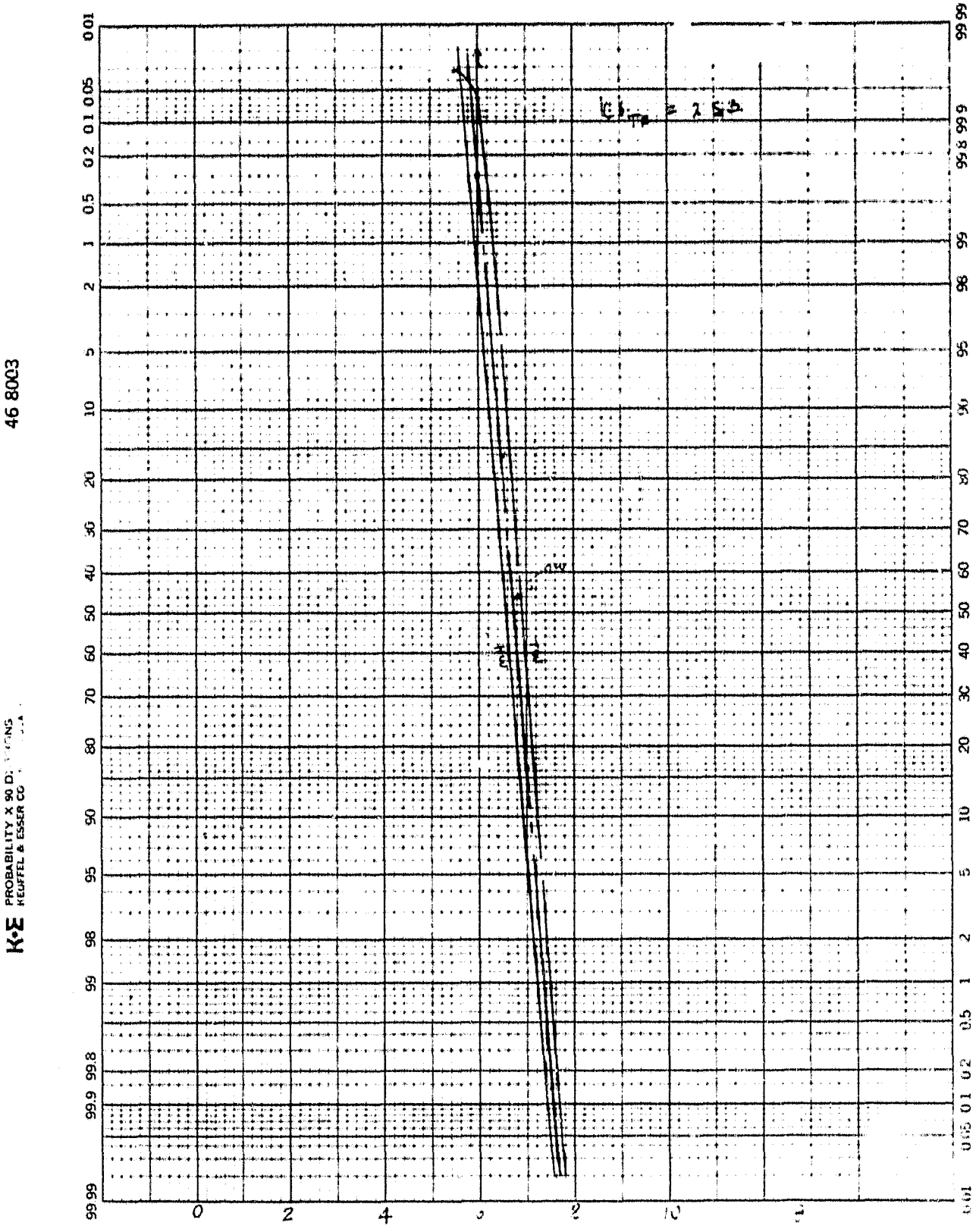

FIGURE B-79. HOT, THREE CONTROLS

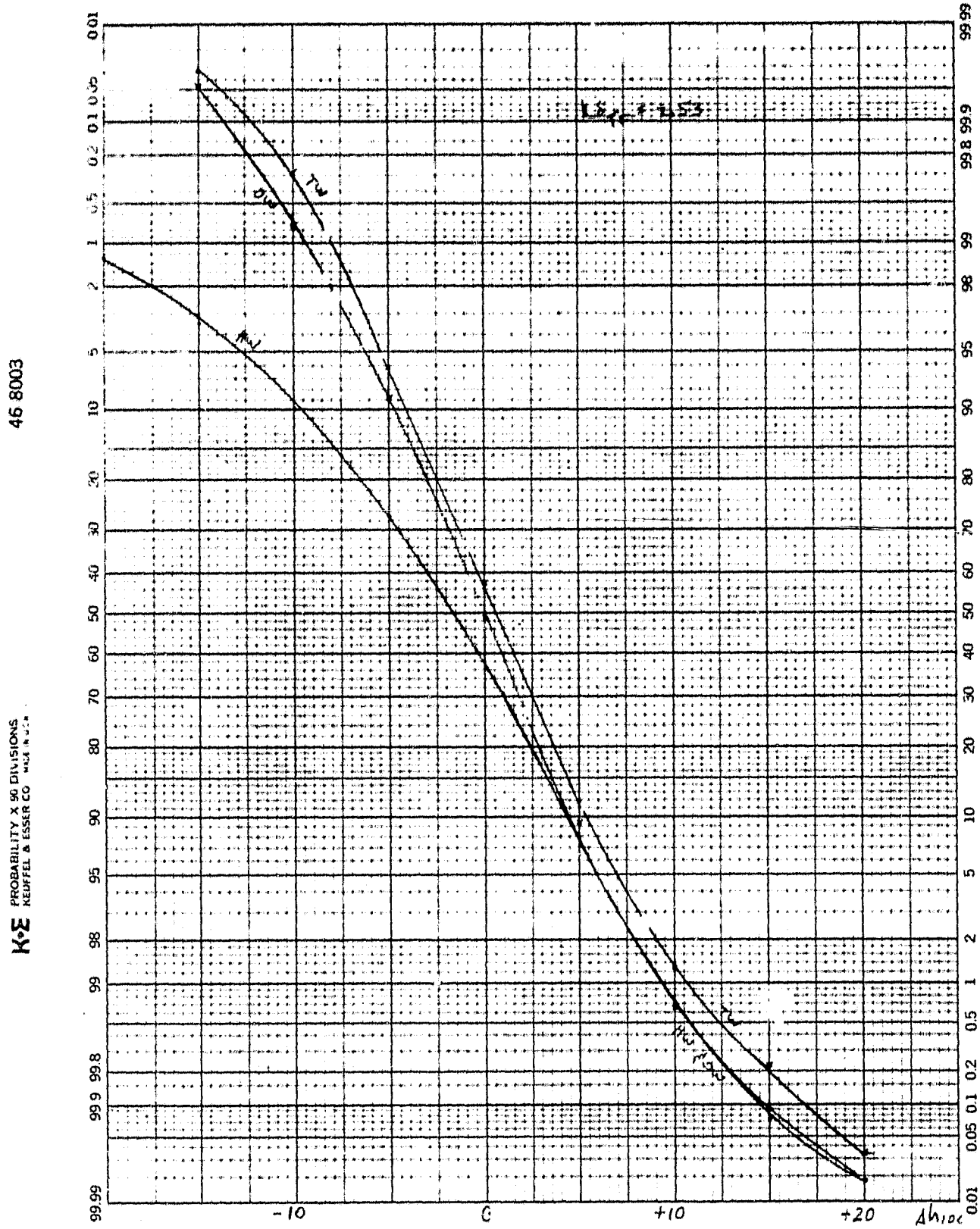

FIGURE B-80. HOT, THREE CONTROLS

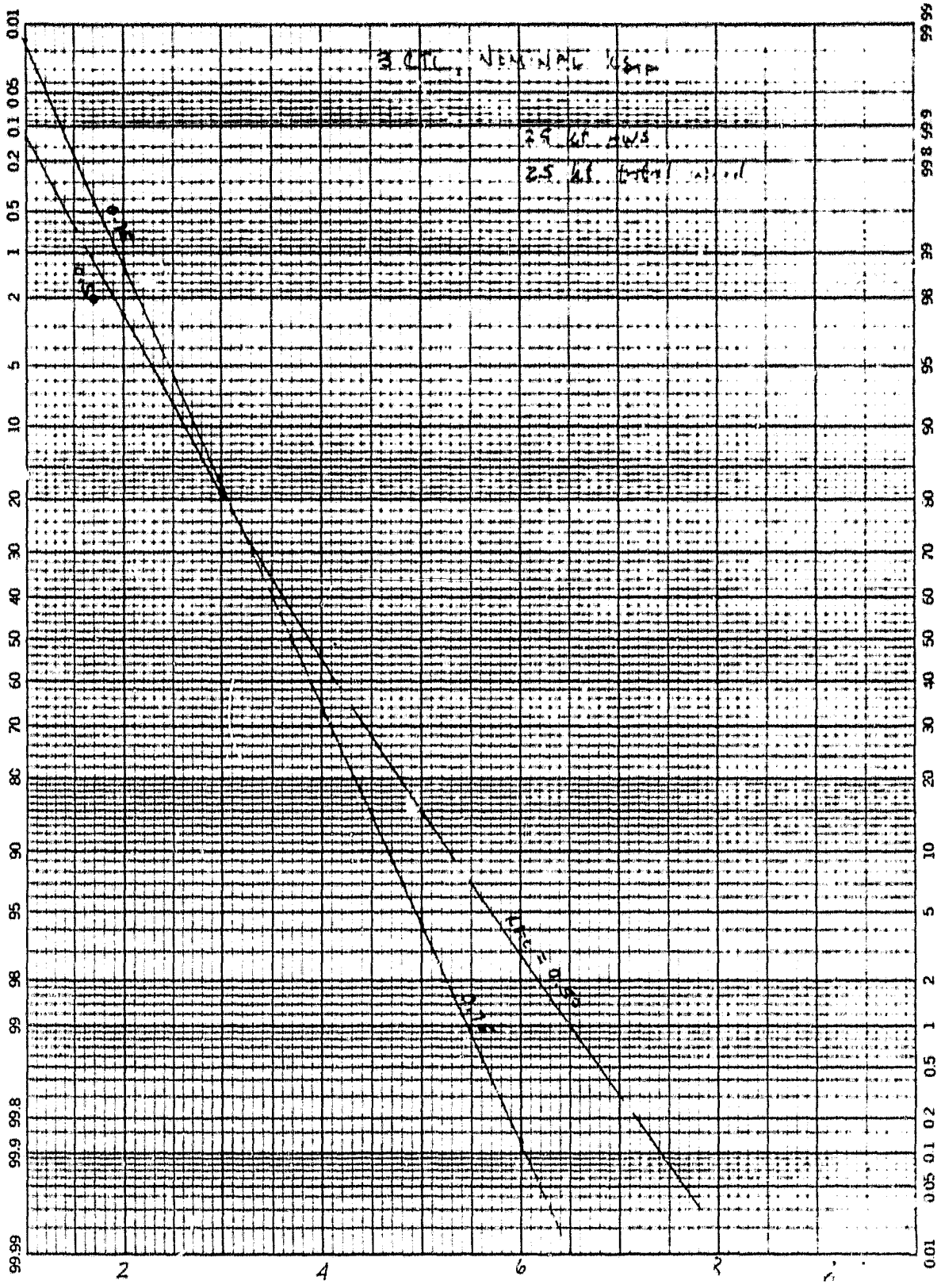

FIGURE B-81. THROTTLE GAIN VARIATION

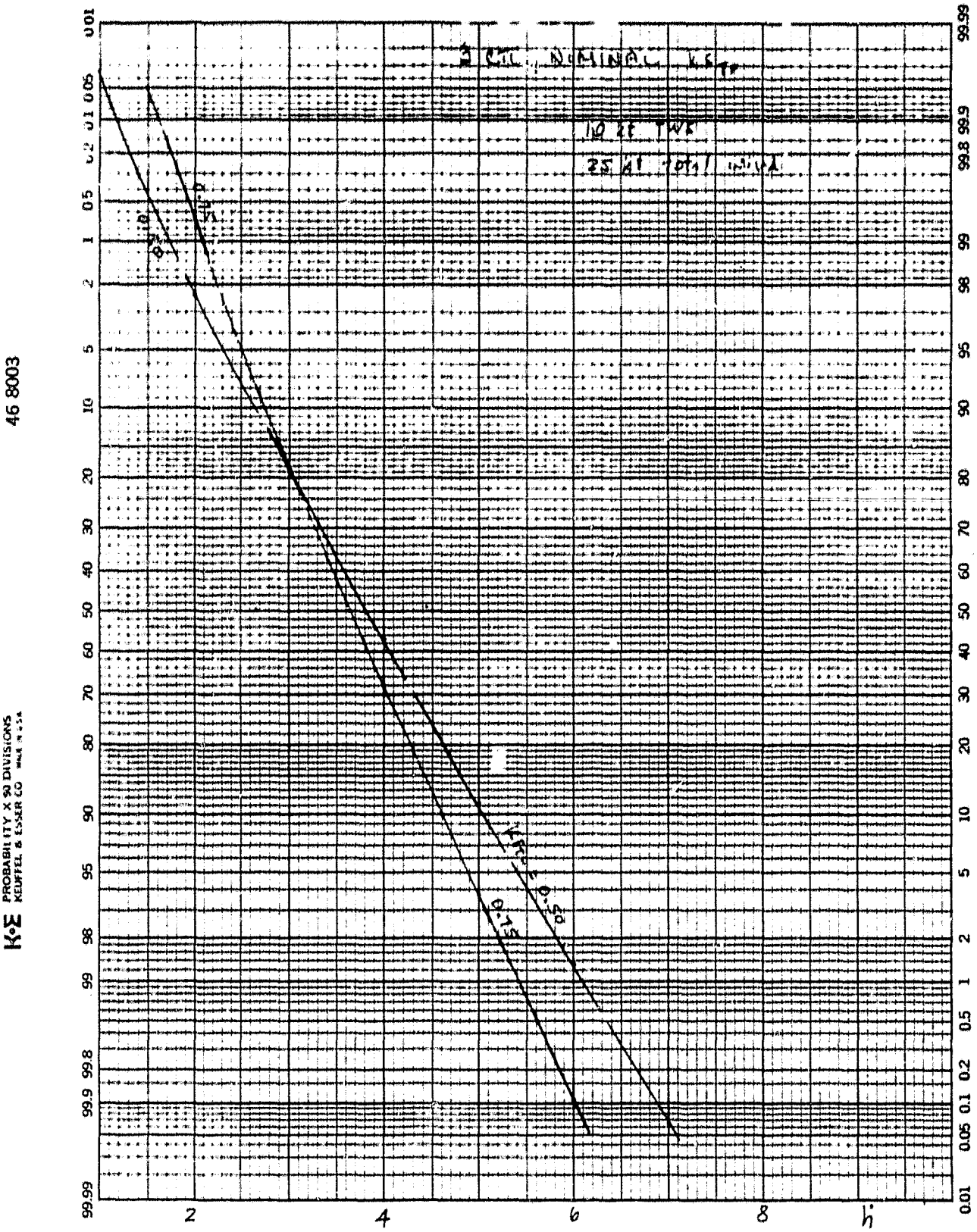

FIGURE B-82. THROTTLE GAIN VARIATION

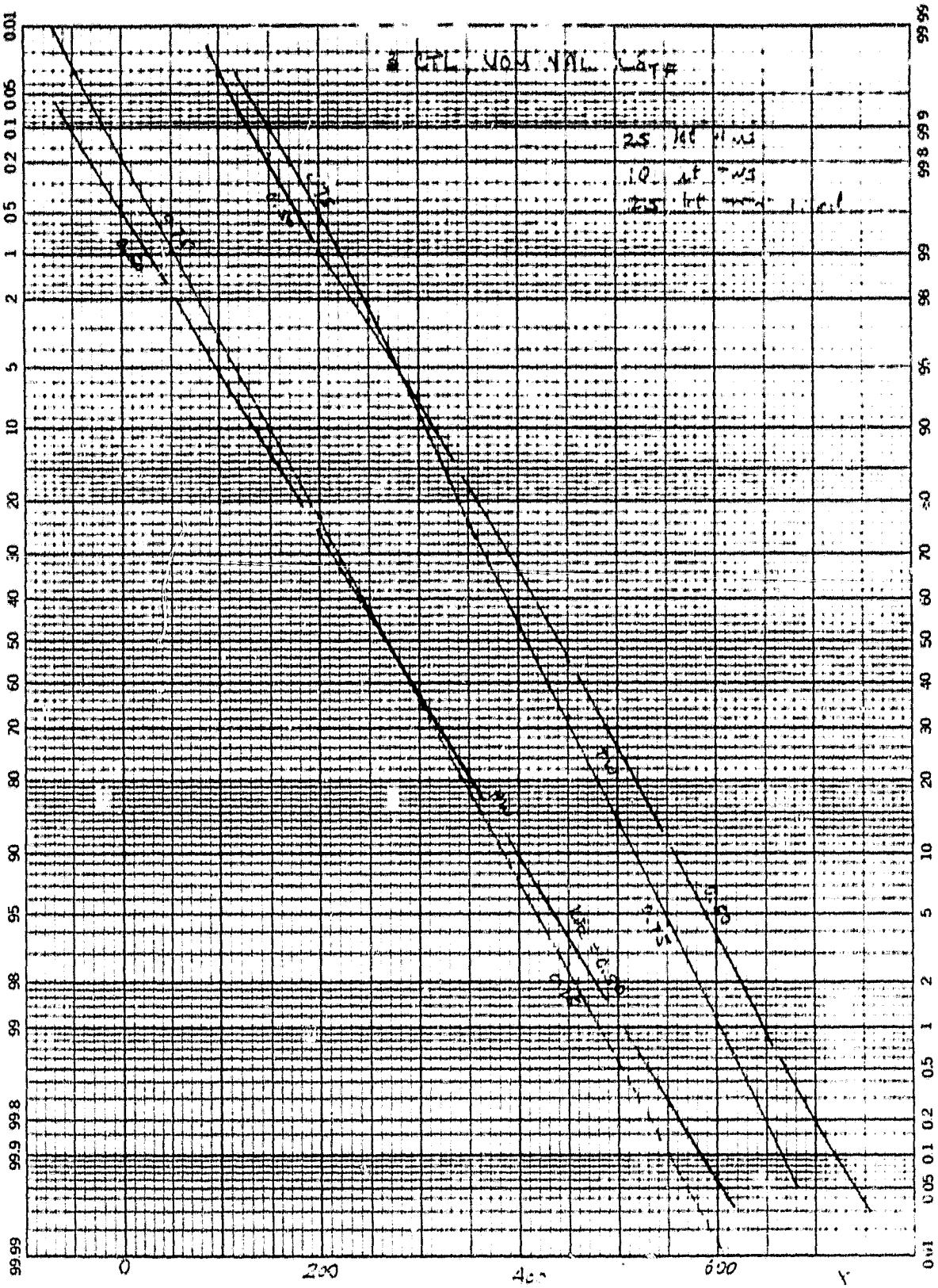

FIGURE B-83. THROTTLE GAIN VARIATION

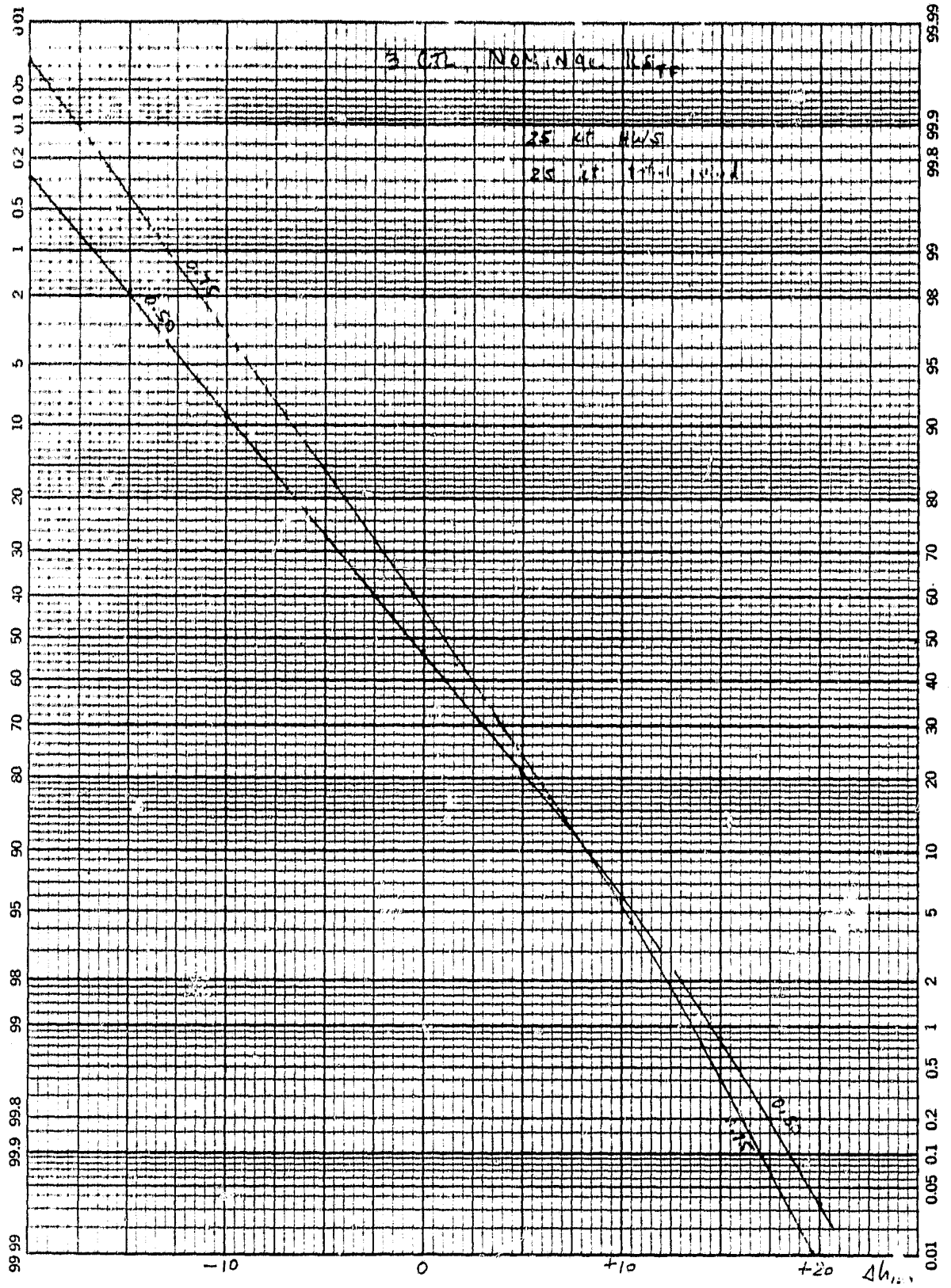

46 8003

KE PROBABILITY X 9u DIVISIONS
KEUFFEL & ESSER CO MADE IN U.S.A.

FIGURE B-84. THROTTLE GAIN VARIATION

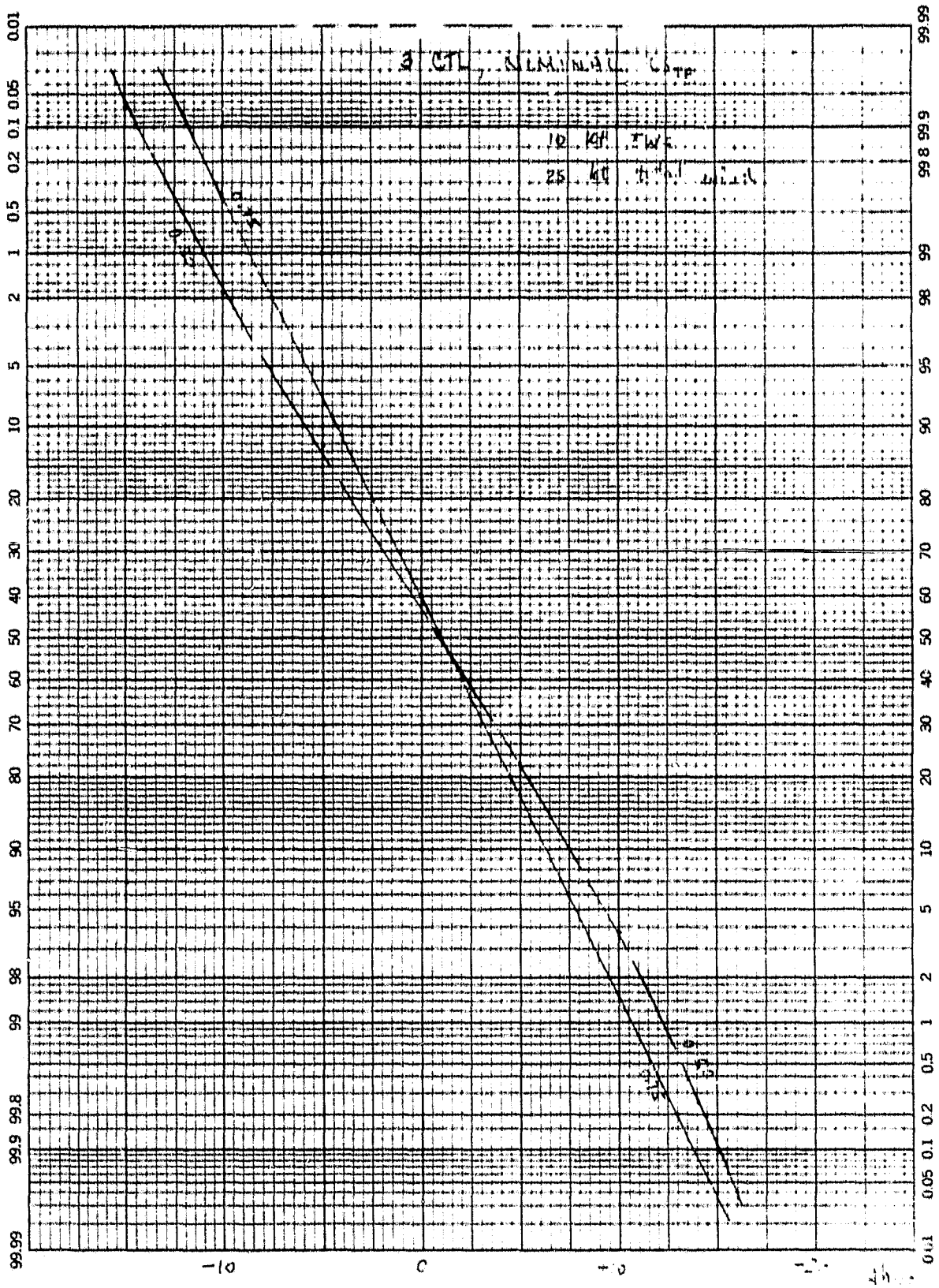

FIGURE B-85. THROTTLE GAIN VARIATION

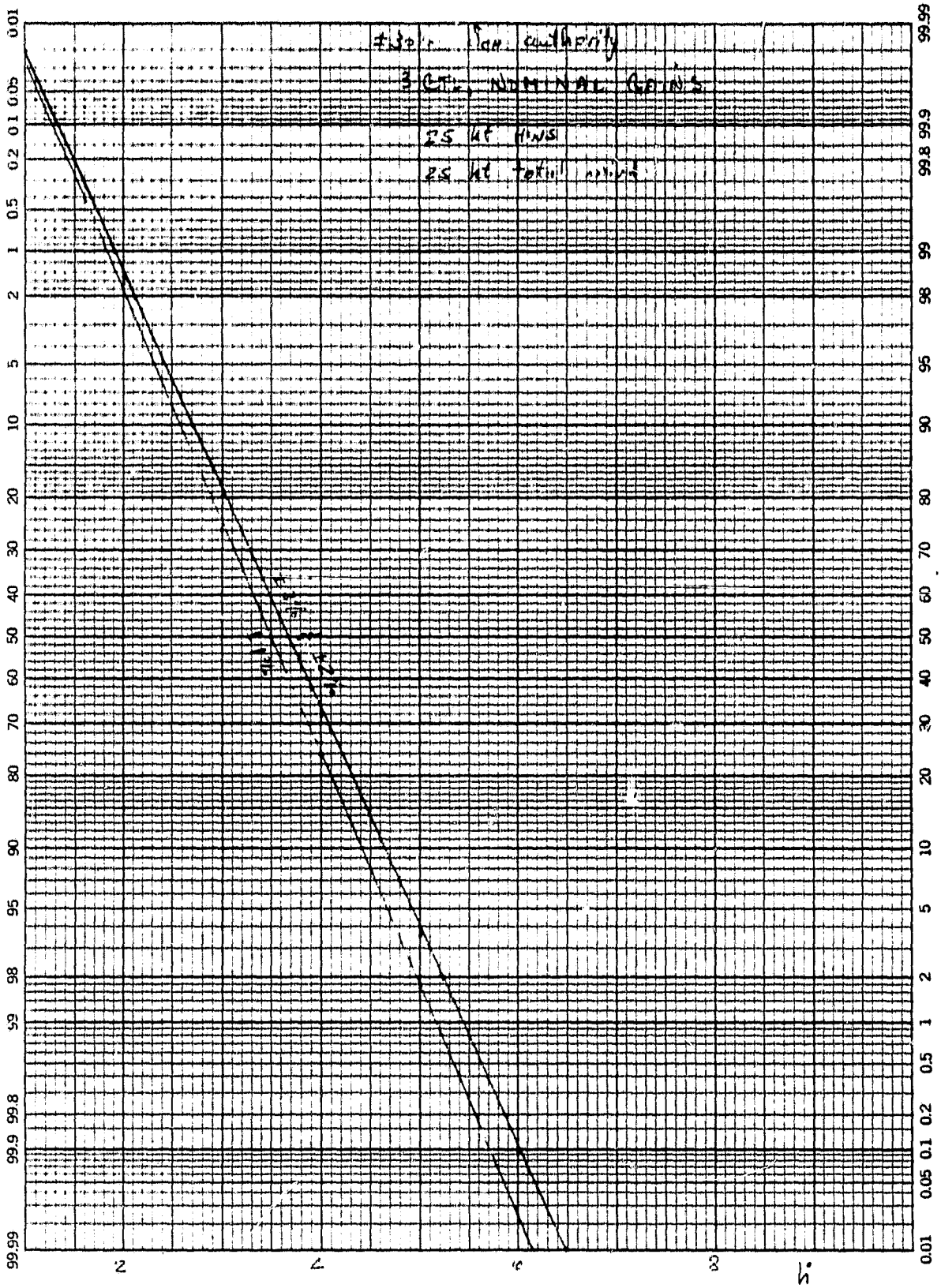

FIGURE B-86. RPM AUTHORITY VARIATION

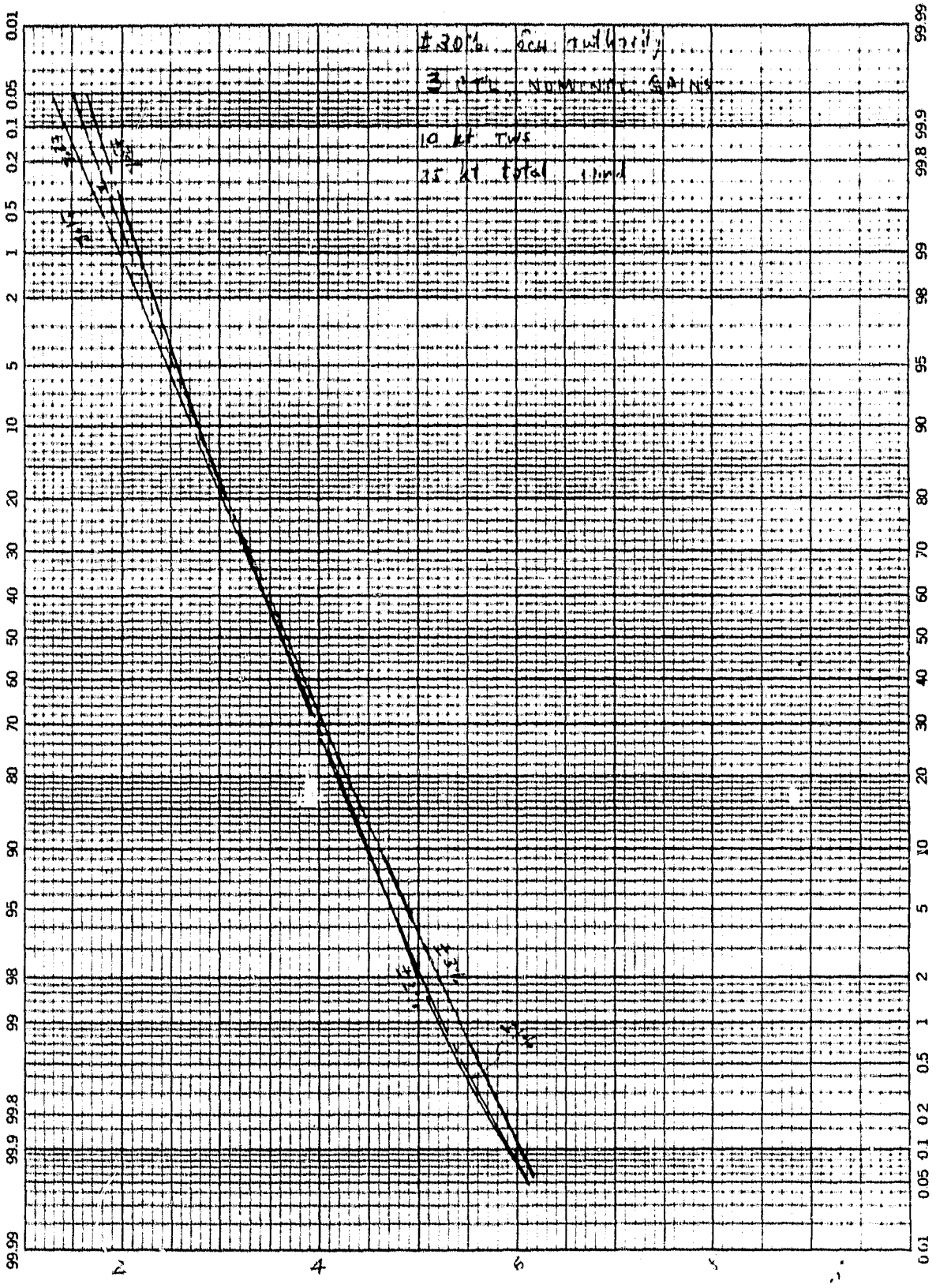

FIGURE B-87. RPM AUTOHRITY VARIATION

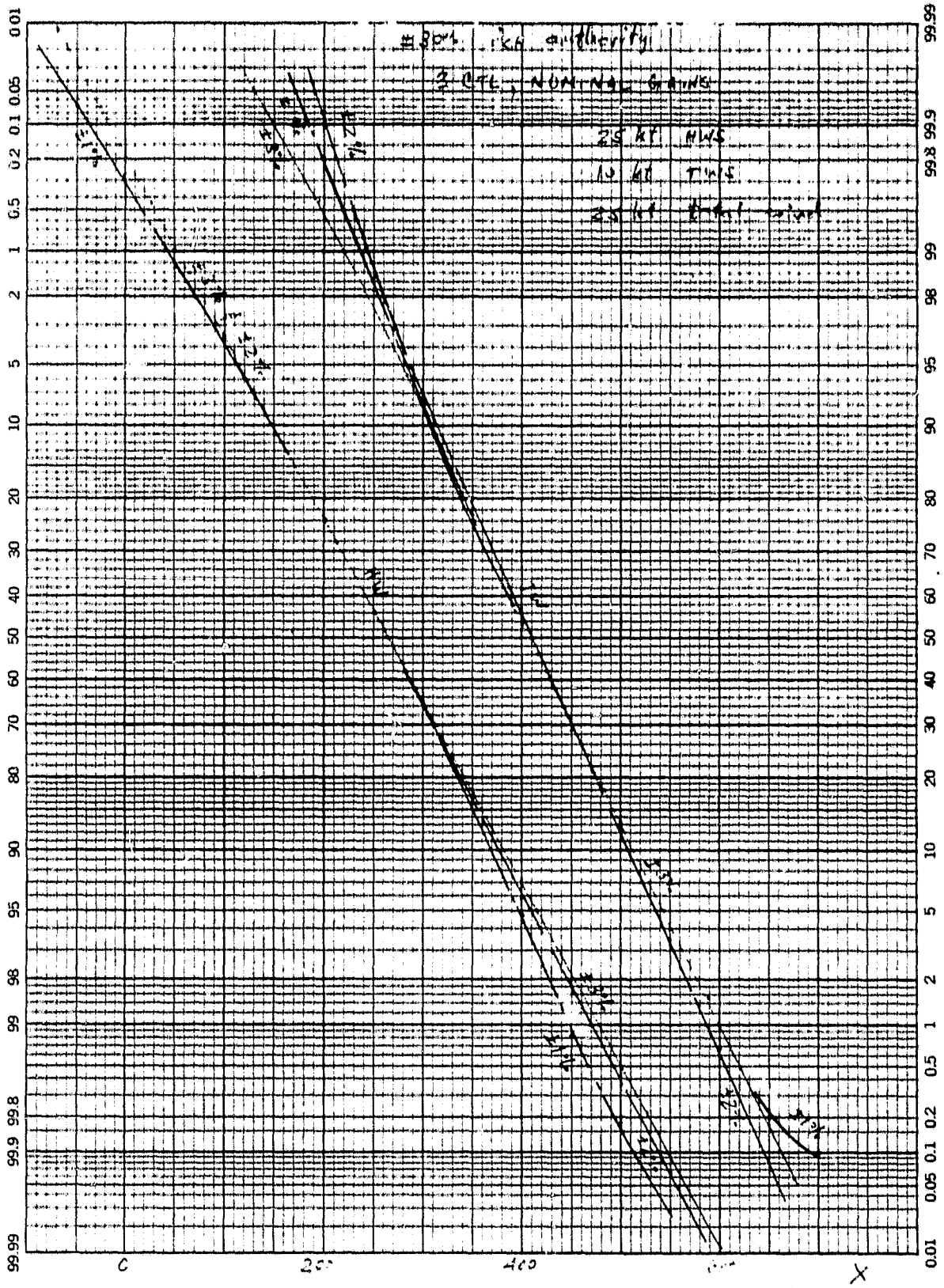

FIGURE B-88. RPM AUTHORITY VARIATION

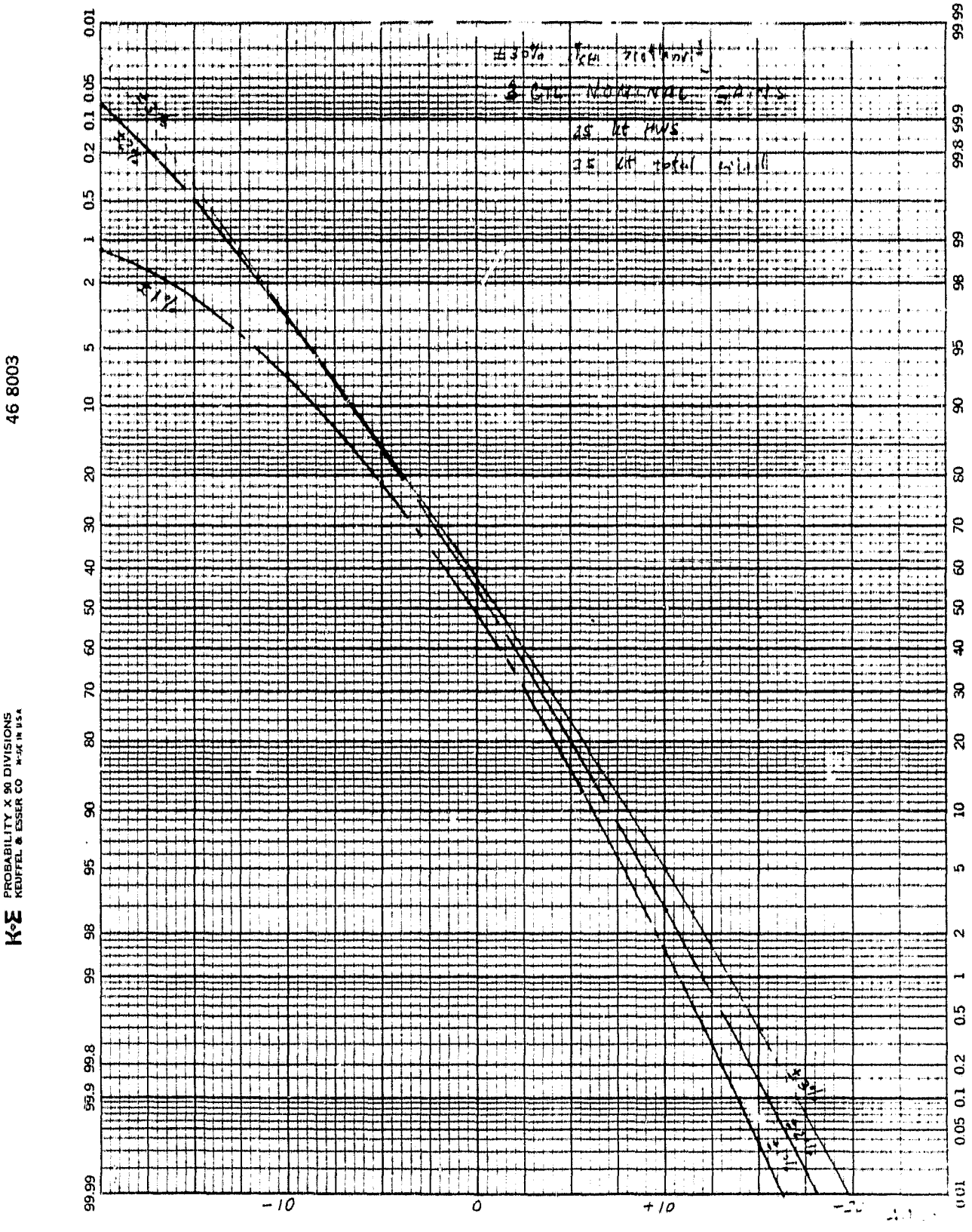

FIGURE B-89. RPM AUTHORITY VARIATION

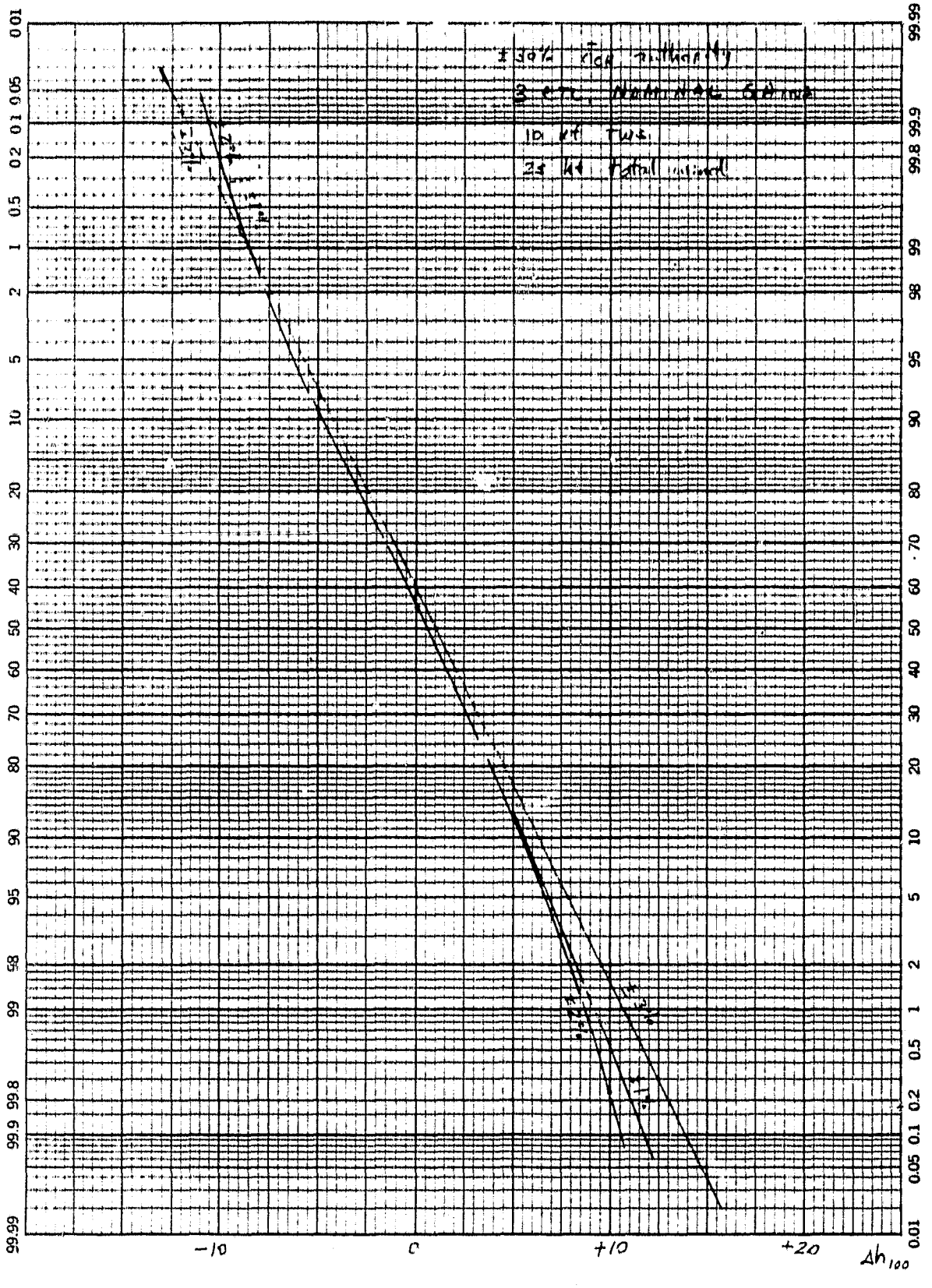

FIGURE B-90. RPM AUTHORITY VARIATION

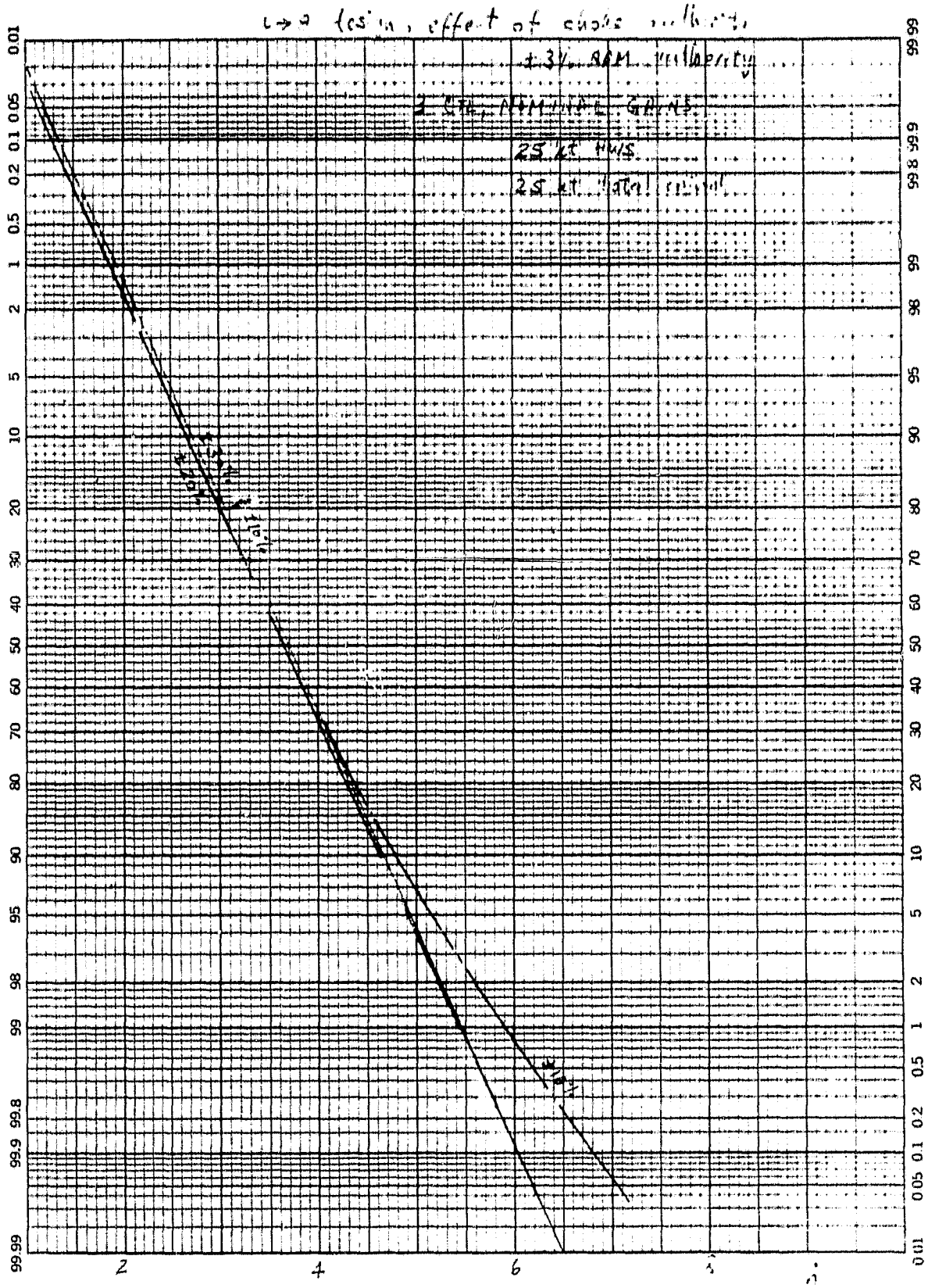

FIGURE B-91. CHOKE AUTHORITY VARIATION

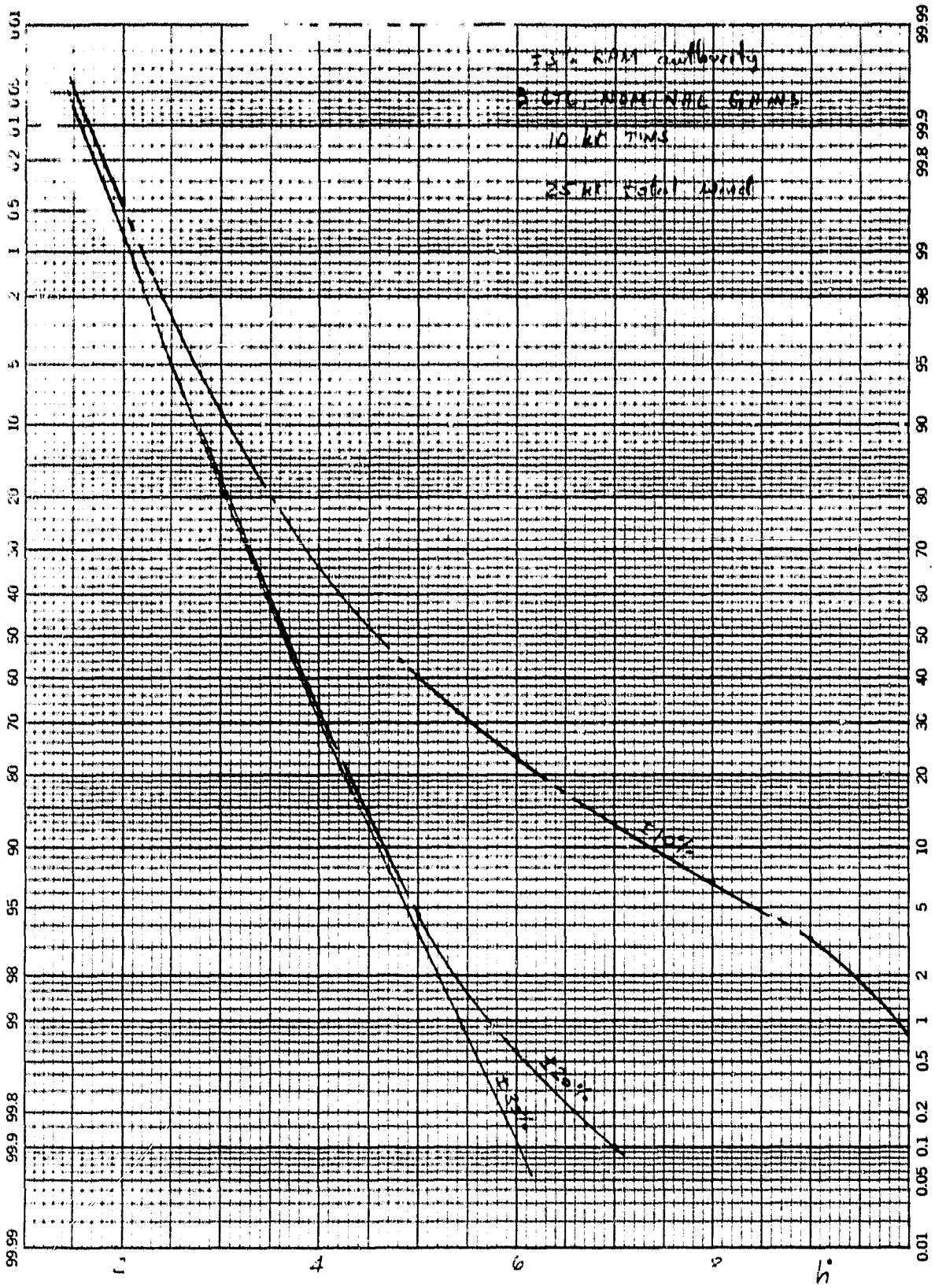

FIGURE B-92. CHOKE AUTHORITY VARIATION

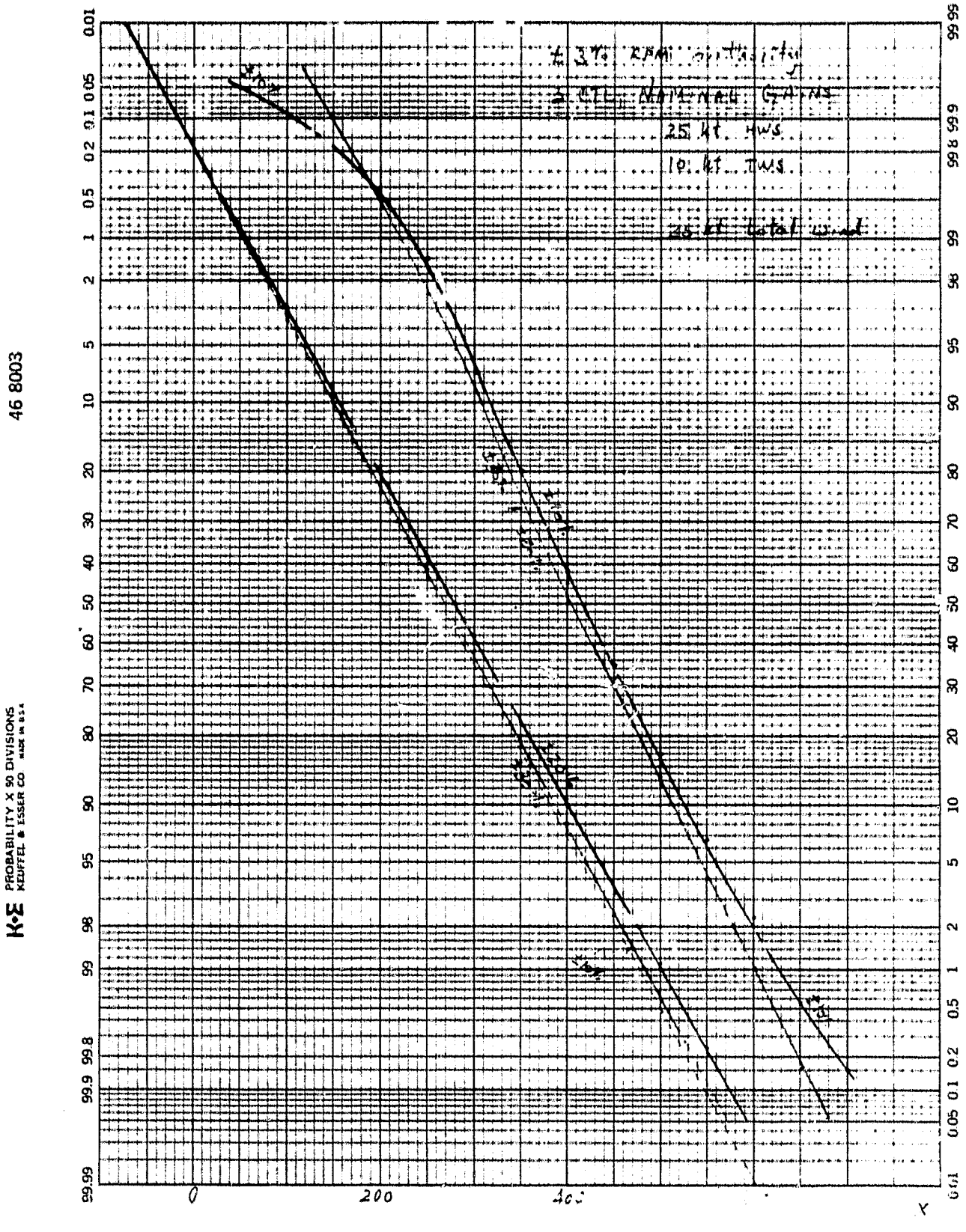

FIGURE B-93. CHOKE AUTHORITY VARIATION

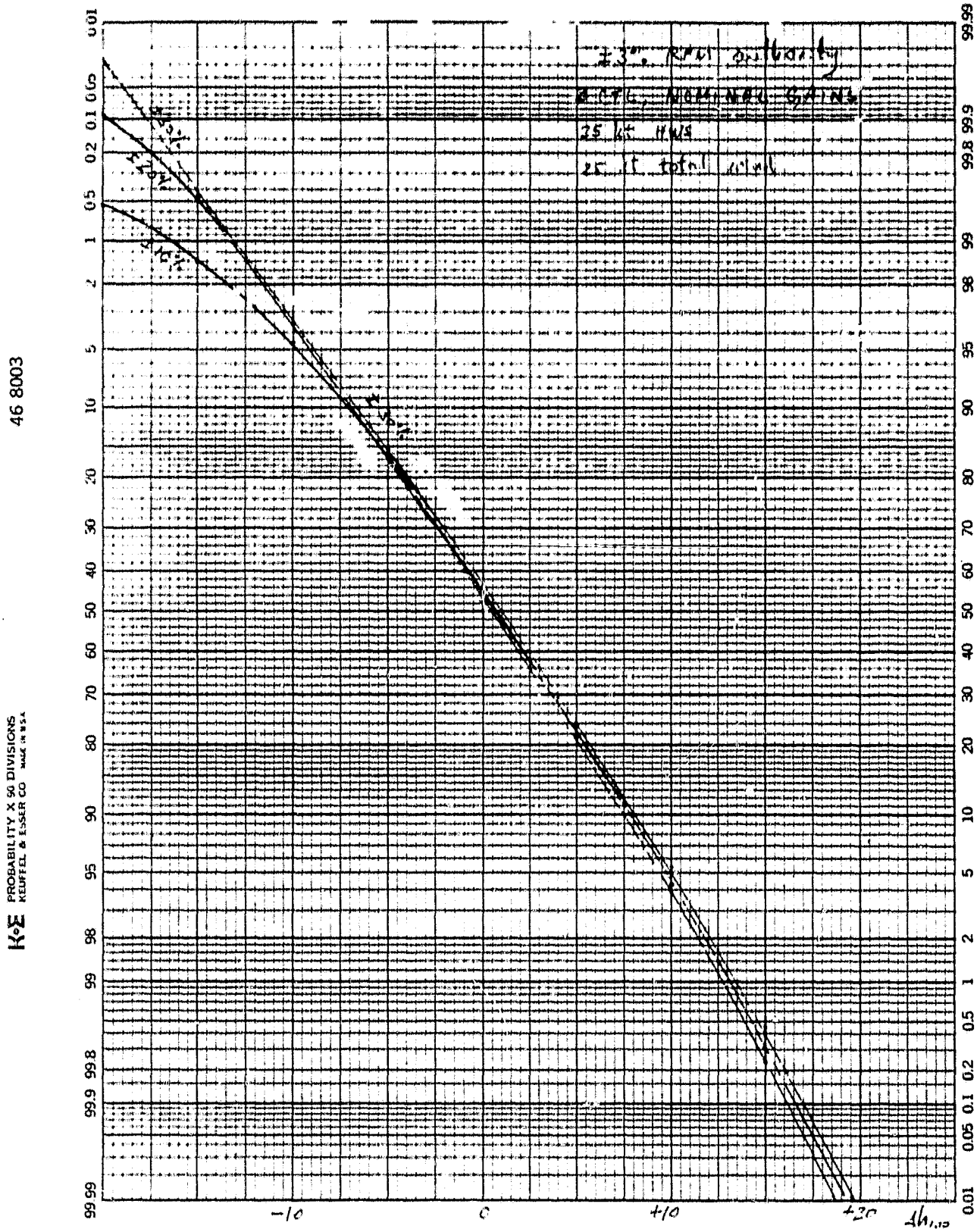

FIGURE B-94. CHOKE AUTHORITY VARIATION

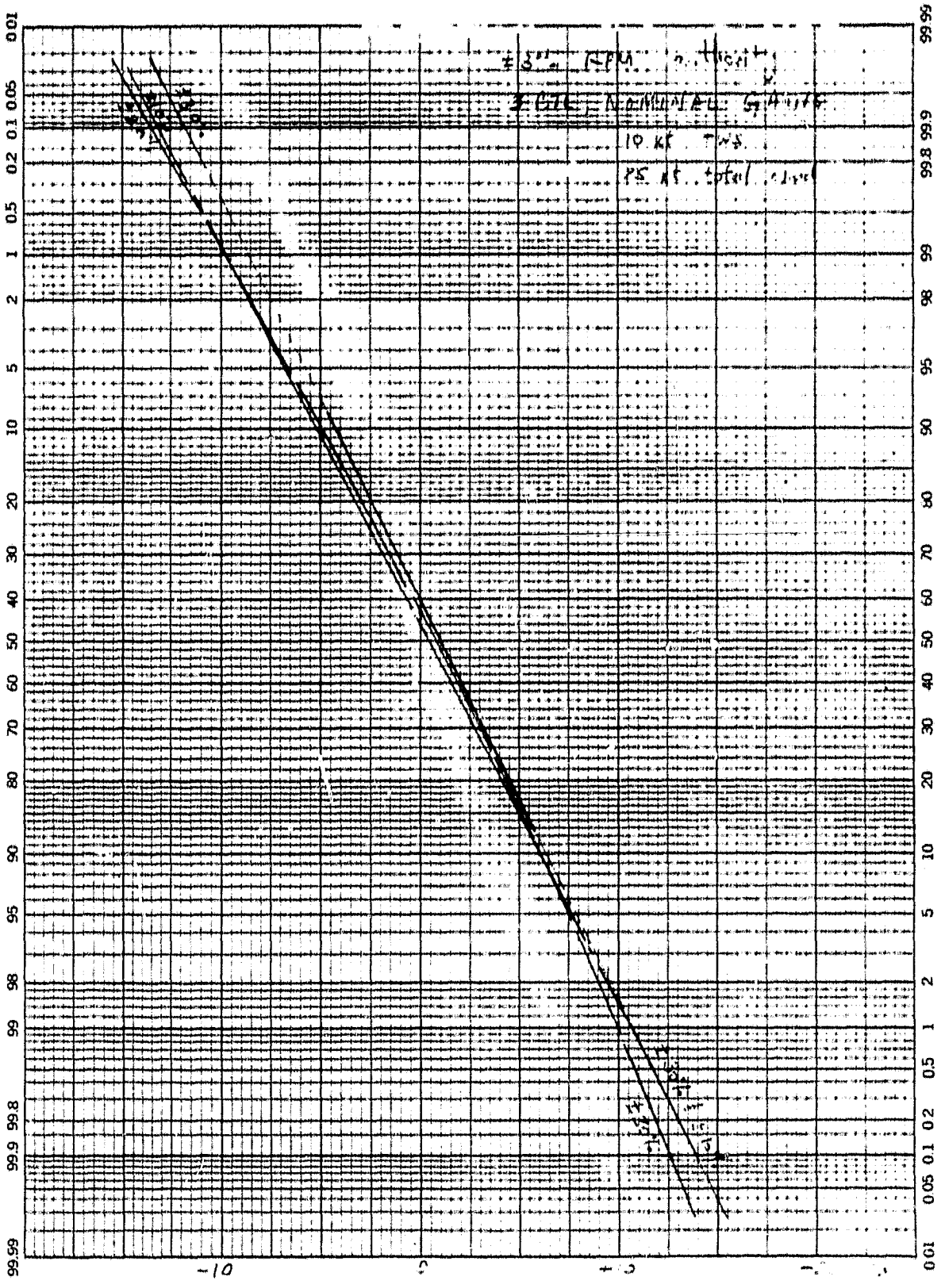

FIGURE B-95. CHOKE AUTHORITY VARIATION

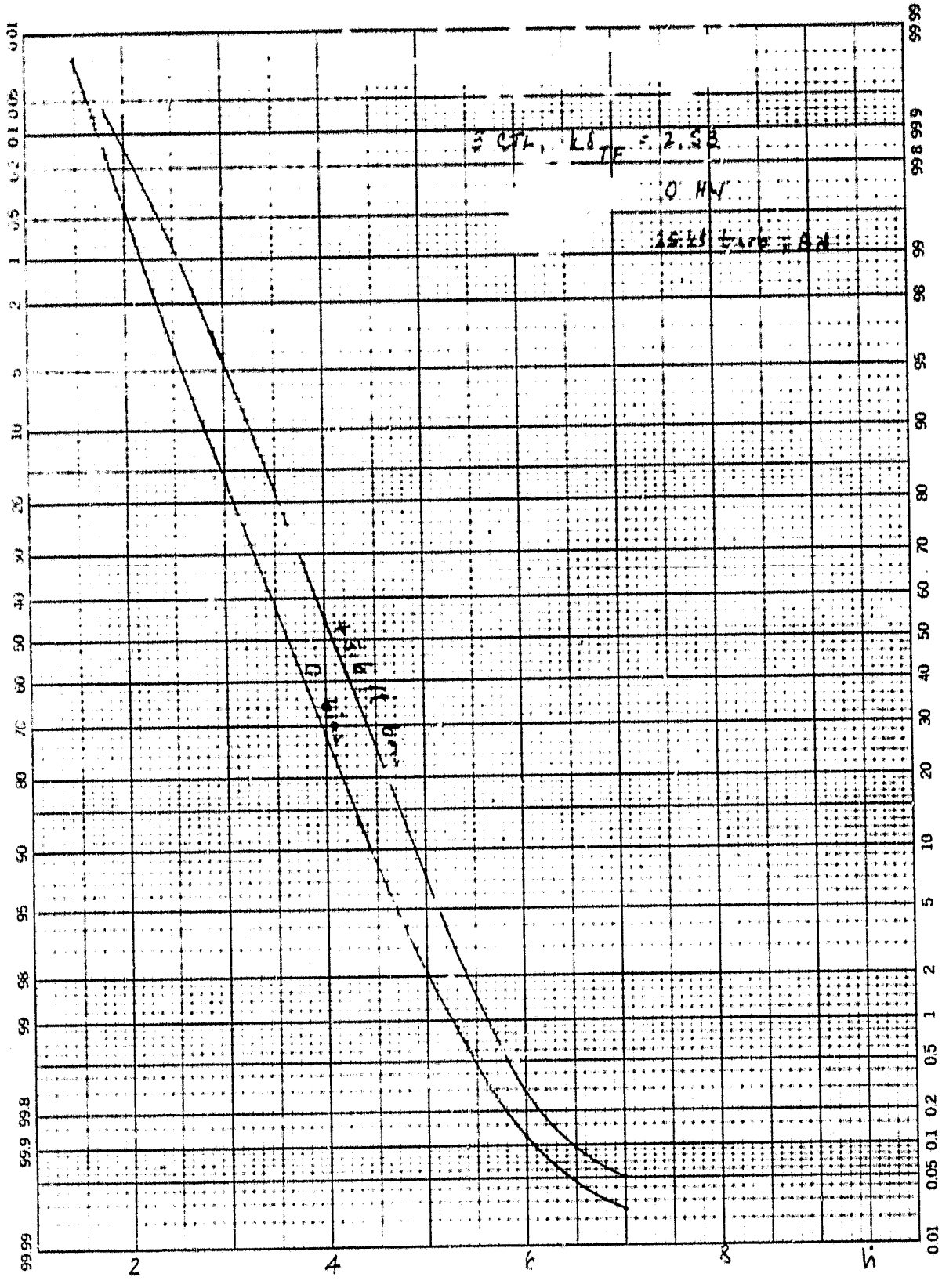

FIGURE B-96. RADAR ALTIMETER BIAS

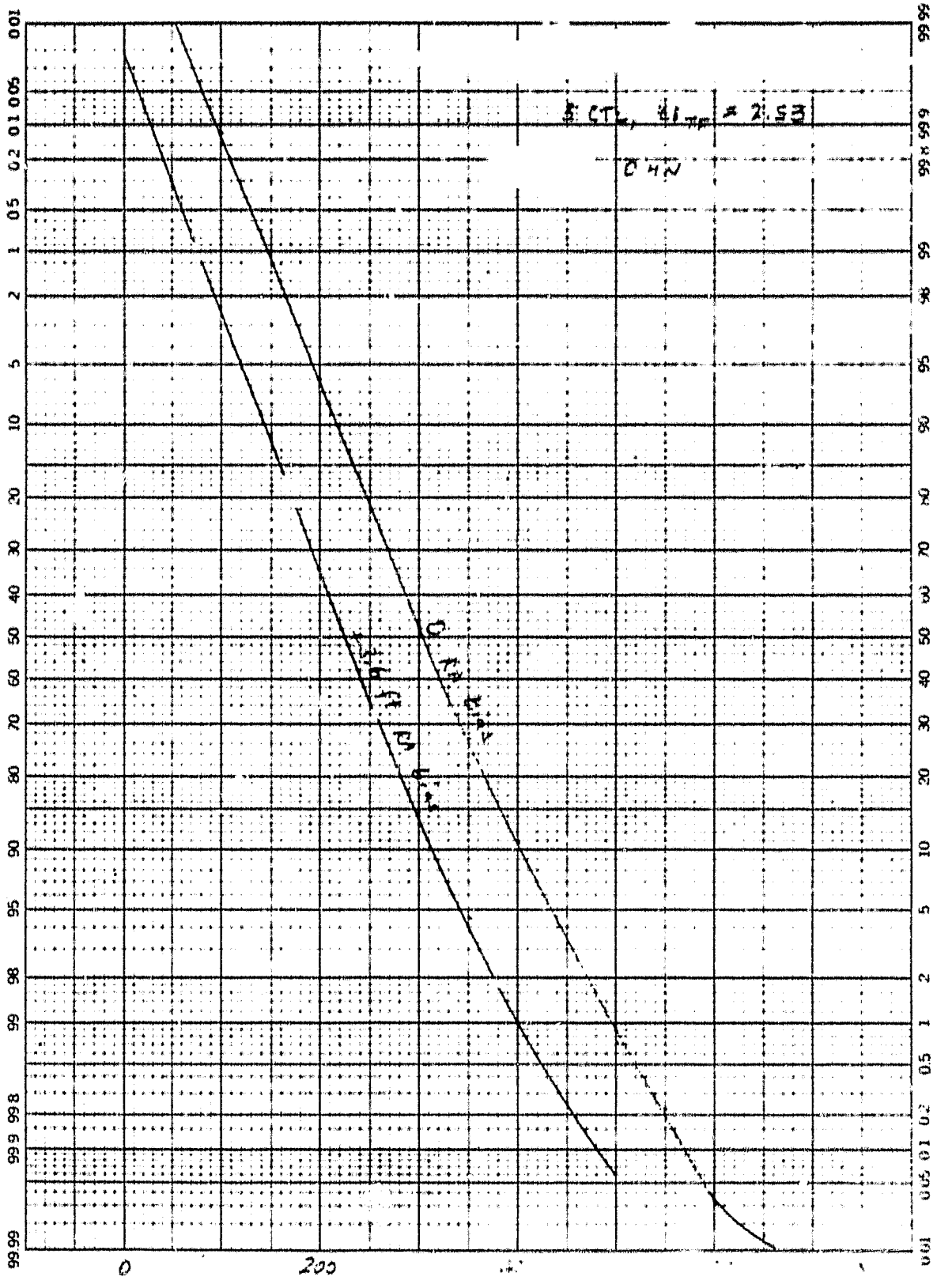

FIGURE B-97. RADAR ALTIMETER BIAS

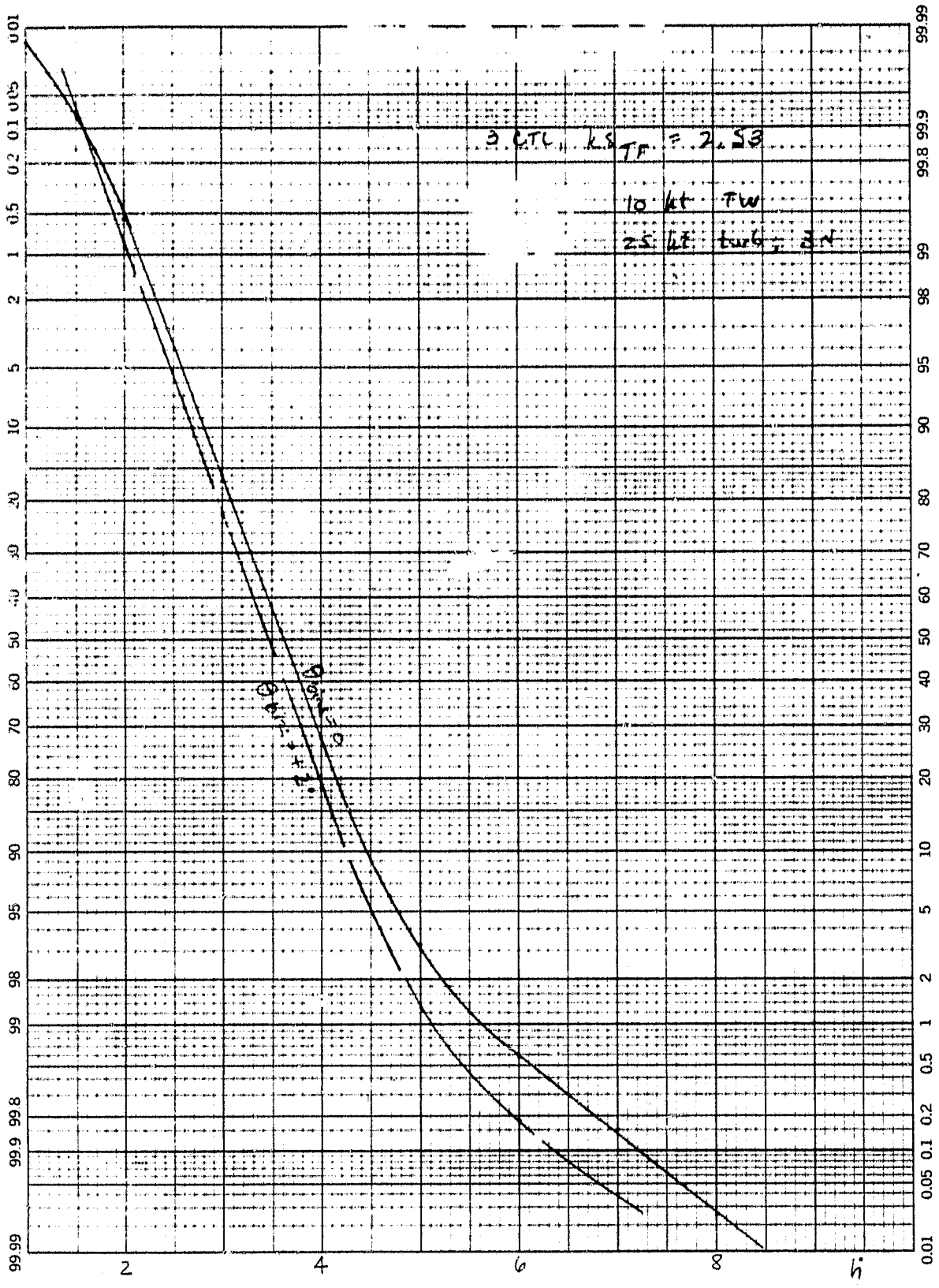

46 8003

K&E PROBABILITY X 3G DIVISIONS
KEUFFEL & ESSER CO

FIGURE B-98 GYRO BIAS

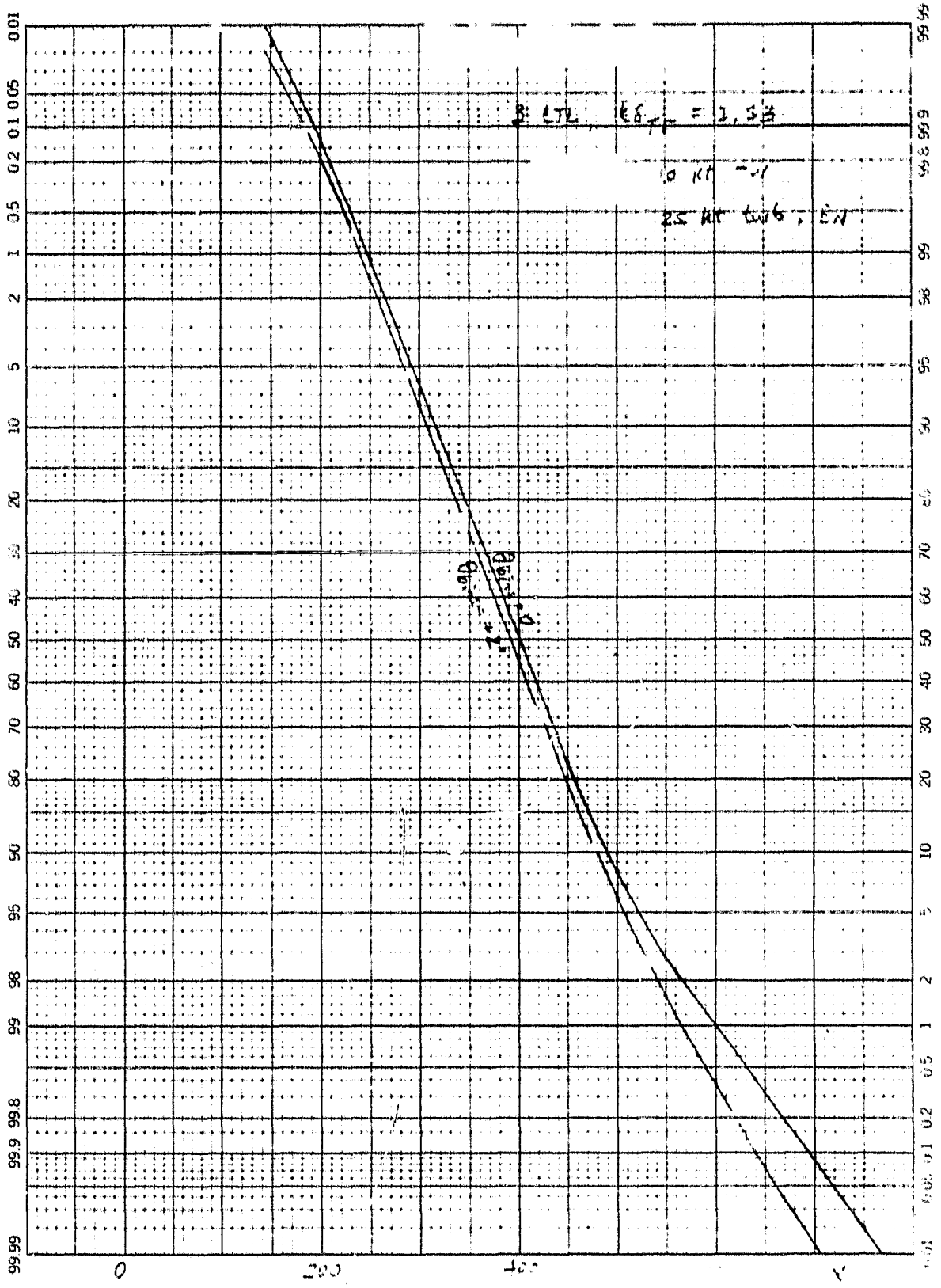

FIGURE B-99. GYRO BIAS

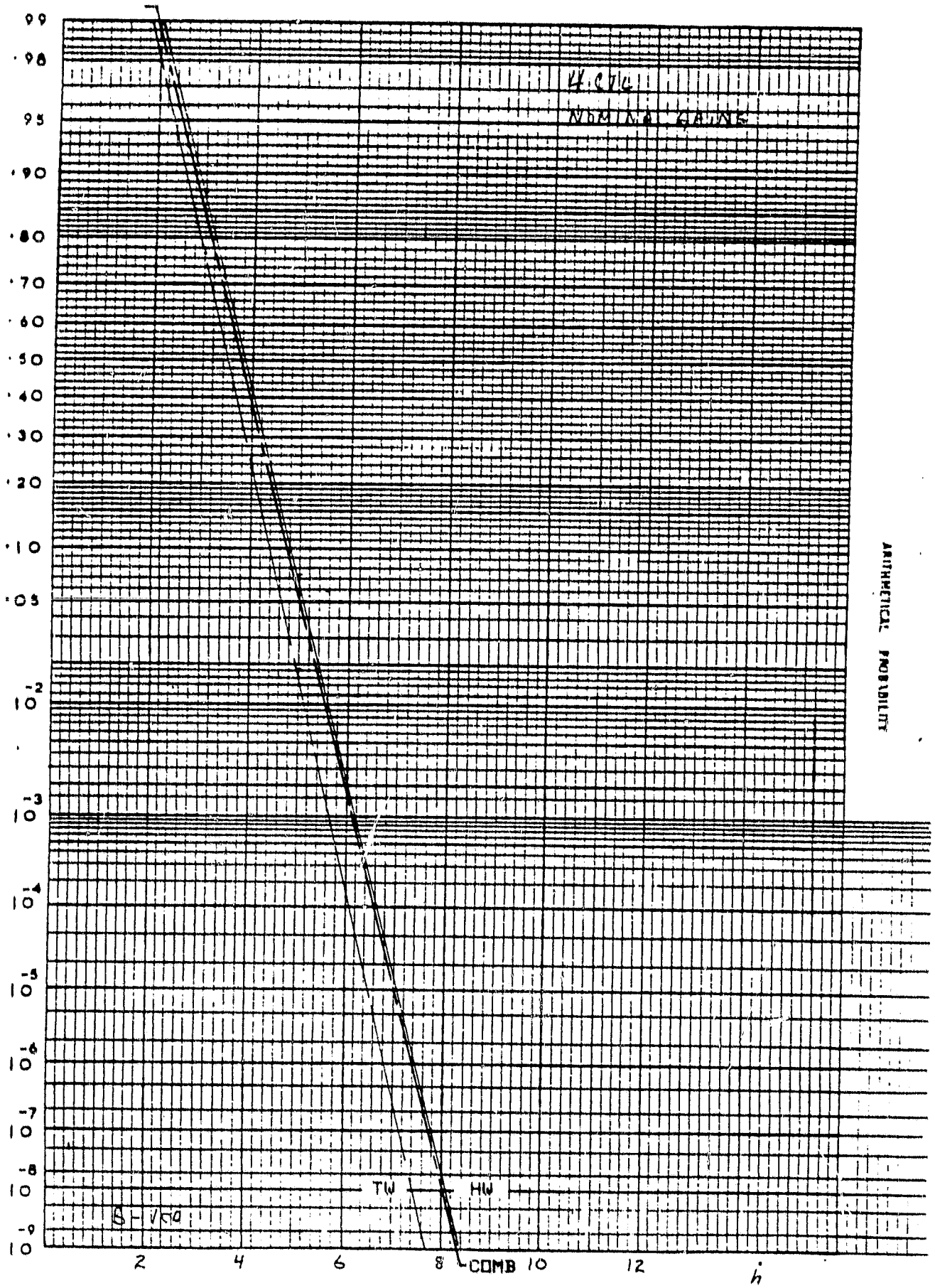

FIGURE B-100. RUNS OUTSIDE WINDOW REJECTED

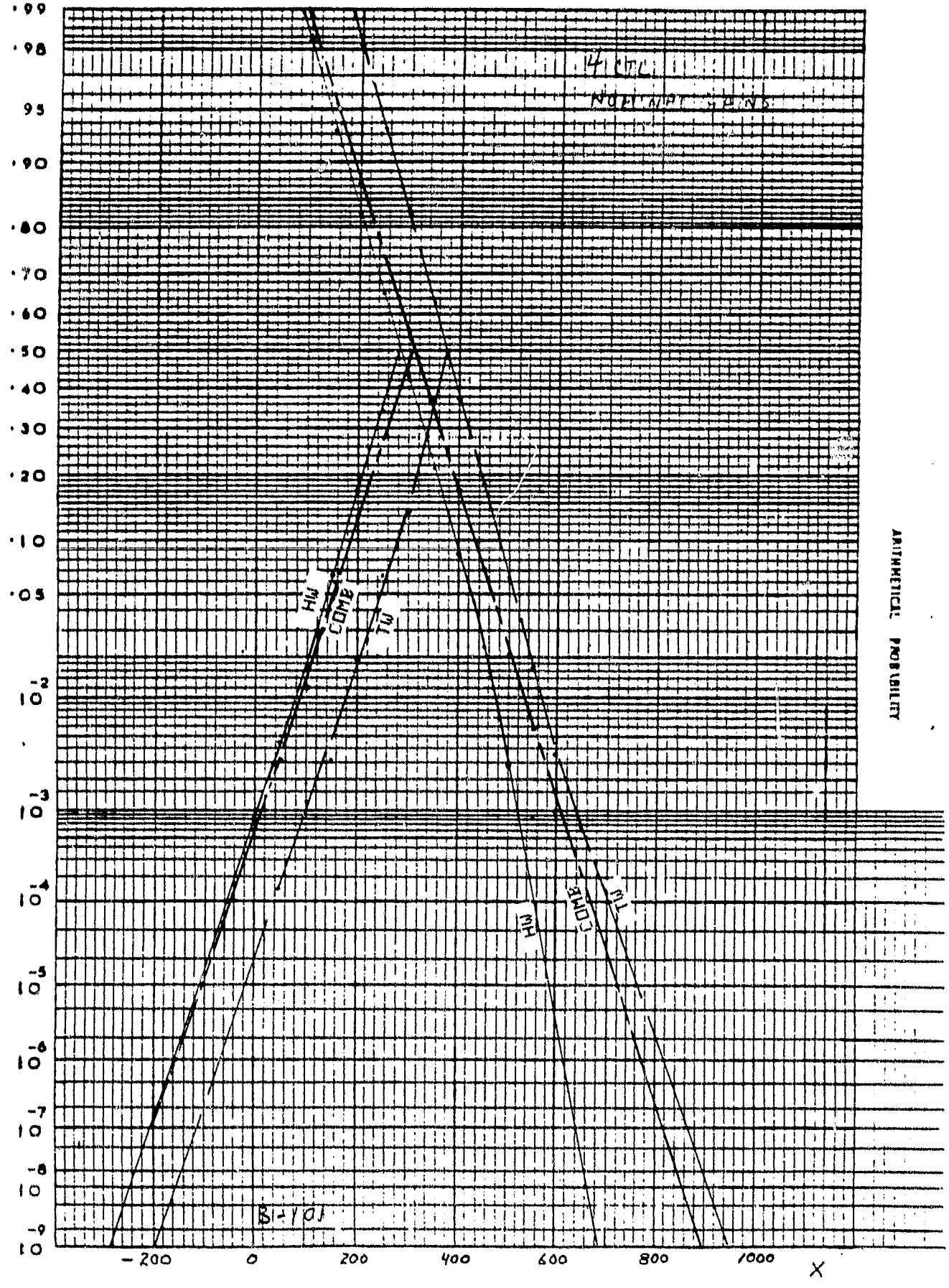

FIGURE B-101. RUNS OUTSIDE WINDOW REJECTED

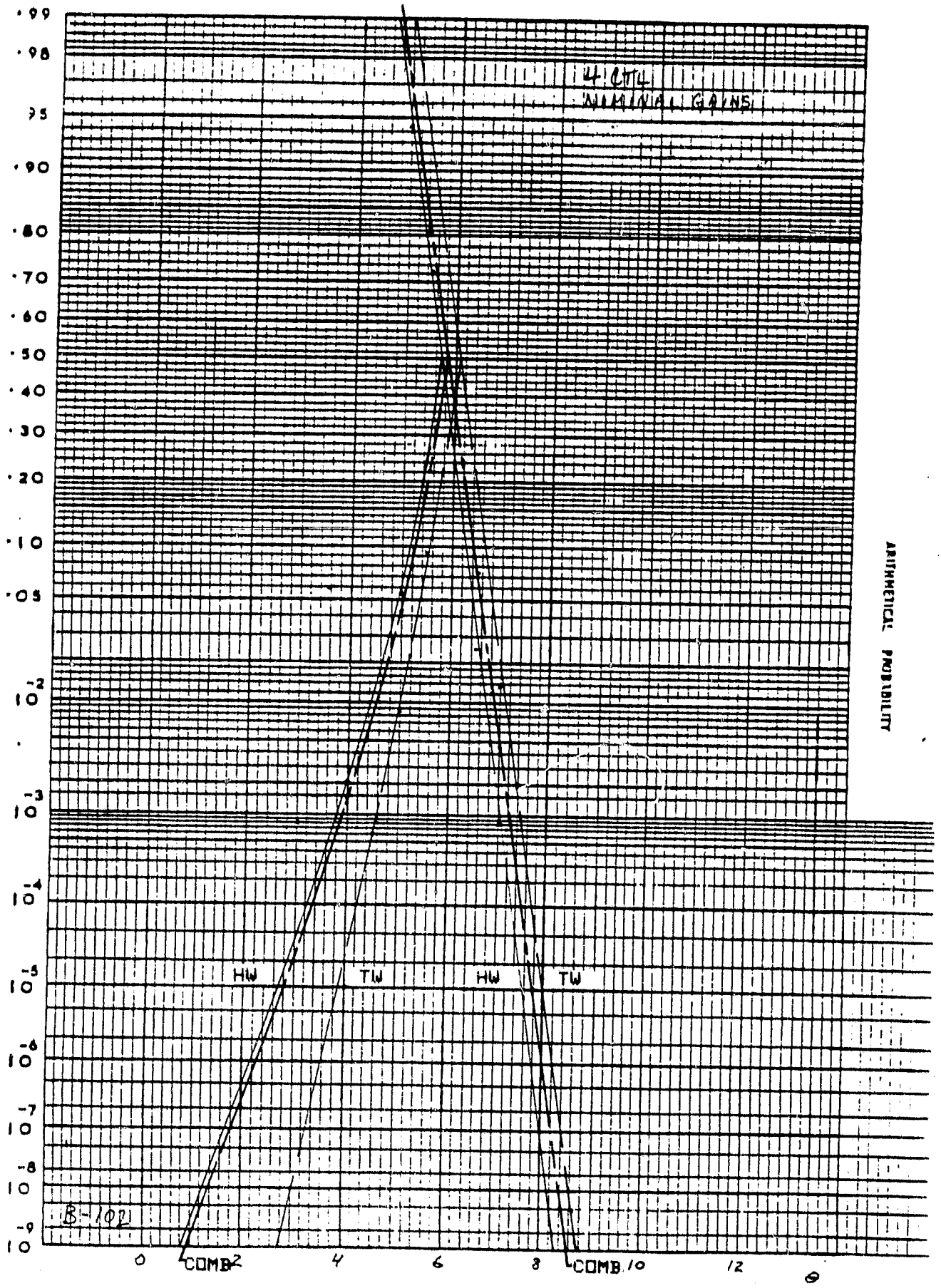

FIGURE B-102. RUNS OUTSIDE WINDOW REJECTED

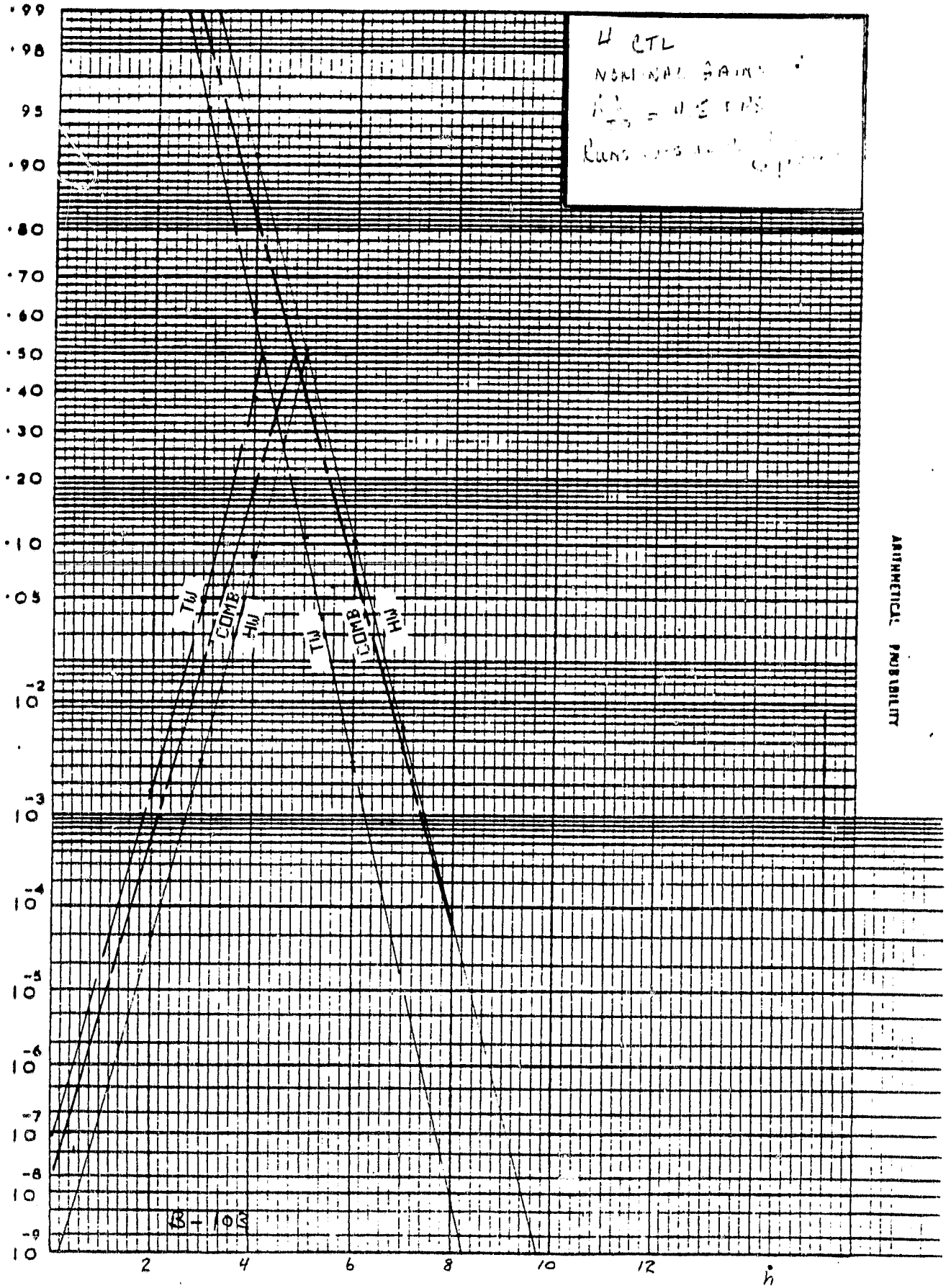

FIGURE B-103. INCREASED TOUCHDOWN SINK RATE

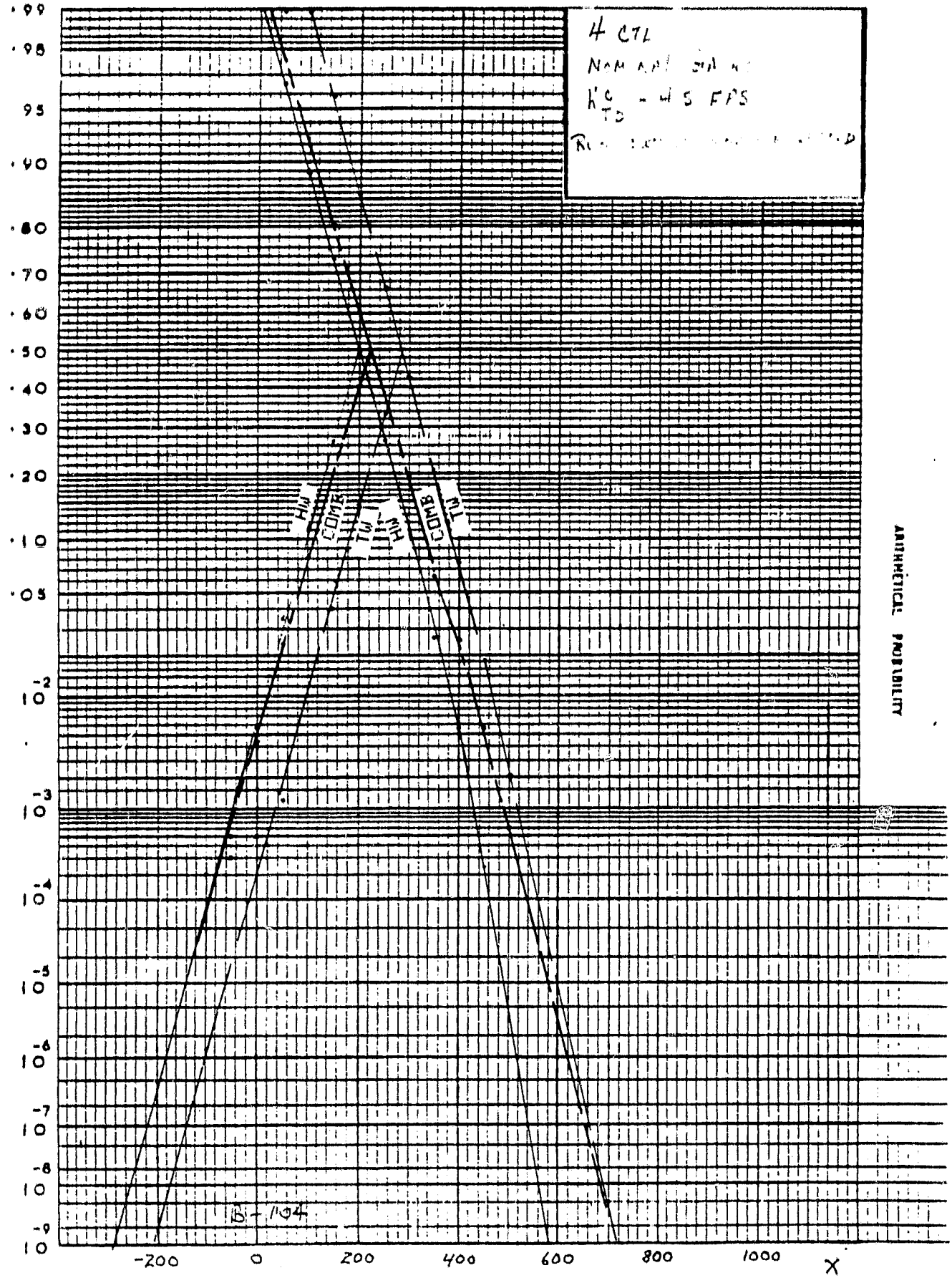

FIGURE B-104. INCREASED TOUCHDOWN SINK RATE

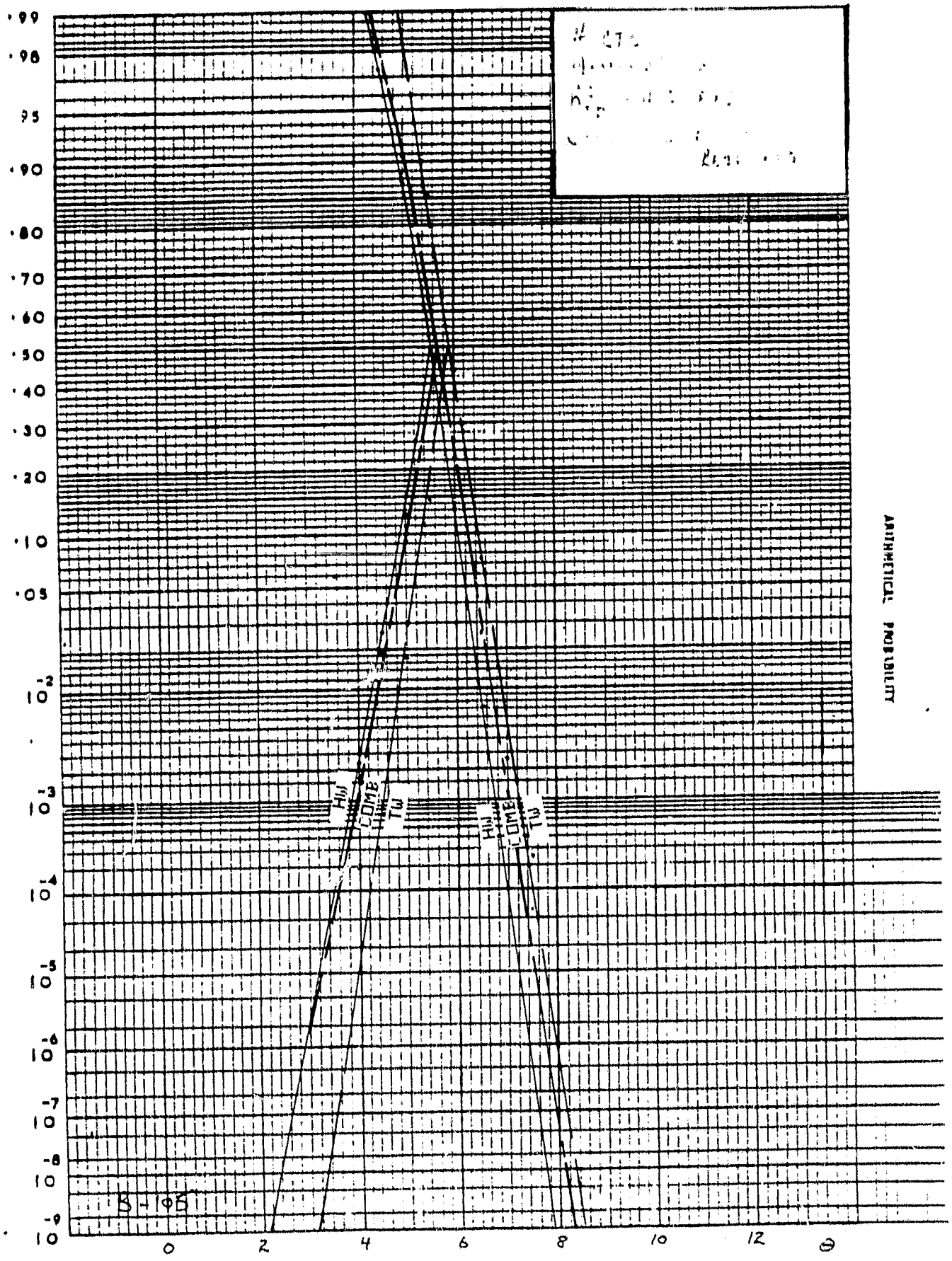

FIGURE B-105. INCREASED TOUCHDOWN SINK RATE

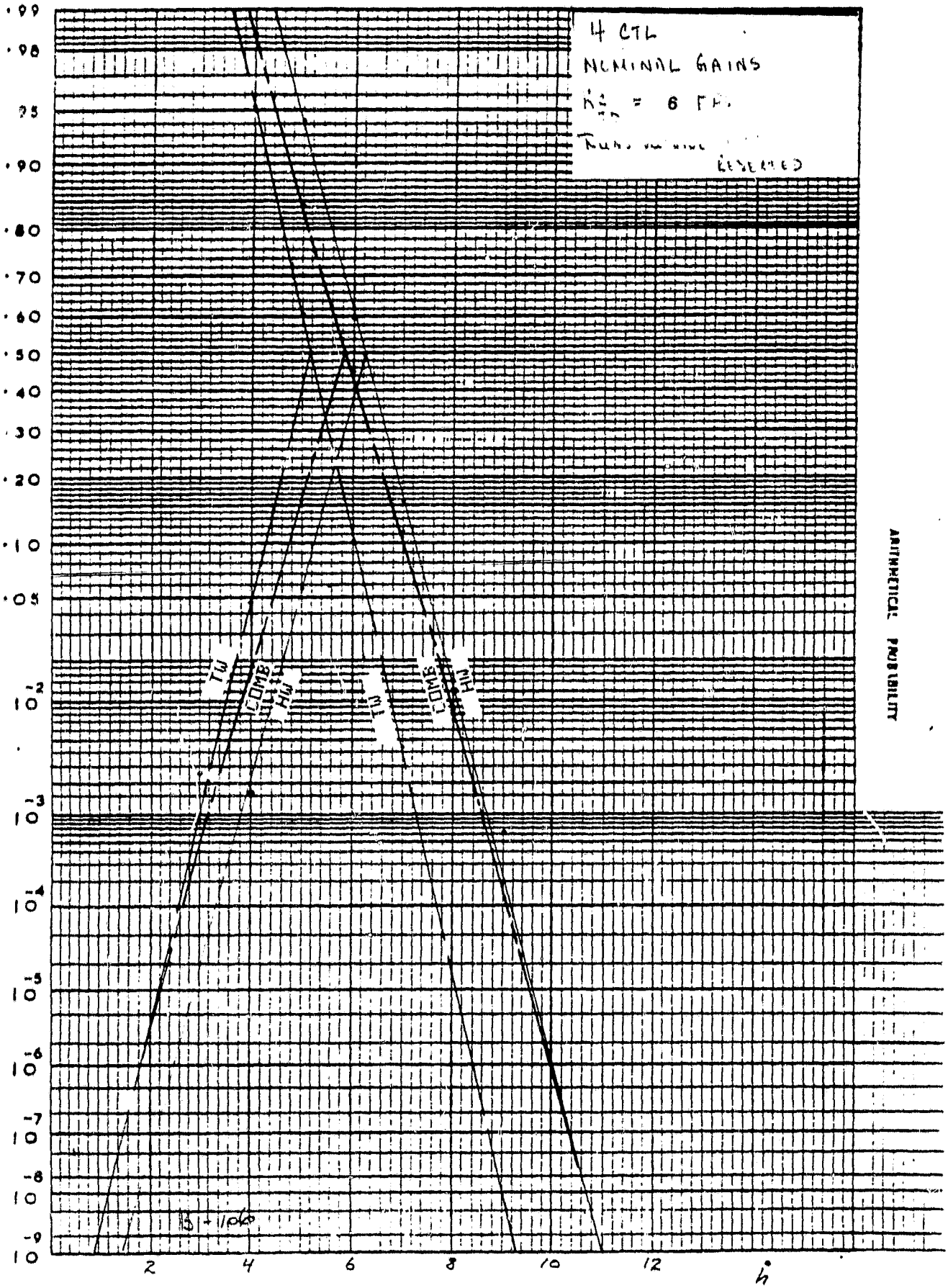

FIGURE B-106. INCREASED TOUCHDOWN SINK RATE

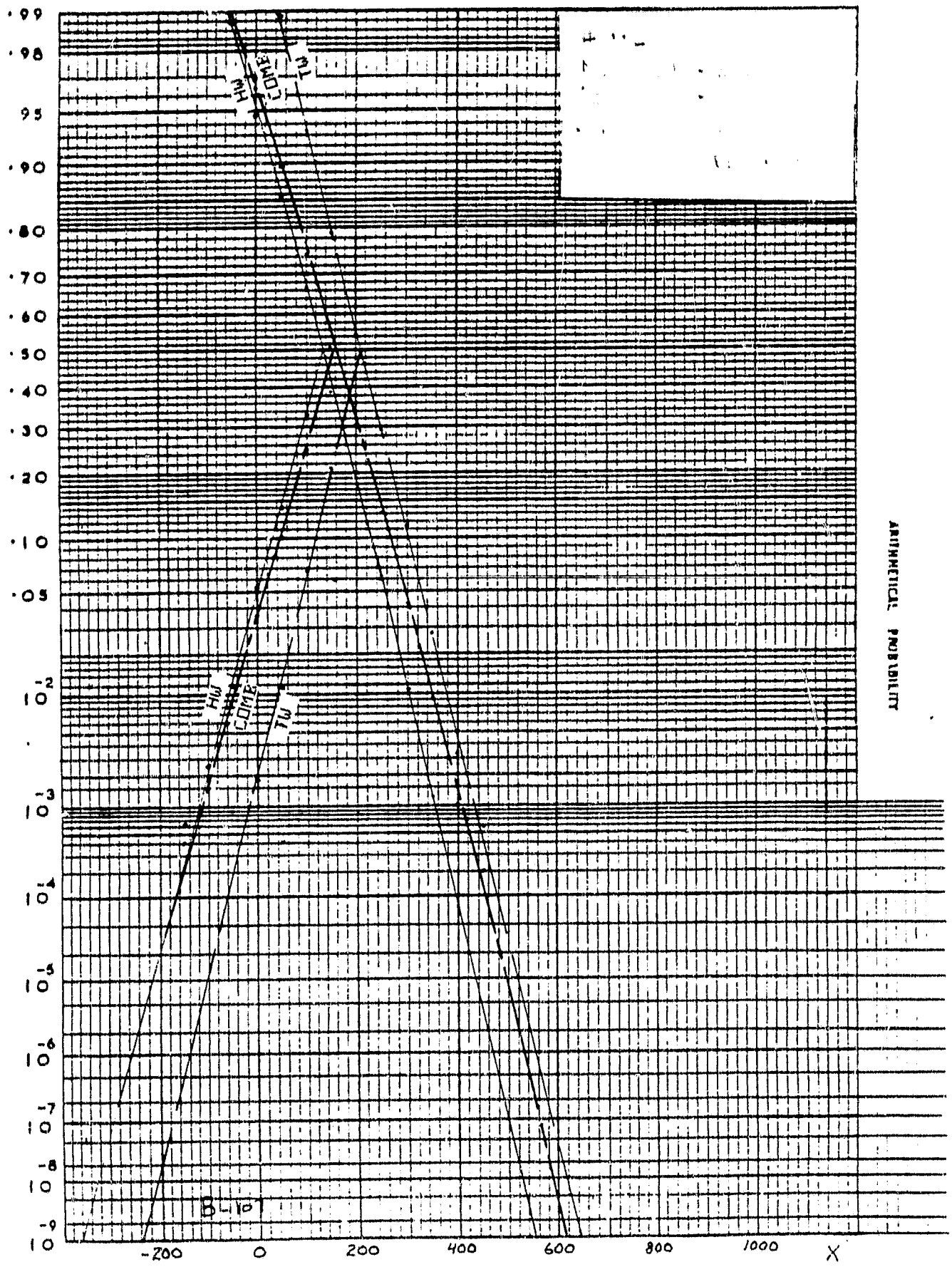

FIGURE B-107. INCREASED TOUCHDOWN SINK RATE

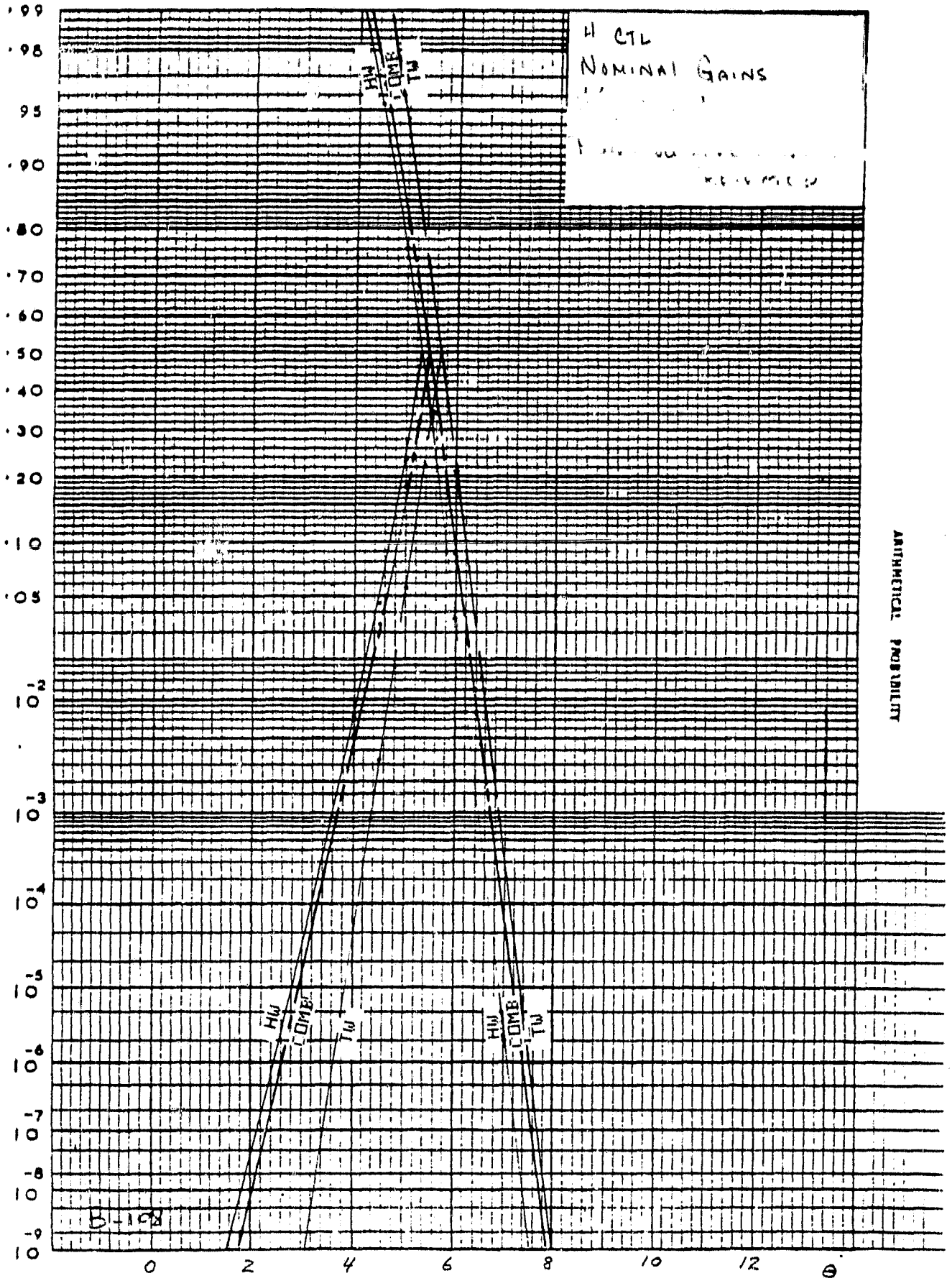

FIGURE B-108. INCREASED TOUCHDOWN SINK RATE